DISSERTATION

INVESTIGATION INTO PRODUCER GAS UTILIZATION IN HIGH PERFORMANCE NATURAL GAS ENGINES

Submitted by

Daniel M. Wise

Department of Mechanical Engineering

In partial fulfillment of the requirements

For the Degree of Doctor of Philosophy

Colorado State University

Fort Collins, Colorado

Spring 2013

Doctoral Committee:

Advisor: Daniel B. Olsen

Gary Caille
Anthony Marchese
Sybil Sharvelle

ABSTRACT

INVESTIGATION INTO PRODUCER GAS UTILIZATION IN HIGH PERFOMANCE NATURAL GAS ENGINES

A wide range of fuels are used in industrial gas fueled engines including well-head gas, pipeline natural gas, producer gas, coal gas, digester gas, landfill gas, and liquefied petroleum gas. Many industrial gas fueled engines operate both at high power density for increased efficiency and at ultra-lean air-fuel ratios for low NOx emissions. These two conditions require that engine operation occurs in a narrow air-fuel ratio band between the limits of misfire and the initiation of knock. The ability to characterize these limits for a given fuel is essential for efficient and effective engine operation. This work pursues two primary research objectives:

(1) to characterize producer gas blends by developing prognostic tools with respect to a given blend's resistance to knock and

(2) to develop a process to determine knock onset for a given fuel gas through direct indication from pressure transducer data at varied air-fuel ratios (ranging from stoichiometric to ultra-lean) as well as varied intake conditions (ranging from naturally aspirated to boosted intake pressures replicating turbocharged engines) and to quantitatively characterize the knock event using discreet and repeatable metrics derived from the analysis of the data.

Methane number determination for natural gas blends is traditionally performed with research engines at stoichiometric conditions where the onset of knock is identified through subjective audible indication. To more closely replicate the operating conditions of a typical industrial engine, a Cooperative Fuel Research (CFR F2) engine is modified for boosted fuel/air intake and variable exhaust back pressure (to simulate turbocharger operation) with the

incorporation of piezoelectric pressure transducers at the cylinder head to allow quantitative analysis of cylinder pressure conditions and transients precursive to, during, and following a knock event of varying magnitude. The interpretation of this data provides for evaluation of unique analytical methods to quantify and characterize engine knock under these conditions.

In the course of this study an objective and consistent method for measuring methane number is developed, measured methane number for a total of 35 producer gas blends is provided, and a prognostic tool for predicting methane number, utilizing neural networks, is presented.

ACKNOWLEDGEMENTS

I would like to express my gratitude to Dr. Dan Olsen, my advisor, for his remarkable support throughout the course of my graduate studies. In addition, I would like to express my appreciation to my faculty committee members, Dr. Gary Caille, Dr. Anthony Marchese, and Dr. Sybil Sharvelle for their interest in this work, for the time they have invested on my behalf and for the guidance provided me throughout this process.

Many thanks to the staff of the Engines and Energy Conversion Laboratory, in particular to Phil Bacon for his help and support offered on so many occasions and to Kirk Evans, without whose expertise and innovation this project would not have been possible. I also sincerely appreciate the help and support provided by my fellow graduate students, always willing to lend their expertise, as well as the undergraduate students working with me in the CFR laboratory, constructing the test cell nearly from scratch. To Chris Fischer, whose hard work and tireless contribution have been invaluable to the success of this project, thank you.

Finally, to Kathy, my loving wife and partner, for your support throughout this process. It's been far too much to ask but you've stayed with me every step of every journey, this one included. I can't thank you enough.

TABLE OF CONTENTS

ABSTRACT ii

ACKNOWLEDGEMENTS iv

LIST OF TABLES viii

LIST OF FIGURES x

LIST OF SYMBOLS xv

LIST OF ACRONYMS xvi

1 INTRODUCTION AND GENERAL BACKGROUND 1

1.1 Engine Knock 3

1.2 Fuel Knock Ratings 7

1.3 Problem Statement and Research Objectives 9

2 LITERATURE REVIEW 11

2.1 Metrics to Rate Resistance to Knock for Gaseous Fuels 11

2.1 Characterization of Producer Gas as a Fuel in IC Engines 21

3 EXPERIMENTAL APPARATUS 23

3.1 Hardware Set-Up 23

3.2 Engine 26

3.3 Knock Measurement System 28

3.4 Engine Intake System 30

3.5 Engine Exhaust System 40

3.6 Electronic Ignition 48

3.7 Fuel Blending System 49

3.8 Enabling Software and Virtual Instrumentation (VI) 54

4 TEST PLAN AND FUEL SELECTION 56

4.1 Test Cell Demonstration Testing 56
4.2 Crank Angle/Piston Top Dead Center (TDC) Indication 57
4.3 Ignition Timing Sweeps and MBT Timing Determination 58
4.4 Methane Number Sensitivity to Engine Operating Parameters 59
4.5 Producer Gas Blend Selection 61
4.6 Knock Measurement Method Development 65
4.7 Knock Level Thresholds 74
4.8 Knock Integral 76

5 TEST RESULTS 83

5.1 Measured Methane Numbers 83
5.2 Critical Compression Ratio, Measured Methane Number and NMEP 84
5.3 Methane Number Sensitivity to Operational Parameters Results 87
5.4 Heating Value, Methane Number, NMEP and Intake Boost Pressure 89
5.5 Combustion Analysis 92
5.6 Correlation of Measured Methane Number to Predicted 94
5.7 Impact of Diluent and Fuel Gas Content on Measured Methane Number 97

6 PREDICTING METHANE NUMBER FOR PRODUCER GAS BLENDS 100

6.1 CHEMKIN Modeling of Producer Gas Blends 100
6.2 Neural Network Methodology 107
6.3 Neural Network Model for Producer Gas Methane Number 111

7 CONCLUSIONS AND RECOMMENDATIONS 114

7.1 Overview 114
7.2 Conclusions 114
7.3 Research Recommendations 116

REFERENCES 119

Appendix A TEST PROCEDURES 122

Appendix B ENGINE CONTROL & LOGGING OVERVIEW 140

B-1 CFR Test Cell Vi 148
B-2 Electronic Ignition 155

Appendix C NEURAL NETWORK STATISTICAL ANALYSIS 156

Appendix D DATA TABLES 174

Appendix E Acoustic Velocity Calculations..... 185

LIST OF TABLES

Table 4- 1 Methane Number Measurement Case Definition 61

Table 4- 2 Initial Test Blend Constituent Makeup 62

Table 5- 1 Producer Gas Blend Constituent Definition and Characterization 84

Table 6- 1 CHEMKIN IC Engine Model Input Parameters 101

Table 6- 2 Methane Number Determination Summary 106

Table C- 1 Results of Neural Network Predictive Model for Producer Gas Blends 157

Table C- 2 Neural Network Data Set #1 Summary 158

Table C- 3 Data Set #1 RMS Error 161

Table C- 4 Neural Network Data Set #2 Summary 162

Table C- 5 Data Set #2 RMS Error 165

Table C- 6 Neural Network Data Set #3 Summary 166

Table C- 7 Data Set #3 RMS Error 169

Table C- 8 Neural Network Data Set #4 Summary 170

Table C- 9 Data Set #4 RMS Error 173

Table D- 1 Methane Number Raw Data, Blends 3, 5, and Check Case 175

Table D- 2 Equivalence Ratio Sweeps, Raw Data (Blends 3 and 4) 176

Table D- 3 Methane/Hydrogen Baseline Data - NA 177

Table D- 4 Methane/Hydrogen Baseline Data – 10 bar nmep 178

Table D- 5 Methane/Hydrogen Baseline Data – 11 bar nmep 179

Table D- 6 Methane/Hydrogen Baseline Data – 12 bar nmep 180

Table D- 7 Motoring Data 1 – Daily Verification of Dynamic TDC 181

Table D- 8 Motoring Data 2 – Daily Verification of Dynamic TDC 182

Table D- 9 Motoring Data 3 – Daily Verification of Dynamic TDC 183

Table D- 10 Motoring Data 4 – Daily Verification of Dynamic TDC 184

Table E- 1 Worksheet to calculate γ_{avg} and MW_{avg} 189

Table E- 2 Producer Gas Combustion Equation Coefficients and Calculated Acoustic Velocity 190

Table E- 3 Matching CH_4/H_2 Blend Combustion Equation Coefficients and Calculated Acoustic Velocity 191

LIST OF FIGURES

Figure 1-1 Auto-Ignition of End Gas in a Combustion Chamber. 4

Figure 1-2 Cylinder Pressure vs. Time in a Typical SI Engine Application. 5

Figure 1-3 Definition of Combustion Phenomena in Spark-Ignition Engines. 6

Figure 2-1 Schematic of knock indices determination 17

Figure 2-2 DKI Representationfor a Knocking Cycle 19

Figure 3-1 Schematic representation of the test cell constructed for this work. 25

Figure 3-2 Cylinder and Clamping Sleeve Sections, Waukesha F-2 CFR. 27

Figure 3-3 CFR Engine Knock Measurement System, Original. 29

Figure 3-4 Sectional View Of The CFR Type D-1 Detonation Pick-Up. 31

Figure 3-5 CFR Engine Knock Measurement System, Post-Modification. 31

Figure 3-6 Pressure vs. Volume Diagram for the CFR Engine. 33

Figure 3-7 Engine Intake Air Piping from Facility Compressed Air System 36

Figure 3-8 Intake Air Piping to Include Rupture Disc and Solenoid Vent Valve 36

Figure 3-9 Schematic Depiction of the Test Cell Intake Air System. 37

Figure 3-10 Schematic Depiction of the Test Cell Engine Exhaust System. 40

Figure 3-11 Exhaust components. 41

Figure 3-12 Turbocharger Schematic 42

Figure 3-13 Overhead Suspension of Exhaust Components. 49

Figure 3-14 Fuel Blending System Installed Components. 50

Figure 3-15 Schematic Depiction of the Test Cell Fuel Blending System. 51

Figure 4-1 Motoring Indicated Peak Pressure (TDC) Location Test Results 58

Figure 4-2 Ignition Timing Sweep Results - Power vs. Timing 59

Figure 4-3 Expanded Producer Gas Blend List by Air Fuel Ratio. 63

Figure 4-4 Expanded Producer Gas Blend List by Diluent Percentage. 63

Figure 4-5 Blend List by Air-Fuel Ratio, Gap Blends Inserted. 64

Figure 4-6 Blend List by Diluent Percentage, Gap Blends Inserted. 64

Figure 4-7 Pressure Trace and FFT Plot - Light Knock. 68

Figure 4-8 Pressure Trace and FFT Plot - Moderate Knock 69

Figure 4-9 Pressure Trace and FFT Plot - Heavy Knock 70

Figure 4-10 Average knock frequency for tested blends. 71

Figure 4-11 In-Cylinder Acoustic Velocity for Tested Blends. 73

Figure 4-12 Acoustic Velocity As a Function of Methane Number. 74

Figure 4-13 FFT Knock Amplitude 75

Figure 4-14 Two Recorded Knock Measurement Traces Superimposed. 77

Figure 4-15 Check Case Results - 90% CH4, 10% C2H6 79

Figure 4-16 Average Knock Amplitude for Blends Tested 80

Figure 4-17 COV of Recorded Knock Amplitude for Tested Blends. 80

Figure 4-18 Average Integral Values By Blend For 500 Cycle Test Runs 82

Figure 5-1 Methane Number vs. Critical Compression Ratio, nmep = 9 bar. 85

Figure 5-2 Methane Number vs. Critical Compression Ratio, nmep = 10 bar. 85

Figure 5-3 Methane Number vs. Critical Compression Ratio, nmep = 11 bar. 86

Figure 5-4 Methane Number vs. Critical Compression Ratio, nmep = 12 bar. 86

Figure 5-5 Methane Number vs. Critical Compression Ratio, Combined. 86

Figure 5-6 Natural Gas Measured Methane Number. 87

Figure 5-7 Critical Compression Ratio for NG and Blends 3 & 5 89

Figure 5-8 NMEP Developed Under Naturally Aspirated Operation and LHV 90
Figure 5-9 Heating Value vs. Methane Number 91
Figure 5-10 Intake Pressure to Achieve 12 bar NMEP and Fuel LHV 91
Figure 5-11 Measured Methane Number vs. Ignition Delay 92
Figure 5-12 Methane Number vs. Combustion Phasing (50% Burn Location) 93
Figure 5-13 Methane Number vs. Location of Peak Pressure 94
Figure 5-14 Measured and Predicted (AVL) Methane Numbers. 95
Figure 5-15 CH4 Percentage vs. Measured/Predicted Methane Number Delta. 96
Figure 5-16 CO and H2 Percentage vs. Measured/Predicted Delta. 96
Figure 5-17 CO2 + N2 Percentage vs. Measured/Predicted Delta. 96
Figure 5-18 Measured Methane Number vs. Diluent Content 98
Figure 5-19 Measured Methane Number vs. Fuel Gas Content 98
Figure 5-20 Syngas Blend Lower Heating Value vs. Methane Number 99
Figure 6-1 CHEMKIN Model Pressure vs. Crank Angle for the Güssing Blend. 103
Figure 6-2 CHEMKIN Model Pressure vs. Crank Angle for CH_4-H_2 Blend. 105
Figure 6-3 CHEMKIN Model for CH_4-H_2 Blend, scale expanded for clarity. 105
Figure 6-4 Methane number estimates derived from various approaches. 107
Figure 6-5 Perceptron learning algorithm flowchart (Coolen, et al., 2005). 109
Figure 6-6 Neural Network schematic. 110
Figure 6-7 Neural Network Predicted Values for Methane Number 112
Figure 6-8 Error comparison for predicted values of methane number. 113

Figure A- 1 Compression ratio worksheet 129
Figure B- 1 Combustion Analyzer configuration input opening screen. 142
Figure B- 2 Engine operations monitoring page, cylinder pressure display. 143
Figure B- 3 Engine operations monitoring page, cylinder pressure display. 144
Figure B- 4 Engine operations monitoring page, P-V plot displayed (operating) 145
Figure B- 5 Engine operations monitoring page, instantaeous RPM plot displayed. 146
Figure B- 6 Engine operations monitoring page, FFT amplitude displayed. 147
Figure B- 7 Combustion loop module of combustion analyzer block diagram. 148
Figure B- 8 CFR Host VI Operational Parameters screen. 149
Figure B- 9 Fuel blending control display of the CFR Host VI program. 151
Figure B- 10 5-Gas Emissions display for the CFR Host VI. 153
Figure B- 11 Block Diagram of CFR Host VI Fuel Blending Module 154
Figure B- 12 Electronic Ignition Terminal Program Display 155
Figure C- 1 Data Set #1 Residuals 159
Figure C- 2 Data Set #1: Predicted vs. Actual Values 159
Figure C- 3 Data Set #1: Residual vs. Actual Values 160
Figure C- 4 Data Set #1: Residual vs. Predicted Values 160
Figure C- 5 Data Set #1 Sensitivity Analysis 161
Figure C- 6 Data Set #2 Residuals 163
Figure C- 7 Data Set #2: Predicted vs. Actual Values 163
Figure C- 8 Data Set #2: Residual vs. Actual Values 164
Figure C- 9 Data Set #2: Residual vs. Predicted Values 164
Figure C- 10 Data Set #2 Sensitivity Analysis 165

Figure C- 11 Data Set #3 Residuals 167
Figure C- 12 Data Set #3: Predicted vs. Actual Values 167
Figure C- 13 Data Set #3: Predicted vs. Actual Values 168
Figure C- 14 Data Set #3: Residual vs. Predicted Values 168
Figure C- 15 Data Set #3 Sensitivity Analysis 169
Figure C- 16 Data Set #3 Residuals 171
Figure C- 17 Data Set #4: Predicted vs. Actual Values 171
Figure C- 18 Data Set #4: Residual vs. Actual Values 172
Figure C- 19 Data Set #3: Residual vs. Predicted Values 172
Figure C- 20 Data Set #4 Sensitivity Analysis 173

LIST OF SYMBOLS

γ = Ratio of specific heats, c_p/c_v.

η = Efficiency.

η_v = Volumetric efficiency. Defined as the ratio of the mass of air into the engine (or cylinder) to the product of intake air density and displacement volume. Algebraically stated:

$$\eta_a = {}^{m_a}/_{\rho_a V_d}$$

λ = Relative air/fuel ratio – the actual air to fuel ratio divided by the stoichiometric air to fuel ratio. Values less than 1.0 indicate fuel rich mixtures, values greater than 1.0 indicate fuel lean mixtures. The inverse of equivalence ratio (ϕ). Algebraically stated:

$$\lambda = \phi^{-1} = \frac{({}^{A}/_{F})_{actual}}{({}^{A}/_{F})_{stoichiometric}}$$

ϕ = Equivalence ratio – the stoichiometric air to fuel ratio divided by the actual air to fuel ratio. Values less than 1.0 indicate fuel lean mixtures, values greater than 1.0 indicate fuel rich mixtures. The inverse of relative air/fuel ratio (λ). Algebraically stated:

$$\phi = \lambda^{-1} = \frac{({}^{A}/_{F})_{stoichiometric}}{({}^{A}/_{F})_{actual}}$$

θ = Crank angle; given in degrees of crank rotation, 0° to 360°, beginning at the crank position associated with the piston location at top dead center (0°) to bottom dead center (180°) and back to top dead center (360°).

Ψ = Phase angle.

ω = Frequency.

LIST OF ACRONYMS

AVL	=	Anstalt für Verbennungskraftmaschinen, Prof. Dr. Hans List (Institute for Internal Combustion Engines founded by Dr. Hans List) Graz, Austria.
AVL "Methane"	=	Computer program developed at AVL to predict the methane number of a given gaseous fuel blend.
AVL MN	=	Methane Number predicted from the AVL software "Methane".
BDC	=	Bottom Dead Center; the point at which the piston has travelled to its full extent outward from the cylinder and corresponds to maximum cylinder volume (V_{max}) and 180° crank angle.
CFR	=	Cooperative Fuel Research; designation of the Waukesha engine designed and built for fuels testing.
CHP	=	Combined Heat and Power.
MBT	=	Maximum Brake Torque; the point of ignition timing where compression stroke work transfer from the piston is just offset by expansion stroke work transfer to the piston. [°bTDC].
mep	=	mean effective pressure; a relative engine performance measure equal to the work produced each engine cycle divided by the displacement volume. [kPa or bar].
NA	=	Naturally Aspirated; engine intake pressure is not boosted. In this project naturally aspirated conditions correspond to absolute pressure of 1 atmosphere (sea level conditions) at the intake.
bmep	=	brake mean effective pressure; engine brake work divided by displacement volume [kPa or bar].
fmep	=	friction mean effective pressure; engine lost work (due to friction) divided by displacement volume [kPa or bar].
KI	=	Knock Integral.
KOCA	=	Knock onset crank angle.
nmep	=	net mean effective pressure; engine net work divided by displacement volume, the sum of bmep and fmep [kPa or bar].

TDC = Top Dead Center; the point at which the piston has travelled to its full extent inward to the cylinder and serves as the reference for minimum cylinder volume (clearance volume or V_c) and 0° crank angle.

°bTDC = Crank angle, measured in degrees before Top Dead Center.

°aTDC = Crank angle, measured in degrees after Top Dead Center.

ICE = Internal Combustion Engine.

PCI = Peripheral Component Interconnect or Peripheral Controller Interface. A computer bus for attaching hardware devices in a computer.

SI = Spark Ignited.

SLM = Standard liters per minute; a mass flow measurement for a gas referenced to the density of the gas at a standard reference temperature and pressure. Reference pressure is generally defined as 1.0 atmospheres or 100 kPa. Reference temperature varies substantially depending on the referencing source. Materials encountered in the course of this work have included reference temperatures of 0° C, 25°C, and 60°F.

TEL = Tetraethyl Lead. Chemical formula $Pb(C_2H_5)_4$. A colorless, poisonous, oily liquid, used in gasoline blends for internal-combustion engines as an antiknock agent. TEL was phased out in the United States in the early 1970's due to documented public health impact and deleterious effect on catalytic converters. (Considine, 1977) It is still used for refinery octane number testing and for aviation gasoline blends.

V_c = Clearance Volume. The volume in the cylinder when the piston is at top dead center.

V_{disp} = Displacement Volume. The volume of the cylinder through which the piston travels from top dead center to bottom dead center. Equal to the difference between minimum and maximum cylinder volume.
e.g. $V_{disp} = V_{max} - V_{min}$

V_{max} = Maximum cylinder volume. The volume of the cylinder when the piston is at bottom dead center.

V_{min} = Minimum cylinder volume. Equivalent to clearance volume, the volume in the cylinder when the piston is at top dead center.

KLSA = Knock limited spark advance.

1 INTRODUCTION AND GENERAL BACKGROUND

Spark ignited engines designed to consume natural gas as a fuel are widely used in commercial power generation, other stationary applications, and increasingly in over-the-road applications such as commercial trucks and buses. The design and production of such engines represent a substantial market world-wide. These engines typically operate under lean-burn conditions achieving higher overall fuel efficiency and cleaner emissions when compared to engines of similar size burning gasoline as a fuel. It is desirable that these engines be able to operate effectively to burn alternative or renewable gaseous fuel, such as producer gas, with little or no modification from natural gas operation.

The term producer gas refers to a mixture of hydrogen (H_2), carbon monoxide (CO), carbon dioxide (CO_2), nitrogen (N_2) and methane (CH_4) or other trace hydrocarbons. It is produced through gasification of organic materials, such as biomass, at relatively low temperatures, typically between 700°C and 1000°C, and is widely desired to be used directly as a fuel gas. It is noted that the term synthesis gas, also commonly referred to as syngas, applies to gas blends generally limited to a combination of hydrogen and carbon monoxide that are suitable for use as an intermediate in the synthesis of synthetic natural gas (SNG) and synthetic petroleum (Sadaka, 2011). While the terms producer gas and syngas are frequently used interchangeably, the gas blends for this work will be referred to as producer gas.

The ability to use producer gas as a fuel for internal combustion engine (ICE) applications requires a full understanding of the fuel properties of the gases and the ability of engine designers to make modifications to engine designs that accommodate those properties. As a general statement producer gases have lower energy content than natural gas and will produce less power per unit mass of fuel. Lower power production of an engine based on fuel

energy content is readily understood and can be compensated for, however, the fuel trait that can limit the usability of producer gas blends is resistance to engine knock. Engine knock, an abnormal combustion phenomenon experienced in spark ignited engines, will readily damage an engine and fuels that tend to knock under set engine operating conditions cannot be used successfully in that application. The characterization of a given fuel blend's tendency to knock will indicate whether or not the fuel is suitable for use in a given spark ignited (SI) engine application.

Producer gas use in SI engines must then be the result of integrating the properties of the fuel and the operating parameters of the engine. The ideal situation is to use producer gas blends directly from a gasification plant in an established engine. However, if a producer gas blend is unsuitable for use, it can be modified by adding favorable constituents to the blend thereby resulting in fuel property changes. Also, some engine performance parameters may be adjusted to accommodate the knock tendencies of a fuel gas blend. Producer gases can be blended with natural gas, for example, in cases where knock tendencies are very high. Examples of engine parameters that are available to the engine designer for adjustment or change include compression ratio, ignition timing, intake boost pressure, intake temperature, exhaust backpressure, spark plug placement, valve configuration, and combustion chamber geometry. With the assumption that fixed engine parameters are more restrictive to change than are the constituent composition of the fuel gas, the focus of this research is to understand the knock tendencies of various producer gas blends and quantify constituent make-up suitable for use in lean-burn natural gas engines.

1.1 ENGINE KNOCK

A reciprocating, spark ignition, piston-cylinder engine will compress a mixture of fuel and air as the piston travels inward toward the cylinder head with both the intake and exhaust valves shut. At a set point of crank rotation and piston travel, determined by ignition timing, and prior to reaching top dead center (TDC), a spark will be initiated igniting the fuel-air mixture and causing a rapid increase in cylinder pressure and temperature. After the piston has achieved TDC the high temperature, high pressure products of combustion force the travel of the piston outward and away from the cylinder head producing power in the process. During normal combustion the flame formed at the spark source travels away from the source and across the combustion chamber causing rapid temperature increase which causes rapid pressure increase. The unburned gas in front of the flame experiences rapid temperature and pressure increase which can cause self-ignition of the end gas and knock to occur. The following is a commonly referenced definition of engine knock:

"*Knock* is the name given to the noise which is transmitted through the engine structure when essentially spontaneous ignition of a portion of the end-gas – the fuel, air, residual gas, mixture ahead of the propagating flame – occurs." (Heywood, 1988)

Figure 1-1 provides an illustration and graphical depiction of knock resulting from fuel-air end gas auto-ignition in a typical SI engine cylinder.

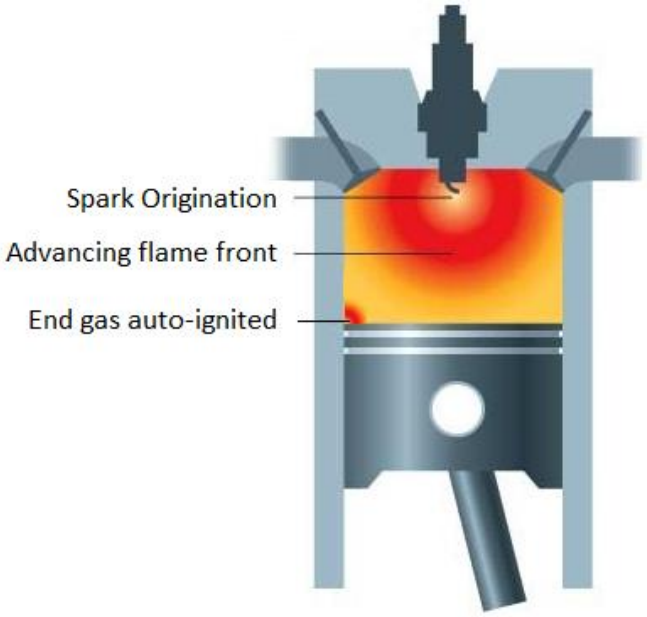

Figure 1-1 Auto-Ignition of End Gas in a Combustion Chamber.

Abnormal combustion events in SI engines are described as occurring in two forms, auto-ignition and surface ignition. Auto-ignition occurs when the air-fuel mixture in the end gas of the combustion chamber is compressed and heated sufficiently to ignite spontaneously. The separate ignition in the end gas region will cause dramatic fluctuation of pressure and temperature in the combustion chamber and in turn cause accelerated mechanical wear to bearings, piston rings, valves, and valve seats as well as pitting and erosion of the surfaces of the piston and cylinder walls. Prolonged operation under conditions of heavy knock can result in severe engine damage. Knock that occurs in a recurrent and repeatable manner can be controlled by ignition timing, retarding the timing of the spark event relative to crank angle will reduce the intensity of the knock. Figure 1-2 shows a depiction of typical plots of recorded cylinder pressure as a function of time for the cases of (a) normal combustion, (b) light knock, and (c) heavy knock.

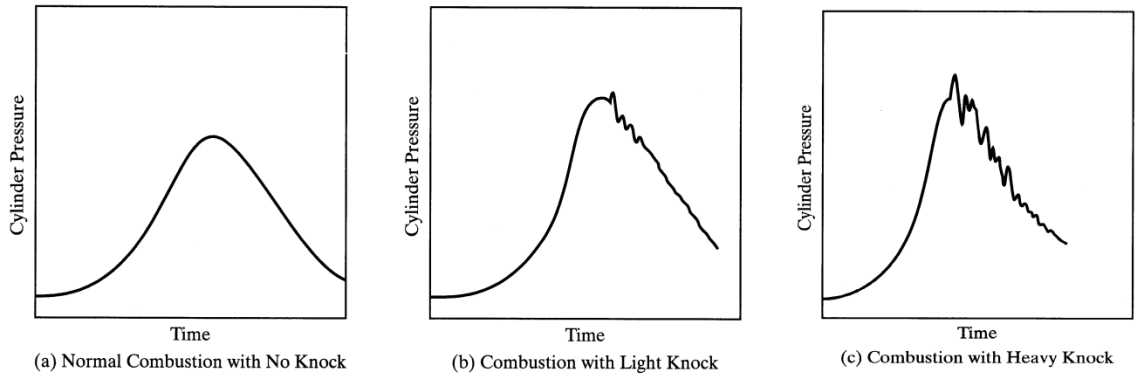

Figure 1-2 Cylinder Pressure vs. Time in a Typical SI Engine Application. (Pulkrabek, 2004)

Hot spots in the combustion chamber due to residue deposits, overheated valves or spark plugs can cause ignition of the air-fuel mixture before (pre-ignition) or after (post-ignition) the normal spark plug firing. Pre-ignition is the most problematic and can result in knock, but even surface post-ignition can compromise the performance of the engine due to loss of positive control of the combustion process. Note that knock from surface ignition will not be reduced in intensity by changing spark timing. Figure 1-3 offers a description of abnormal combustion events in an SI engine and serves to illustrate how these events can compromise the performance and reliability of the engine.

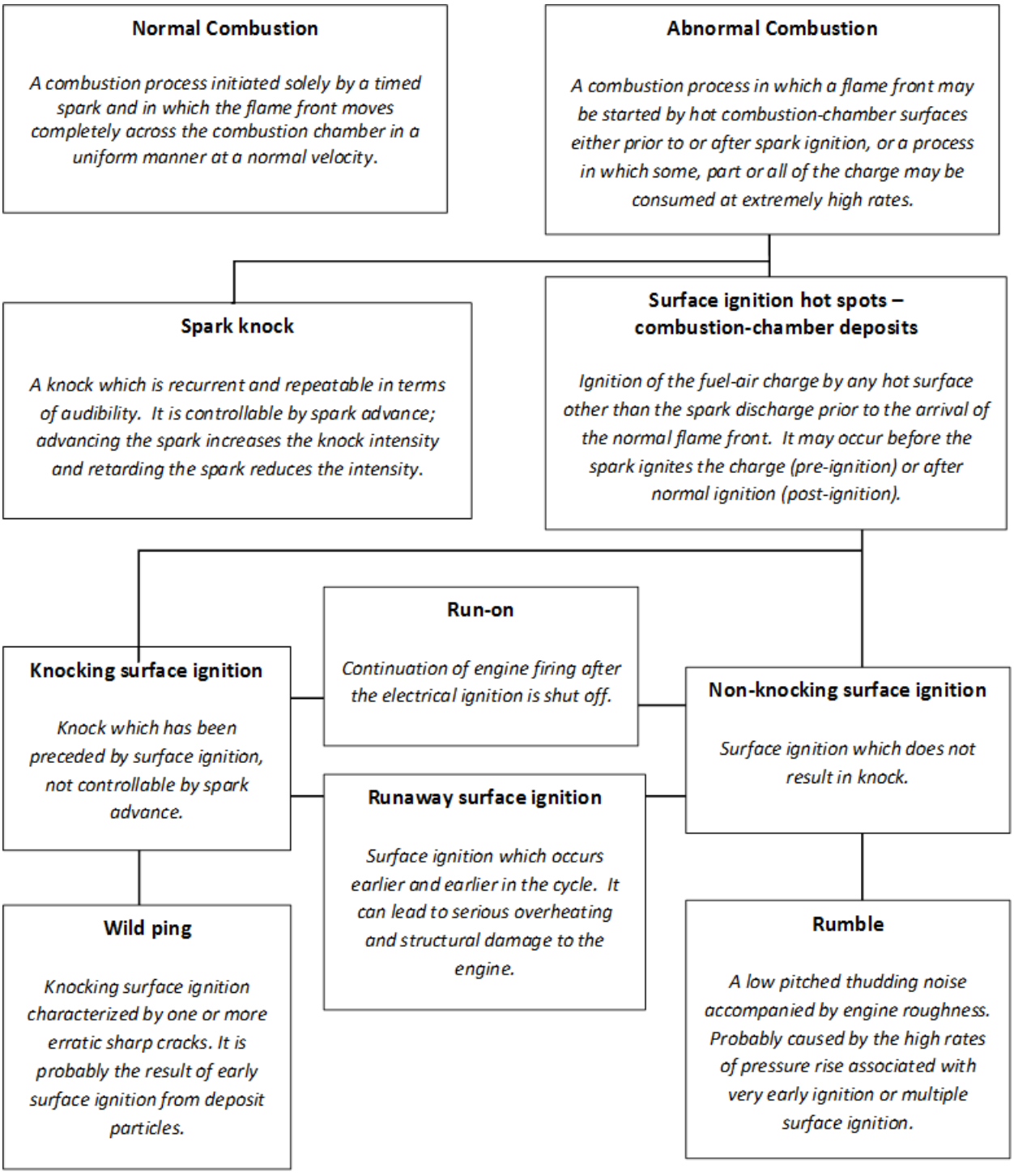

Figure 1-3 Definition of Combustion Phenomena in Spark-Ignition Engines. Adapted from Heywood (Heywood, 1988).

1.2 FUEL KNOCK RATINGS

The tendency for fuels to knock in SI engines is quantified by means of a comparative scale with reference fuels. The first of the fuel knock ratings were established to assign a rating of a fuel's tendency to knock to gasoline. Gasoline blends are a combination of many different hydrocarbon compounds that include paraffins (alkanes), napthenes (cyclanes), olefins (alkenes), and aromatics. The resistance to knock exhibited by any gasoline blend is quantified in terms of octane number, which is a value determined by direct comparison of the knock tendencies of the tested fuel blend to a two-constituent blend of isooctane (C_8H_{18}: 2,2,4-trimethylpentane) and normal heptane (n-C_7H_{16}). The percentage of isooctane is varied until the observed knock behavior matches that of the gasoline blend under test. The percentage of isooctane in the reference blend is stated as the octane number. That is, isooctane alone has an octane number of 100, normal heptane alone has an octane number of 0, an 80% to 20% blend of isooctane and normal heptane has an octane number of 80. Isooctane and n-heptane were chosen to serve as a reference blend because of wide differences in their resistance to knock, the commercial availability of n-heptane in high purity, and the fact that isooctane had a higher resistance to knock than any gasoline blends available at the time (Heywood, 1988). Subsequent to the development of the original test method and after discovery of fuel blends with higher resistance to knock than isooctane, the method was modified to add tetraethyl lead (TEL) to isooctane and define the resultant octane number as 100 plus the percentage TEL added.

The American Society for Testing and Materials (ASTM) have established specific test methods for determination of octane number. Two methods defined by the testing codes ASTM D-2699 and ASTM D-2700 are the research octane method and motor octane method, respectively. These tests differ somewhat in terms of specified inlet temperature, engine speed

and ignition timing. The standard test platform for octane testing is a single cylinder, 4-stroke engine known as the CFR engine as it was developed under direct oversight of the Cooperative Fuel Research Committee in 1928 (Waukesha Engine Division, Dresser Industries, 1980).

The methane number, a resistance to knock quantification methodology for gaseous fuels, was introduced in 1972 by Dr. Max Leiker and associates. The methane number rating method was the result of work carried out between 1964 and 1969 at the Institute for Internal Combustion Engines (Anstalt für Verbennungskraftmaschinen) or AVL, in Graz, Austria. As octane number uses a mixture of isooctane and n-heptane as the reference fuel, the reference fuel for methane number method is a mixture of methane (CH_4) and hydrogen (H_2). The method is analogous to octane number in that knock characteristics for a test fuel matched by 100% methane is deemed to have a methane number of 100, 100% hydrogen has a methane number of 0, and a mixture of 80% methane to 20% hydrogen has a methane number of 80. Methane and hydrogen were chosen as reference fuel constituents since methane has the highest resistance to knock of any gaseous hydrocarbon and is the principal constituent in natural gas whereas hydrogen is a principal constituent of town gas and refinery gases, "…notorious for their knocking tendency" (Leiker, et al., 1972). As with the octane number, a measuring method was developed to assign methane numbers greater than 100 with the addition of carbon dioxide (CO_2) to the pure methane, defining the methane number as 100 plus the percentage of carbon dioxide added to the blend.

1.3 Problem Statement and Research Objectives

The problems for which solutions are pursued in this research effort are stated separately as follows:

(1) Producer gas used to power industrial, lean burn natural gas engines varies significantly in formulation and performance as a fuel. The ability to characterize producer gas blends in terms of resistance to knock is essential to establish predictive metrics for engine configuration and operation.

(2) The determination of a given fuel's resistance to knock has been a largely subjective process comparing an unknown fuel blend to a known reference fuel blend (methane and hydrogen for gaseous fuels) relative to the onset of knock. A quantitative and readily repeatable metric for objective measurement of knock onset is desired.

(3) Standard testing protocol for methane number measurement uses CFR engines that are characterized as having relatively low values of mean effective pressure (mep), are naturally aspirated, and are operated under stoichiometric conditions. The typical natural gas engine operates at higher mean effective pressure (mep), is turbocharged or supercharged to elevate intake pressure, and is operated under lean air-fuel ratios. It is unknown if these operating conditions substantially impact measured methane number and, if so, render methane numbers misleading as a predictive indicator of knock tendency in natural gas engines.

Given the problem statements above, the research objectives for this work are to seek:

(1) development of metrics to be used as predictive indicators of how varying producer gas blends will perform when used to fuel lean burning natural gas engines.

(2) quantification of knock onset by analysis of cylinder pressure data to determine if reliable and repeatable methods of knock quantification can be developed to more accurately and consistently measure a given gaseous fuel blend's resistance to knock.

(3) determination of impact that engine operating parameters have on measured methane number and to demonstrate the differences in measured methane number under these varied operating conditions.

2 LITERATURE REVIEW

The literature reviewed in support of this project and detailed herein address three general subject areas:

(1) Metrics to rate resistance to knock of gaseous fuels used in internal combustion engines.

(2) The quantification of knock in spark ignited engines.

(3) The characterization and evaluation of producer gas as a fuel in internal combustion engines.

The following sections provide a synthesis of the literature review conducted and presented. A synopsis of the work and methodology employed are provided for publications cited relative to the conduct of this study.

2.1 METRICS TO RATE RESISTANCE TO KNOCK FOR GASEOUS FUELS

The establishment of gasoline octane rating systems provided the model for defining resistance to knock ratings for gaseous fuels. The most common is methane number, although the literature does reveal a number of studies insisting on the applicability of octane number as the suitable standard for knock resistance measurement, even for gaseous fuels.

(Leiker, et al., 1972) As previously mentioned, in 1972 Dr. Max Leiker and associates published a paper through the American Society of Mechanical Engineers documenting their work defining methane number, a metric to quantify the anti-knock characteristics of gaseous fuels. As a basis for the study, it was recognized that the highest octane number that can be measured directly is 120.34 which corresponds to the octane number of a mixture of 6 ml

tetraethyl lead (TEL) per U.S. gallon isooctane. TEL was used to suppress the onset of knock in gasoline until the 1970's when environmental concerns forced the cessation of the practice. Octane numbers greater than 120 were derived by extrapolation and not direct measurement. Natural gas blends containing high percentages of methane were observed to exceed knock resistance corresponding to an octane number of 120 therefore, as postulated by Dr. Leiker, gas engine designers could not rely on fuel knock ratings defined with liquid fuels. To establish a knock resistance metric for gaseous fuels, Leiker chose pure methane to serve as the reference standard for highest knock resistance and hydrogen, due to its well-known tendency to induce knock, to serve as the counter constituent to methane in a manner completely analogous to the octane number system established for gasoline blends using isooctane and n-heptane.

(Callahan, et al., 1996) (Kubesh, et al., 1992) Other studies contend that the methane number method is unreliable with gas blends containing even small amounts of heavier hydrocarbons such as butane (C_4H_{10}), pentane (C_5H_{12}), and hexane/heptane (C_6H_{14}/C_7H_{16}). The assertion is that methane numbers do not track linearly with increased levels of heavier hydrocarbons, therefore octane number is the better fuel knock resistance rating method. Even though high percentage methane blends require an extrapolated octane number (>120), for most common pipe-line natural gas blends enough heavier hydrocarbons are present to have octane numbers in the range of 90 to 95.

No similar studies were encountered in the literature relative to producer gas blends with correlated methane number impact due to high or low percentages of hydrogen (H_2), carbon monoxide (CO), nitrogen (N_2), or carbon dioxide (CO_2).

The need to quantify the intensity of knock and determine the exact point of knock onset has long been the subject of study. Earlier studies explore combustion pressure data, later studies

establish the advantage of identifying the rate of change of combustion chamber pressure as a function of crank position, and more current publications emphasize pressure data reduction and applied statistical methods.

(Barton, et al., 1970) A number of studies appear in the literature relative to assigning a quantitative index to knock events in spark ignited engines. The method commonly invoked is to establish a knock intensity metric based on the rate of pressure change in the combustion chamber. In earlier work several studies sought to classify knock by the resulting noise and mechanical vibration imparted on the engine. Accelerometers, being both inexpensive and fairly robust, are commonly used to construct relatively simple knock detection systems in a variety of engine applications. (Brecq, et al., 2003) However, in a study performed at Pennsylvania State University, published in 1970, Barton, et al. present a metric chosen such that it is tied to the combustion event rather than the resulting impact manifested in the engine. Due to wide variation in mounting and acoustical properties in different engine designs, mechanical reaction can mask the characteristics of a knock event and would not be easily translated to different engines. The approach chosen was to instead concentrate on a frequency domain representation of combustion chamber pressure through the compression and power strokes using a Fourier Series. For a Fourier Series, representation of cylinder pressure in a spark ignited engine the n^{th} harmonic can be described with a single trigonometric expression incorporating phase angle by the expression:

$$P = P_o \sin(\omega t + \psi)$$

and it follows that

$$\frac{dP}{dt} = P_o \omega \cos(\omega t + \psi)$$

where:

ω = frequency of the n^{th} harmonic

P_o = maximum amplitude

ψ = phase angle

The maximum value for the rate of change of pressure (dP/dt) occurs when

$$\cos(\omega t + \psi) = 1$$

Equation 2-1

So, the ratio of maximum value of *dP/dt* to P is given by

$$\left({}^{dP}/_{dt}\right)_{max} \Big/ {}_{P_{max}} = \omega$$

Equation 2-2

The relationship given by equation 2-2 implies that for any frequency greater than 1 radian/second, the amplitude of (*dP/dt*) will be greater than P. To confirm the decision to rely on rate of pressure change rather than direct combustion pressure measurement two ratios were defined. The ratio of pressure magnitude at the knocking frequency to the magnitude occurring at engine speed is given by

$$\frac{P(\omega_{knock})}{P(\omega_{engine})} = \eta_1$$

Equation 2-3

The ratio of the magnitude at the mechanical vibration frequency to the magnitude at the knock frequency is given by

$$\frac{P(\omega_{mechanical})}{P(\omega_{knock})} = \eta_2$$

Equation 2-4

The frequencies of interest for the CFR engine used in that particular study were determined to be as follows:

Engine speed = 600 rpm = 10 Hz

Knock vibration = 6,000 Hz

Engine vibration = 50,000 Hz

From Equation (2-1) it follows that

$$\frac{dP}{dt}(6000\ Hz) \Big/ \frac{dP}{dt}(10\ Hz) = 600\eta_1$$

and

$$\frac{dP}{dt}(50000\ Hz) \Big/ \frac{dP}{dt}(6000\ Hz) = 8.3\eta_2$$

This analysis establishes that the rate of pressure change amplifies the pressure ratio, η_1, which increases sensitivity. Unfortunately, the rate of pressure change also increases sensitivity

due to mechanical vibration by amplifying the pressure ratio, η_2, although to a much lesser extent. The authors conclude that knock intensity, when defined with respect to rate of pressure change in the combustion chamber, provides a repeatable means to quantify knock. The authors do not address applicability of the measurement method considering the random nature of knock observed in the course of this work in terms of widely varying intensity of individual pre-ignition events or the frequency of recurrence of such events.

(Brunt, et al., 1998) The authors base a knock intensity metric on a "peak knock pressure" which they define as the maximum positive value of the high frequency pressure component. Digital filtering was employed for pressure transducer signals due to concerns over transducer and combustion chamber natural frequency vibration modes and also to account for higher frequency signals tending to be mistaken for low frequency signals as a result of aliasing. A knock intensity metric was calculated based on the summation of individual cycle peak corrected knock pressures. The authors conclude that large variability exists in peak knock pressure data and the resulting knock intensity calculation requires large sample windows (at least 1000 cycles). The final conclusive remark in the paper is: "Knock pressure and knock intensity results are sensitive to all measurement and analysis parameters and a definitive quantitative measure of knock pressure and knock intensity is not possible."

(Brecq, et al., 2003) The authors describe a methodology to enable ignition timing control to maintain what they term "knock margin", the difference between a given spark advance and that corresponding to knock onset. Combustion pressure analysis was accomplished by defining two primary indices based on high frequency analysis of combustion chamber pressure data. The first index, termed the Integral of Modulus of Pressure Oscillations (IMPO) is intended to represent total energy contained in the high frequency oscillations of cylinder pressure occurring

due to knock. The second index is maximum amplitude of pressure oscillations (MAPO). IMPO and MAPO are expressed as

$$IMPO = \frac{1}{N}\sum_{1}^{N}\int_{ST}^{ST+W}|\tilde{p}|d\theta$$

Equation 2-5

and

$$MAPO = \frac{1}{N}\sum_{1}^{N}\max_{ST,ST+W}|\tilde{p}|$$

Equation 2-6

where

N = Number of computed cycles

ST = spark timing [crank angle degrees]

W = width of computational window [crank angle degrees]

$\tilde{p}$ = filtered pressure

Figure 2-1 provides a schematic representation of the determination of IMPO and MAPO indices. Computation of the IMPO and MAPO is performed with *"Indiwin"* software developed by AVL.

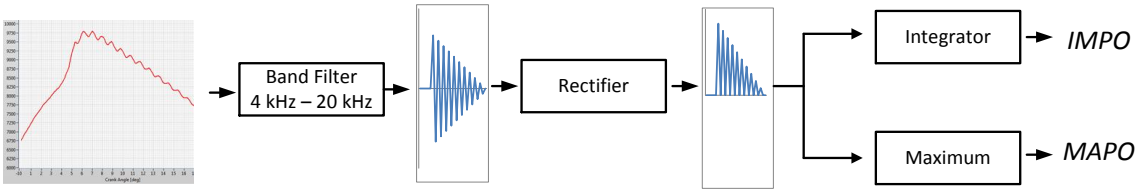

Figure 2-1 Schematic of knock indices determination
Adapted from (Brecq, et al., 2003)

The authors introduce a dimensionless knock indicator (DKI) based on the indices established above given by

$$DKI = \frac{IMPO}{MAPO \; x \; W}$$

Equation 2-7

The calculated values for the knock indices during a given knock event are plotted as shown in Figure 2-2. The start of auto-ignition is clearly evident and shown as a function of crank angle. Several authors have conducted studies using the IMPO and MAPO indices at different threshold levels with considerably mixed results. The consensus opinion appears to be that an appropriate threshold level determination will depend on the individual engine and operating conditions of equivalence ratio, volumetric efficiency, and ignition timing (Millo & Ferraro, 1998). However, Brecq, et al. offer that DKI will account for noise in the signal occurring prior to the start of auto-ignition and thus can be viewed as an image of knock intensity. The clear indication of the crank angle at which knock inception occurs defines the value of knock limited spark advance (KLSA) and allows knock margin, or KLSA overstep, to be defined for various operating conditions (volumetric efficiency, equivalence ratio, and spark advance) and fuels for specific engine configurations.

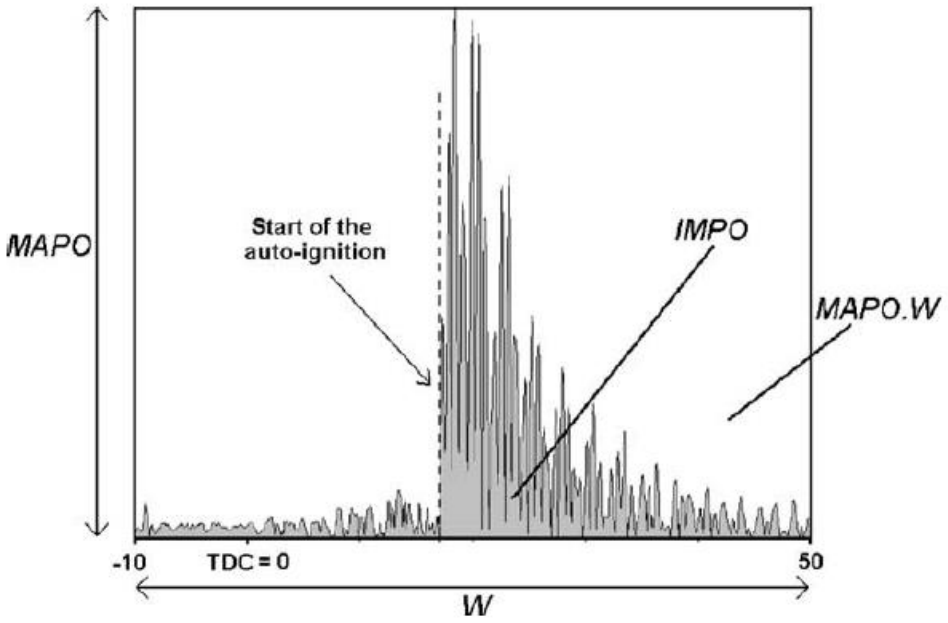

Figure 2-2 DKI Representationfor a Knocking Cycle

(Brecq, et al., 2003)

(Rahmouni, et al., 2004) In an extension of the work of Brecq, et al. and using the same knock onset metrics, Rahmouni et al. develop a methane number requirement (MNR) to correlate the impact of varying engine operating parameters (spark advance, equivalence ratio, and volumetric efficiency) to the fuel resistance to knock or what the authors term service methane number. The authors conclude that experimental results of measured methane number are highly consistent with those values predicted by the AVL software *"Methane"*. It is noted that the fuels tested were natural gas blends with representative percentages of constituent gases based on those commonly encountered in field applications.

(Coetzer, et al., 2006) The authors describe knock-point estimation for different liquid fuel blends of ethanol, iso-propanol, hexane, and toluene. Knock intensity for this study was determined to be related to fractional change in the pressure rise rate during a knock event. This general approach, using statistical curve fit methods, shows promise to characterize producer gas

blends under varied equivalence ratios from stoichiometric to lean conditions typical of industrial natural gas engine operation. The study offers a compelling description of the suitability of statistical methods to perform data reduction and estimate actual knock point and relative intensity, determined by the slope of the pressure curve, for a given knock event. However, the study does not offer a solution for overall knock index in terms of a metric to characterize knock level to facilitate direct and repeatable measurement of fuel performance when conducting methane number measurement.

(Soylu & Van Gerpen, 2003) The authors develop an autoignition model for an engine combustion chamber based on ignition delay, the time necessary to establish the radical species pool in the end gas favorable to autoignition. The ignition delay is modeled with a form of the Arrhenius equation to match experimental data as the actual chemical kinetics process is unknown. The knock onset crank angle (KOCA) then coincides with ignition delay associated with a fictitious species building up in the end gas. The authors conclude that, though simple, the autoignition sub model is accurate for predicting KOCA in engines for which extensive experimental data exists and can be coupled to analytical engine modeling tools without requiring extensive computational capabilities. Another study asserts that the approach by Soylu and Van Gerpen is inadequate specifically due to the ambiguity of the chemical kinetics process and variability of end gas temperature with engine speed. The authors contend that an empirical model they derived is able to predict KOCA to ± 2° which is sufficient to be used as an initial estimate for design of new engine concepts. (Elmqvist, et al., 2003)

2.1 Characterization of Producer Gas as a Fuel in IC Engines

The literature is generally limited with regard to studies that characterize producer gas performance in spark ignited engines. Two studies have been published documenting research work accomplished at the Technical University of Denmark specific to the Viking plant, a two-stage downdraft gasifier fueled with woodchips. In one paper the combined heat and power (CHP) capability of the Viking plant is described to include the constituent make-up of the evolved gas, emissions characteristics from the plant, and engine performance related to load and efficiency. (Ahrenfeldt, et al., 2005) A second study from the same institution provides a comparison between natural gas and producer gas from the Viking plant in terms of engine performance (load and efficiency) and emissions. (Ulfvik, et al., 2011) Neither study investigates anti-knock characteristics of the producer gas.

Related studies are found investigating the effect of varying natural gas blends on the knock limit of lean burn natural gas engines. For example, Soylu and Van Gerpen evaluated the increase in knock propensity with propane addition to natural gas in heavy-duty natural gas engines. (Soylu & Van Gerpen, 1998). References in the literature are limited regarding producer gas characterization. This work addresses that gap and provides experimental results of anti-knock performance observed with varying producer gas blends.

Arunachalum (Arunachalam, 2010), in her Master of Science thesis work at Colorado State University, did direct comparison of methane number for specific producer gas blends determined experimentally, predicted by use of the AVL software "*Methane*", and predicted through modeling in the chemical kinetics software, CHEMKIN. The resulting characterization of the gas blends was hampered somewhat due to the following factors:

1. High sensitivity to the chemical mechanism used in the CHEMKIN analysis and subsequent variation in predicted methane number.
2. Subjectivity of determining knock onset at the point of “light audible knock” to establish the knock reference point.
3. Limits to the performance of the gas blending system and repeatability of gas blend make-up.

This work seeks to address and mitigate the factors hampering gas blend characterization.

3 EXPERIMENTAL APPARATUS

This research project requires the availability of a test cell capable of conducting engine operations with virtually any producer gas fuel blend desired, with engine operational parameters that are controllable with regard to compression ratio, mean effective pressure (MEP), intake boost pressure, intake temperature, exhaust back-pressure, air-fuel ratio and ignition timing with instrumentation and controls capable of establishing stable engine operation and data recording to enable the analysis of the experiment results.

3.1 HARDWARE SET-UP

The engine test cell system requirements necessary to meet the project goals are summarized by the following:

- Ignition system permitting maximum brake torque (MBT) evaluation.
- Blending system capable of producing blends of desired constituent composition.
- Ability to increase brake mean effective pressure (bmep) to levels closer to typical lean burn natural gas engines by boosting intake.
- Ability to match exhaust pressure simulating demand from a turbocharger.

The engine test cell at the Colorado State University Engines & Energy Conversion Laboratory (EECL) is modified to provide the capability of meeting the projects goals described above. Engine operation can be performed with virtually any producer gas fuel blend desired, with engine operational parameters that are controllable with regard to compression ratio, mean effective pressure (mep), intake boost pressure, intake temperature, exhaust back-pressure, air-

fuel ratio and ignition timing with instrumentation and controls capable of establishing stable engine operation and data recording to enable the analysis of the experiment results.

The overall test cell design is depicted schematically in detail in Figure 3-1. A narrative description of the principal components and integration of those components to establish the test cell is provided in the sections that follow.

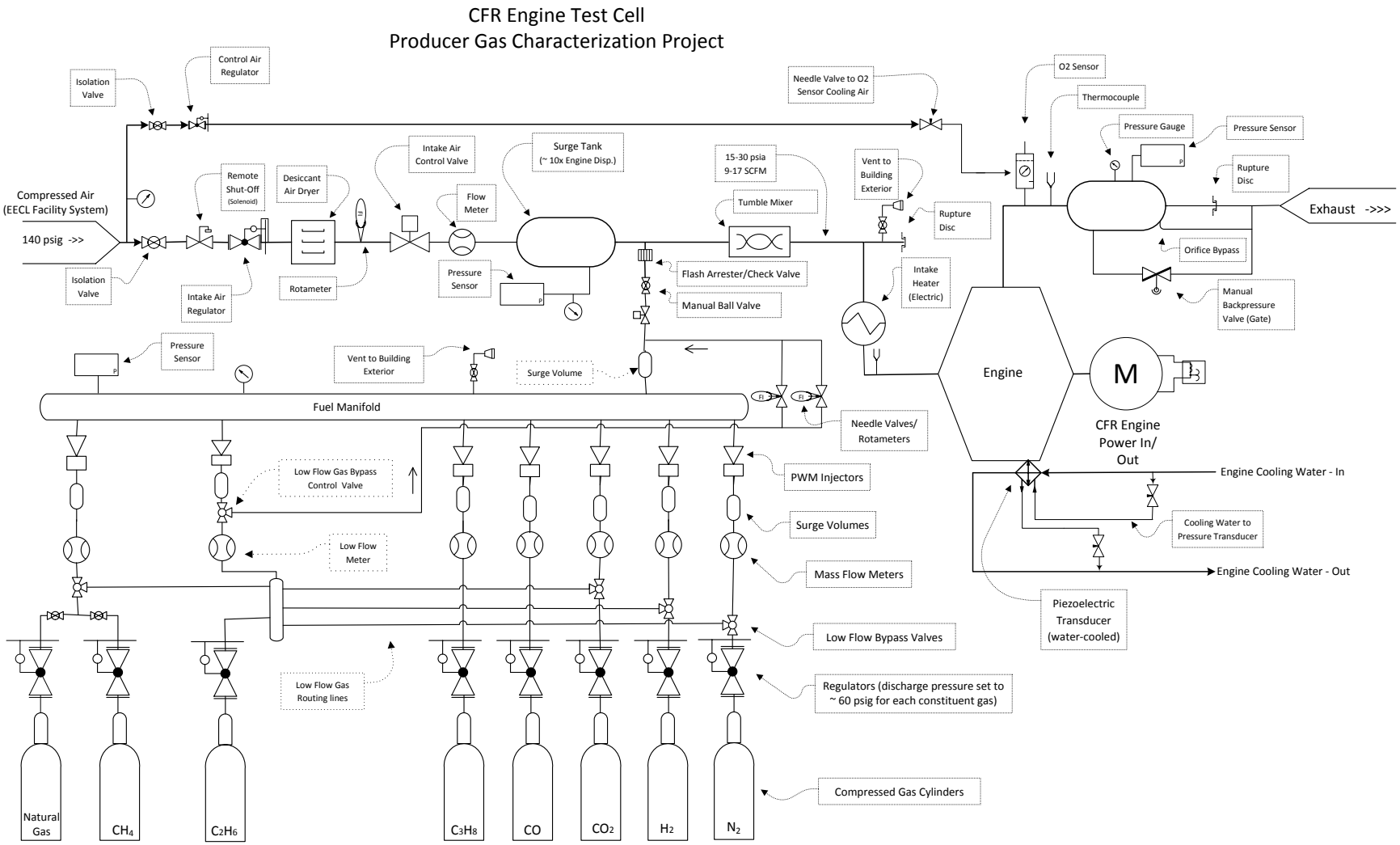

Figure 3-1 Schematic representation of the test cell constructed for this work.

3.2 ENGINE

The type of engine used in this project is a Cooperative Fuel Research (CFR) F-2 model manufactured by Waukesha Engine, Dresser Industries. It is a stationary, constant speed (~900 rpm), un-throttled, single cylinder, 4-stroke engine with a cylinder bore of 3.250 inches (8.255 cm) and piston stroke of 4.500 inches (11.43 cm). The displacement volume of the engine is 37.33 in^3 (611.7 cm^3). To enable operation at a range of compression ratios from 4:1 to 18:1 the engine is constructed with a can-type casting forming the cylinder and cylinder head as a single part. The exterior of the cylinder is configured with a jack-screw type threaded race allowing an engaged worm-gear to raise and lower the cylinder relative to the piston/connecting rod assembly, held laterally stable in a clamping sleeve. By raising or lowering the cylinder the clearance volume (that volume formed from the top of the piston at TDC, the cylinder wall and the cylinder head) is increased or decreased resulting in adjustment of compression ratio. The total vertical travel of the cylinder relative to the fixed position of the crankshaft is 1.235 inches which allows compression ratio adjustment. The engine is designed to allow adjustment of compression ratio while operating. Figure 3-2 provides a cut-away drawing of the engine cylinder and clamping sleeve sections. (Waukesha Engine Division, Dresser Industries, 2003)

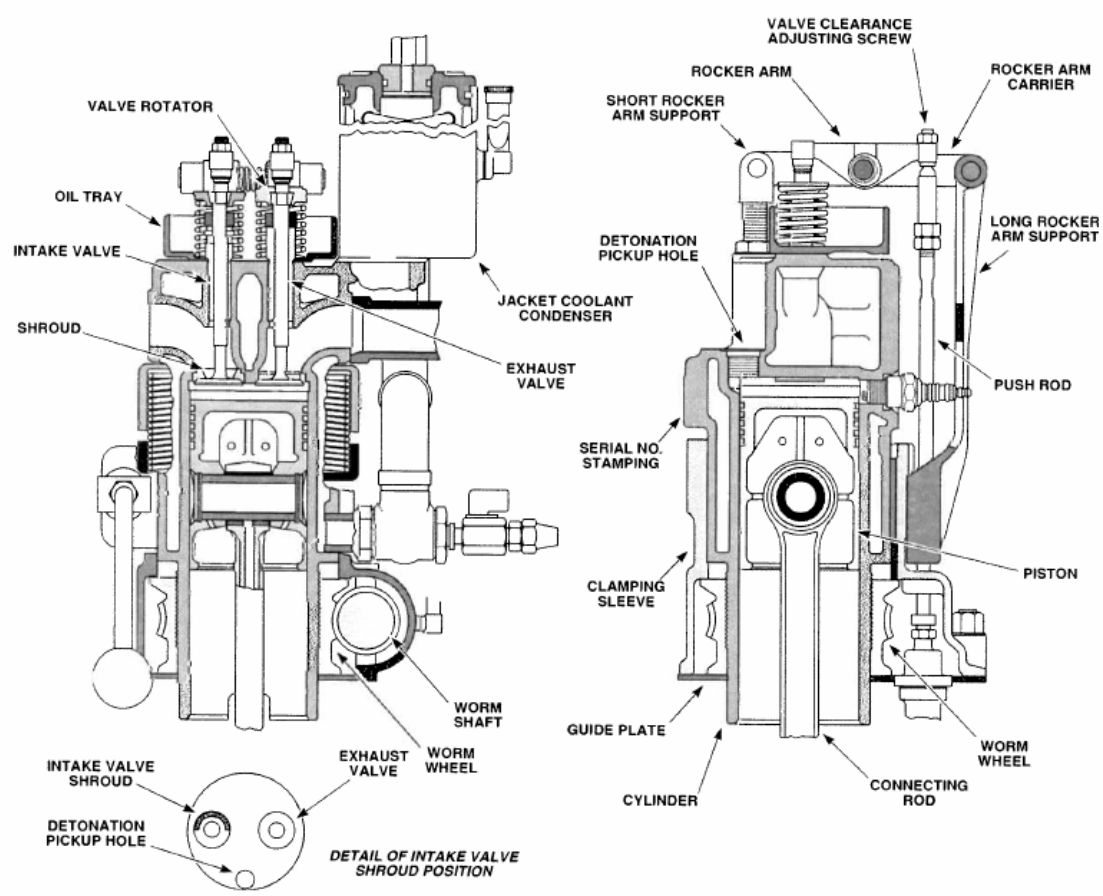

Figure 3-2 Cylinder and Clamping Sleeve Sections, Waukesha F-2 CFR.
From Waukesha CFR F-1 & F-2 Octane Rating Units Operations & Maintenance (Form 875), 2nd Ed. © 2003, Dresser, Inc.. Reprinted with permission from General Electric Company

The particular engine used in this project was manufactured in 1957 and is a model still manufactured and sold today, designed specifically for testing knock tendencies of fuels. Originally configured for octane number testing of gasoline blends, the engine is currently configured to burn gaseous fuels. The original CFR engine was designed in 1928 by the (then) Waukesha Motor Company at the request of the Co-operative Fuel Research (CFR) Committee to provide a standardized means to measure and define the combustion characteristics of gasoline blends. The engine was first displayed in January 1929 at the Society of Automotive Engineers annual meeting and served as the standard for fuel testing by both refiners and engine builders. The original design underwent slight modification but the mechanical configuration for the CFR

F-2 has remained essentially unchanged since 1952. (Waukesha Engine Division, Dresser Industries, 1980)

The engine is operated through a belt driven connection with a 5 horsepower synchronous motor. On start-up and while operating without producing power (motoring operation) the engine is rotated by the motor, when fueled and producing power the synchronous motor operates as a generator feeding power to the electrical grid (powered operation). Engine speed is limited by the set constant motor speed during motoring operation and corresponding electric grid frequency during powered operation.

3.3 KNOCK MEASUREMENT SYSTEM

As originally manufactured and configured the knock measurement system on the CFR engine consists of a power supply, detonation meter, detonation pickup, and knock meter. The pick-up sensor, mounted through the head of the cylinder, offers a thin flexible diaphragm cover which is exposed to the combustion chamber. As the diaphragm surface reacts to combustion chamber pressure variation the magnetic field varies around a magneto-restrictive alloy wound with a copper wire coil. The magnetic field variance induces a voltage in the coil which is directly proportional to the rate of change of cylinder pressure, and is output to the detonation meter. The detonation meter is an analog device that is able to isolate the relative knock amplitude through averaging and filtering the received signal which is then transmitted to the knockmeter. The knockmeter display reflects the relative intensity of the knock event to establish a comparative scale used as the basis for measuring the intensity of knock experienced in the engine. An analog strip chart recorder may also be attached to provide a permanent record of a

data set. Figure 3-3 shows a signal flow diagram for the original knock measurement system. Figure 3-4 provides a sectional view of the originally installed type D-1 detonation pickup.

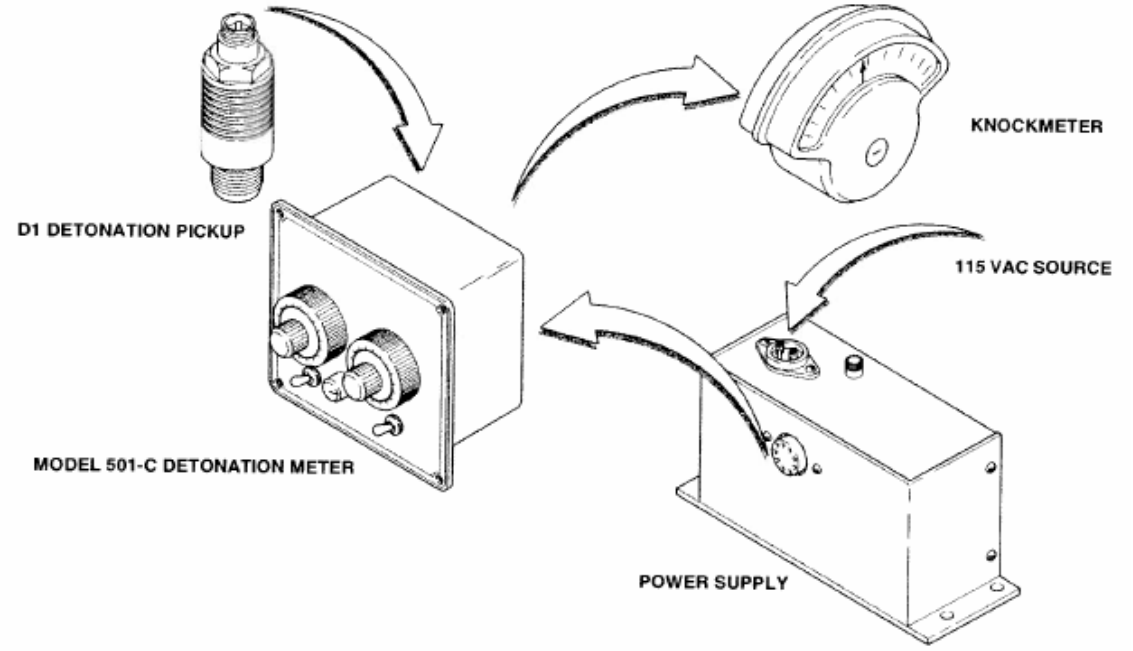

Figure 3-3 CFR Engine Knock Measurement System, Original.
From Waukesha CFR F-1 & F-2 Octane Rating Units Operations & Maintenance (Form 875), 2nd Ed. © 2003, Dresser, Inc.. Reprinted with permission from General Electric Company

The original knock measurement system requires that the operator determine the onset of knock audibly and then adjust the meter reading and spread dial settings (controlling resistive networks that adjust the sensitivity of the instrument), establish an operate/zero point, and then select a time constant (1 of 6 positions determining the integration interval). The process and instrumentation force a subjective measurement of knock intensity which is certainly acceptable for comparing tested fuels to reference blends to assign an octane number. For this project it is desired to establish an objective knock intensity measurement less prone to variability due to operator interpretation and sufficiently detailed to allow more refined analysis of the knocking phenomenon.

The modified knock measurement system begins with a water-cooled, piezoelectric transducer (Kistler model 6061A) mounted in the same cylinder detonation port previously housing the Type D-1 pickup. The signal from the transducer is fed to a charge amplifier which relays pressure signal input to the controlling software. A rotary 0.1° incremental optical engine encoder (BEI model L25) provides positive crank angle position indication enabling real-time display of cylinder pressures as a function of crank rotation. Due to high dynamic response and resolution (3600 discreet data points per engine revolution) detailed pressure history is available allowing direct analysis of the combustion event in the cylinder. Figure 3-5 provides a signal path depiction of the post-modification knock measurement system.

3.4 ENGINE INTAKE SYSTEM

The in-cylinder pressure versus volume trace for a typical operating cycle of the CFR engine is shown in Figure 3-6. This cycle consists of two complete revolutions of the crankshaft which constitutes four strokes of the piston. The upper loop, area A, is formed during the compression and power strokes; the lower loop, Area B, is formed during the exhaust and intake strokes as the

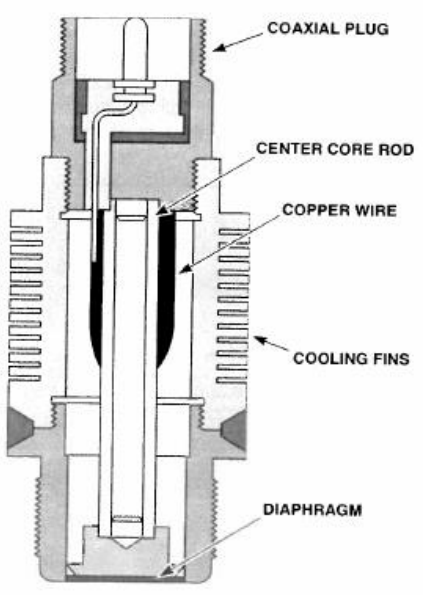

Figure 3-4 Sectional View Of The CFR Type D-1 Detonation Pick-Up.
From Waukesha CFR F-1 & F-2 Octane Rating Units Operations & Maintenance (Form 875), 2nd Ed. © 2003, Dresser, Inc..
Reprinted with permission from General Electric Company

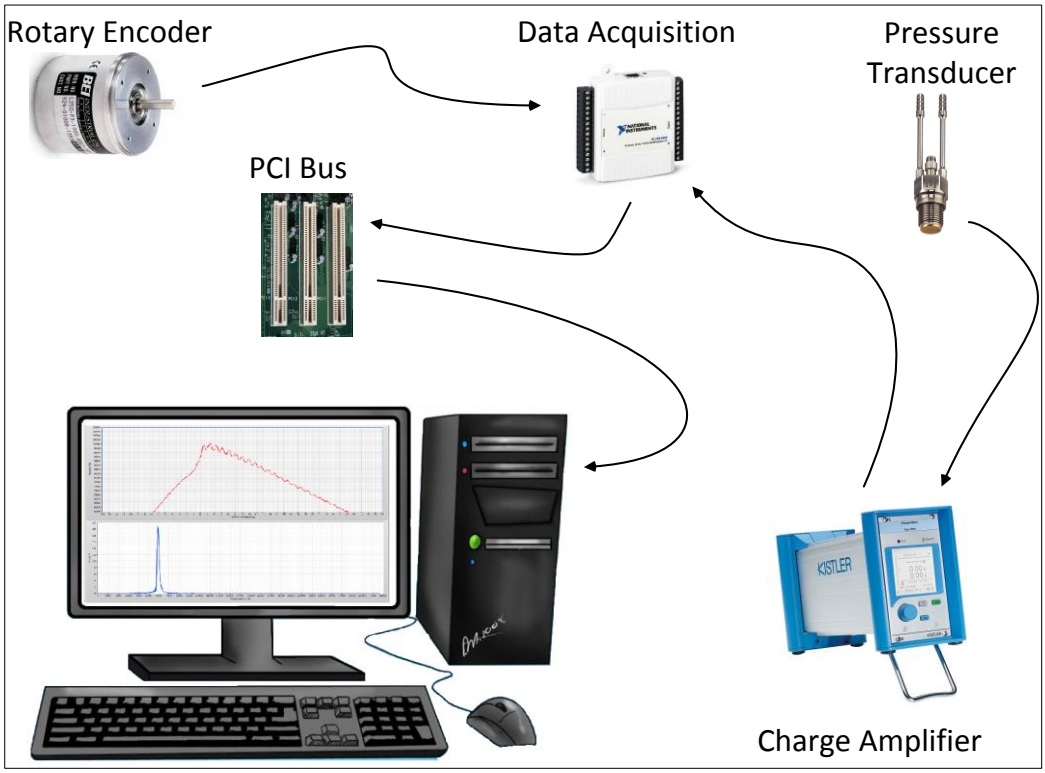

Figure 3-5 CFR Engine Knock Measurement System, Post-Modification.

engine is aspirated. Area A is indicated work, the work delivered by the crankshaft is brake work which is slightly less than indicated work and includes losses due to friction. Brake work is given by

$$w_b = w_i - w_f$$

Equation 3-1

Where

w_i = indicated specific work generated inside the cylinder
w_f = specific work lost due to friction

Area B formed during aspiration is called pump work. Net work is related to pump work as given by

$$w_{net} = w_b - w_p$$

Equation 3-2

Where

w_p = work performed by the engine during the exhaust and intake strokes

The parameter mean effective pressure (mep) is used to facilitate the comparison of different engines because it is independent of both engine size and rotating speed. The definition of mep is given by the relationship

$$w = (mep)\Delta v$$

Equation 3-3

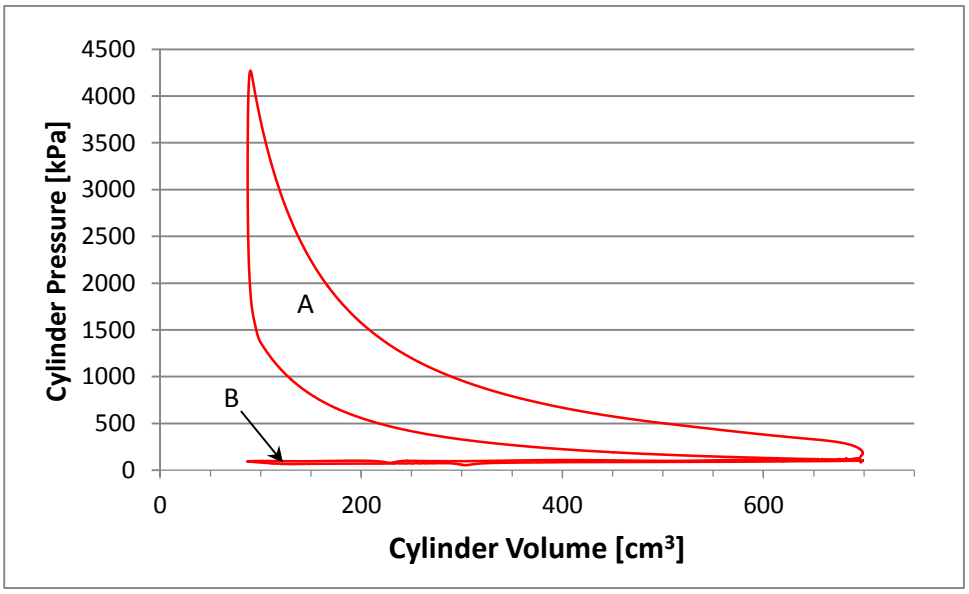

Figure 3-6 Pressure vs. Volume Diagram for the CFR Engine.

It follows that Equation 3-3 can be written as

$$mep = \frac{w}{\Delta v} = W/V_d$$

Equation 3-4

where

$$\Delta v = v_{BDC} - v_{TDC}$$

and

W = work of one cycle
w = specific work of one cycle
v = specific volume of the cylinder contents
v_{BDC} = specific volume of the cylinder contents at bottom dead center
v_{TDC} = specific volume of the cylinder contents at top dead center
V_d = displacement volume

The definition of mep is often further distinguished by incorporating indicated work, gross work, brake work, friction work, and net work. Detailed definition for these parameters vary slightly

(Heywood, 1988) (Pulkrabek, 2004). For the purposes of this study, the following subsets of mep are defined and utilized:

Brake mean effective pressure (bmep): Defined in terms of brake work, given by

$$bmep = \frac{w_b}{\Delta v} = W_b/V_d$$

Equation 3-5

Pump mean effective pressure (pmep): Defined in terms of the actual work available at the crankshaft lost to both pumping (aspiration) and friction losses, given by

$$pmep = \frac{w_p}{\Delta v} = W_p/V_d$$

Equation 3-6

Net mean effective pressure (nmep): Defined in terms of net work, given by

$$nmep = \frac{w_{net}}{\Delta v} = W_{net}/V_d$$

Equation 3-7

The CFR F-2 engine is originally configured to operate under naturally aspirated conditions. During normal operation, burning natural gas as a fuel, the net mean effective pressure (nmep) of the engine is approximately 7.5 bar. In order to operate at conditions more representative of commercial lean burn natural gas engines the desire is to elevate the nmep to as high as 14 bar; however, the amount of intake boost for this CFR engine is based on recommended pressure limits from the OEM.

The OEM responded to an information request and indicated that F-2 engines have been modified for boosted intake for aviation gasoline testing and operated successfully with intake pressure up to 90 psia (621 kPa). However, since the aviation gasoline test engines have been structurally modified to accommodate higher pressures the OEM recommends no more than 50 to 60 psia (345 to 414 kPa) intake boost for this particular engine. For this project, based on the recommended limit indicated by the OEM and operating pressures of ancillary components, an operating target of 400 kPa maximum intake pressure is selected. Operational history of this engine indicates that for naturally aspirated conditions an intake air flow of approximately 200 SLM is realized. Assuming ideal gas behavior for intake air, the increase in air flow will be directly proportional to pressure increase and a maximum boosted air flow of 800 SLM is desired. A product search for a blower or compressor operating at those pressures and flow rates revealed difficulties in procuring and adapting a suitable device available off-the-shelf. Alternatively, facility compressed air is available to the test cell. The intake air system is developed from that capability. Figures 3-7 and 3-8 provide photographs of the installed system in the test cell. Figure 3-9 shows a schematic depiction of the installed intake air system.

Figure 3-7 Engine Intake Air Piping from Facility Compressed Air System

Figure 3-8 Intake Air Piping to Include Rupture Disc and Solenoid Vent Valve

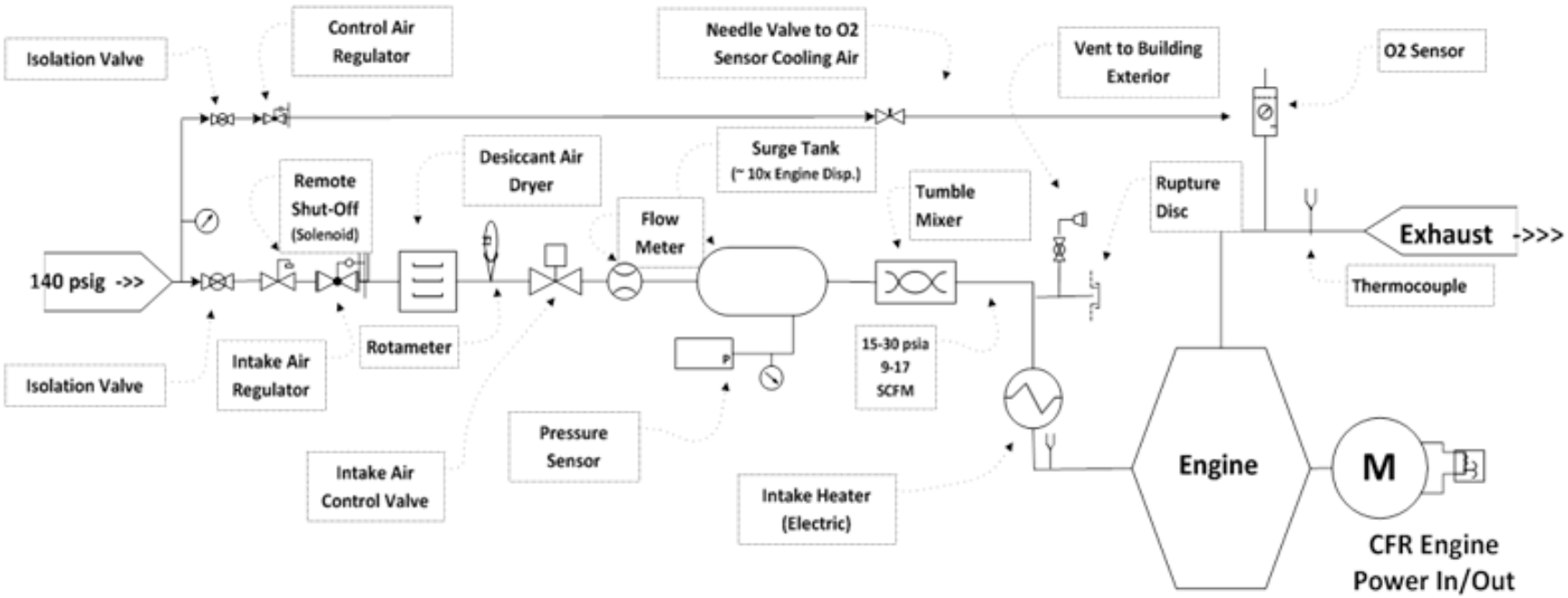

Figure 3-9 Schematic Depiction of the Test Cell Intake Air System**.**

The piping and selected components for the intake air system are sized to ensure adequate mass flow to the engine with minimal pressure drop, appropriately conditioned (clean and dry), under controlled and safe conditions. Features of the boosted intake air are described as follows:

3.4.1 Conditioning Combustion Air

As a function of predominant climate conditions in Fort Collins, Colorado the ambient air at the EECL is consistently at low relative humidity, typically less that 40%. The facility compressed air system contains in-line filters and desiccant air dryers to clean and condition the air prior to introduction to the system and/or storage in the system receiver. As an added precaution a separate filter and desiccant drier assembly is installed downstream of the test cell pressure regulator, as can be seen in Figure 3-7.

Additionally, the engine intake has an installed electrical resistance heater with power supplied by the control panel 110VAC bus and operation controlled by a manually operated rheostat. Intake heater operation is controlled by the LabVIEW© controller software cycling the heater on until the indicated minimum temperature is met.

3.4.2 Instrumentation

A rotameter is installed in the system providing the test cell operator a visual flow indication for combustion air. An in-line mass flow meter (heated tube or calorimetric type electronic mass flow meter, Model FMA 1700 Series, 0-500 SLM, from Omega Engineering, Inc.) is installed to provide direct measurement of combustion air mass flow to the engine used to control the air-

fuel mixture. A pressure transducer mounted in the buffer volume of the intake system provides the signal to the controlling program used to trigger positioning of the intake air admission valve.

3.4.3 Safety Isolation and Emergency Shutdown

The intake system can be isolated from the facility compressed air system by two valves in series. The first isolation valve is a hand operated ball type valve. The second is a normally shut solenoid operated diaphragm type valve.

In the event of interrupted power to the solenoid operated admission valve, whether through an inadvertent loss of power or intentional isolation of the system in the event of an emergency, the valve will fail shut isolating combustion air from the engine. Additionally, a normally open solenoid vent valve is installed in the proximity of the intake port venting to ambient air exterior to the building. As with the solenoid at the admission side, in the event of interrupted power to the solenoid the vent valve will position to its normal position (open) depressurizing the intake system.

3.4.4 Dampening, Fuel-Air Mixing and Precautions for Pre-Ignition

A buffer volume approximately ten times the displacement volume of the engine (10 liters) is installed to dampen pressure fluctuation upstream of the engine intake.

An in-line tumble mixer is installed immediately downstream of the fuel admission port to promote uniform distribution of the fuel gas in the combustion air stream.

A 2-inch diameter graphite rupture disc is installed near the engine intake to allow a rapid vent path in the event of pre-ignition detonation of the air-fuel mixture at the intake. The rupture disc is shown in Figure 3-8.

3.5 ENGINE EXHAUST SYSTEM

Figure 3-10 shows a schematic depiction of the engine exhaust system for the test cell. Modifying the engine exhaust system to perform suitably for this test cell requires a number of specific design considerations. The exhaust requires a buffer volume to dampen pressure fluctuations in the exhaust stream and sufficient, controllable, flow restriction is necessary to establish back pressure that mimics the parameters realized in a turbo charged engine. Figure 3-11 is a photograph of the installed connection piping and surge volume.

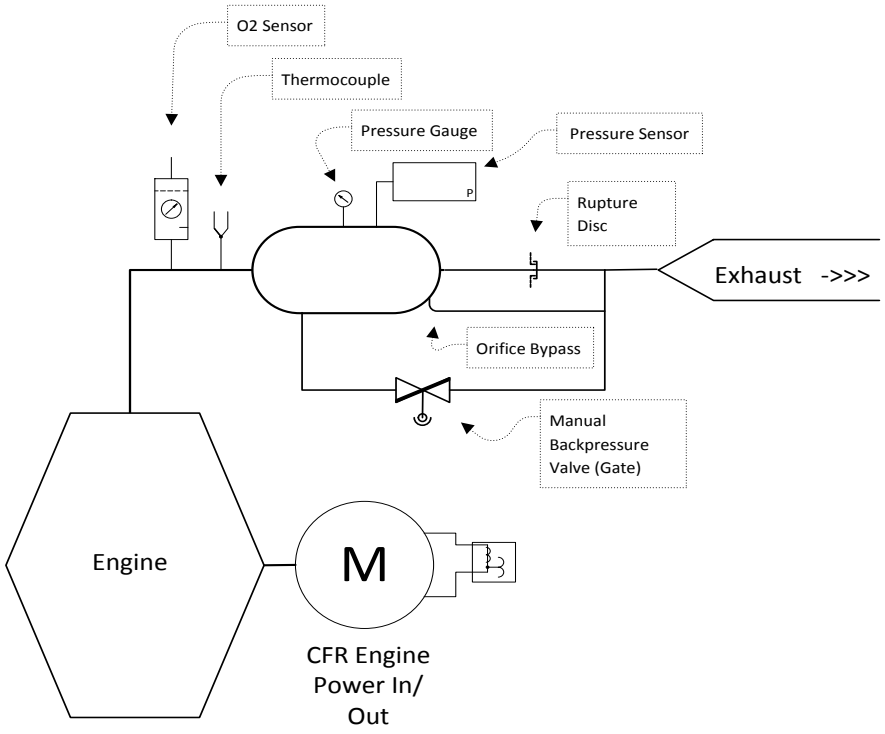

Figure 3-10 Schematic Depiction of the Test Cell Engine Exhaust System.

Figure 3-11 Exhaust components

It is desired to establish a relationship between exhaust backpressure, intake pressure, and other engine parameters to mimic a typical turbocharger installation in an engine. Figure 3-12 shows a schematic depiction of a turbocharger where point (1) is the compressor inlet from ambient atmosphere, point (2) the engine intake at the compressor discharge, point (3) the engine exhaust to the turbine intake, and point (4) turbine exhaust to ambient atmosphere.

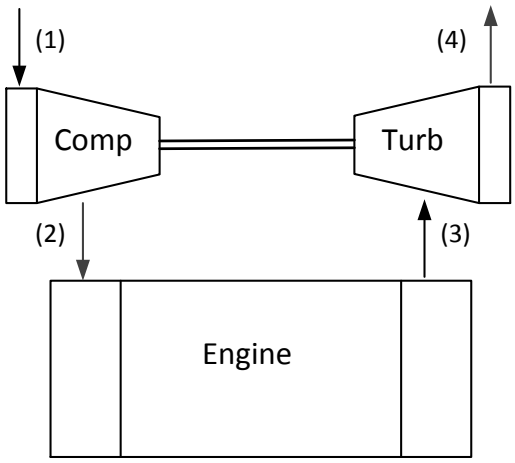

Figure 3-12 Turbocharger Schematic

The exhaust gas flows through the buffer volume to an orifice sized to allow minimal flow and maximum back pressure of approximately 2 atm (gauge). Bypass piping with an in-line manual gate valve is installed to allow sufficient flow, when fully open, to reduce back pressure to nearly zero gauge pressure. The gate valve is adjusted manually to control the amount of exhaust gas bypassing the orifice thus controlling back pressure.

The desired back pressure is calculated based on intake conditions, exhaust temperature, turbocharger efficiency and gas properties, as given by the derivation shown below – as adapted from Heywood (Heywood, 1988).

The required exhaust backpressure, or P_3, is obtained by evaluating the operation of the compressor and turbine. The isentropic efficiency, η_c, for the compressor is given by

$$\eta_c = \frac{reversible\ power}{actual\ power} = \frac{h_{2s} - h_1}{h_2 - h_1}$$

Equation 3-8

where

h_1 = Enthalpy of the air mixture entering the compressor

h_{2s} = Enthalpy of the air mixture at the compressor discharge for an isentropic process

h_2 = Enthalpy of the air mixture at the compressor discharge

Assuming ideal gas behavior and constant specific heat for the engine intake air entering and leaving the compressor, Equation 3-8 can be expressed as

$$\eta_c = \frac{c_{p,i}(T_{2s} - T_1)}{c_{p,i}(T_2 - T_1)} = \frac{(T_{2s} - T_1)}{(T_2 - T_1)}$$

Equation 3-9

where

$c_{p,i}$ = constant pressure specific heat of the intake air

T_1 = Temperature of the air mixture entering the compressor

T_{2s} = Temperature of the air mixture at the compressor discharge for an isentropic process

T_2 = Temperature of the air mixture at the compressor discharge

For the isentropic compression of an ideal gas

$$\left(\frac{T_{2s}}{T_1}\right) = \left(\frac{P_2}{P_1}\right)^{(\gamma_i - 1)/\gamma_i} \; and \; T_{2s} = T_1\left(\frac{P_2}{P_1}\right)^{(\gamma_i - 1)/\gamma_i}$$

where

γ_i = ratio of specific heats, c_p/c_v, for the intake air mixture

P_1 = Pressure of the air mixture entering the compressor

P_2 = Pressure of the air mixture at the compressor discharge

Equation 3-9 can now be written as

$$\eta_c = \frac{\left(\frac{P_2}{P_1}\right)^{(\gamma_i - 1)/\gamma_i} - 1}{\left(\frac{T_2}{T_1}\right) - 1}$$

Equation 3-10

Rearranging,

$$\left(\frac{T_2}{T_1}\right) - 1 = \frac{\left(\frac{P_2}{P_1}\right)^{(\gamma_i - 1)/\gamma_i} - 1}{\eta_c}$$

Equation 3-11

And multiplying both sides of the equation by T_1 it follows that

$$T_2 - T_1 = \frac{T_1}{\eta_c}\left\{\left(\frac{P_2}{P_1}\right)^{(\gamma_i - 1)/\gamma_i} - 1\right\}$$

Equation 3-12

The 1st Law of Thermodynamics for an open system is given by

$$\dot{Q} - \dot{W} = \dot{m}\left\{(h_2 - h_1) + \frac{1}{2}(V_2^2 - V_1^2) + g(z_2 - z_1)\right\}$$

Applying the simplifying assumptions that heat transfer, change in kinetic energy, and change is potential energy are small across the control volume of the compressor and can therefore be neglected, it follows that

$$\dot{W} = \dot{m}(h_2 - h_1)$$

Equation 3-13

Given that, for constant specific heat,

$$h_2 - h_1 \approx c_{p,i}(T_2 - T_1)$$

Equation 3-14

Combining equations (3-12), (3-13), and (3-14) the power required to drive the compressor, $\dot{W}_c$, can be expressed as

$$\dot{W}_c = \frac{\dot{m}_i c_{p,i} T_1}{\eta_c}\left\{\left(\frac{P_2}{P_1}\right)^{(\gamma_i - 1)/\gamma_i} - 1\right\}$$

Equation 3-15

As similar analysis is carried out for the turbine; isentropic efficiency, η_T , is given by

$$\eta_T = \frac{actual\ power\ output}{reversible\ power\ output} = \frac{h_3 - h_4}{h_3 - h_{4s}}$$

Equation 3-16

If the exhaust is considered to be an ideal gas with constant specific heats, equation (3-16) can be written as

$$\eta_T = \frac{T_3 - T_4}{T_3 - T_{4s}} = \frac{1 - ({}^{T_4}/_{T_3})}{1 - ({}^{P_4}/_{P_3})^{({\gamma_e - 1})/{\gamma_e}}}$$

Equation 3-17

An expression for the power produced by the turbine is derived from equations 3-13 and 3-17 using the same assumptions of ideal gas behavior and constant specific heat.

$$\dot{W}_T = \dot{m}_e(h_3 - h_4) = \dot{m}_e c_{p,e}(T_3 - T_4) = \dot{m}_e c_{p,e}\eta_T T_3 \left(1 - \left(\frac{P_4}{P_3}\right)^{({\gamma_e - 1})/{\gamma_e}}\right)$$

Equation 3-18

Next, overall turbine efficiency, η_{turbo}, is introduced. Since the compressor and turbine are mechanically joined in a turbocharger,

$$-\dot{W}_c = \eta_{turbo}\dot{W}_T$$

Equation 3-19

Substituting equations (3-15) and (3-18) into equation (3-19) it follows that

$$\frac{\dot{m}_i c_{p,i} T_1}{\eta_c}\left\{\left(\frac{P_2}{P_1}\right)^{({\gamma_i - 1})/{\gamma_i}} - 1\right\} = \eta_{turbo}\dot{m}_e c_{p,e}\eta_T T_3 \left(1 - \left(\frac{P_4}{P_3}\right)^{({\gamma_e - 1})/{\gamma_e}}\right)$$

Since $\dot{m}_i = \dot{m}_e$ and $\eta_c\eta_T = \eta_{turbo}$ a simplified form of the equation becomes

$$\left(1-\left(\frac{P_4}{P_3}\right)^{(\gamma_e-1)/\gamma_e}\right)=\frac{\dot{m}_i c_{p,i} T_1}{\eta_{turbo}/\eta_T}\left\{\left(\frac{P_2}{P_1}\right)^{(\gamma_i-1)/\gamma_i}-1\right\}\frac{1}{\eta_{turbo}\dot{m}_e c_{p,e}\eta_T T_3}$$

and, isolating P_3,

$$P_3 = P_4\left[1-\left\{\frac{c_{p,i}T_1}{(\eta_{turbo})^2 c_{p,e}T_3}\left[\left(\frac{P_2}{P_1}\right)^{\frac{\gamma_i-1}{\gamma_i}}-1\right]\right\}\right]^{\frac{\gamma_e}{1-\gamma_e}}$$

Equation 3-20

where:

P_1 = compressor inlet pressure (assumed ambient condition)

P_2 = compressor outlet pressure (boost pressure)

P_3 = turbine inlet pressure (exhaust system pressure)

P_4 = turbine outlet pressure

T_1 = compressor inlet temperature (assumed ambient condition)

T_3 = exhaust system temperature

$c_{p,i}$ = specific heat at constant pressure for inlet

$c_{p,e}$ = specific heat at constant pressure for exhaust

γ_i = ratio of specific heats for inlet conditions

γ_e = ratio of specific heats for exhaust conditions

η_{turbo} = overall turbocharger efficiency (assumed to be 65% for this project)

3.5.1 Exhaust System Weight Support

For the CFR engine the cylinder head is raised and lowered in order to adjust compression ratio and the exhaust port from the engine is fixed to the cylinder head, therefore accommodation must be made to allow the entire exhaust assembly to travel vertically by roughly 1.25 inches (3.2 cm) without imposing excessive stress on the two, 3/8 inch fasteners at the exhaust port that provide cantilevered support for the weight of the entire exhaust system. In the original configuration of the engine the exhaust system consisted of a simple thin walled exhaust pipe bolted to the exhaust port of the engine with a total weight of approximately 5 kg. This test cell application increases the weight of the exhaust components to 50 kg of new materials. The new test cell is arranged to suspend the exhaust components from springs mounted overhead such that the bulk of the system weight is not assumed by the exhaust port bolts and adequate flexibility is afforded to allow free vertical travel when adjusting the cylinder head to vary compression ratio. Figure 3-13 provides a photograph of the installed suspension components.

3.6 ELECTRONIC IGNITION

The engine, originally configured with a capacitive discharge type ignition system, is currently configured with an electronic ignition system (Altronic model CD200) adapted to a single cylinder engine. The system consists of a controller unit, magnetic pickup sensor, input and output harness and ignition coil. Terminal program software enables supervisory operation of the system to allow ignition timing to be set and changed as desired during engine operation without mechanical adjustment.

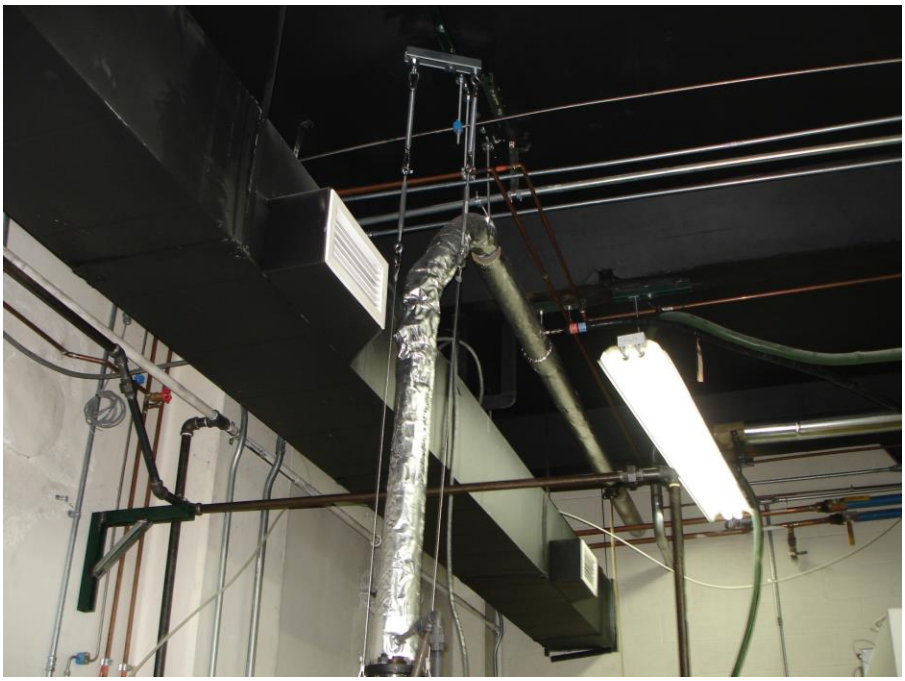

Figure 3-13 Overhead Suspension of Exhaust Components

3.7 FUEL BLENDING SYSTEM

The fuel blending system is designed to allow proportioning of any combination of constituent gas desired to create specific fuel gas blends. The system consists of a number of compressed gas cylinders with regulators discharging flow first into mass flow meters, then into a buffer volume, then to the inlet of a pulse width modulated (PWM) injector for each gas. The PWM injectors introduce respective gases to a common manifold and the blended gas mixture is then allowed to flow through a combination flash arrestor/check valve and finally mix with combustion air prior to entering the engine intake. Figure 3-14 provides a photograph of the installed components. Figure 3-15 provides a schematic depiction of the test cell fuel blending system. The gases available for blending include methane (CH_4), ethane (C_2H_6), propane (C_3H_8), carbon monoxide (CO), carbon dioxide (CO_2), nitrogen (N_2), and hydrogen (H_2). Facility natural gas is also compressed and connected to the system for use as a direct fuel gas for general engine

operation and testing. The system lay-out and component function are described in the following sections.

Figure 3-14 Fuel Blending System Installed Components.

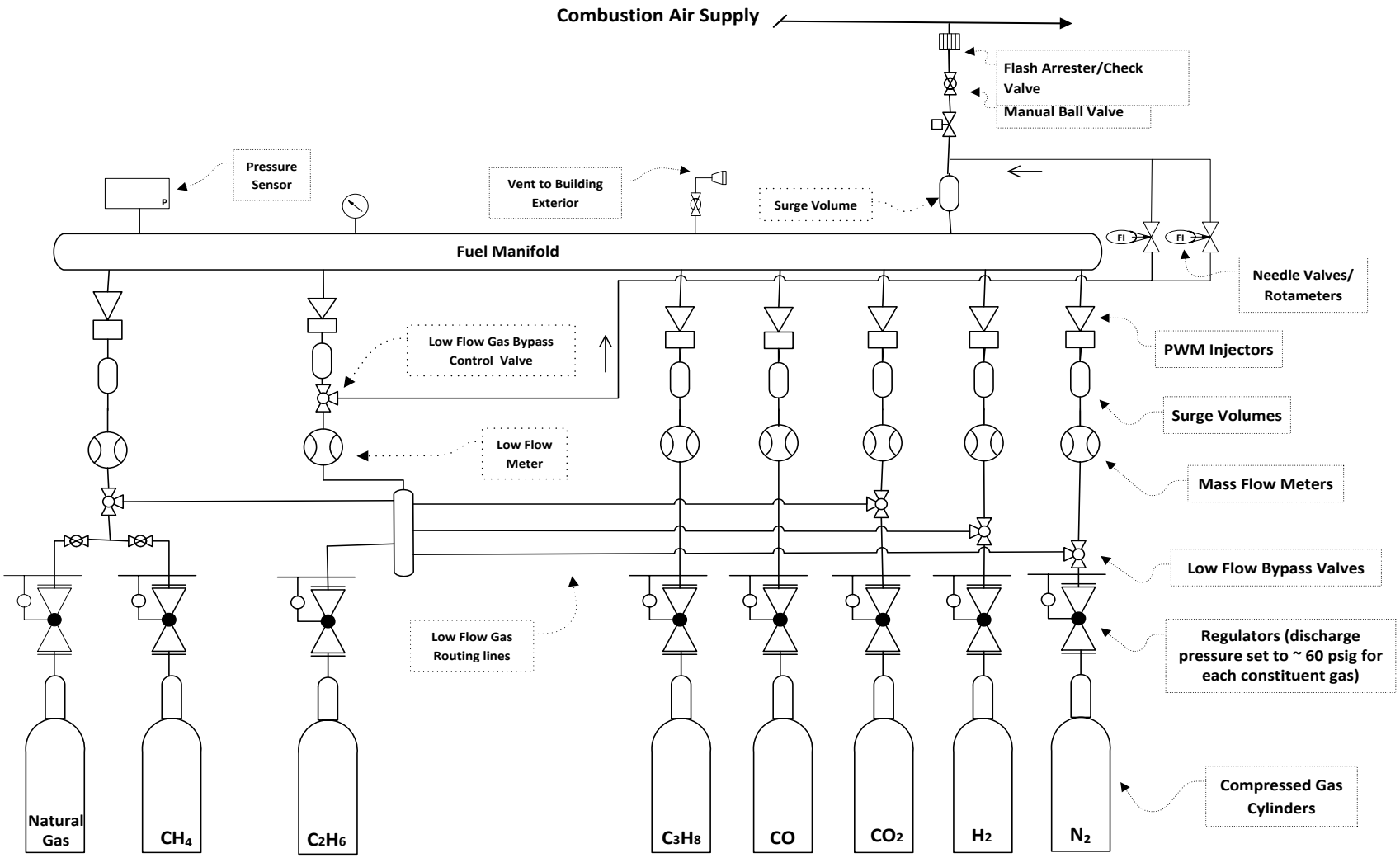

Figure 3-15 Schematic Depiction of the Test Cell Fuel Blending System.

3.7.1 Compressed Gas Storage and Staging

Individual gases (CH_4, C_2H_6, CO, CO_2, H_2, and N_2) are purchased either as chemically pure (CP) grade or ultra-high purity (UHP) grade in 200 or 300 standard cubic foot (SCF) cylinders. The gases remain stored and staged in the delivered cylinders. A natural gas compressor at the EECL is used to compress natural gas 300 SCF cylinders. When natural gas is used for this project it must be in compressed form due to inadequate line pressure to overcome blending system pressures dictated by engine intake boost pressure. While the blending system has a propane (C_3H_8) station, none of the test blends for this project require its use.

3.7.2 Mass Flow Measurement

An in-line mass flow meter (heated tube or calorimetric type electronic mass flow meter, Model FMA 1700 Series,0-15 SLM, 0-100 SLM, and 0-200 SLM, from Omega Engineering, Inc.) is installed for each constituent gas to provide direct measurement of net fuel gas flow to the engine. The operating range of the meters were selected based on the peak flow requirements identified by constituent percentage in projected producer gas blends.

3.7.3 Fuel Injection

The blending system uses PWM injectors (model SP-051 manufactured by Clean Air Power, Inc.) to introduce constituent gases into the fuel manifold. The injectors were sized based on initial producer gas blend constituent percentages and sizing methodology provided by the injector manufacturer. The injector model purchased was the smallest size available and matched the requirements for higher percentage constituents, e.g. > 15%.

For gas blend constituents less than roughly 10% to 15% of total volume the duty cycle of the individual PWM can be less than 10% which is problematic for positive control of the constituent flow into the manifold. For this reason a low flow by-pass loop is included allowing the injector to be by-passed and gas flow routed through either of two manually controlled rotameters (Models FL-3601ST FL-3688C, from Omega Engineering) depending on desire flow rate. The rotameters installed in the low flow loop serve two purposes; (1) they provide a visual indication to the operator of gas flow rate admitted to the system and (2) the rotameter valves allow precise manual control of gas flow to be achieved. A flow signal is transmitted by the low flow mass flow meter to the LabVIEW© control software so that total fuel flow includes the low flow loop contribution even though a PWM injector is not engaged.

Each mass flow meter was received with current calibration certification established for nitrogen flow and requires that a correction factor be employed for measurement of any gas other than nitrogen. Those correction factors are embedded in the LabVIEW© control software for each constituent gas line. However, since the low flow loop can flow a number of different constituent gases at any given time the LabVIEW© control software requires that the low flow constituent gas be identified by the operator in order for the appropriate flow correction factor to employed. It is noted that the failure to input the proper low flow gas identity will cause significant distortion of test results, particularly with regard to measured methane number.

3.7.4 Safety Isolation

The blending system incorporates both a manual isolation valve as well as a normally shut solenoid operated valve in series. In the event of interrupted power to the solenoid operated valve, whether through an inadvertent loss of power or intentional isolation of the system in the event of an emergency the valve will fail shut isolating fuel from the engine. A combination flash arrestor/check valve is installed at the union connecting the fuel line to combustion air serving to isolate the fuel line in the event of a detonation or rapid pressure surge in the combustion air system. A manual vent valve to the building exterior is installed at the fuel manifold and nitrogen purge is conducted through the low pressure gas flow line up.

3.8 ENABLING SOFTWARE AND VIRTUAL INSTRUMENTATION (VI)

The project test cell monitoring and control system uses a software package developed by the staff of the Colorado State University Engines and Energy Conversion Laboratory written with LabVIEW©. The Virtual Instrumentation software developed specifically for this engine and this project accepts input from installed sensors (flow meters, thermocouples, pressure transducers) and provides automated output to control fuel injector PWM duty cycles in response to calculated fuel system mass flow, combustion air control valve for controlling intake air pressure and flow rate (also regulating stoichiometry), and calculates desired exhaust backpressure for the engine operator. The VI program displays engine operating status allowing the operator to monitor and control intake air pressure and temperature, fuel mixture, air-fuel ratio, exhaust temperature and pressure, coolant temperature, and power generation level.

A separate program, also developed at the CSU EECL, written with LabVIEW© used in this project is the combustion logger. A high speed data acquisition card receives input from the

cylinder pressure transducer, through the charge amplifier, as well as crank shaft position indication from the digital encoder. The information is processed and relayed into real-time monitoring and recording of combustion activity in the operating engine. A synopsis of these programs is provided in Appendix B to this work.

4 TEST PLAN AND FUEL SELECTION

The project test plan consists of initial verification of test cell performance, demonstration of the proposed knock measurement process, and then methane number measurement of a variety of producer gas blends. The definition of fuel blends to be tested was developed based on a combination of engine operating limitations (principally air-fuel ratio) and sponsor indicated compositions, based primarily on gas produced from existing gasifiers. The following sections provide a synopsis of tests conducted and fuel blends selected for the project.

4.1 TEST CELL DEMONSTRATION TESTING

The initial tests conducted for this project are intended to prove design goal accomplishment associated with the construction of the test cell. These tests are performed with compressed facility natural gas and demonstrate the performance of the test cell features including intake boost system, exhaust backpressure controls, VI control of the engine, ignition timing, and knock measuring methodology developed for the project. In addition to test cell function an engine maintenance tear-down is conducted following the initial set of tests. The cylinder is found to be within OEM tolerances for internal diameter, taper, and out-of-round. Valves are found to have some pitting and corrosion present. However, stems and valve guide dimensions are within OEM tolerances. Free and loaded valve spring heights are within OEM guidelines. The cylinder wall is honed, piston rings replaced, valve seats lapped, and the engine reassembled.

4.2 CRANK ANGLE/PISTON TOP DEAD CENTER (TDC) INDICATION

In order to evaluate repeatability regarding true TDC an inspection is conducted on the engine to determine crank position relative to the flywheel stamped crank angle match marks. A micrometer is mounted magnetically through the cylinder head detonation pickup port and place in contact with the piston, the flywheel rotated by hand noting the peak position of the piston (occurring at TDC) by observing the micrometer indication and noting the corresponding flywheel match marks. In repeated tests, rotating the flywheel in successive opposite directions the point of TDC corresponded to approximately 1° lag of indicated 0° crank angle. The lead design engineer at the OEM was contacted to verify OEM intended tolerance for indicated TDC and the response was that ± 1° was consistent with their manufacturing specifications and represented intended backlash. It was emphasized that this engine is designed with generous backlash in order to withstand intended operation under conditions of light to heavy knock.

Consistency of dynamic TDC is evaluated by recording cylinder pressure as a function of crank angle while motoring. The motoring data test set is repeated each test day over 22 test days. Figure 4-1 is a plot of indicated motoring peak pressure in °aTDC for each date recorded. For the 22 data sets, the average peak pressure occurs at 0.371°aTDC, the median peak pressure occurs at 0.373°aTDC, and the standard deviation of the readings is 0.0565°.

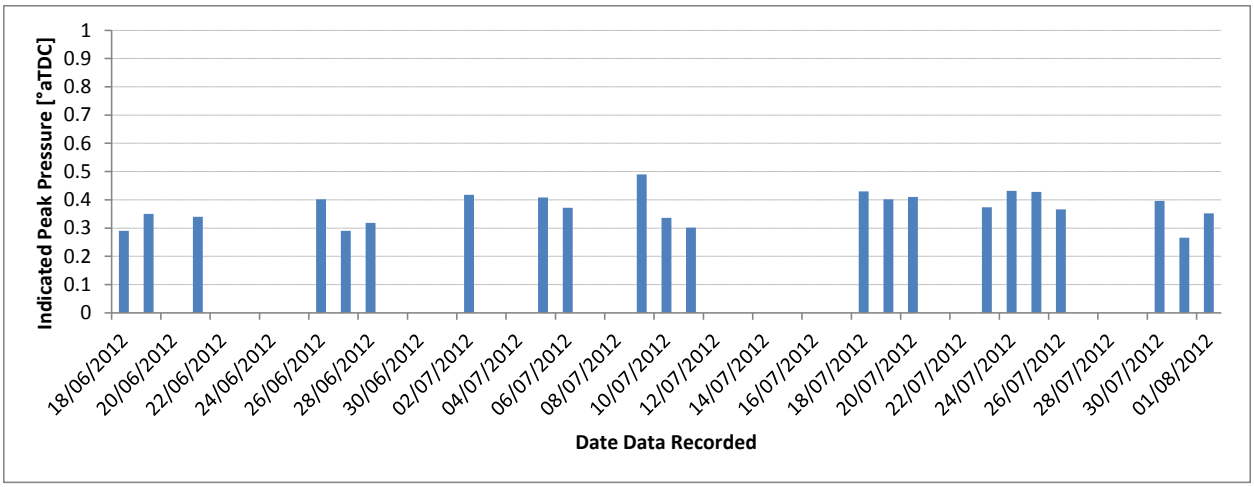

Figure 4-1 Motoring Indicated Peak Pressure (TDC) Location Test Results

4.3 Ignition Timing Sweeps and MBT Timing Determination

The first tests conducted in the new test cell are ignition timing sweeps to determine the point of ignition timing corresponding to maximum brake torque (MBT) for the engine. The ignition system is capable of altering ignition timing as desired, verified by an induction type timing light and marked timing match marks. Figure 4-2 shows the results from the ignition timing sweep engine runs. The plot shows the variation in engine power produced to ignition timing while burning natural gas under naturally aspirated conditions, at a compression ratio of 6:1, with no imposed exhaust back pressure.

The results indicate that, for this engine, power output does not vary substantially (< 2%) with ignition timing between the settings of 17° and 26°bTDC.

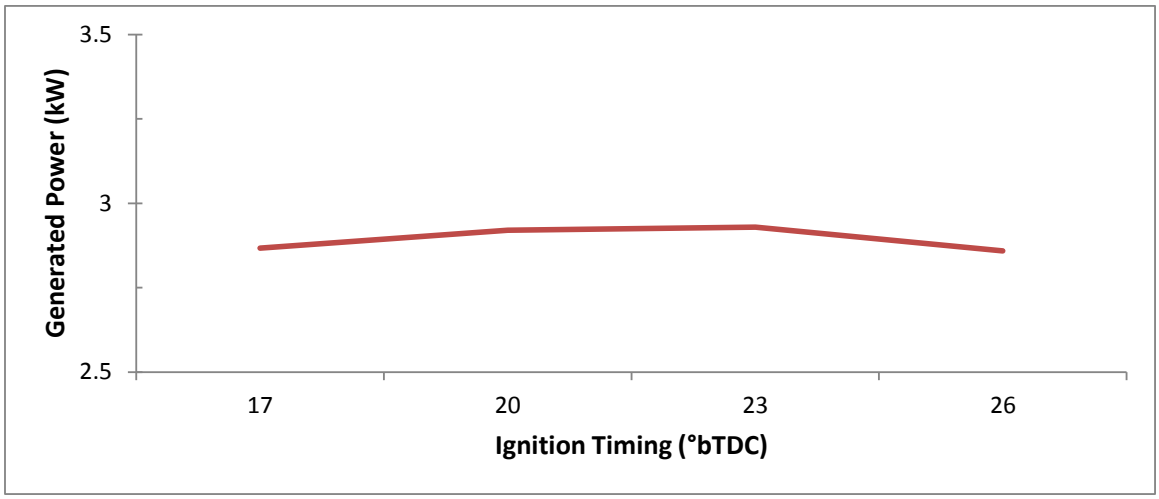

Figure 4-2 Ignition Timing Sweep Results - Power vs. Timing

4.4 Methane Number Sensitivity to Engine Operating Parameters

The initial methane number measurement tests are conducted with parameters adjusted as nearly as possible to replicate those described in the original methane number measurements at AVL (Leiker, et al., 1972), specifically:

Engine speed…….. n = 900 rpm

Ignition timing……..... α_i = 15°bTDC

Combustion air ratio……...…… λ = 1 (100% chemically correct mixture)

Intake air temperature……. T_i = 20°C

Cooling water outlet temperature…. T_w = 80°C

Knock intensity……. KI = 50

It is noted that the apparatus will not allow certain parameters listed above to be met. Specifically, engine speed, cylinder head geometry, intake air temperature, cooling water temperature and knock intensity will vary from the standard test conditions stipulated by Leiker. The following limitations apply:

1. Engine speed for the CFR engine is determined by the speed of the synchronous motor/generator driving the engine or being driven by the engine subjected to frequencies on the electrical grid. Typical engine speeds under load are ~940 ± 5 rpm.
2. The test engine described by Leiker, et al, was configured with a Removable Dome Head (RDH) which consists of a domed shaped combustion chamber with the spark plug located near the center of the dome. The CFR F2 engine has a disk shaped combustion chamber with the spark plug located on the periphery of the chamber.
3. Intake air temperature in ambient conditions vary from approximately 30°C to 40°C and no means is currently available to decrease that temperature to 20°C.
4. Cooling water outlet temperature for this engine in operation is consistently 95 ± 2°C and no means is currently available to decrease that temperature to 80°C.
5. Knock intensity with the originally installed analog knock sensor corresponds to a comparative measure at light audible knock. One of the objectives of this test program will be to use the FFT algorithm to establish a direct and quantifiable measure of frequency domain magnitude that corresponds to a repeatable knock index for this engine configuration.

The tests to measure methane number under varying operating parameters are designed to reveal sensitivity to (1) ignition timing, (2) intake boost and nmep level, and (3) equivalence ratio, ϕ. Table 4-1 lists the specific test cases defined for this portion of the project.

Table 4- 1 Methane Number Measurement Case Definition

Case #	Ignition Timing	nmep/Intake Boost	Φ
I	17°bTDC	NA – 101.3 kPa	1.0
II	23°bTDC	NA – 101.3 kPa	1.0
III	17°bTDC	12 bar nmep	1.0
IV	23°bTDC	12 bar nmep	0.7
V	23°bTDC	12 bar nmep	1.0

Tests outlined for sensitivity to operating parameters were conducted first with facility natural gas, then with the original five producer gas blends defined for this project, and finally with a gas blend of 90% methane and 10% ethane (CH_4/C_2H_6). Specific results and discussion are provided in Chapter 5 of this work. However, the first test conducted with facility natural gas indicated that sensitivity of measured methane number to the variations in Table 4-1 was relatively small. Consequently, it was decided to perform methane number measurements at conditions close to those used by Leiker et al.

4.5 Producer Gas Blend Selection

The initial producer gas blends chosen for this project are given in Table 4-2 and were intended to be representative of constituent blend make-up from common biomass gasification plants. After completing initial methane number measurements for these blends a matrix of blends was provided by Caterpillar, Inc. listing approximately 60 producer gas blends

specifically encountered by their natural gas engine research group in previous work and testing. A number of these blends were chosen for methane number measurement to expand the total number of blends measured in this work. The criteria imposed for inclusion in this work was that the stoichiometric air-fuel ratio should be greater than a value of approximately 2.0. One of the test cell limitations noted in early testing is that the fuel blending system is difficult to control at very low air-fuel ratios due to the volume of fuel gas necessary to maintain equivalence ratios of 1.0. This test cell limitation is correctable and can be resolved by re-sizing the fuel constituent lines and fuel manifold to accommodate higher fuel constituent flow rates. The test cell lines are sized to accommodate fuel blends ranging from wood gas ($A/F_{stoic} \approx 2$) to natural gas ($A/F_{stoic} \approx 16$) for naturally aspirated conditions. Test conditions outside these boundaries can create engine control instabilities.

Table 4- 2 Initial Test Blend Constituent Makeup

Constituent	Blend #1	Blend #2	Blend #3	Blend #4	Blend #5
CH_4	0%	2%	45%	0%	15%
CO	37%	18%	12%	20%	20%
CO_2	17%	14%	6%	15%	0%
N_2	7%	48%	11%	15%	15%
H_2	39%	18%	26%	50%	50%
A/F_{stoic}	2.55	1.20	8.96	2.78	6.80

In addition to fuel blends selected from the matrix of additional producer gas blends, 6 producer gas blends were selected from a characterization study conducted at Colorado State University as part of a master of science thesis project. (Arunachalam, 2010)

The expanded list of test blends is parsed into characteristics of air-fuel ratio and total percentage diluent (CO_2 and N_2). Figures 4-3 and 4-4 show the blend characteristics parsed as described with arrows inserted indicating gaps in gradual transition of those characteristics.

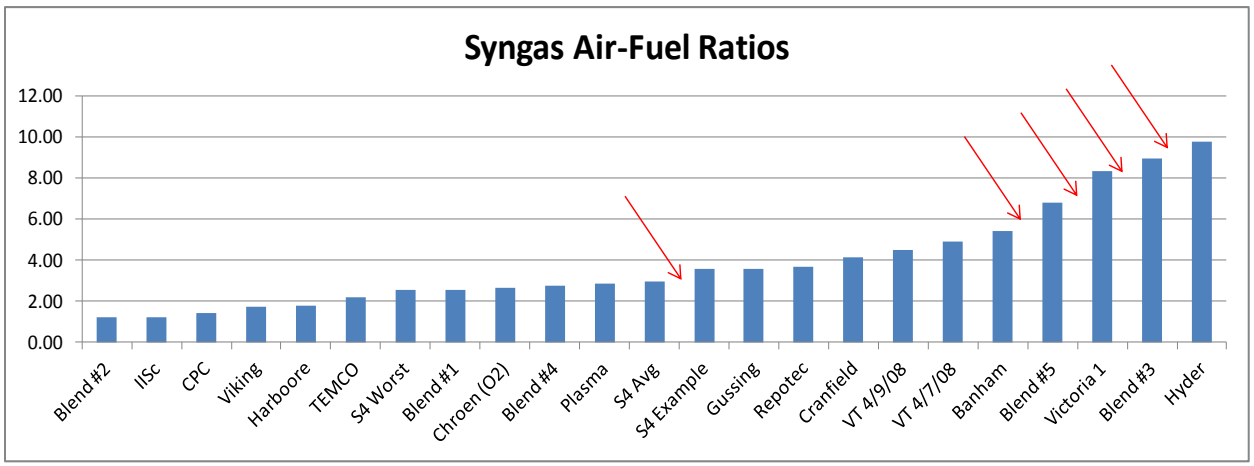

Figure 4-3 Expanded Producer Gas Blend List by Air Fuel Ratio.

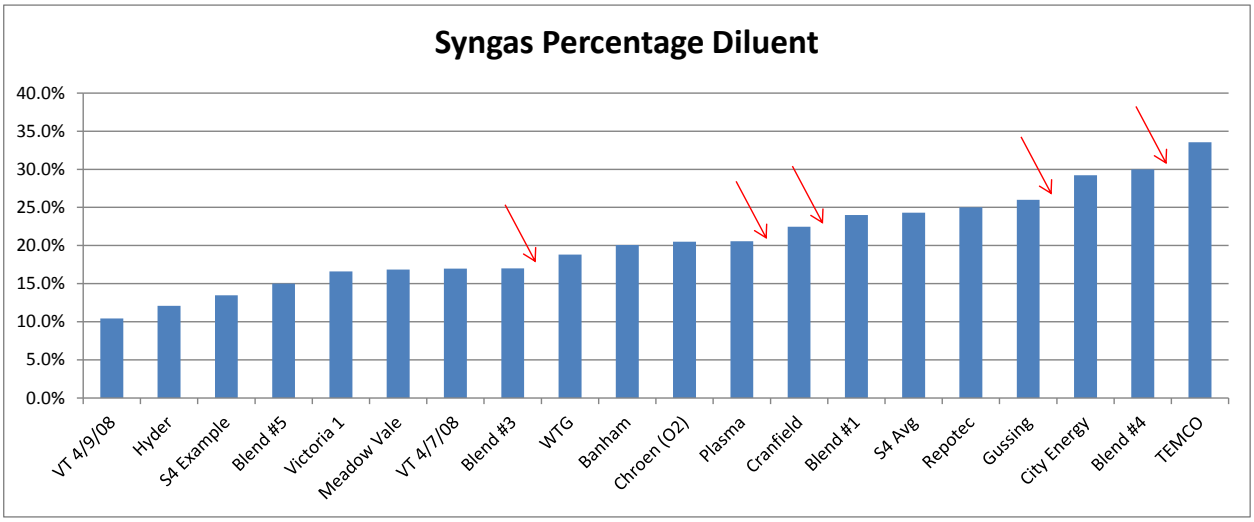

Figure 4-4 Expanded Producer Gas Blend List by Diluent Percentage.

Additional syngas blends were developed with constituent percentages selected to fill these gaps. The complete list, shown with the gap blends inserted is shown in Figures 4-5 and 4-6. A matrix form of this list is provided in Chapter 5 of this dissertation, Table 5-1.

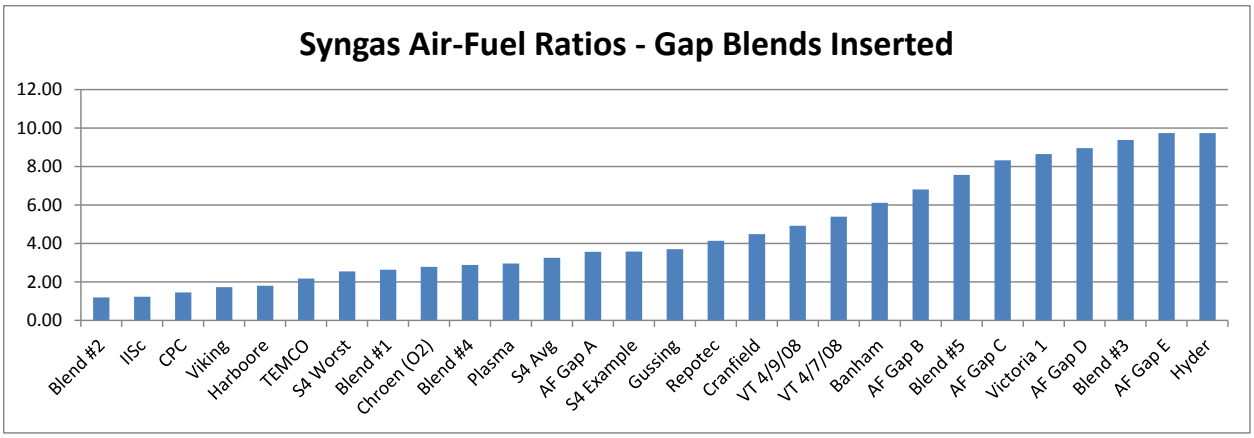

Figure 4-5 Blend List by Air-Fuel Ratio, Gap Blends Inserted.

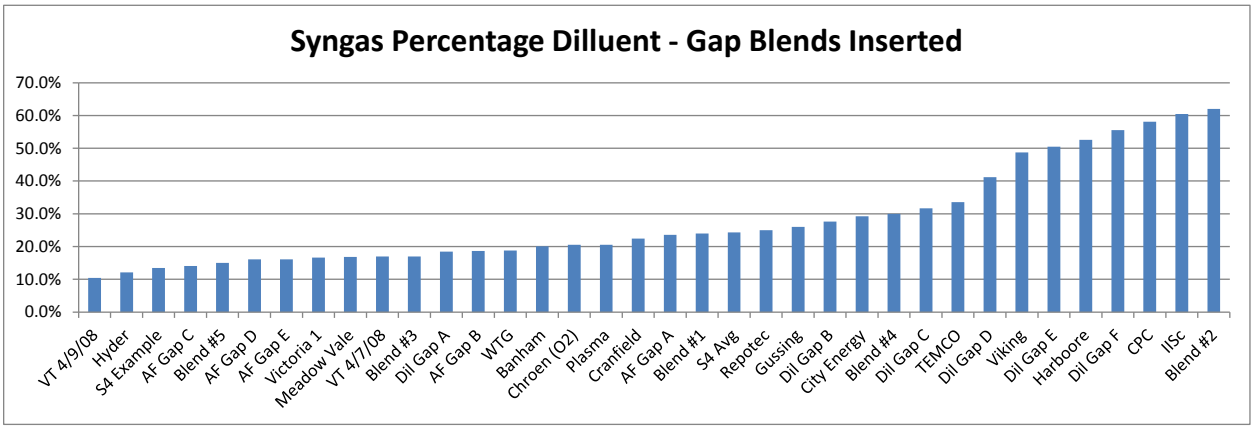

Figure 4-6 Blend List by Diluent Percentage, Gap Blends Inserted.

4.6 KNOCK MEASUREMENT METHOD DEVELOPMENT

Methane number measurement requires the identification of a quantitative knock indicator. The approach taken is to evaluate a Fast Fourier Transform (FFT) of the cylinder pressure readings to evaluate the dynamics of the pressure trace in the frequency domain. This method is similar in approach to that of Brunt (Brunt, et al., 1998) as well as Elmqvist (Elmqvist, et al., 2003). As a predictive exercise a hypothetical knock event in which pre-detonation occurs is evaluated as follows:

Assume the point of pre-detonation occurs directly across the combustion chamber from the spark plug as a result of excessive temperature in front of the advancing flame front. The period of the event should correlate to the geometry of cylinder and equate to the time required for a pressure wave to travel the diameter of the cylinder and back – or twice the diameter of the cylinder. The pressure wave is assumed to travel at the local speed of sound. First, the speed of sound is given by the relationship:

$$c = \sqrt{\gamma RT}$$

Equation 4-1

Where

c = speed of sound
γ = ratio of specific heats; c_p/c_v
R = ideal gas constant
T = temperature of the gas

The period of the event is given by:

$$\tau = 2\ x\ Diameter/c$$

Equation 4-2

The frequency is the inverse of the period, so that:

$$f = 1/\tau$$

Equation 4-3

And, substituting from above:

$$f = \sqrt{\gamma RT}/2xDiameter$$

Equation 4-4

Given the values of:

$\gamma = 1.3$
R = 0.2870 kJ/kg·K
T = 2500 K
Bore Diameter = 3.250 inch = 0.08255 m

The anticipated frequency for this case will be 5850 Hz. LabVIEW, the software with which the combustion logger program is written has an FFT function embedded which is able to be imposed on the cylinder pressure signal in real time. In-cylinder pressure measurements are

detected as discrete values occurring every 0.1 degree of crankshaft rotation and grouped corresponding to 2 engine revolutions (one complete thermodynamic cycle with 7200 individual pressure values). An average engine speed is calculated over every two engine revolutions and that value is used for frequency approximation. A band pass filter is applied to the pressure data corresponding to the average engine speed to remove the operating pressure trace and expose pressure data distortion outside of normal operating parameters, those distortions attributable to the effects of knocking. The CFR F2 engine operates at a nominal speed of 900 rpm (corresponding to 15 Hz) and when producing power at approximately 940 rpm (~15.67 Hz). When translated to the frequency domain, with the signal cleaned of the 15 Hz operating pressure trace and a Hanning window applied, it is possible to detect ringing corresponding to engine knock. A frequency domain plot of the signal reveals both the frequency at which the knock occurs and a magnitude directly corresponding to the energy associated with the knock event.

Figures 4-8, 4-9, and 4-10 each show two data plots, the upper display being the measured in-cylinder pressure [kPa] vs. crank angle [°bTDC] and the second being the result of the FFT, amplitude [kPa·rms^2] vs. frequency [Hz]. The figures show recorded data from conditions of light, moderate, and heavy engine knock, respectively. The FFT plot shows a clear indication or "spike" at the frequency associated with the knock event. The location of the frequency spike in the FFT plot corresponds to values near 6 kHz (as predicted) and the magnitude of the spike increasing with knock intensity.

Figure 4-7 Pressure Trace and FFT Plot - Light Knock.

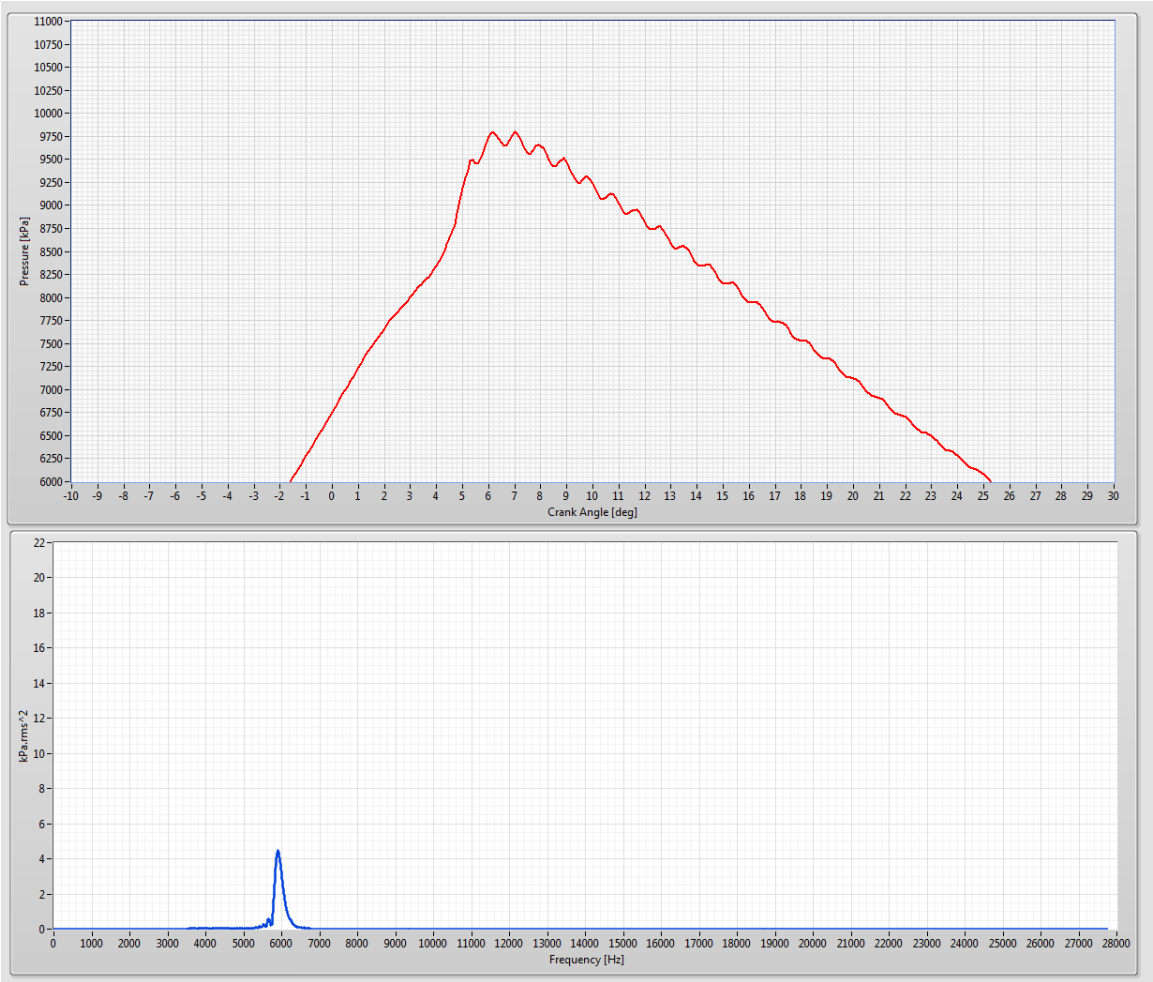

Figure 4-8 Pressure Trace and FFT Plot - Moderate Knock

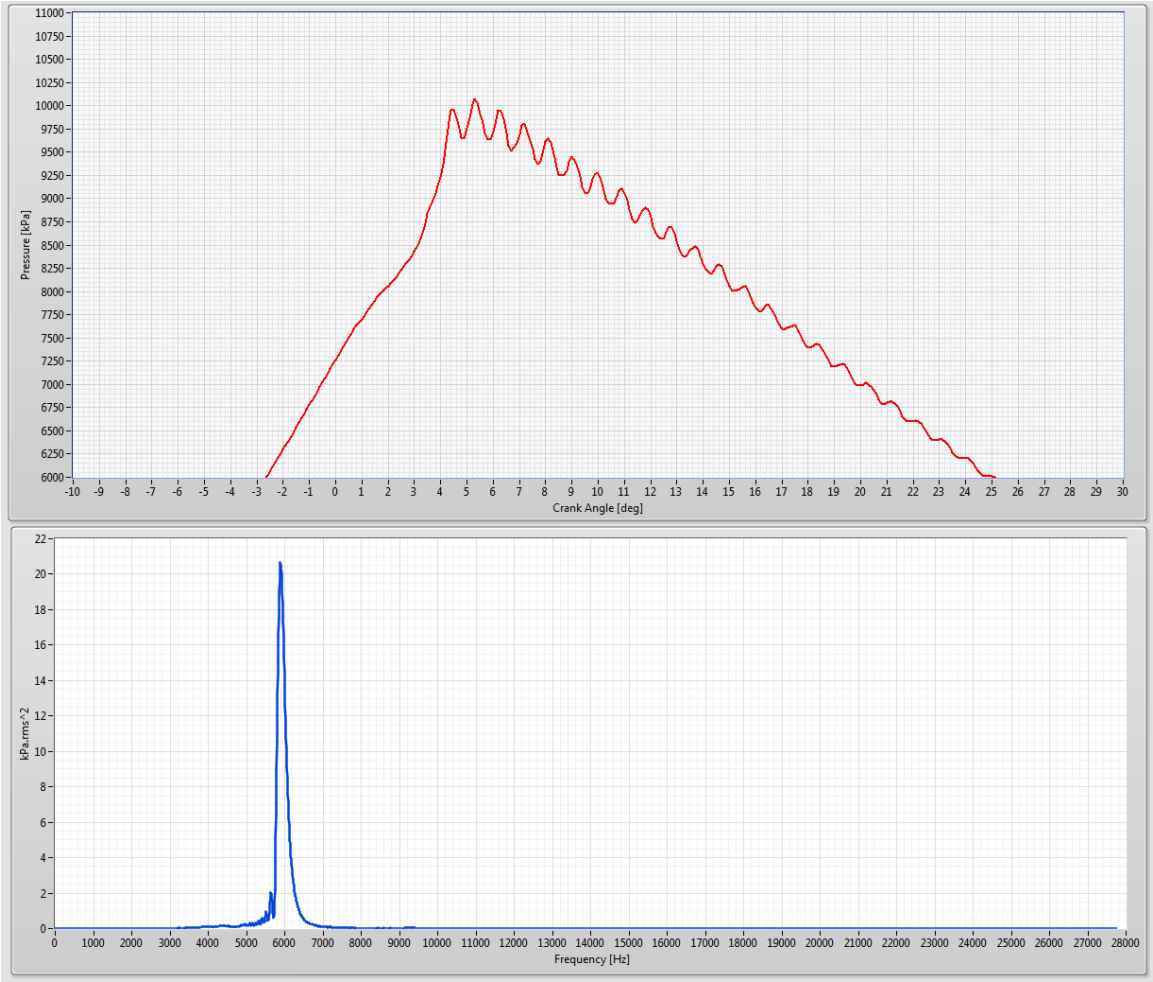

Figure 4-9 Pressure Trace and FFT Plot - Heavy Knock

The frequency at which knocking occurs for each of the tested fuel blends as well as the matching blend of methane and hydrogen is shown in Figure 4-10. It is noted that the knock frequency of the producer gas blend is less than that of the CH_4/H_2 blend in all but one of the 35 test cases. A principle contributor to knock frequency is acoustic velocity, as discussed previously and described in Equation 4-4. It is anticipated that the acoustic velocity, determined by temperature in the cylinder and the ratio of specific heats, γ, as shown in Equation 4-1, will

have similar comparative values between the producer gas blends and the matching CH_4/H_2 blends.

To model the process the assumption is made that the complete combustion occurs with 100% air under adiabatic conditions. Adiabatic flame temperature is determined by evaluating

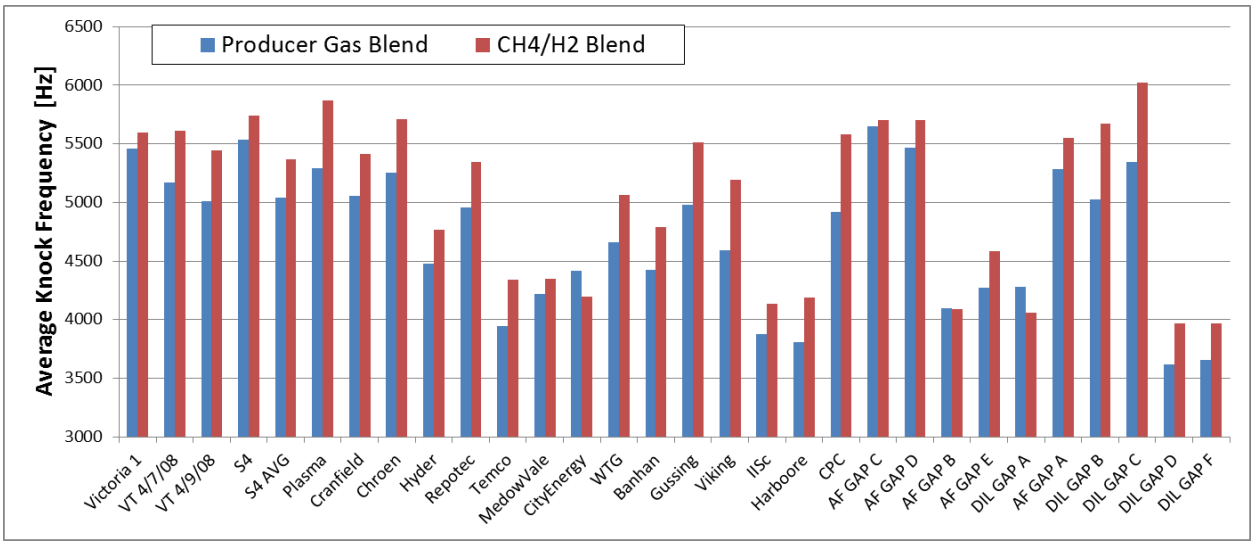

Figure 4-10 Average knock frequency for tested blends.

the energy balance equation as expressed by

$$Q - W = \sum N_p\left(\bar{h}_f^0 + \bar{h} - \bar{h}^0\right)_p - \sum N_r\left(\bar{h}_f^0 + \bar{h} - \bar{h}^0\right)_r$$

Equation 4-5

Where

Q = Net heat transfer to the system

W = Net work performed by the system

N_r and N_p = Number of moles of reactants and products, respectively

$\bar{h}_f^0$ = Enthalpy of formation

$\bar{h} - \bar{h}^0$ = Sensible enthalpy relative to 25°C, 1 atm

In simplified form,

$$Q - W = H_{products} - H_{reactants}$$

Equation 4-6

Where

$$H_{products} = \sum N_p \left(\bar{h}_f^0 + \bar{h} - \bar{h}^0\right)_p$$

$$H_{reactants} = \sum N_r \left(\bar{h}_f^0 + \bar{h} - \bar{h}^0\right)_r$$

In the limiting case where no heat is transferred and no work is done by or on the system, the maximum temperature reached by the products is called the adiabatic flame temperature or adiabatic combustion temperature. The energy balance equation becomes

$$\sum N_p \left(\bar{h}_f^0 + \bar{h} - \bar{h}^0\right)_p = \sum N_r \left(\bar{h}_f^0 + \bar{h} - \bar{h}^0\right)_r$$

Equation 4-7

For the reactants, enthalpy is known based on an assumed initial temperature. For the products, since enthalpy is a function of temperature, the temperature is determined for which the combined values of enthalpy satisfy the equality (Cengel & Boles, 2011). This iterative solution was performed with the use of the software EES (Engineering Equation Solver by F-Chart Software, Academic Commercial V9.224 (9/12/2012) for all 35 producer gas blends and the matching CH_4/H_2 blends. Figure 4-11 shows the average values for acoustic velocity based on

calculated adiabatic flame temperatures and averaged specific heats. Figure 4-12 is a plot of acoustic velocity as a function of methane number, showing a clear trend toward lower acoustic velocity as methane number increases. Details of the calculations are provided in Appendix E.

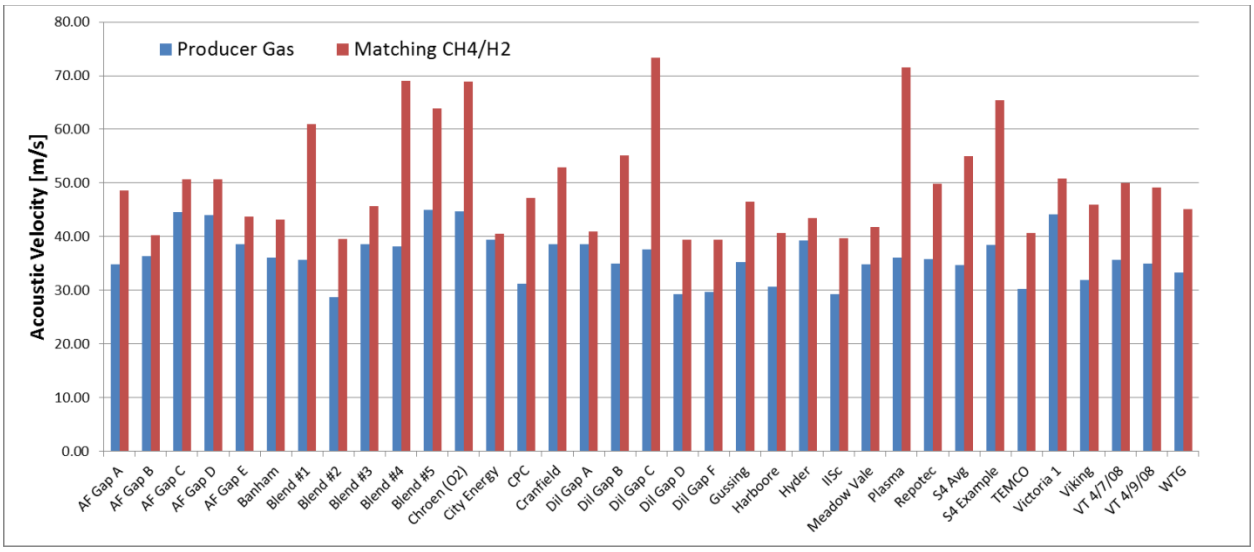

Figure 4-11 In-Cylinder Acoustic Velocity for Tested Blends.

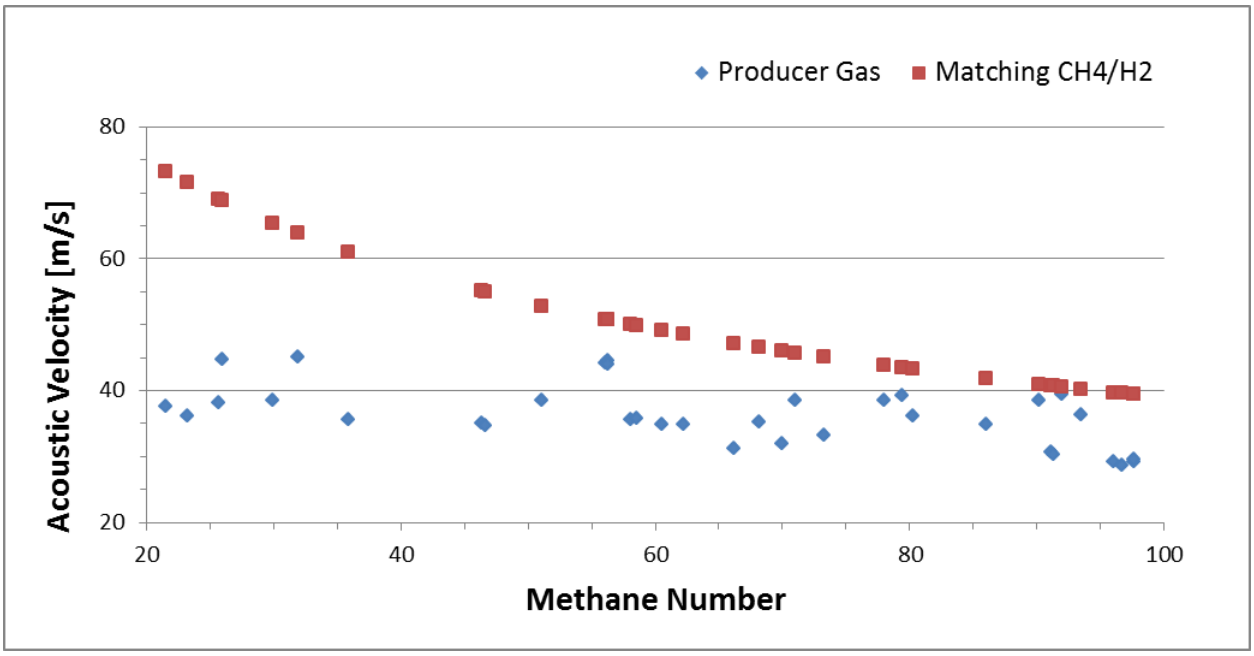

Figure 4-12 Acoustic Velocity As a Function of Methane Number.

4.7 KNOCK LEVEL THRESHOLDS

The next step in establishing a definitive knock index is to evaluate the magnitude of the spike resulting from a knock event coupled to the frequency of occurrence, e.g. how many events are manifested in a given number of cycles. Figure 4-13 shows a typical recording of moderate knock, plotting only the magnitude of the spike for each combustion cycle

.

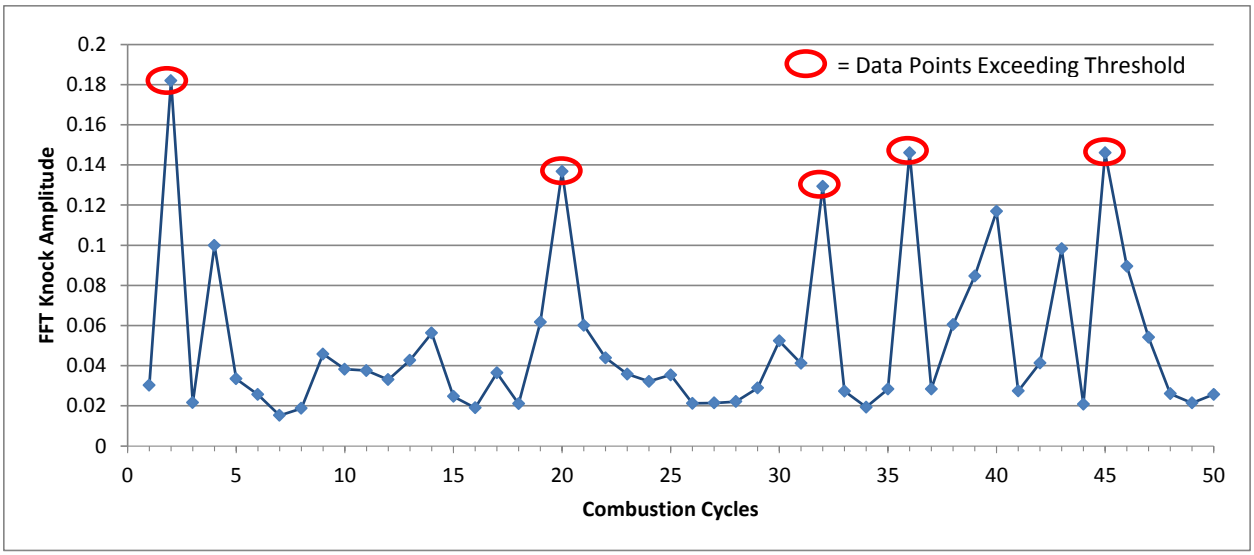

Figure 4-13 FFT Knock Amplitude

The recorded FFT magnitude of pre-detonation in the combustion chamber varies widely during engine operation, as illustrated in Figure 4-12 by the differences in spike magnitude in each cycle. Even during engine operation with relatively high, consistent, and clear ongoing knock, a pre-detonation event does not occur on each cycle and the severity of each individual pre-detonation event will also vary widely. The approach chosen for this project is to establish a threshold for both magnitude and rate of recurrence to define a knock level. For example, in Figure 4-12 illustrates a knock level defined by a threshold of 0.12 magnitude, occurring at least 5 times in every 50 combustion cycles.

4.8 KNOCK INTEGRAL

The term knock integral is used referring to the area under the curve bounded by FFT spike magnitude over a set number of combustion cycles. Since a discreet value for amplitude is known for every cycle the area under the curve is given by

$$KI = Area_{bounded} = \sum_{i=0}^{n} \{(i+1) - i\}\{KL(i+1) + KL(i)\}/2$$

Equation 4-8

Where

n = number of combustion cycles in a data set
KL(x) = knock level magnitude at a given combustion cycle, x

It follows that

$$KI = \frac{1}{2}\{KL(1) + KL(0) + KL(2) + KL(1) + \cdots + KL(n+1) + KL(n)\}$$

Equation 4-9

and

$$KI = \frac{1}{2}\{KL(0) + 2KL(1) + 2KL(2) + \cdots + 2KL(n) + KL(n+1)\}$$

Equation 4-10

Since KL(0) and KL(n+1) define the beginning and end of the data set, respectively, those values are set to zero and

$$KI = \ KL(1) + KL(2) + \cdots + KL(n)$$

Equation 4-11

The knock index then must be referenced to the specific data set combustion cycle count, e.g. "10 for 200 cycles".

The area under the curve is evaluated by summing the magnitude seen at each cycle point over the block of successive cycles for each data set – usually 200 cycles. By using the integral value for comparison both severity of individual knock events and persistence in recurrence are taken into account. The determination of a knock integral to describe a repeated knock condition offers objective quantification of the phenomena. Figure 4-13 shows the results from two separate data runs of 200 combustion cycles with nearly matched integral values.

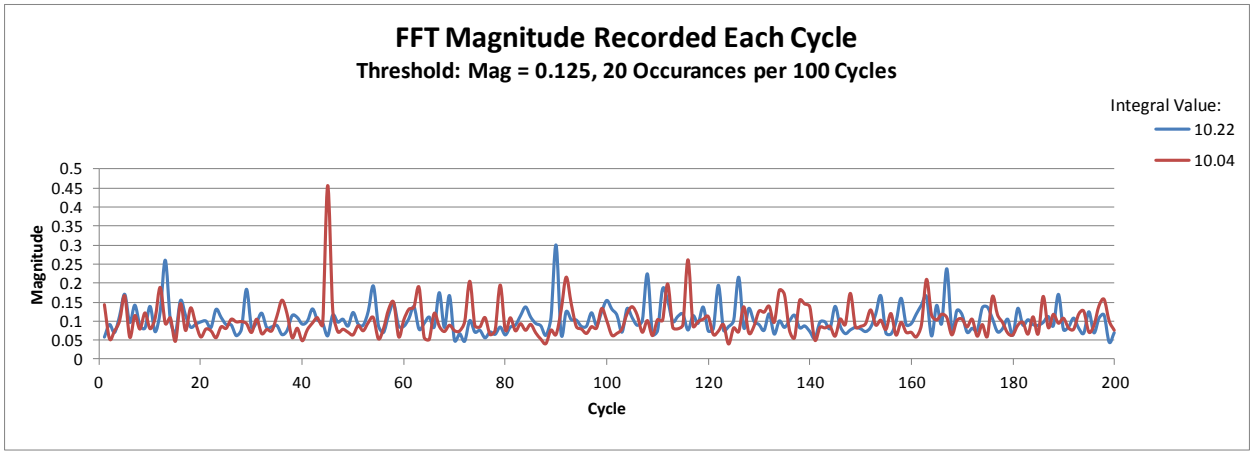

Figure 4-14 Two Recorded Knock Measurement Traces Superimposed.

Using the knock integral method developed for this project allows methane number measurement to be conducted by ascertaining a specific knock integral value with a tested fuel blend at set engine operating parameters (compression ratio, ignition timing, intake boost pressure, intake temperature, exhaust backpressure, and nmep) and then allows the operator to objectively match that integral value with a measured blend of methane and hydrogen.

The knock integral method was found to be a stable and repeatable method for consistent methane number measurements. Due to the random nature of the knock events (i.e. the knock amplitude is different for each cycle) accounting for both the intensity of frequency of knock allows the best fit for matching knock characteristics of fuel blends under to test to the methane and hydrogen mixture used for comparison. The integral method is also similar to the operation of the original knock meter, providing some consistency with previous data using the knock meter.

4.8.1 Consistency and Repeatability of Knock Measurement

To determine the repeatability of the method a check case methane number measurement is conducted each test day for the project. The check case blend chosen is 90% methane (CH_4) and 10% ethane (C_2H_6). The constituent gases for the check case were chosen because of the ease of blending that ratio. Figure 4-14 shows the resulting methane number results for the check case tests. The data suggests that the methane number measurement method developed in this work is repeatable to less than ± 2%. Note that the average methane number value for the check blend is 77.9, the mean value is 78.0, and the standard deviation is 1.85. Further, the AVL software "Methane" estimates the methane number for this mixture to be 78.9.

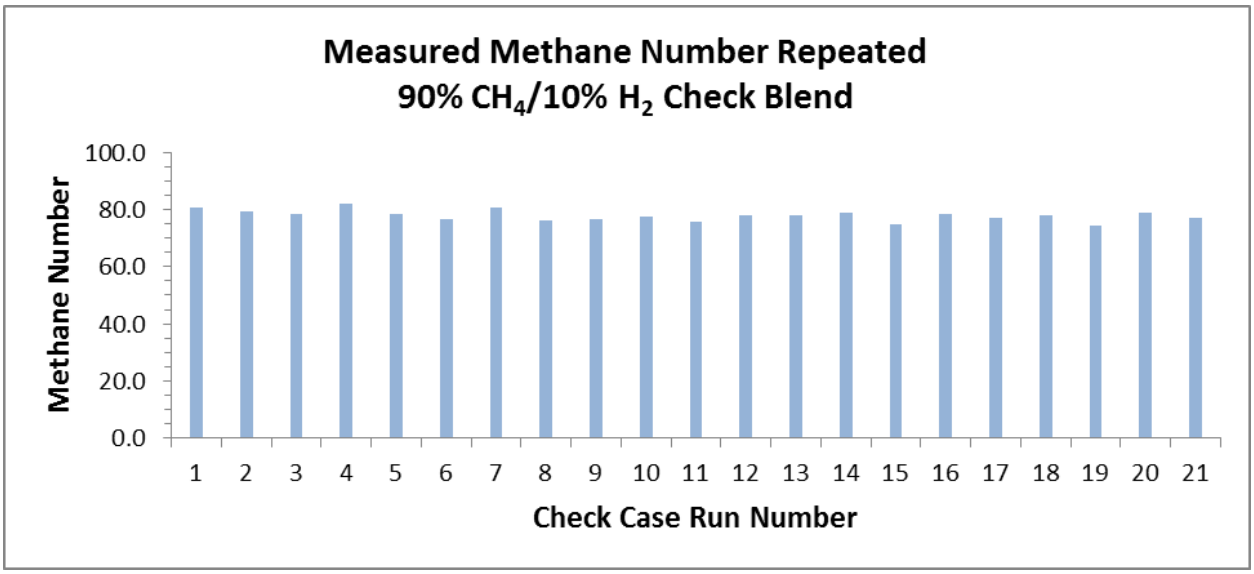

Figure 4-15 Check Case Results - 90% CH4, 10% C2H6

Details of knock integral data component data are provided for information. Figure 4-15 shows the average knock amplitude values for tested blends and their matching CH_4/H_2 blend. No consistent trend is observed examining those blends with the highest mismatch in average knock amplitude with regard to relative concentrations of carbon monoxide and hydrogen in the blends.

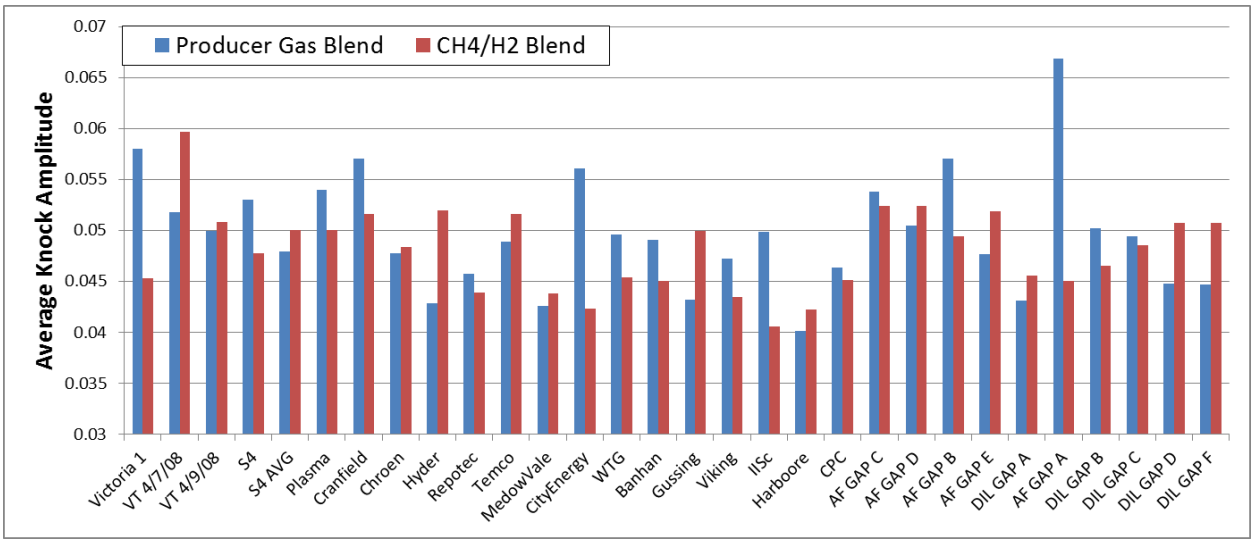

Figure 4-16 Average Knock Amplitude for Blends Tested

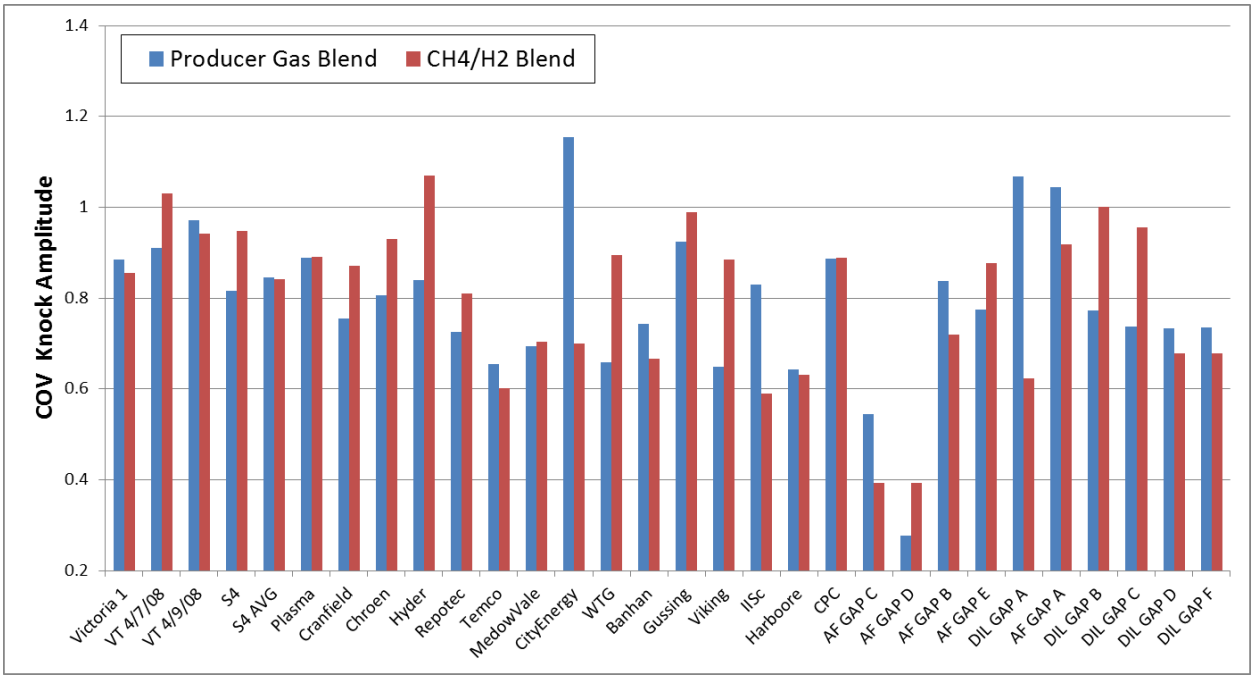

Figure 4-17 COV of Recorded Knock Amplitude for Tested Blends.

Figure 4-16 provides the values for Coefficient of Variance (COV) for the knock amplitude data recorded for each of the test blends. There is no apparent correlation of COV values to the magnitude of difference between the average knock amplitudes recorded.

Figure 4-17 provides a plot of average integral values for each of the test blends and the matching CH_4/H_2 blends. For the purpose of direct comparison, during the data collection process effort was made to capture the data at a consistent knock levels, this plot illustrates the variance encountered.

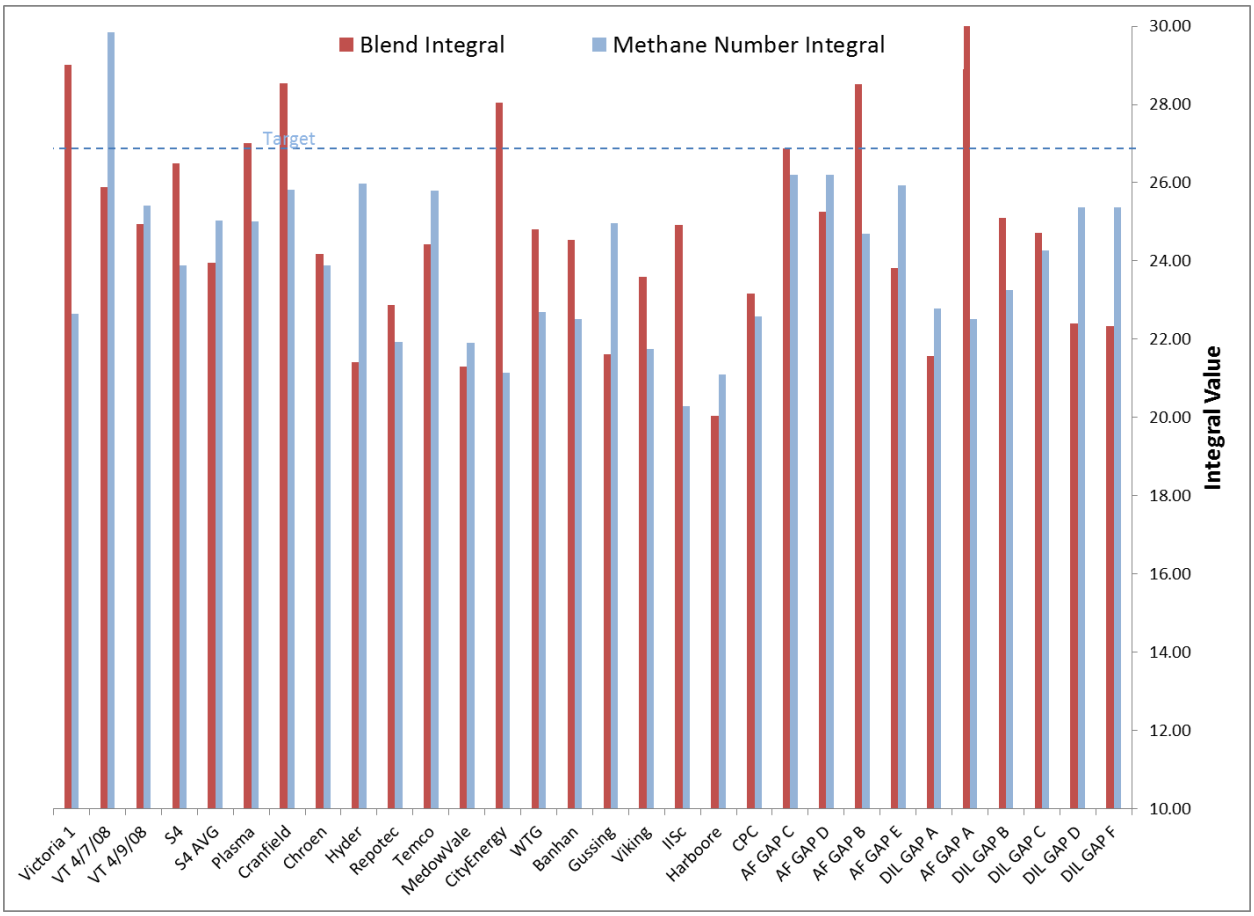

Figure 4-18 Average Integral Values By Blend For 500 Cycle Test Runs

5 TEST RESULTS

5.1 MEASURED METHANE NUMBERS

Table 5-1 provides a detailed list of the syngas blends tested. The table includes a volumetric percentage breakdown of constituent gases, total H_2 and CO percentage, total diluent percentage, heating value, stoichiometric air-fuel ratio, measured methane number, and methane number predicted by AVL software "Methane" (hereinafter referred to as AVL MN). A more detailed evaluation of the results is provided in following sections.

Table 5- 1 Producer Gas Blend Constituent Definition and Characterization

	N2	CO2	CO	H2	CH4	CO+H2	Diluent	MN	AVL MN	A/Fs	LHV
AF Gap A	4.95%	18.6%	34.3%	34.3%	7.8%	68.7%	23.6%	62.2	63.4	3.26	11472
AF Gap B	0.00%	18.6%	19.6%	33.0%	28.8%	52.6%	18.6%	93.5	71.6	6.11	19307
AF Gap C	14.08%	0.0%	18.8%	47.0%	20.2%	65.7%	14.1%	56.3	43.7	7.56	24548
AF Gap D	10.95%	5.1%	9.3%	47.1%	27.5%	56.4%	16.1%	56.3	49	8.65	27128
AF Gap E	10.43%	5.7%	11.4%	24.6%	47.9%	36.0%	16.1%	78.0	75.6	9.37	28348
Banham	0.00%	20.1%	21.1%	35.6%	23.3%	56.7%	20.1%	80.3	68.5	5.39	17316
Blend #1	7.00%	17.0%	37.0%	39.0%	0.0%	76.0%	24.0%	35.9	55.1	2.55	9664
Blend #2	48.00%	14.0%	18.0%	18.0%	2.0%	36.0%	62.0%	96.7	85	1.20	4362
Blend #3	11.00%	6.0%	12.0%	26.0%	45.0%	38.0%	17.0%	71.0	73.9	8.96	27214
Blend #4	15.00%	15.0%	20.0%	50.0%	0.0%	70.0%	30.0%	25.7	41.4	2.78	10195
Blend #5	15.00%	0.0%	20.0%	50.0%	15.0%	70.0%	15.0%	31.9	39.4	6.80	22536
Chroen (O2)	0.10%	20.4%	39.3%	40.2%	0.0%	79.5%	20.5%	25.9	56.5	2.64	10004
City Energy	28.9%	0.3%	0.3%	26.4%	44.0%	26.7%	29.2%	92.0	73.2	8.81	26273
CPC	56.70%	1.4%	21.0%	18.7%	2.2%	39.7%	58.1%	66.2	74.8	1.45	5292
Cranfield	0.30%	22.2%	17.1%	52.4%	8.1%	69.5%	22.5%	51.1	48.8	4.14	14121
Dil Gap A	11.94%	6.5%	13.0%	28.2%	40.3%	41.3%	18.5%	90.2	71	8.28	25360
Dil Gap B	3.19%	24.5%	25.5%	42.6%	4.3%	68.1%	27.7%	46.3	57.8	2.89	10285
Dil Gap C	15.84%	15.8%	18.8%	49.5%	0.0%	68.3%	31.7%	21.5	42	2.67	9785
Dil Gap D	22.54%	18.6%	45.1%	6.9%	6.9%	52.0%	41.2%	97.6	96.9	1.94	7024
Dil Gap F	41.06%	14.5%	22.2%	17.4%	4.8%	39.6%	55.6%	97.6	86.6	1.62	5570
Gussing	3.00%	23.0%	24.0%	40.0%	10.0%	64.0%	26.0%	68.2	61.6	3.58	12186
Harboore	40.70%	11.9%	22.8%	19.3%	5.3%	42.1%	52.6%	91.1	80.6	1.80	6335
Hyder	5.40%	6.7%	13.3%	27.3%	47.3%	40.6%	12.1%	79.4	73.1	9.74	29625
IISc	48.50%	12.0%	19.0%	19.0%	1.5%	38.0%	60.5%	96.0	81.5	1.23	29625
Meadow Vale	8.8%	8.0%	31.0%	15.6%	36.6%	46.6%	16.8%	86.0	81.6	6.40	20088
Plasma	3.30%	17.3%	38.0%	39.8%	1.6%	77.8%	20.6%	23.2	55.4	2.88	10720
Repotec	5.00%	20.0%	25.0%	40.0%	10.0%	65.0%	25.0%	58.5	59.6	3.70	12629
S4 Avg	5.10%	19.2%	35.4%	35.4%	5.1%	70.7%	24.3%	46.6	61.8	2.95	10613
S4 Example	2.10%	11.4%	41.1%	42.7%	2.8%	83.8%	13.5%	29.9	49.8	3.56	13129
TEMCO	19.20%	14.3%	52.8%	6.6%	7.0%	59.4%	33.5%	91.3	89.9	2.18	7993
Victoria 1	11.30%	5.3%	9.6%	48.6%	25.2%	58.2%	16.6%	56.1	47.1	8.32	26237
Viking	33.30%	15.4%	19.6%	30.1%	1.6%	49.7%	48.7%	70.0	63.4	1.73	6282
VT 4/7/08	8.40%	8.6%	37.7%	24.2%	21.2%	61.9%	17.0%	58.1	69.5	4.92	16293
VT 4/9/08	2.30%	8.1%	51.7%	20.3%	17.5%	72.0%	10.4%	60.5	70.4	4.48	15327
WTG	1.2%	17.6%	44.0%	22.1%	15.1%	66.1%	18.8%	73.3	76.2	3.75	12838

5.2 CRITICAL COMPRESSION RATIO, MEASURED METHANE NUMBER AND NMEP

Data is collected for the critical compression ratio corresponding to methane number (% methane in hydrogen) at fixed ignition timing (17°bTDC) and varied nmep levels starting at naturally aspirated conditions and progressing through 9, 10, 11, and 12 bar nmep. Figures 5-1

through 5-5 provide the data plots for the first five conditions, Figure 5-6 provides the combined data plots.

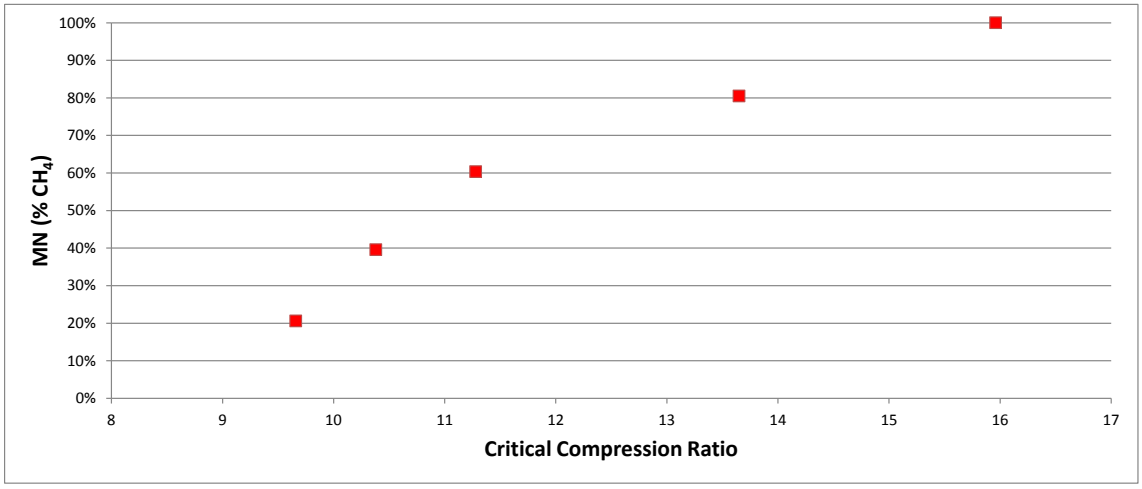

Figure 5-1 Methane Number vs. Critical Compression Ratio, nmep = 9 bar.

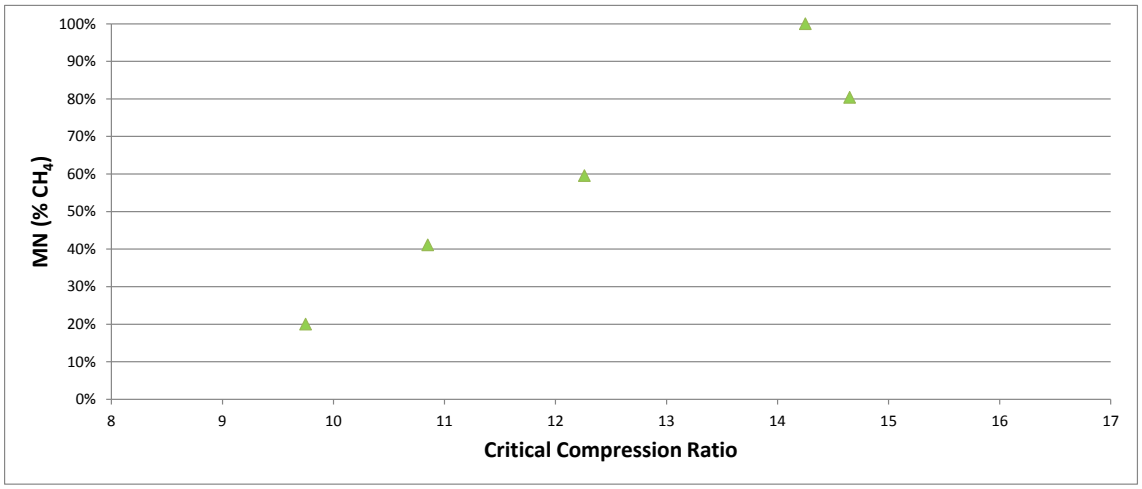

Figure 5-2 Methane Number vs. Critical Compression Ratio, nmep = 10 bar.

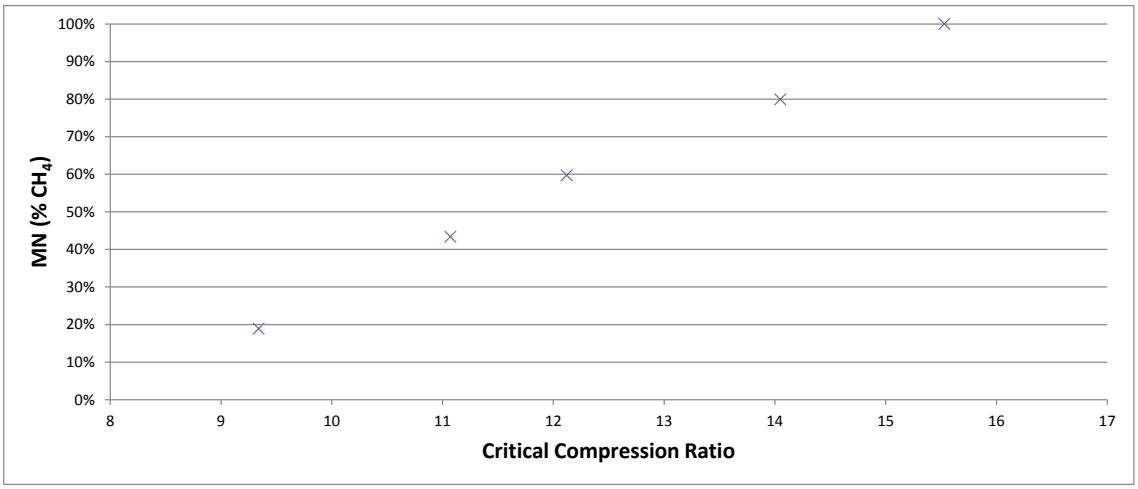

Figure 5-3 Methane Number vs. Critical Compression Ratio, nmep = 11 bar.

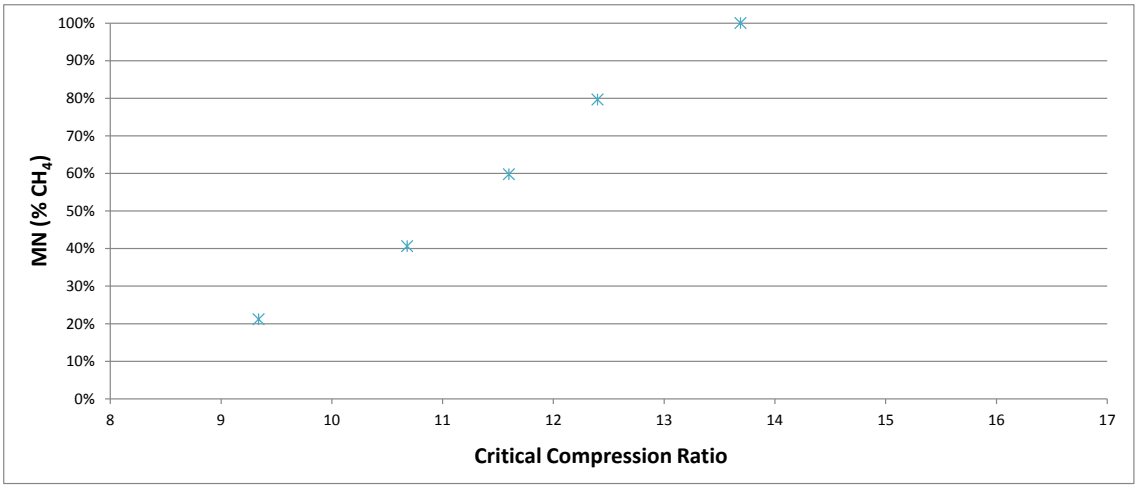

Figure 5-4 Methane Number vs. Critical Compression Ratio, nmep = 12 bar.

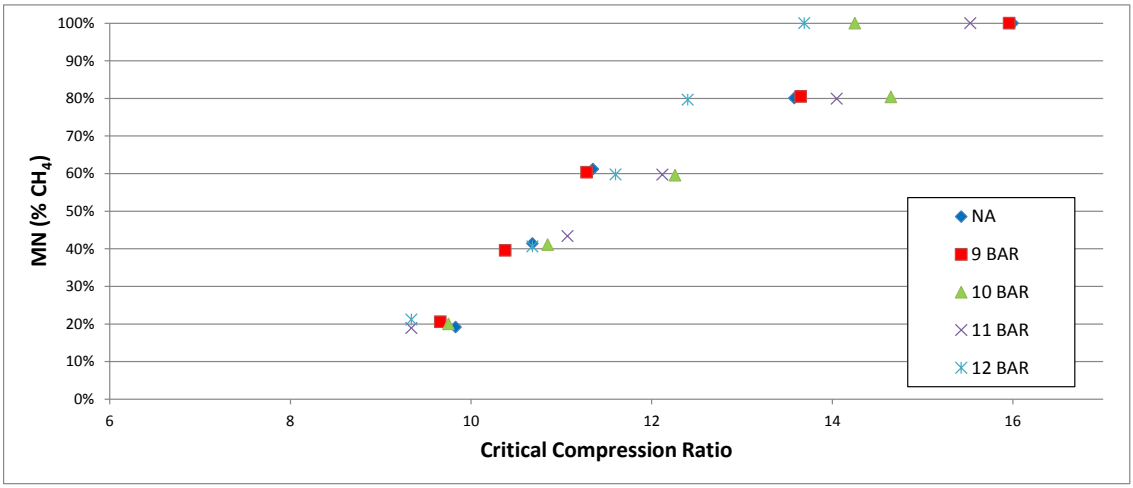

Figure 5-5 Methane Number vs. Critical Compression Ratio, Combined.

5.3 Methane Number Sensitivity to Operational Parameters Results

As discussed in Section 4-4 of this dissertation methane number measurements are conducted for varying engine operating parameters of ignition timing, stoichiometric air-fuel ratio, and intake boost (nmep) as defined in Table 4-1. The results for these tests conducted for natural gas are given in Figure 5-7 along with a charted value for the AVL MN.

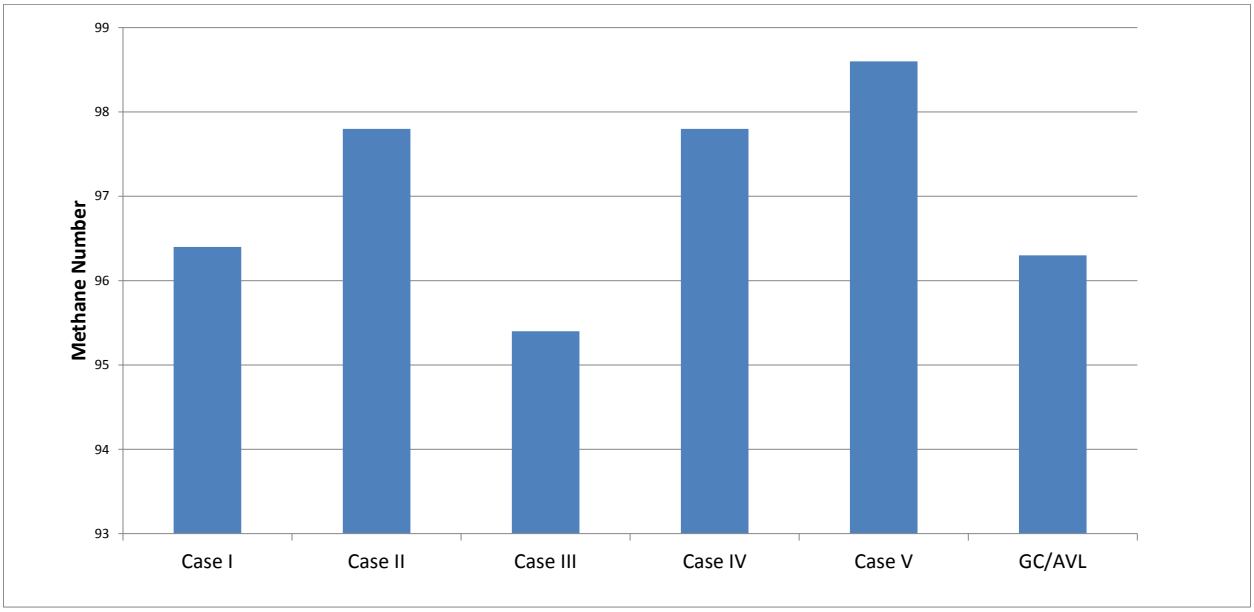

Figure 5-6 Natural Gas Measured Methane Number.

Varied parameter testing is attempted for producer gas blends 1 through 5. When intake boost is increased to raise nmep for blends with low stoichiometric air-fuel ratios the test cell is unable to maintain controlled operation of the engine, therefore the data is not complete for blends 1, 2 and 4. Substantial time is required to establish each fuel blend so that for varied parameter testing of blends 3 and 5 critical compression ratio is recorded at the point of knock inception and steady knock integral rather than collapsing the blend mix to switch to methane/hydrogen for direct methane number measurement. The results of varied parameter

testing, by critical compression ratio, for syngas blends 3 and 5 are provided in Figure 5-8. Note that critical compression ratio indicates the critical compression ratio where the methane/hydrogen blend would be used to evaluate methane number. It does not constitute the complete methane number measurement. To obtain an accurate indication of methane number variability with ignition timing, nmep, and equivalence ratio the complete methane number measurement would need to be executed, as was done to generate the data in Figure 5-7.

The trends evident in transitioning from one case to another are interesting and warrant more thorough investigation. The engine operating difference from Case I to Case II is advancing ignition timing from 17°bTDC to 23°bTDC and one would expect knock to occur more readily, at lower compression ratio, with advanced spark timing. From Case II to Case III ignition timing is retarded from 23°bTDC back to 17°bTDC, which should serve to delay knock onset but at the same time nmep is dramatically increased, from approximately 8 bar to 12 bar. The net effect is slight reduction of critical compression ratio. From Case III to Case IV nmep level is held constant, ignition timing is advanced, which should increase knock onset, and combustion is made lean (ϕ from 1.0 to 0.7), which should diminish knock onset. The net effect is that natural gas and blend 5 see a slight increase in critical compression ratio, blend 3 a slight reduction. Finally, in the transition from Case IV to Case V ignition timing and nmep are held constant and combustion is brought to stoichiometric from lean conditions, the effect is slight reduction in critical compression ratio for all three fuel gases.

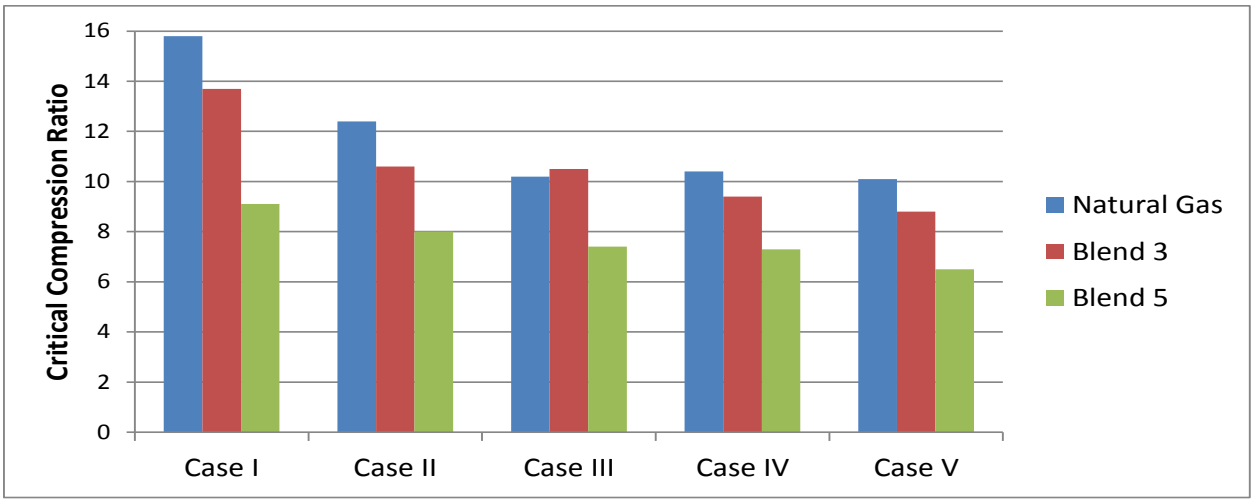

Figure 5-7 Critical Compression Ratio for NG and Blends 3 & 5

5.4 Heating Value, Methane Number, NMEP and Intake Boost Pressure

Measured methane number and calculated Lower Heating Value (LHV) are plotted to investigate possible trends and tendencies between the two properties. Figure 5-8 provides a plot of developed nmep under naturally aspirated conditions as well as lower heating value for syngas blends 3 and 5 and the check-case blend (90% CH_4/10% C_2H_6). The syngas blends have significantly smaller LHV values. However, the nmep is not proportionally decreased. This is because the energy per unit volume of the stoichiometric mixtures does not change nearly as much, 3.13 kJ/std. liter for the check-case, 3.01 kJ/std. liter for Syngas Number 3, and 2.96 kJ/std. liter for Syngas Number 5. These values explain the nmep general trend, assuming that the same volume of gas at the same temperature and pressure is inducted in each case. For the syngas blends the fuel flow is increased to partially compensate for the reduced heating value. However, the increase in fuel flow displaces air so the nmep is still lower than the value

for natural gas. There also may be differences in brake efficiency due to variation in combustion phasing.

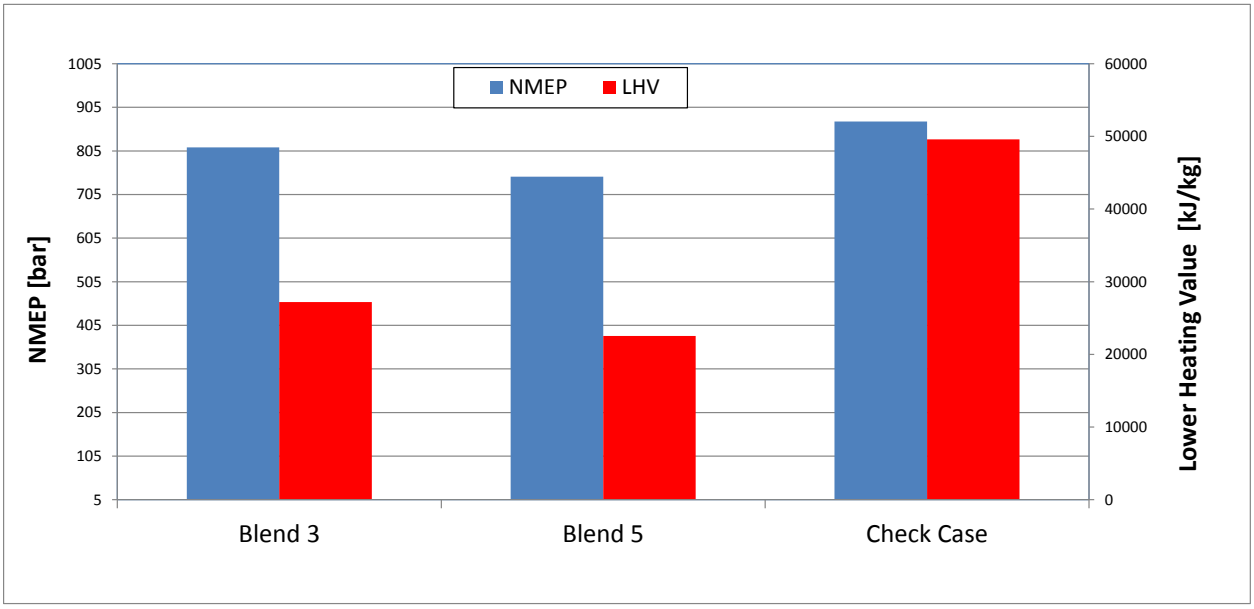

Figure 5-8 NMEP Developed Under Naturally Aspirated Operation and LHV

Figure 5-9 provides a scatter plot of methane number and lower heating value of tested syngas blends with relative percentages of fuel gas (CO and H_2) identified. High (>60%), medium (30-60%), and low percentages are indicated. The correlation between lower heating value and methane number is nonexistent. This is because the percentage of pro-knock species ($CO+H_2$) is more critical than the fuel energy content.

An evaluation was made of general syngas blend performance with the CFR engine with regard to developed nmep, intake boost pressure to achieve a desired nmep and lower heating value of the fuel. Figure 5-10 provides plotted results of these comparisons.

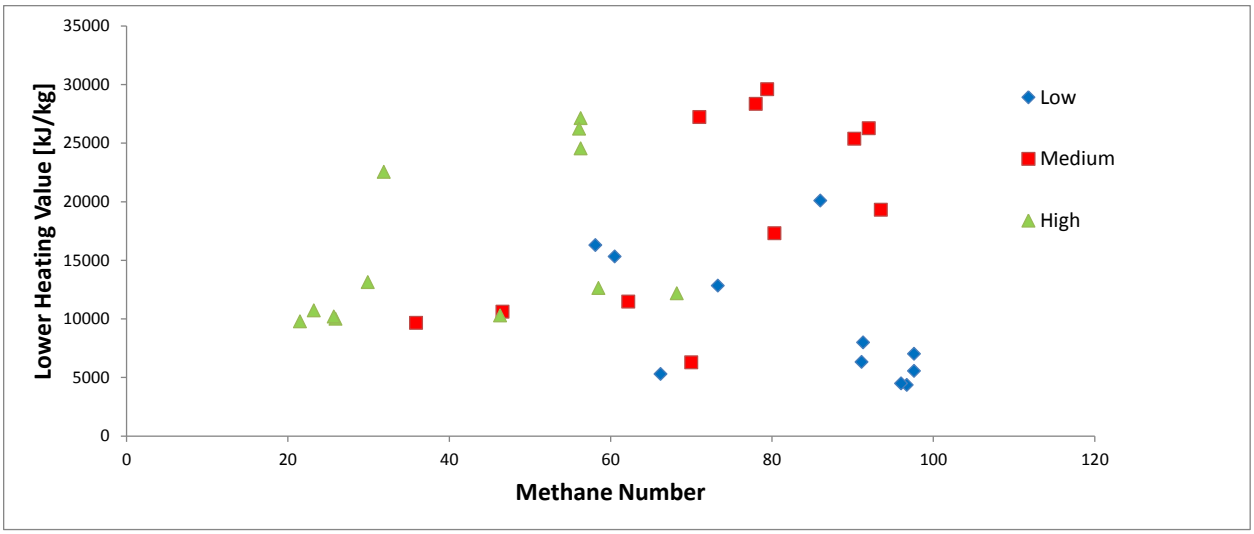

Figure 5-9 Heating Value vs. Methane Number

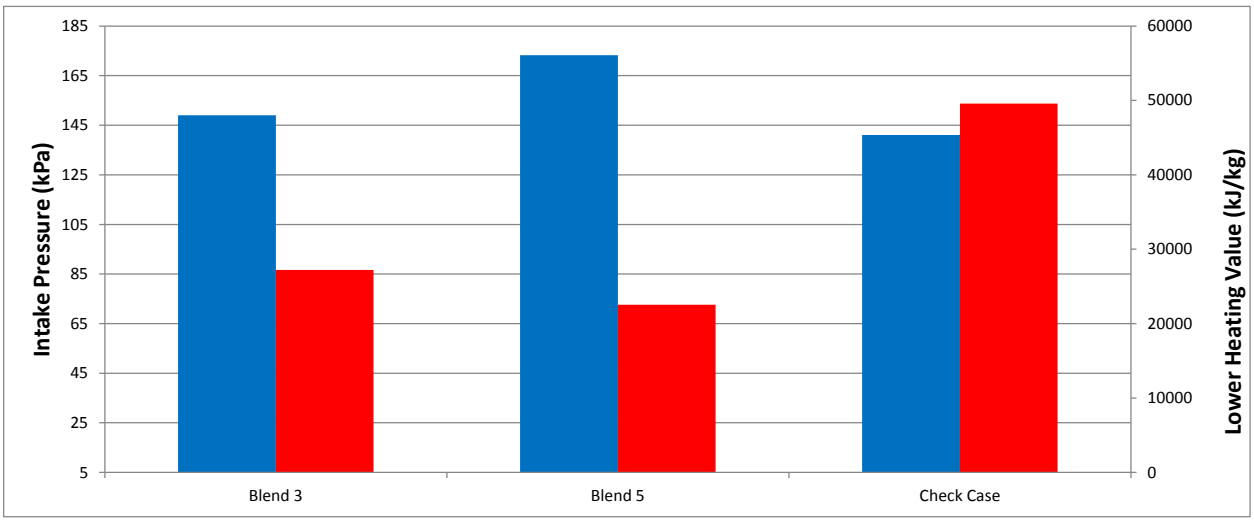

Figure 5-10 Intake Pressure to Achieve 12 bar NMEP and Fuel LHV

5.5 COMBUSTION ANALYSIS

Data is presented correlating measured methane number to ignition delay. Figure 5-11 provides a scatter plot of all tested blends correlating methane number and ignition delay while highlighting relative diluent percentage. With the exception of two outlying data points it appears that there is a clear trend of increased ignition delay and resistance to knock. To state this in a different way, there is a direct correlation between the flame initiation process and the spontaneous combustion of the end gas. A fuel with a shorter flame initiation period will have a lower methane number and knock more readily. Conversely, a fuel with a longer flame initiation period will have a higher methane number and be less likely to knock. Early flame development is strongly related to laminar flame speed; consequently, methane number is expected to correlate to laminar flame speed.

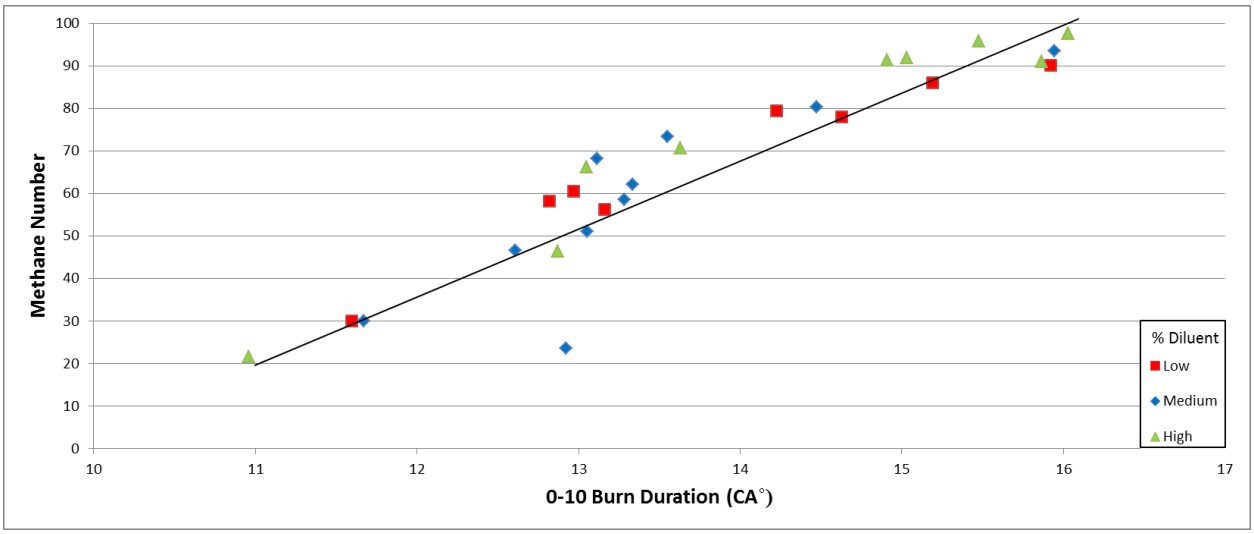

Figure 5-11 Measured Methane Number vs. Ignition Delay

Combustion phasing and the correlation to methane number is illustrated in Figure 5-12. Ignition timing for all tests is set at 17°bTDC. Relative entrained diluent percentage is highlighted. The trend is that the 50% burn location is retarded with the fuel's resistance to knock. The 50% burn location is a measure of overall combustion rate, which is related to ignition delay, laminar flame speed, and turbulence level. Turbulence level for all NA cases is similar, since engine operating parameters that influence turbulence such as speed and combustion chamber geometry do not change. Similar to the arguments above, this data indicates that laminar flame speed is related to the methane number and the knock tendancy of a fuel.

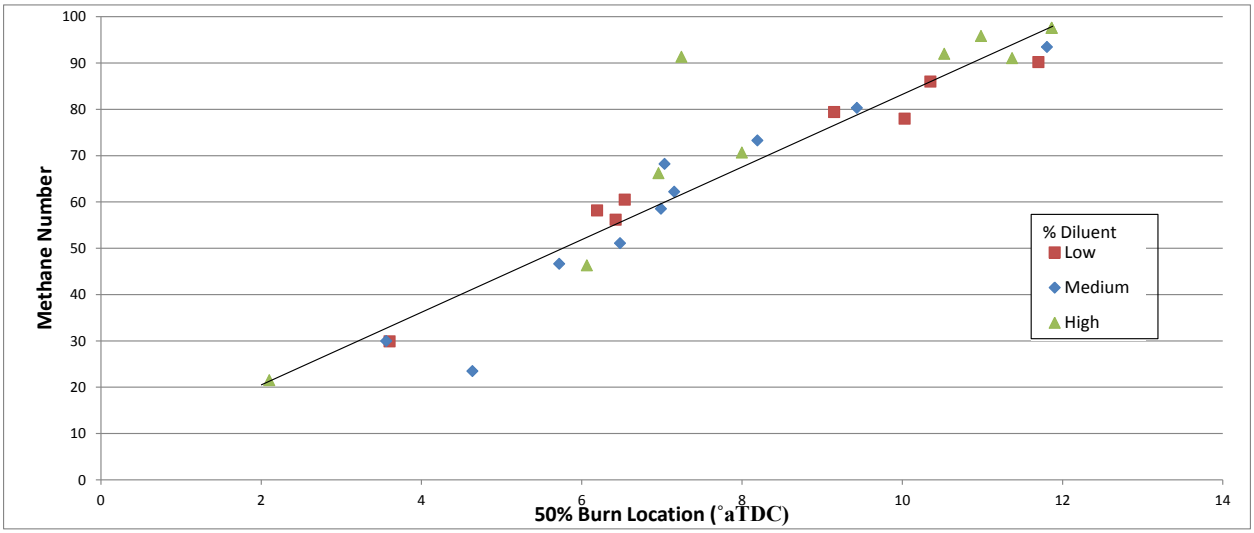

Figure 5-12 Methane Number vs. Combustion Phasing (50% Burn Location)

The impact of measured methane number on the location of peak pressure is shown in Figure 5-13. Relative entrained diluent percentage is highlighted. While the location of peak pressure is generally retarded with increased resistance to knock, the trend is less linearly progressive. This is most likely due to the non-linear relationship between crank angle and cylinder volume.

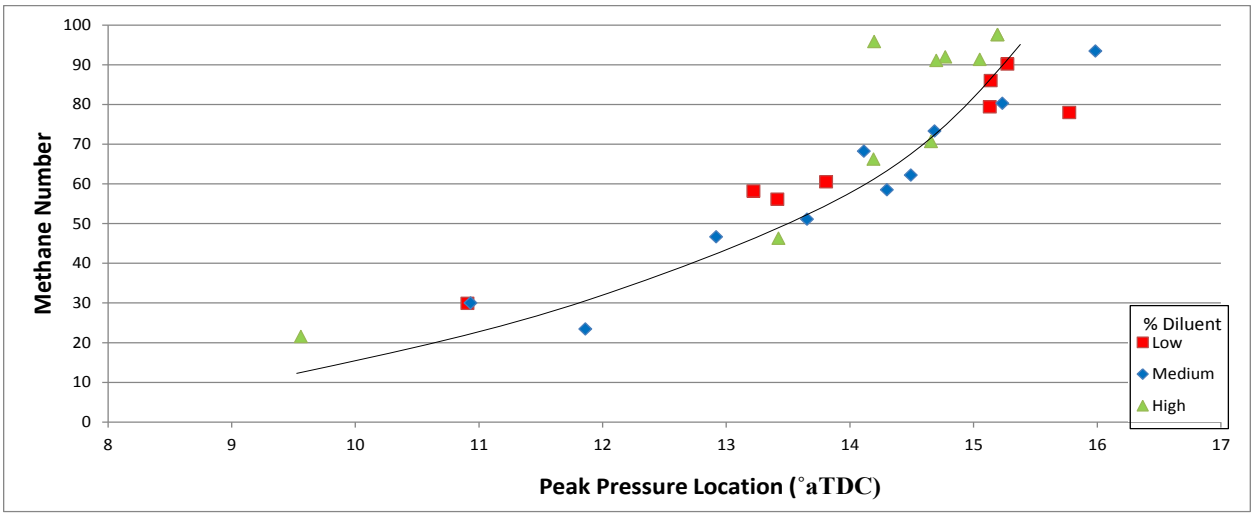

Figure 5-13 Methane Number vs. Location of Peak Pressure

5.6 Correlation of Measured Methane Number to Predicted

A comparison is made to the difference between measured methane number and the AVL methane number. Figure 5-14 shows a bar chart showing the tested blends arranged in order beginning with blends in which the AVL predicted methane number was higher than the methane number measured.

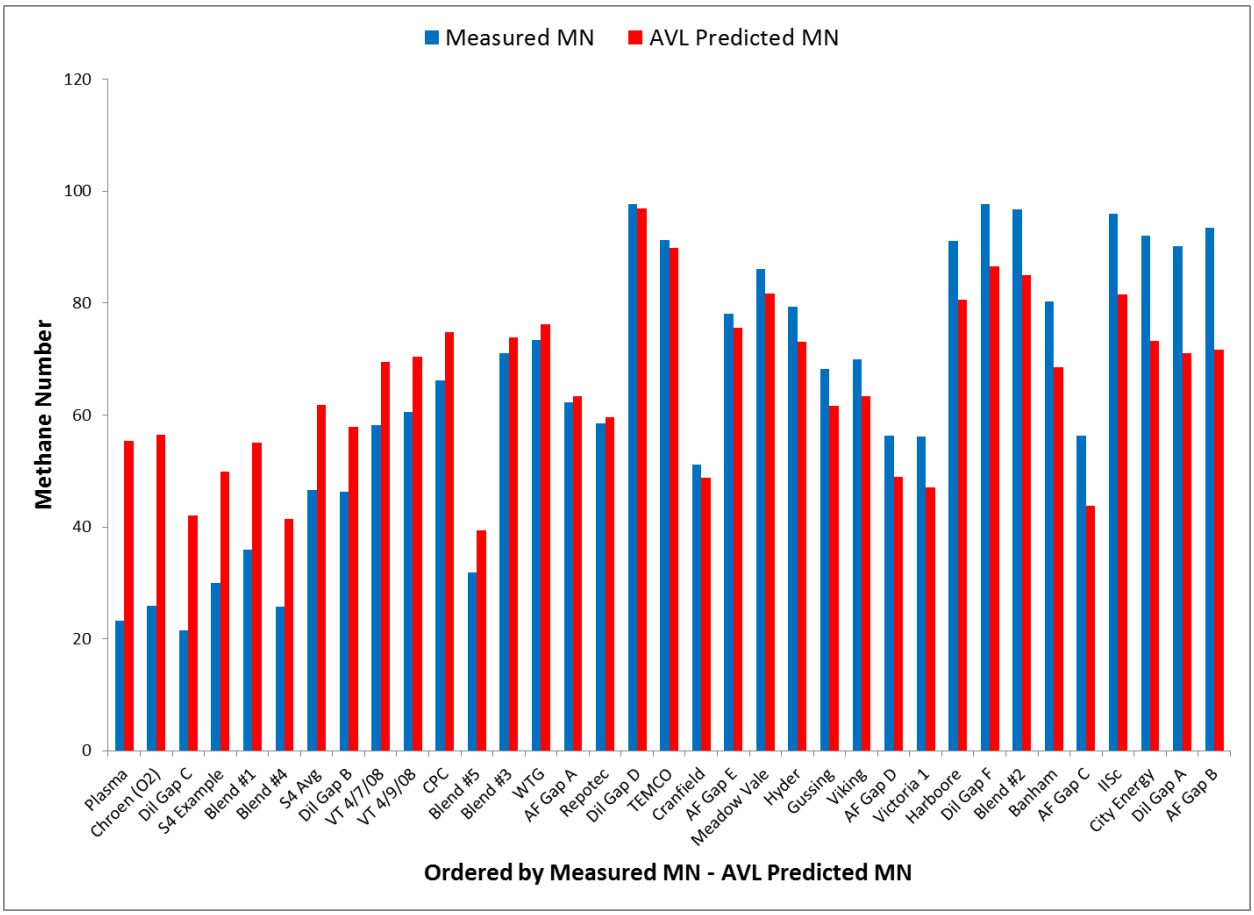

Figure 5-14 Measured and Predicted (AVL) Methane Numbers.

The next group of data plots are compiled to illustrate the relationship, if any, between the difference of measured and predicted (AVL) methane numbers and characteristic gas content in the syngas blend; specifically methane percentage, fuel gas (CO and H_2) percentage, and diluent (CO_2 and N_2) percentage are presented in Figures 5-15, 5-16, and 5-17, respectively.

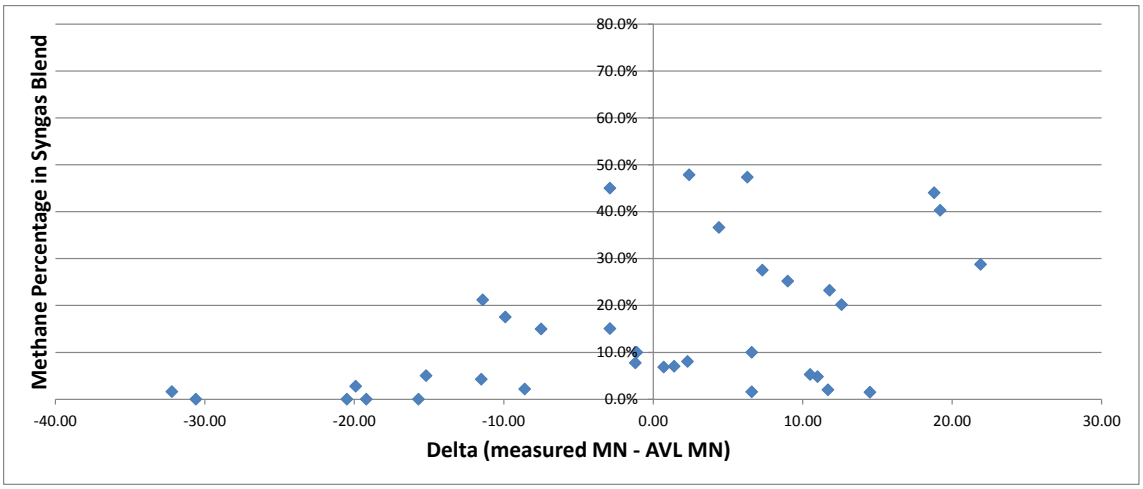

Figure 5-15 CH4 Percentage vs. Measured/Predicted Methane Number Delta.

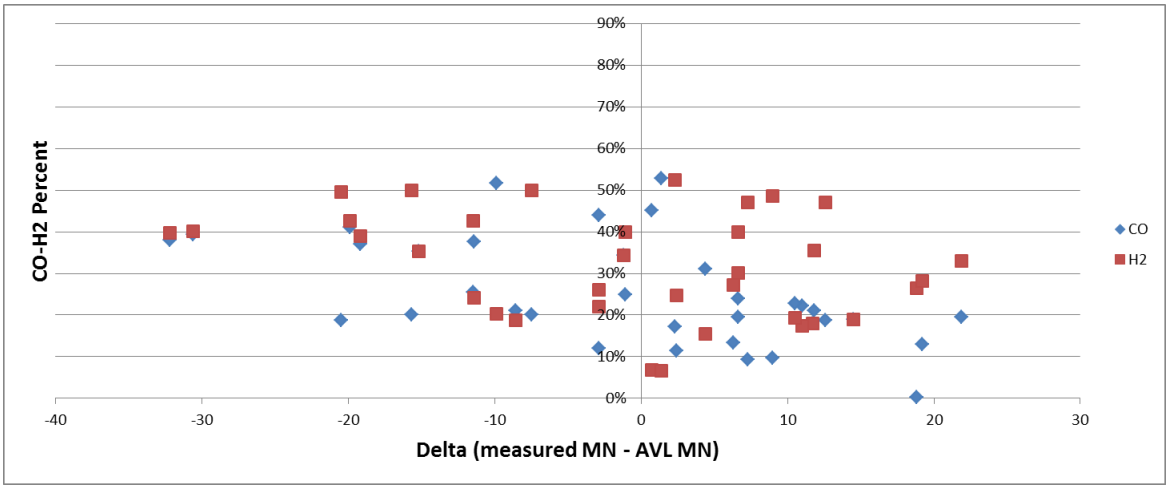

Figure 5-16 CO and H2 Percentage vs. Measured/Predicted Delta.

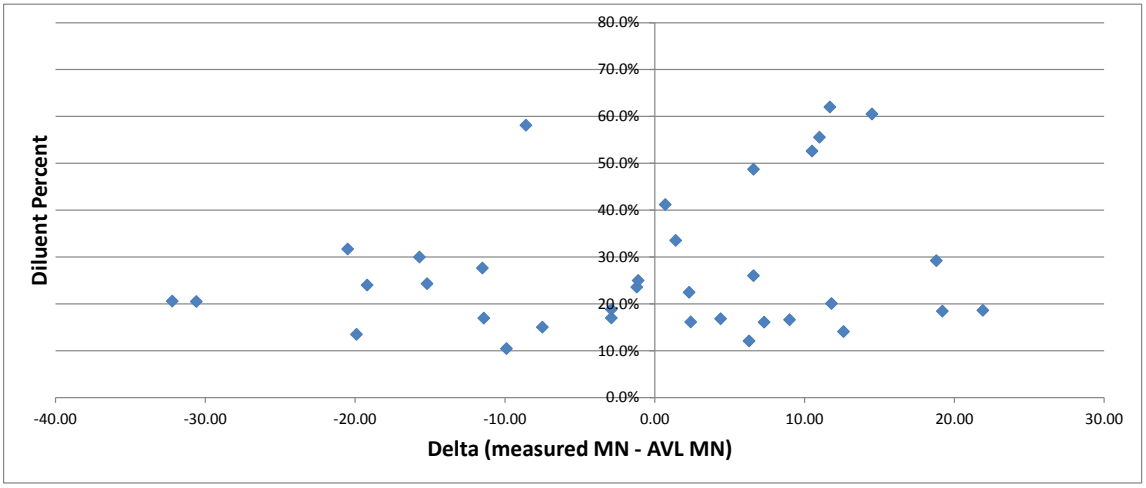

Figure 5-17 CO2 + N2 Percentage vs. Measured/Predicted Delta.

It is difficult to draw definitive conclusions from the data because the effects of diluent and combustible composition are not isolated. However, some general observations can be made. The data show the magnitude of the difference between measured and AVL methane numbers larger than 30 methane number units in some cases. The largest difference magnitude occurs for two blends with large CO and H_2 content and very little methane content; for these cases the difference is negative, meaning the AVL model over-predicts methane number. Figure 5-16 shows that as the CO and H_2 content increase, the amount that the AVL method over predicts increases (difference decreases). It appears that the AVL method is not highly sensitive to CO and H_2 content. There is no observable trend in AVL method accuracy with diluent as depicted in Figure 5-17.

5.7 Impact of Diluent and Fuel Gas Content on Measured Methane Number

Figure 5-19 provides a scatter plot of the measured methane number and the entrained percentage of diluent (CO_2 and N_2) in the syngas blends. No strong correlation presents itself.

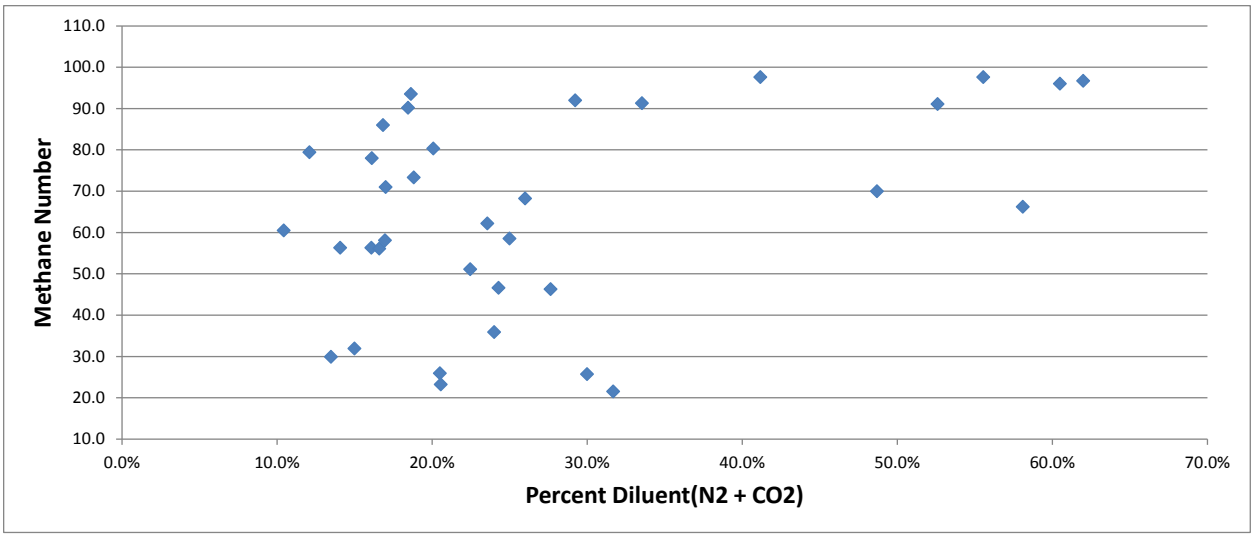

Figure 5-18 Measured Methane Number vs. Diluent Content

Figure 5-20 provides a scatter plot of the measured methane number and the entrained percentage of fuel gas (CO and H_2, CH_4 not included) in the syngas blends. Generally methane number decreases as fuel H_2+CO content increases. This trend is identifiable in spite of variations in fuel diluent. Presumably, the scatter in the data is due to variations in diluent. Significant concentration of methane also causes scatter in the data.

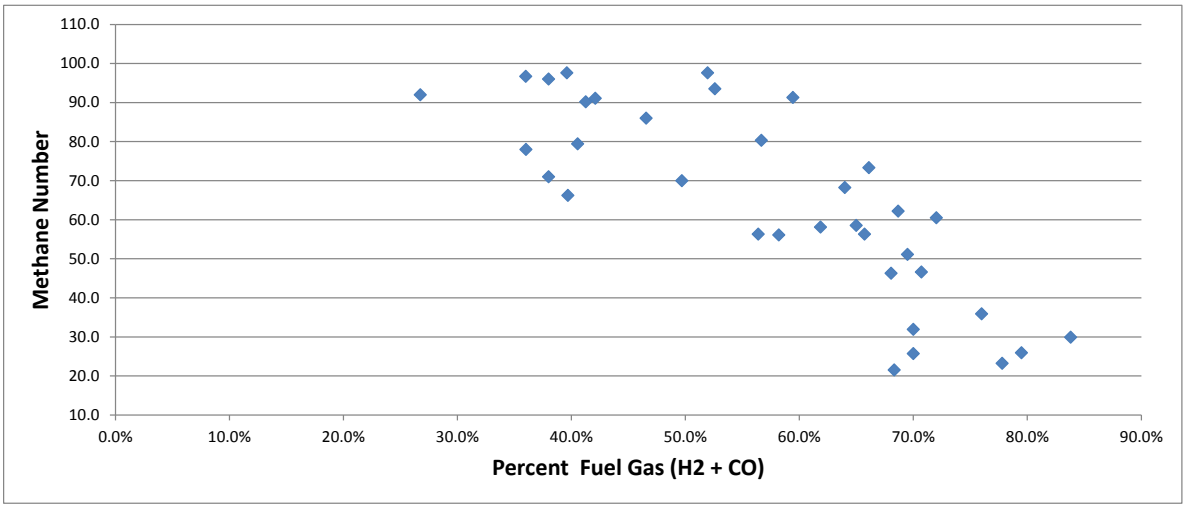

Figure 5-19 Measured Methane Number vs. Fuel Gas Content

Figure 5-21 provides a scatter plot showing energy content of the syngas blend (lower heating value) vs. measured methane number. The percentage of entrained fuel gas is indicated. No apparent correlation exists.

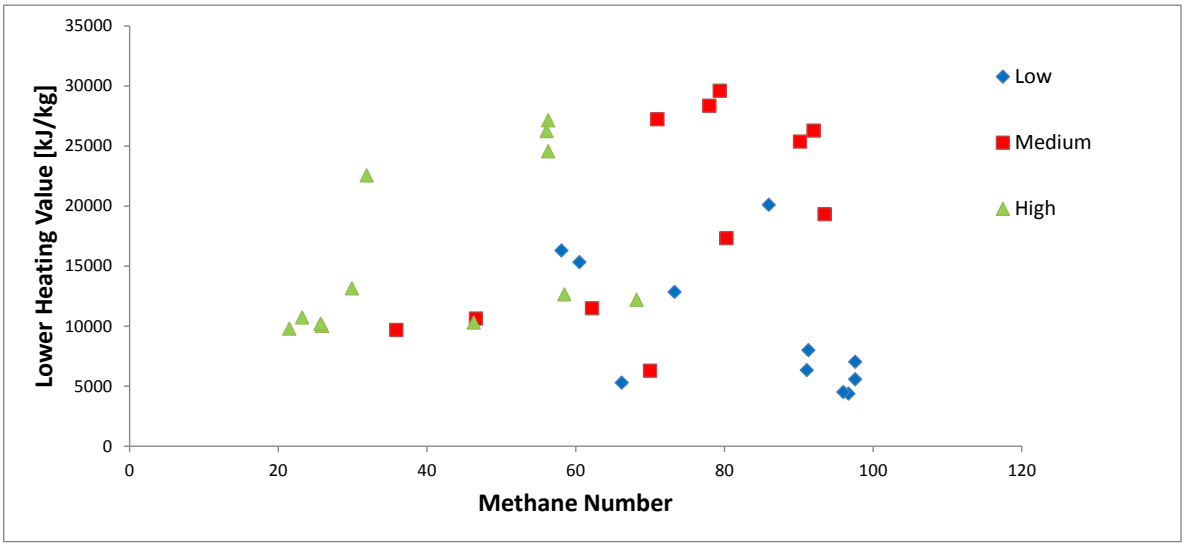

Figure 5-20 Syngas Blend Lower Heating Value vs. Methane Number

6 PREDICTING METHANE NUMBER FOR PRODUCER GAS BLENDS

A variety of methods and algorithms to predict methane number for natural gas blends exist and are made available by engine manufacturers as well as industry groups, energy research organizations and consultants. The methane number predicting software most commonly referenced is the AVL program "Methane" developed based on the work by Leiker, et. al. in the early 1970's. As described in Chapter 5 of this work the results for predicted versus actual methane number for producer gas blends using the AVL software is observed to be inconsistent. In this chapter an investigation is presented regarding the use of two approaches to develop a consistent and reliable predictive tool for producer gas methane number. The first is the evaluation of a chemical kinetics model enabled by the use of the software "CHEMKIN" (Release 10112) in which the point of auto-ignition of a producer gas blend is modeled and then compared to the modeled auto-ignition point of a blend of methane and hydrogen wherein the percentages of methane and hydrogen are adjusted until the modeled results very nearly match that of the original producer gas blend. The resulting percentage of methane in the mixture is defined to be the methane number. The second approach is through the use of neural network methodology software to establish methane number solely based on the input variables of constituent percentage and observed experimental methane number measurement.

6.1 CHEMKIN MODELING OF PRODUCER GAS BLENDS

CHEMKIN is a chemical kinetics simulation program originally developed at Sandia National Laboratory. The software includes an internal combustion engine module that provides a zero dimensional model of an internal combustion engine simulating auto-ignition of stipulated

air-fuel mixtures. Input parameters to the program include specific engine geometries, operating speed, fuel composition, stoichiometric conditions, and heat transfer models (Kee, et al., 1996). Engine geometries include displacement volume, connecting rod to crank radius ratio, starting crank angle and compression ratio. Fuel composition is entered into the program by individual constituent and stoichiometric conditions are specified to define air flow to the engine. The program allows heat transfer characteristics through the cylinder wall to be selected ranging from adiabatic assumptions, constant heat rejection, heat rejection based on an input time dependent profile, or use of the Woschni heat transfer correlation (Chang, et al., 2004). For the purpose of this work the engine geometries and operating speed of the CFR F2 engine are input to the program, and the default cylinder wall heat rejection model is used. The rationale for use of the default heat transfer mechanism is that the methane number determination is based on comparison of the stipulated fuel gas to a mixture of methane and hydrogen. The comparison should be valid provided the same heat transfer mechanism is employed in both cases. The input parameters describing engine characteristics used in this model are provided in Table 6-1.

Table 6- 1 CHEMKIN IC Engine Model Input Parameters

Displacement Volume	37.331 in^3 [611.7 cm^3]
Connecting Rod to Crank	4.444
Engine Speed	940 rpm
Starting crank angle	-180°

6.1.1 Chemical Kinetics Mechanism Selection

Arunachalam incorporated the CHEMKIN IC Engine Model to predict methane number for selected producer gases in a previous study (Arunachalam, 2010). Several chemical kinetic mechanisms were evaluated in that study concluding that the modeled results for the "Güssing" producer gas blend most nearly matched experimental results for methane number when utilizing the USCII mechanism, a compilation of 784 chemical reactions and 111 species comprehensive of high temperature H_2/CO/C_1-C_4 combustion (Wang, et al., 2007).

The chemical kinetics mechanism utilized in this work is the natural gas mechanism developed at the National University of Ireland, Galway, NUIG NGM, a compilation of 1359 reactions and 229 species, optimized for natural gas and methane combustion (Zsély, et al., 2011).

6.1.1 Procedural Method for Methane Number Prediction

In the course of using CHEMKIN as a modeling vehicle it is desired to closely replicate the experimental procedure used to measure methane number. The following section provides a description of the process used to determine methane number.

The model is executed using input values for the producer gas in question, under stoichiometric conditions, with all input conditions constant less compression ratio which stepped in appropriate increments. The actual CFR F2 engine has the capability to vary compression ratio from 4:1 to 18:1; however, this model simulates auto-ignition in the cylinder and not auto-ignition in an end gas concentration after spark initiation. Consequently it was determined that very low compression ratio values will not initiate combustion, so a starting

value of 10:0 is chosen as the lower compression ratio input. Figure 6-1 shows the modeled pressure versus crank angle plots for a sequence of compression ratios.

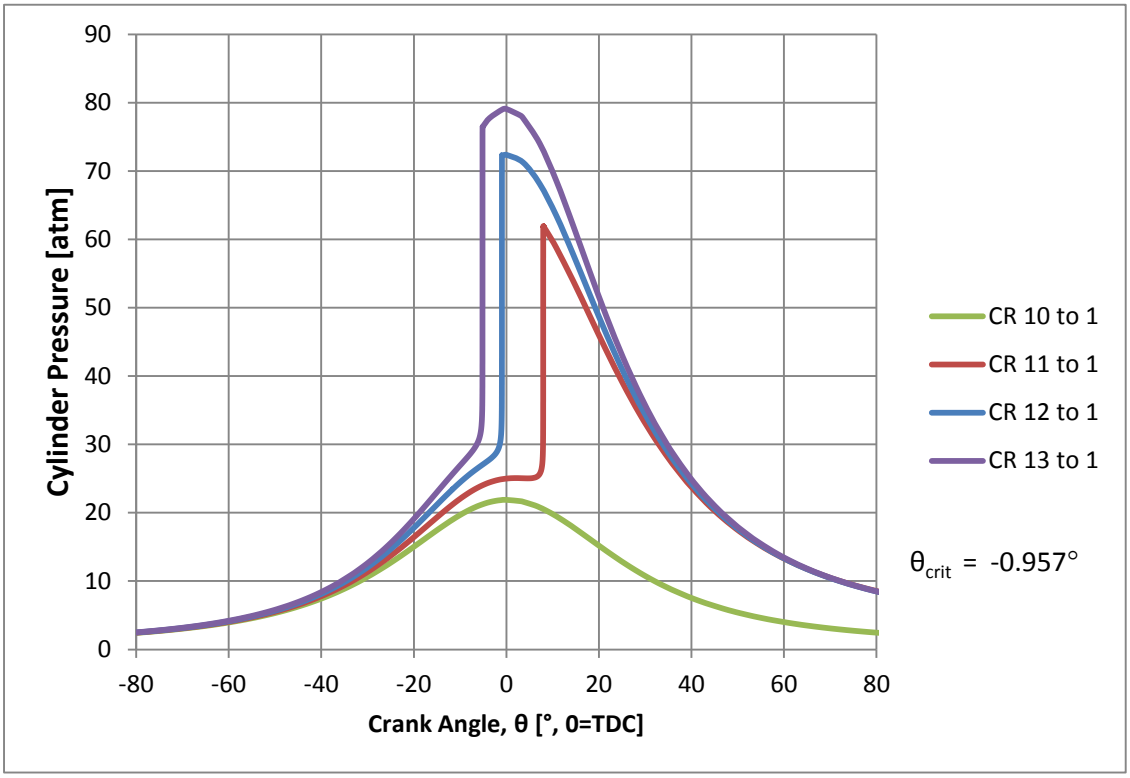

Figure 6-1 CHEMKIN Model Pressure vs. Crank Angle for the Güssing Blend.

The point of simulated auto-ignition is determined by the peak change in pressure per unit change in crank angle, a form of in-cylinder $dP/d\theta$ which has been used previously as a metric to define initiation of engine knock (Barton, et al., 1970). It can be observed in Figure 6-1 that the point of simulated auto-ignition advances with increased compression ratio. The results of the initial sequence for the Güssing and subsequent producer gas blends are further refined by running additional sequences with smaller incremental steps to determine the compression ratio that results in the point of auto-ignition occurring reasonably near to TDC (within ±1°). That crank angle is designated θ_{crit} for the simulation. The corresponding compression ratio is held as

the critical compression ratio for the blend, and designated r_{crit}. It is noted that Arunachalam, in her simulation using CHEMKIN, adjusted compression ratio until auto-ignition first occurred not noting specific crank angle. The approach in this work is attempted in an effort to refine the process (Arunachalam, 2010).

The simulation is then repeated with all input values held constant, including r_{crit}, for a methane and hydrogen mixture under stoichiometric conditions. The percentage of hydrogen in the mixture is varied until the point of auto ignition, θ_{crit}, very nearly matches that determined for the associated producer gas blend. Figures 6-2 and 6-3 show the results obtained for methane number matching the Güssing blend. Figure 6-3 is merely expanded for clarity around TDC (θ = 0) to illustrate the effect of slight variance in methane-hydrogen proportioning.

In the event that 100% methane auto-ignites too early for a given value of r_{crit} the procedure is to add carbon dioxide to methane until auto-ignition occurs at θ_{crit}. The methane number is determined by summing the percentage of CO_2 in the blend to 100. For example, a methane number of 110 would result if the matching gas blend consisted of 90% methane and 10% CO_2. For the producer gas blends evaluated in this work, both experimentally and those modeled in CHEMKIN, a methane number greater than 100 was not encountered.

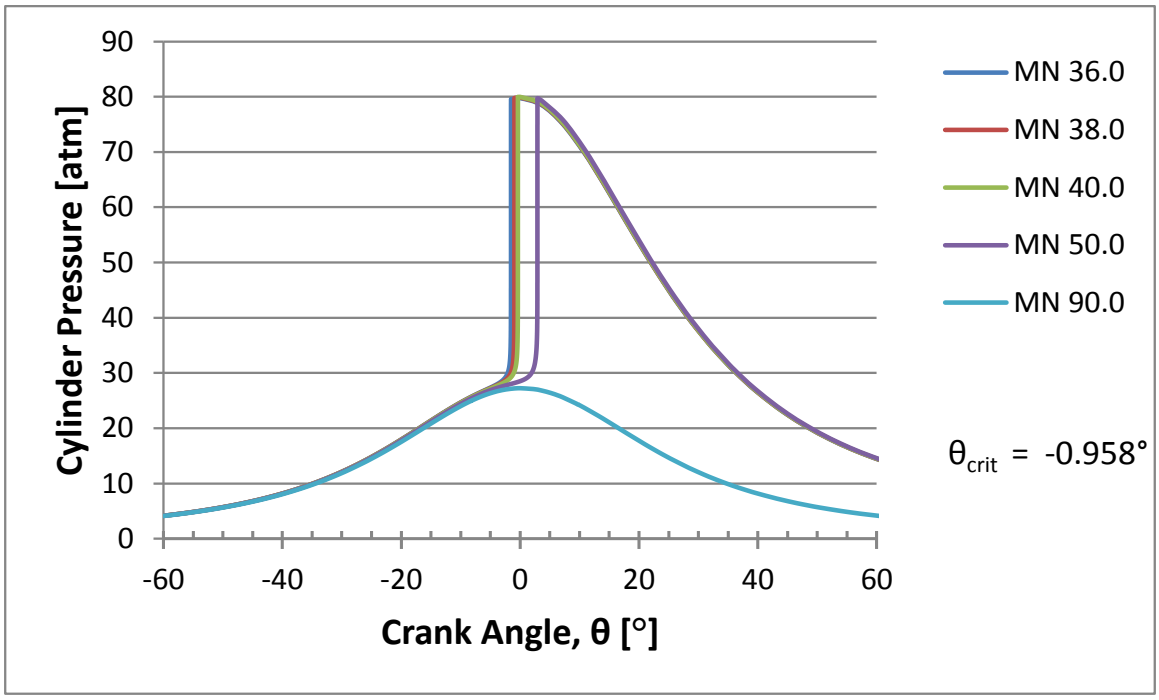

Figure 6-2 CHEMKIN Model Pressure vs. Crank Angle for CH_4-H_2 Blend.

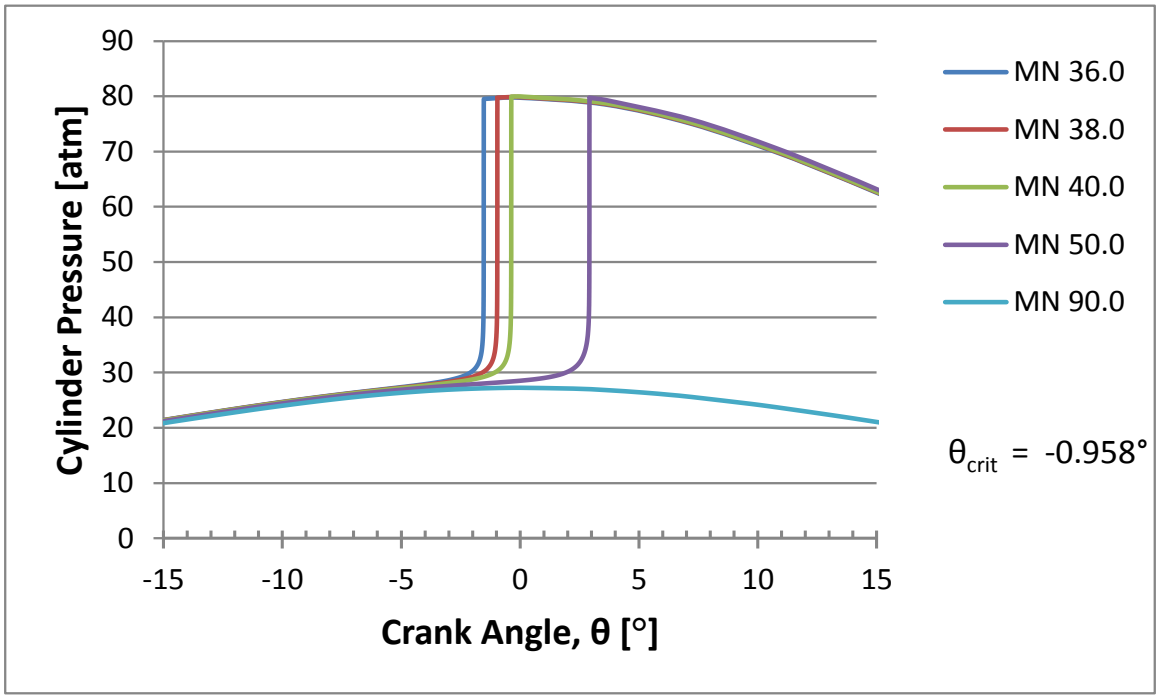

Figure 6-3 CHEMKIN Model for CH_4-H_2 Blend, scale expanded for clarity.

6.1.2 Results and discussion

For the purpose of comparison methane number estimates were developed by CHEMKIN simulation, using the NUIG NGM mechanism, for the same producer gas blends investigated by Arunachalam. Table 6-2 lists the results of the simulation with the USCII and NUIG NGM mechanisms as well as experimental methane number measurement derived in that study along with experimental results from this work.

Table 6- 2 Methane Number Determination Summary

Producer Gas Blends	Constituent Gas Percentages					Methane Number				
						Measured (this work)	AVL	CHEMKIN Mechanism		Previous Measured Data*
	N_2	CO_2	CO	H_2	CH_4			USC II*	NUIG NGM	
IISc	48.5	12.0	19.0	19.0	1.5	96.0	81.5	38	27.5	122.0
CPC	56.7	1.4	21.0	18.7	2.2	66.2	74.8	13	10.2	58.5
Güssing	3.0	23.0	24.0	40.0	10.0	68.2	61.6	51.5	38.0	57.2
Harboore	40.7	11.9	22.8	19.3	5.3	91.1	80.6	42	33.6	106.0
Viking	33.3	15.4	19.6	30.1	1.6	70.0	63.4	33	25.5	53.7

* (Arunachalam, 2010)

Figure 6-4 provides the methane number data in column chart form for the same five producer gas blends. The two CHEMKIN models, while trending reasonably closely with each other, differ widely from experimentally measured values and values predicted by the AVL program "Methane". The USCII mechanism is closer to measured values than the NUIG NGM mechanism. It is concluded that methane number estimates derived from modeling producer gases using the CHEMKIN IC engine module and common chemical kinetics mechanisms have not been established to be consistent with experimental measurement conducted with the methodology developed in this work. It is important to note that these results are not presented

as an indictment of the chemical kinetics mechanisms. An actual SI engine will experience a flame propagation process not represented in the homogeneous charge compression ignition (HCCI) model. The significance of the flame propagation process is not known relative to the auto-ignition assumptions applied to HCCI.

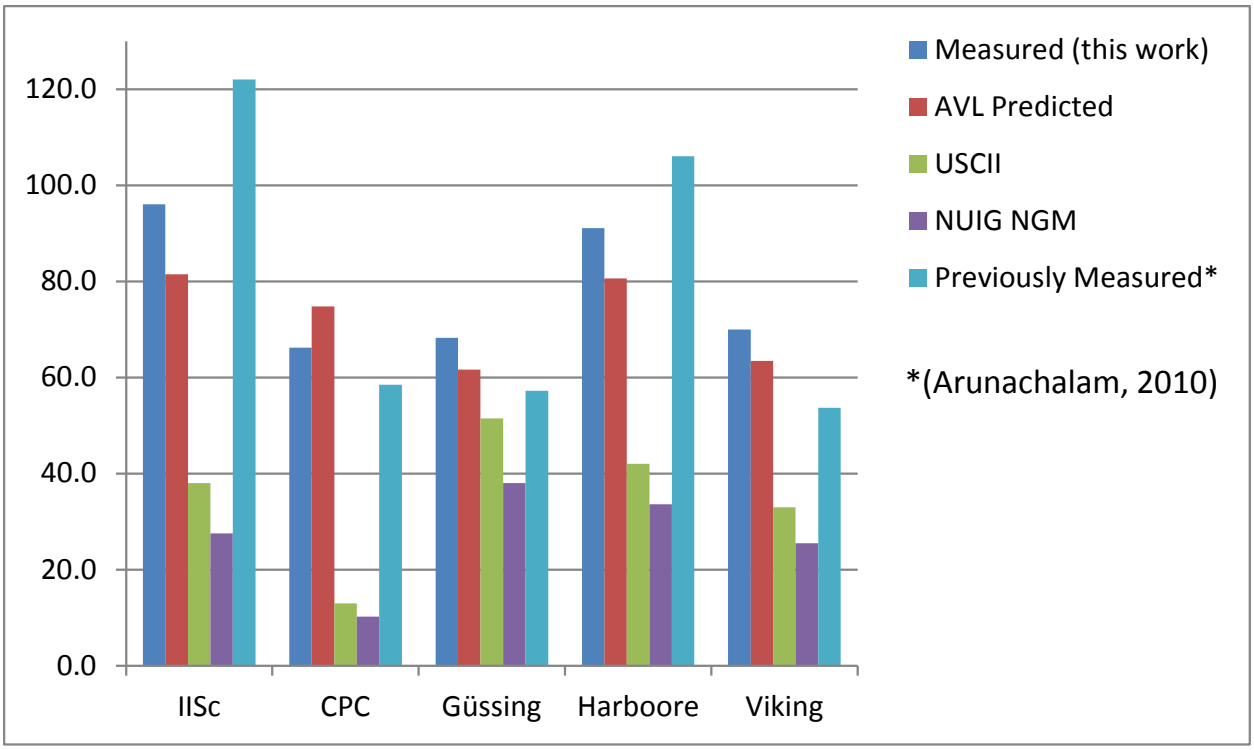

Figure 6-4 Methane number estimates derived from various approaches.

6.2 Neural Network Methodology

In a neural network methodology no mathematical correlation between producer gas constituent make-up and methane number is established based on physical principles or chemical kinetics modeling. This predictive model is purely empirical, based on neural information processing theory or neural network modeling. Neural network modeling is based solely on

interpretive correlation between input information and output result, which in this case is producer gas constituent make-up and measured methane number, respectively. The use of neural networks is a common approach in artificial intelligence methodologies that essentially mimic learning processes in natural biological systems. In a simple approximation of a neurological process, information is provided to an interconnected series of receptor nodes or neurons that process the information resulting in a weighted output function. Emerging patterns identified in the learning process, comparing input to output, are applied to establish predictive models for new input data (Anderson, 1995).

The specific commercial software used in this work is a neural network constituent module, "Neural Tools", a subset of the risk management software "Decision Tools" published by Palisade Corporation. This software is an overlay program to Microsoft Excel using spreadsheet formatting for data input, applying the most common type of neural network formulation known as a feed forward network. Data is organized as connected input and output layers with at least one interconnected intermediate layer, called a hidden layer, between the input and output. Information is fed from input to output and then back propagated through all layers. Each cycle of data forward feed and back propagation for the complete data set used for training the system is called an epoch. The learning algorithm employed in this software is termed a perceptron algorithm in which every connection within the network is weighted; weighting of the neural nodes is accomplished following an iterative process to update weights assigned that achieve the best correlative fit possible. A flowchart of the perceptron learning algorithm is shown in Figure 6-5.

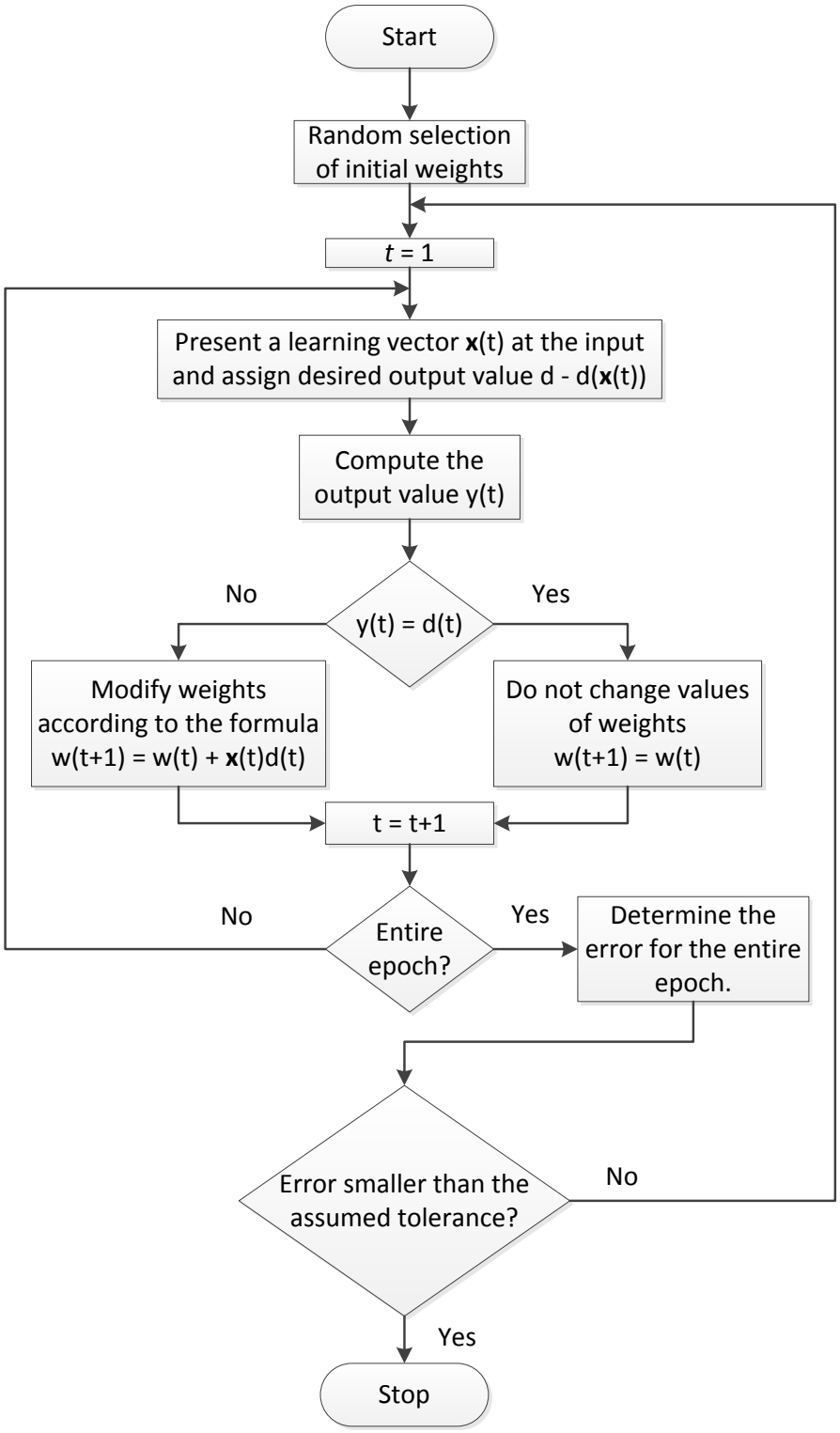

Figure 6-5 Perceptron learning algorithm flowchart (Coolen, et al., 2005).

For this work the specific input data consists of percentages of the five individual constituent gases (H_2, CO, CH_4, CO_2 and N_2), the total percentage of fuel gases (H_2, CO, and CH_4 combined) and the total percentage of diluent gases (CO_2 and N_2 combined). The output result is methane number. Figure 6-6 provides a schematic illustration for this specific model depicting a single hidden layer. It is noted that the Palisade Neural Tools software uses a variable number of hidden layers and transfer functions.

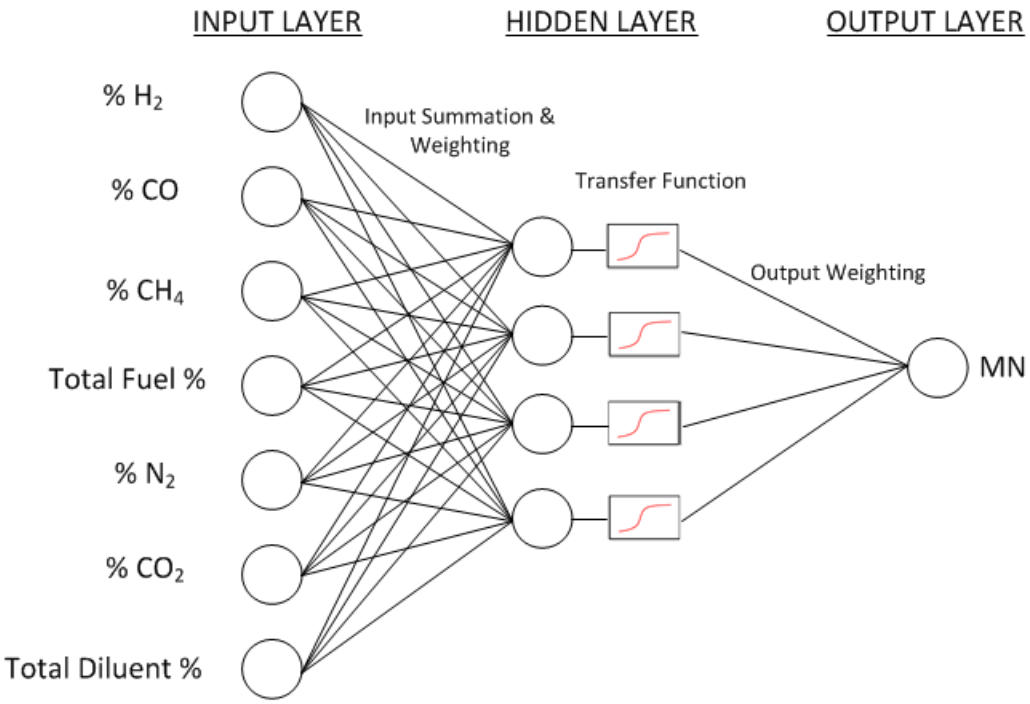

Figure 6-6 Neural Network schematic.
(Steyskal, 2001), as adapted.

6.3 Neural Network Model for Producer Gas Methane Number

Producer gas characteristics compiled in Table 5-1 (including percentage of constituent blends, percentage of fuel gas, percentage of diluent gas, stoichiometric air-fuel ratio, and calculated lower heating value), are provided as input data (independent variables) to the Neural Tools software. Measured methane numbers are provided as output (dependent variable). The software uses the input data to train the program for the data set and then tests the results. This particular program does not provide input parameter characterization as dominant or non-critical, only statistical data derived from error analysis of the model results.

The order of the blends is rearranged and the process repeated on 10 attempts, the predicted MN values are exactly the same following each attempt. Next, to assess the sensitivity of the neural network to all the data groups the model is repeated, first eliminating diluent and fuel gas percentages, next eliminating stoichiometric air-fuel ratio, and finally eliminating lower heating values. Table 6-7 provides the results for the test trials. The predicted values highlighted are assessed as "bad." The general trend is that the model is more accurate after eliminating independent variables other than constituent gas percentage. This is consistent with the observations in chapter 5 of this work regarding the apparent lack of correlation between methane number and those same variables. Statistical data for the neural network trial runs including sensitivity analysis and predictive error analysis are provided in Appendix B.

The validity of a neural network in terms of consistency and reliability as a prognostic tool is impacted by a number of factors relative to the data comprising the independent variables and sulting dependent variables used to train the model. If the data is of insufficient quantity to allow development of adequate neural input weighting the model will suffer. In contrast, over-

Blend Name	N2	CO2	CO	H2	CH4	CO+H2	Diluent	A/Fs	LHV	MN	Methane Number Prediction, Neural Network Model Base on: All Variables:	Less CO+H2 & Diluent:	Less A/Fs	Less LHV
AF Gap A	0.05	0.19	0.34	0.34	0.08	0.69	0.24	3.26	11472	62.2	53.6	54.6	58.9	59.6
AF Gap B	0.00	0.19	0.20	0.33	0.29	0.53	0.19	6.11	19307	93.5	83.0	79.5	91.4	93.4
AF Gap C	0.14	0.00	0.19	0.47	0.20	0.66	0.14	7.56	24548	56.3	46.7	44.5	52.2	56.5
AF Gap D	0.11	0.05	0.09	0.47	0.28	0.56	0.16	8.65	27128	56.3	58.4	56.1	56.4	56.3
AF Gap E	0.10	0.06	0.11	0.25	0.48	0.36	0.16	9.37	28348	78.0	98.1	90.6	78.2	77.4
Banham	0.00	0.20	0.21	0.36	0.23	0.57	0.20	5.39	17316	80.3	75.7	74.1	81.9	80.3
Blend #1	0.07	0.17	0.37	0.39	0.00	0.76	0.24	2.55	9664	35.9	33.8	34.4	29.6	30.2
Blend #2	0.48	0.14	0.18	0.18	0.02	0.36	0.62	1.20	4362	96.7	103.8	106.5	94.0	93.7
Blend #3	0.11	0.06	0.12	0.26	0.45	0.38	0.17	8.96	27214	71.0	93.5	86.3	79.7	73.7
Blend #4	0.15	0.15	0.20	0.50	0.00	0.70	0.30	2.78	10195	25.7	29.3	29.3	24.3	25.7
Blend #5	0.15	0.00	0.20	0.50	0.15	0.70	0.15	6.80	22536	31.9	39.4	37.9	36.1	60.5
Chroen (O2)	0.00	0.20	0.39	0.40	0.00	0.79	0.21	2.64	10004	25.9	33.2	33.9	29.0	28.3
City Energy	0.29	0.00	0.00	0.26	0.44	0.27	0.29	8.81	26273	92.0	88.3	79.5	85.2	73.4
CPC	0.57	0.01	0.21	0.19	0.02	0.40	0.58	1.45	5292	66.2	72.1	70.0	75.3	67.2
Cranfield	0.00	0.22	0.17	0.52	0.08	0.69	0.22	4.14	14121	51.1	44.7	45.7	51.8	62.6
Dil Gap A	0.12	0.07	0.13	0.28	0.40	0.41	0.18	8.28	25360	90.2	86.7	79.4	86.5	89.6
Dil Gap B	0.03	0.24	0.26	0.43	0.04	0.68	0.28	2.89	10285	46.3	48.9	46.8	42.9	42.5
Dil Gap C	0.16	0.16	0.19	0.50	0.00	0.68	0.32	2.67	9785	21.5	31.7	32.0	24.5	26.0
Dil Gap D	0.23	0.19	0.45	0.07	0.07	0.52	0.41	1.94	7024	97.6	104.1	106.9	97.3	95.3
Dil Gap F	0.41	0.14	0.22	0.17	0.05	0.40	0.56	1.62	5570	97.6	93.5	94.5	94.3	94.3
Gussing	0.03	0.23	0.24	0.40	0.10	0.64	0.26	3.58	12186	68.2	60.3	61.1	61.5	63.8
Harboore	0.41	0.12	0.23	0.19	0.05	0.42	0.53	1.80	6335	91.1	89.3	89.8	93.1	93.6
Hyder	0.05	0.07	0.13	0.27	0.47	0.41	0.12	9.74	29597	79.4	92.4	84.4	78.1	77.1
IISc	0.49	0.12	0.19	0.19	0.02	0.38	0.61	1.23	4503	96.0	95.0	96.8	92.9	93.6
Meadow Vale	0.09	0.08	0.31	0.16	0.37	0.47	0.17	6.40	20088	86.0	93.7	87.1	86.1	86.1
Plasma	0.03	0.17	0.38	0.40	0.02	0.78	0.21	2.88	10720	23.2	33.8	35.2	30.7	29.7
Repotec	0.05	0.20	0.25	0.40	0.10	0.65	0.25	3.70	12629	58.5	55.1	55.1	61.0	62.5
S4 Avg	0.05	0.19	0.35	0.35	0.05	0.71	0.24	2.95	10613	46.6	52.1	57.0	48.4	48.0
S4 Example	0.02	0.11	0.41	0.43	0.03	0.84	0.13	3.56	13129	29.9	24.3	26.8	29.6	30.0
TEMCO	0.19	0.14	0.53	0.07	0.07	0.59	0.34	2.18	7993	91.3	83.0	82.8	97.2	93.6
Victoria 1	0.11	0.05	0.10	0.49	0.25	0.58	0.17	8.32	26237	56.1	52.0	47.6	56.3	56.2
Viking	0.33	0.15	0.20	0.30	0.02	0.50	0.49	1.73	6282	70.0	70.1	71.0	69.9	70.5
VT 4/7/08	0.08	0.09	0.38	0.24	0.21	0.62	0.17	4.92	16293	58.1	63.0	58.6	59.1	58.4
VT 4/9/08	0.02	0.08	0.52	0.20	0.18	0.72	0.10	4.48	15327	60.5	48.8	43.7	59.9	60.5
WTG	0.01	0.18	0.44	0.22	0.15	0.66	0.19	3.75	12838	73.3	67.7	66.4	60.6	73.0

Figure 6-7 Neural Network Predicted Values for Methane Number

training or over-fitting is a common concern that can occur in cases where the network can be trained with plentiful data that includes sufficient error or noise as to mask generalized trends of the model (Anderson, 1995). With this model the concern is the former case, that the quantity of available blends used to establish and train the model is limited to 35 blends. Typical neural network models will input an order of magnitude more sets of independent variables used to train the model. For the software "Neural Tools" used in this work, the predicted values are considered "good" if they fall within approximately 25% of the dependent variable input for the case and "bad" if beyond 25%, as indicated in Table 6-7. The default target is for "bad" predicted values to occur in less than 30% of the cases. As can be seen in Table 6-7, for the first trial including all independent variables this model provides 3 in 35 predictive models in the "bad" category which is less than 10% of the predicted values. Subsequent trials contain 2, 1, and 1 "bad" predictions. While the consistency of the neural model is better than that of the AVL model for predicting methane number for producer gases, more data sets will be required to improve the neural network. Table 6-8 compares the error between the predicted and measured methane numbers for the neural network model and the AVL software "Methane" model for the 35 producer gas blends.

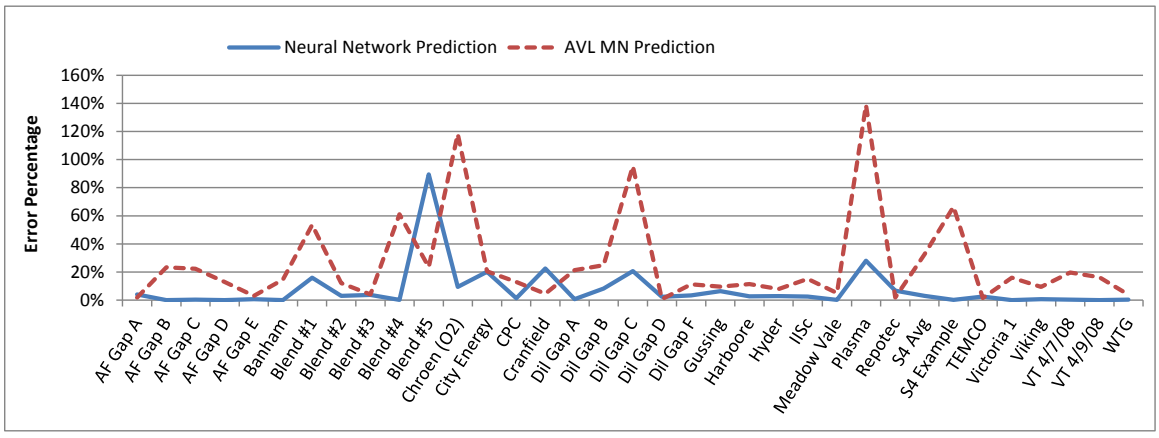

Figure 6-8 Error comparison for predicted values of methane number.

7 CONCLUSIONS AND RECOMMENDATIONS

7.1 OVERVIEW

This work seeks to advance the characterization of producer gas as an alternative fuel for use in lean burn natural gas engines. It provides research results that are supportive of engineering applications and germane to current industry challenges as well as contributing to the science associated with energy conversion processes and internal combustion engine design and operation.

The completed work has addressed the research objectives to:

(1) develop metrics used as predictive indicators of how varying producer gas blends will perform when used to fuel lean burning natural gas engines.

(2) quantify knock onset by analysis of cylinder pressure data and develop reliable and repeatable methods of knock quantification.

(3) determine the impact that engine operating parameters have on measured methane number and demonstrate the differences in measured methane number under varied engine operating conditions.

7.2 CONCLUSIONS

Conclusions for the investigation into producer gas utilization in high performance natural gas engines are as follows:

- Engine test cell design and operation can successfully incorporate a CFR engine in a system to reliably blend producer gases, monitor and record engine combustion data, and control stoichiometric conditions, all while simulating turbocharger operation

through positive control of intake boost pressure and exhaust backpressure allowing achievement of desired nmep levels.

- The use of in-cylinder pressure data in a Fast Fourier Transform method to quantify knock intensity in real time (as detailed in chapter 4, sections 4-6 through 4-8) provides a reliable and repeatable metric for use in conducting methane number measurement. Repeatability is illustrated by the results for the check blend mixture of 90% methane and 10% ethane with a standard deviation of less than 2% (as described in detail in chapter 4, part 4.8.1).
- Engine operating characteristics of boosted intake (simulating turbocharger operation), lean stoichiometric conditions, and variation of ignition timing have minimal effect on measured methane number. For the testing parameters defined in Table 4-1 the variation in measured methane number is less than 4%, as shown in Figure 5-6.
- The measured values of methane number for producer gas blends are not consistent with the values predicted by the AVL program "Methane." Specifically, for the 35 tested producer gas blends, the average difference (absolute value) between the AVL MN and measured methane number is 11.1 with a standard deviation of 8.02.
- The measured values of methane number for producer gas blends are not consistent with values obtained with modeling of producer gas blends using the IC engine module of the software CHEMKIN. As stipulated in the literature review the accepted indicator of knock is the dramatic rate of change of in-cylinder pressure (dP/dt or $dP/d\theta$) resulting in auto-ignition as the flame front transverses the combustion chamber and impacts a pocket of end-gas (Barton, et al., 1970) (Brecq, et al., 2003).

The IC engine module in CHEMKIN uses in-cylinder pressure levels based on motoring pressures, sinusoidal changes in cylinder volume as the piston advances and retracts into and from the cylinder with crank rotation. The rate of change of pressure in that model will not reasonably simulate the pressure and temperature transients encountered as a result of spark ignition and an advancing flame front.

- A neural network model for predicting producer gas methane number is developed initially using input (independent) variables of constituent percentage, fuel gas percentage, diluent percentage, stoichiometric air-fuel ratio, and lower heating value and the output (dependent) variable of methane number. It is observed that the model performance, in terms of predicted value error, improved after deleting fuel gas and diluent percentages and further improved after deleting air-fuel ratio and lower heating value. Specifically, the percentage of "bad" predictions reduced from 8.6% to 2.9%, and mean absolute error reduced from 6.84 to 3.39. The values produced by this model are observed to be more reliable for producer gas methane number than those values provided by the AVL program "Methane." A specific indication is standard deviation for percentage error compared to measured data, 16.0% for the neural network model data and 32.9% for the AVL MN data.

7.3 Research Recommendations

Additional work is necessary to develop a more robust and accurate predictive program for producer gas methane number. This effort should incorporate hardware and controls improvements in the test cell which will facilitate expansion of the database used to train the neural network model. A limiting condition for expanding the methane number database is the

time necessary to stabilize producer gas blend constituent make-up as well as settling time for engine operating conditions when conducting methane number measurements. Specific recommendations for test cell hardware and operational improvement are as follows:

- Fuel blending system pulse width modulated (PWM) injectors. The existing fuel injectors are significantly oversized for the CFR fuel cell. The PWM injectors in use are the smallest commercially available but are designed for over-the-road natural gas engines supporting fuel delivery rates associated with approximately 200 horsepower (~150kW) natural gas engines as compare to the CFR engine with typical power output of approximately 4 horsepower (~3kW). As a result the duty cycle for the injectors is typically less than 10% which requires extremely delicate and slow adjustment to maintain engine control.
- Control of nmep. The engine control system adjusts nmep by controlling intake manifold pressure (boost pressure). Each incremental adjustment of intake boost requires a slow and deliberate period to allow maintenance of stoichiometric conditions and power output. Since developed engine output electrical power is proportional to nmep, one approach to improve responsiveness would be to use output electrical power as feedback for intake system boost pressure in a slow control loop.
- Manual control of the exhaust backpressure valve is used to maintain desired backpressure mimicking the operation of a turbocharger. Automated operation of the exhaust backpressure valve will streamline engine operation.

The improvements described above will facilitate expansion of the measured methane number database and subsequent improvement of the neural network model based methane number predictive tool.

Additional research should be directed toward engine controls based on an expanded neural network predictive algorithm. It is established that methane number, the relative resistance to knock in a spark ignited engine, is a fuel property that could eventually be ascertained solely through knowledge of the constituent make-up of the fuel. The potential exists for an accurate methane number sensor to be developed that could be integrated with engine controls to allow more flexible operation of lean-burn natural gas engines. With real time fuel gas analysis a controls system could react to varying methane number to optimize engine performance by taking actions such as automatically adjusting ignition timing, changing stoichiometric settings, or possibly initiating supplemental methane injection to increase the fuel's resistance to knock. These tools would doubtlessly provide a positive impact on the employment of natural gas engines to producer gas fuel applications.

REFERENCES

Ahrenfeldt, J., Jensen, T. K., Henriksen, U. & Schramm, J., 2005. *Investigation of Continuous Gas Engine CHP Operation on Biomass Producer Gas.* San Antonio, SAE International.

Anderson, J. A., 1995. *An Introduction to Neural Networks.* 1st ed. Cambridge(Massachusetts): The MIT Press.

Arunachalam, A., 2010. *Experimental and Analytical Evaluation of Knock Characteristics of Producer Gas Fuel,* Fort Collins: Colorado State University.

Barton, R. K., Lestz, S. S. & Duke, L. C., 1970. *Knock Intensity as a Function of Engine Rate of Pressure Change*, New York: Society of Automotive Engineers.

Brecq, G., Bellettre, J. & Tazerout, M., 2003. A New Indicator for Knock Detection in Gas SI Engines. *International Journal of Thermal Sciences (42),* pp. 523-532.

Brunt, M., Pond, C. & Biundo, J., 1998. *Gasoline Engine Knock Analysis Using Cylinder Pressure Data*, s.l.: SAE Paper 980896.

Callahan, T. J. et al., 1996. *Engine Knock Rating of Natural Gases - Expanding the Methane Number Database.* Fairborn, ASME Internal Combustion Engine Division, pp. 59-64.

Cengel, Y. A. & Boles, M. A., 2011. *Thermodynamics An Engineering Approach.* 7th ed. New York(New York): McGraw-Hill.

Chang, J. et al., 2004. *New Heat Transfer Correlation for an HCCI Engine Derived from Measurements of Instantaneious Surface Heat Flux,* Ann Arbor: Society of Automotive Engineers, Inc..

Coetzer, R. L., Rossouw, R., Swarts, A. & Viljoen, C., 2006. The Estimation of Knock-Points of Fuels by a Weighted Mean Square Error Criterion. *Fuel 85,* pp. 1880-1893.

Considine, D. M., 1977. *Energy Technology Handbook.* 1st ed. New York: McGraw-Hill.

Coolen, A., Kühn, R. & Sollich, P., 2005. *Theory of Neural Informaiton Processing Systems.* 1st ed. Oxford: Oxford University Press.

Elmqvist, C. et al., 2003. *Optimizing Engine Concerpts by Using a Simple Model for Knock Prediction,* s.l.: SAE International.

Hanrahan, G., 2011. Artificial Intelligence: Competing Approaches or Hybrid Intelligent Systems?. In: T. a. F. Group, ed. *Artificial Neural Networks in Biological and Environmental Analysis.* New York: CRC Press, pp. 24-39.

Heywood, J. B., 1988. *Internal Combustion Engine Fundamentals.* New York(New York): McGraw-Hill.

Kee, R. J., Rupley, F. M., Meeks, E. & Miller, J., 1996. *CHEMKIN-III: A FORTRAN CHEMICAL KINETICS PACKAGE FOR THE ANALYSIS OF GAS-PHASE CHEMICAL AND PLASMA KINETICS,* Livermore: Sandia National Laboratory.

Kubesh, J., King, S. R. & Liss, W. E., 1992. *Effect of Gas Composition on Octane Number of Natrual Gas Fuels.* Warrendale(PA): Society of Automotive Engineers, Inc..

Leiker, M. et al., 1972. *Evaluation of Antiknocking Property of Gaseous Fuels by Means of Methane Number and its Practical Application to Gas Engines,* New York: American Society of Mechanical Engineers.

Millo, F. & Ferraro, C., 1998. *Knock in SI Engines, A Comparison Between Different Technicques for Detection and Control.* SAE Paper Number 982477 ed. Milan: SAE.

Pulkrabek, W. W., 2004. *Engineering Fundamentals of the Internal Combustion Engine.* 2nd ed. Upper Saddle River(New Jersey): Pearson Prentice Hall.

Rahmouni, C., Brecq, G., Tazerout, M. & Le Corre, O., 2004. Knock Rating of Gaseous Fuels in a Single Cylinder Spark Ignition Engine. *Fuel 83,* pp. 327-336.

Sadaka, S., 2011. *Gasification, Producer Gas and Syngas,* Little Rock: University of Arkansas Cooperative Extension Service Printing Services.

Soylu, S. & Van Gerpen, J., 1998. *Fuel Effects on the Knocking Limit of a Heavy-Duty Natural Gas Engine.* Dearborne, SAE International, pp. 1-10.

Soylu, S. & Van Gerpen, J., 2003. Development of an Autoignition Submodel for Natural Gas Engines. *Fuel 82,* pp. 1699-1707.

Steyskal, M., 2001. *Development of a Neural Network Model for Predicting NOx Emissions From a Large Bore Natural Gas Engine,* Fort Collins: Colorado State University.

Ulfvik, J. et al., 2011. *SI Gas Engine: Evaluation of Engine Performance, Efficiency and Emissions Comparing Producer Gas and Natural Gas,* s.l.: SAE International.

Wang, H. et al., 2007. *High Temperature Combustion Reaction Model of H2/CO/C1-C4 Compounds,* s.l.: s.n.

Waukesha Engine Division, Dresser Industries, 1980. *The Waukesha CFR Fuel Research Engine.* Waukesha(Wisconsin): Waukesha.

Waukesha Engine Division, Dresser Industries, 2003. *Waukesha CFR F-1 & F-2 Research Method (F-1) Motor Method (F-2) Octane Rating Units Operation and Maintenance.* Second ed. Waukesha(Wisconsin): Dresser Waukesha.

Zsély, I. G., Nagy, T., Simmie, J. M. & Curran, H. J., 2011. *Reduction of a detailed kinetic model for the ignition of methan/propane mixtures at gas turbine condition using simulation error minimization methods,* Amsterdam: Elsevier Inc..

Appendix A TEST PROCEDURES

The following are operating procedures developed for this project in an effort to ensure safe, reliable, and repeatable test cell and engine operation. They are provided here to allow the reader to review the processes followed in conducting this work and collecting the data reflected.

CFR START-UP CHECKLIST

Engine prep to be performed after VI is started and ready to control the engine:

< > Turn on CFR main power

< > Verify engine oil is at a minimum is 100°F

< > Verify that the fuel manifold vent valve is shut

< > Verify exhaust backpressure valve fully open

< > Open valve to GC sample line {if operating}

< > Power up 5-Gas Analyzer pump and heater {if operating}

< > Open combustion air valves

< > Verify compression ratio setting {typical start-up $r_c \approx 10{:}1$, Dial Indicator = 0.235"}

< > Position cooling water valves for engine operation. Drain valve is opened first, then inlet

< > Verify cooling water flow through the cylinder pressure transducer

< > Verify cooling water level in sight glass

< > Verify engine lube oil at ½ sight glass

Starting the engine with VI controls:

At "Operational Parameters" tab:

< > Verify "Inlet Air Manual [%]" is set to 20

< > Verify "Inlet Air Control" is off

< > Click Intake Air Vent to enable (icon should be green)

< > Start CFR engine from Main CFR control panel on engine skid then click "Air Enable" button

< > With engine running set "Air Set point" to the desired inlet air pressure in kPa absolute

< > Select "Inlet Air Control" button to enable closed loop pressure control of the inlet air

< > Shut intake air vent valve

< > Switch on charge amplifier (hit reset button until "operate" is indicated)

< > Switch oil heater off

< > Ensure crankcase condensate drain and exhaust condensate drain valves are shut

< > Set compression ratio to desired level

< > Take a motoring data set (50 cycles) to enable later determination of dynamic TDC at CR

< > Verify manifold isolation valves positioned as necessary for intended fuel blend

< > Verify low flow manifold valves positioned as necessary for low flow fuel line-up

< > Open gas regulators for desired fuel blend

< > Verify downstream fuel isolation valve is open

At "Fuel Blending Control" tab:

< > Set the "Desired Fuel make up[%]" to the desired levels

< > Set the "Desired AF ratio" – based on CR and anticipated knock onset point

< > Set "AFR Range" to 40

< > Set the "Maximum Duty Cycle" (usually to 55)

< > Push the “Fuel System Enable” button

< > Set the “Fuel Manual Control” to 25

< > Verify “AFR Sample to Avg.” is greater than zero (default is 20)

< > Switch ignition system on

< > Verify Altronic software is enabled, set ignition time to desired point

< > Push the “PWM Enable” to start the injection

< > Select desired “AFR control” mode – “AFR Recorder”

< > After air fuel ratio stabilizes (approx. 15 sec.) push “Auto Fuel Control” to enable closed loop air fuel ratio control.

< > Switch air heater on at operating console; set VI intake air heater control to 45°C and Pulse Period to 6, enable intake air heater

CFR SHUT-DOWN CHECKLIST

Normal Shutdown:

< > {Operational Parameters: Air Setpoint} Set boost pressure to 101kPa

< > Open exhaust backpressure valve

< > Isolate fuel system at the downstream fuel isolation valve

< > Open the fuel manifold vent valve

< > Shut all fuel regulators

< > {Fuel Blending Control: Auto Fuel Control} Turn off "Auto Fuel Control"

< > After fuel pressure drops to zero gage turn off "PWM Enable" to stop fuel injection

< > Click the "Fuel System Enable" button to disable the fuel system

< > Bleed off any residual fuel line pressure through the low flow fuel system

< > Turn off power strip to 5 gas analyzer sample line

< > Shut GC sample line valve

< > Switch off air-fuel heater

< > Open drain valve from crankcase vent line

< > Open drain valve from exhaust piping in the overhead

< > Allow engine to cool for approximately 5 minutes {~90°C Engine Coolant Temperature}

< > Stop the Combustion Logger

< > Switch off the charge amplifier

< > {Operational Parameters: Inlet Air Control} Turn off "Inlet Air Control"

< > Shut down engine from main CFR Control Panel

< > {Operational Parameters: Air Enable} Turn off "Air Enable"

< > Open intake air vent in VI using Shut-Down Feature

< > Isolate supply to engine cooling water, inlet first

< > Isolate combustion air supply

< > Switch off engine ignition

< > Switch off charge amplifier

< > Stop Host VI, close

< > Stop EECL-CFRIO, close

< > Collapse CFRIO in menu, disconnect

< > Close out LabView Main Menu

< > Switch off 480VAC power to 24VDC power supply

< > Switch off 208VAC power to CFR engine

Emergency Shutdown:

< > Depress ESD on Main CFR Control Panel

< > Shut all compressed gas regulators

< > Open 208VAC disconnect

< > Switch off 480VAC power switch

< > Open fuel manifold vent

< > Open intake air vent

< > Shut Cooling Water Supply valve

< > Shut Cooling Water Drain Valve

< > Shut Compressed Air Supply Valves

CFR CLEARANCE VOLUME AND PISTON CLEARANCE

The compression ratio of the CFR engine is determined by measuring the vertical position of the cylinder relative to an indexed position of known compression ratio. For this test cell a dial indicator is positioned to read "Zero" at the point of compression ratio set to 18:1. The cylinder will travel vertically as compression ratio is decreased to a minimum value of 4:1. The dial indicator reading corresponds to compression ratio as described below:

Engine compression ratio, r_c, is given by the relationship $r_c = \frac{V_D + V_c}{V_c}$

Where r_c = Compression Ratio
V_D = Displacement Volume
V_c = Clearance Volume

Rearranging terms and solving for clearance volume,

$$V_c = \frac{V_d}{1 - r_c}$$

The height of the cylinder head above the piston face at top dead center is given by

$$DI = \frac{V_c}{\pi \left(\frac{b}{2}\right)^2}$$

Where DI = Dial Indicator Reading
b = cylinder bore

A calculations reference sheet is prepared in Microsoft Excel© to translate dial indicator readings to compression ratio, shown in Figure A-1.

CFR Compression Ratio (r_c) Worksheet:

V_{DISP}	37.331 in^3	=	611.74 cm^3
R	37.330 in	=	94.82 cm
Bore	3.250 in	=	8.26 cm
Stroke	4.500 in	=	11.43 cm

$V_{clearance} = V_{displacement}/(r_c-1)$ and Cylinder Height = $V_c/\pi\cdot(b/2)^2$

At r_c = 18:1

V_c(18:1)= 2.196 in^3

Cyl Ht = 0.265 in

Calculator (indexed to 0= 18:1)

Dial Indicator Reading: 0.225

Calculated Compression Ratio: 10.19 :1

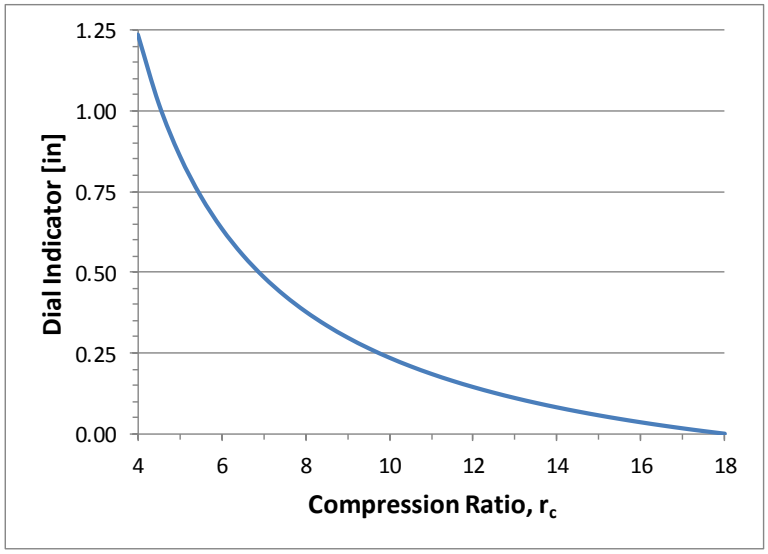

Compression Ratio	Dial Indicator Position [in]
4 :1	1.235
4.5 :1	1.021
5 :1	0.860
5.5 :1	0.735
6 :1	0.635
6.5 :1	0.553
7 :1	0.485
7.5 :1	0.428
8 :1	0.378
8.5 :1	0.335
9 :1	0.298
9.5 :1	0.265
10 :1	0.235
10.5 :1	0.209
11 :1	0.185
11.5 :1	0.164
12 :1	0.144
12.5 :1	0.127
13 :1	0.110
13.5 :1	0.095
14 :1	0.081
14.5 :1	0.069
15 :1	0.057
15.5 :1	0.046
16 :1	0.035
16.5 :1	0.026
17 :1	0.017
17.5 :1	0.008
18 :1	0.000

Figure A- 1 Compression ratio worksheet

TEST PLAN CFR-1

CFR Post-Modification and Methane Verification Tests

Objectives

- Verify operation of the engine, controls, supporting systems, and data acquisition systems in the engine test lab.
- Collect data for development of a Knock Index for this testing configuration.
- Conduct methane number measurement on known constituent gas blends to verify consistency of test results.

Background

The CFR engine test lab has undergone significant modification with the installation of an updated fuel blending system, a pressure boosted engine intake system, exhaust variable backpressure system, new sensors, and substantially upgraded LabVIEW controls and data acquisition program. Additionally, the engine has undergone significant maintenance (valve and valve seat renewal, cooling system restoration, ignition system upgrades, etc.). This test will serve as the initial verification of hardware performance and provide the basis for knock index development.

The CFR engine detonation sensors have been replaced with piezoelectric sensors whose raw signals are routed to a charge amplifier and further processed. This test to determine methane number by comparing the point of knock onset with an unknown test gas blend to that point with a standard blend.

Test Hardware: AF-2 CFR Engine

Part 1: Post Modification Test

Data to be recorded:

Output power, knock indication, and in-cylinder pressure data under varied intake boost pressures, compression ratios, and ignition timing.

Operating conditions:

Fuel blend: Facility Natural Gas (pressurized on site as delivered)

A/F ratio: (a) Stoichiometric as determined by O_2 sensor indications

(b) $\Phi \approx 0.6$, => NOx to 85 ppm @ 15% O_2

Jacket Water Temperature: 95°C

Speed = 900 rpm

Timing, Compression Ratio, and Intake Boost as specified in procedure

Lube Oil Sump Temperature 120˚F

Procedure (Part 1)

CAUTION: Throughout the procedure, do not allow engine to operate under conditions exceeding light knock.

1-I. Prepare the engine for operation in accordance with the general CFR operating procedure:

A. Start the engine with presets as follows:

1. Compression Ratio: 6:1
2. Intake Boost Pressure 1.0 bar
3. Ignition Timing 13˚ bTDC

B. Operate until steady operating conditions are achieved

1- II. Run MBT/Compression Ratio Sweep.

A. With Boost Pressure = 1.0 bar, Compression Ratio = 6:1, $\Phi = 1.0$ {Op Cond (a)}

1. Sweep Ignition Timing from 18˚bTDC to TDC in 6˚ increments

2. Record Power Output [kW], indicate audible knock present, if applicable.

CAUTION: Do not allow engine to operate under conditions exceeding light knock.

3. Repeat ignition timing sweep for increased compression ratios to 14:1 in increments of 2:1

B. Repeat the MBT/Comp Ratio Sweep at discreet increased Boost Pressure

1. Increase boost pressure to 1.5 bar, then continue to a value of 2.0 bar

Record Power Output and indicated knock for each test point. Prepare data tables as follows:

MBT/Compression Ratio Sweep:		C.R. (:1)	Ignition Timing (Ref TDC)						
Repeated for Intake Boost (1.0, 1.5, 2.0 bar)			- 18°	-12°	- 9°	-9°	-6°	-3°	0°
		6							
	Recording	8							
	Power Output [kW] as f(CR,IT)	10							
	or Knock Indicated	12							
		14							

C. Repeat steps II.A and II.B with $\Phi \approx 0.6$ {Op Cond (b)}

Part 2: CFR Methane Number Verification

Data to be recorded:

Compression ratio at the onset of knock. In-cylinder pressure data

Operating conditions:

Fuel blend: As specified in the procedure

A/F ratio: Two conditions: (a) Stoichiometric as determined by O_2 sensor indications and (b) $\Phi \approx 85$ ppm NOx @ 15% O_2

Jacket Water Temperature: 95°C

Speed = 900 rpm

Ignition Timing: MBT* at 0.9 bar intake boost Compression Ratio to be varied through knock onset.

Lube Oil Sump Temperature 120˚F

*{MBT as determined in Part 1 of CFR Test}

Procedure (Part 2)

2-I. Prepare the engine for operation in accordance with the general CFR operating procedure:

A. Start the engine with presets as follows:

1. Compression Ratio: 6:1

2. Intake Boost Pressure 0.9 bar

3. Ignition Timing MBT at 0.9 bar

B. Operate until steady operating conditions are achieved

2-II. Vary Compression Ratio Sweep to determine knock onset.

A. With initial Compression Ratio = 6:1

1. With standard blend fuel [Facility Natural Gas] and A/F at stoichiometric increase Compression Ratio to the point of knock onset. Note instrument indication reading and/or audible knock (thru use of the electronic stethoscope).

B. Return the engine to Compression Ratio = 6:1. Repeat step II.A.1. with standard blend fuel [constituents: XXXX] at A/F ratio deriving 150 ppm NOx. Note instrument indication reading and/or audible knock (thru use of the electronic stethoscope).

C. Return the engine to Compression Ratio = 6:1. Repeat step II.A.1. with the test blend fuel and A/F at stoichiometric. Note instrument indication reading and/or audible knock (thru use of the electronic stethoscope).

D. Return the engine to Compression Ratio = 6:1. Repeat step II.A.1. with test blend fuel A/F ratio deriving 150 ppm NOx. Note instrument indication reading and/or audible knock (thru use of the electronic stethoscope). Record data as follows:

(a) Stoichiometric							
(b) 85 ppm Nox @ 15% O_2				C.R.		Knock Ind.	
			Standard Blend @ (a)				
Recording C.R.			Standard Blend @ (b)				
@ Knock Onset			Test Blend @ (a)				
			Test Blend @ (b)				

2-III. Test Completion:

A. Shut down the engine in accordance with the CFR engine general operating procedure.

B. Isolate, drain, depressurize, and de-energize equipment in accordance with the CFR engine general operating procedure. Conduct all post operation checks.

C. Consolidate data tables, prepare test summary.

End of Test Plan CFR-1

TEST PLAN CFR-2

CFR Methane Number Verification
Sea Level, Stoichiometric, Ignition Timing 15°bTDC

OBJECTIVE

Conduct methane number measurement on known natural gas blends to verify consistency of test results for conditions of naturally aspirated, stoichiometric, and ignition timing at standard 15°bTDC.

BACKGROUND

The CFR engine detonation sensor has been replaced with a piezoelectric sensor (Kistler Model 6061b) whose raw signals are routed to a charge amplifier and further processed. A Fast Fourier Transform algorithm has been developed within the LabVIEW combustion logger to indicate a signal magnitude at the characteristic knock frequency. This program feature will be used to establish a knock index value to provide an objective measure of knock intensity for comparison of conditions with a test fuel blend and a reference fuel blend. For this test bottled natural gas (constituent makeup previously determined by gas chromatograph analysis) will be compared to a reference blend of methane and hydrogen to determine methane number.

TEST HARDWARE: AF-2 CFR ENGINE

DATA TO BE RECORDED:

1. Magnitude at knock frequency to serve as knock index point.
2. Compression ratio at knock index achievement.
3. Full combustion logger data set at knock onset for both the bottled natural gas and reference fuel blends.

OPERATING CONDITIONS:

1. Fuel blend: As contained in the compressed natural gas sample bottle.
2. A/F ratio: Stoichiometric as calculated from GC constituent blend analysis and monitored by O_2 sensor/AF Recorder system.
3. Jacket Water Temperature: 95°C
4. Engine speed: synchronous to electrical grid (~940 RPM)
5. Ignition Timing: 15°bTDC, corresponding to standard methane number test protocol
6. Intake boost: 101.3 kPa
7. Intake mixture temperature: ambient
8. Compression Ratio to be varied through knock index achievement
9. Lube oil sump temperature minimum 120˚F.

CAUTION: Throughout the procedure, do not allow engine to operate under conditions exceeding light knock.

PROCEDURE

I. **Prepare the engine for operation in accordance with the general CFR start up and operating procedure:**

a. Start the engine with presets as follows:

i. Compression Ratio: 6:1

ii. Intake Boost Pressure 101.3 kPa

iii. Ignition Timing 15°bTDC

b. Operate until steady operating conditions are achieved .

II. **Vary compression ratio to determine knock onset with bottled compressed natural gas.**

a. Set compression ratio to 9:1.

b. Using compressed natural gas (whose constituent makeup has been previously determined using the gas chromatograph) set A/F ratio to stoichiometric as indicated in the gas analysis worksheet and tracked in the LabVIEW Virtual Instrumentation controller

c. Increase compression ratio to the point of knock onset.

d. Note LabVIEW knock index magnitude at the point where light knock is audibly discernible by ear or through the use of the electronic stethoscope.

e. Record a 1000 cycle data set using the LabVIEW combustion logger.

III. **Replicate knock condition with reference fuel blend.**

a. Return the engine to Compression Ratio = 9:1.

b. Run the engine using the fuel blending system to establish a fuel reference blend of methane and hydrogen beginning at 100% methane, setting the A/F ratio to stoichiometric corresponding to the table below.

c. Increase compression ratio to that established in Step II.c.

If knock onset occurs prior to target CR, note onset point and proceed to Step IV}

d. Increase hydrogen percentage in the methane/hydrogen fuel blend until knock onset and knock index matches that observed in Step II.c.

e. Record a 1000 cycle data set using the LabVIEW combustion logger.

IV. **Measuring methane number in excess of 100.**

a. Add CO_2 to the methane until knock subsides

b. Increase compression ratio adding enough CO_2 in the process to limit knock onset until reaching the compression ratio established in Step II.c.

c. Adjust CO_2 concentration to match the knock index observed in Setp II.c.

d. Record a 1000 cycle data set using the LabVIEW combustion logger.

Methane %	Hydrogen %	A/F Stoichiometric	H to C	O to C	N to C
100	0	17.238	4.000	0	0
99	1	17.260	4.020	0	0
98	2	17.282	4.041	0	0
97	3	17.304	4.062	0	0
96	4	17.327	4.083	0	0
95	5	17.350	4.105	0	0
94	6	17.374	4.128	0	0
93	7	17.398	4.151	0	0
92	8	17.423	4.174	0	0
91	9	17.448	4.198	0	0
90	10	17.473	4.222	0	0
89	11	17.499	4.247	0	0
88	12	17.526	4.273	0	0
87	13	17.553	4.299	0	0
86	14	17.580	4.326	0	0
85	15	17.608	4.353	0	0

Table CFR-2-1 Stoichiometric A/F ratio for methane concentration from 85% to 100%

Test Completion:

a. Shut down the engine in accordance with the CFR engine general operating procedure**.**

b. Isolate, drain, depressurize, and de-energize equipment in accordance with the CFR engine general operating procedure. Conduct all post operation checks.

c. Consolidate data tables, prepare test summary.

End Test Plan CFR-2

Appendix B ENGINE CONTROL & LOGGING OVERVIEW

ENGINE TEST CELL CONTROLS

This project is conducted using two specific programs developed at the Colorado State University Engines and Energy Conversion Laboratory by the Engineering Manager, Mr. Kirk Evans. Both programs are written in LabVIEW© in support of ongoing research projects at the University. The first program, Combustion Analyzer, is a general internal combustion engine operation monitoring and performance logging program accepting operating parameter input from sensors on the engine and translating that information to combustion characterization of the operating engine. The program is adaptive to a number of different engines and has a module developed specifically for the CFR F2 engine used in this work. The second program, CFR Host VI, is specifically developed for operational control of the CFR F2 engine test cell to include fuel blending, engine operation, and exhaust systems.

COMBUSTION ANALYZER

The combustion logger configuration page is shown in Figure B-1. Inputs are accepted for pegging pressure and location, ignition timing, compression ratio, encoder resolution and offset, bore, stroke, connecting rod length, clearance volume polytropic coefficient and modeled heat release method. Once enabled the program provides active sensor input displayed in real time.

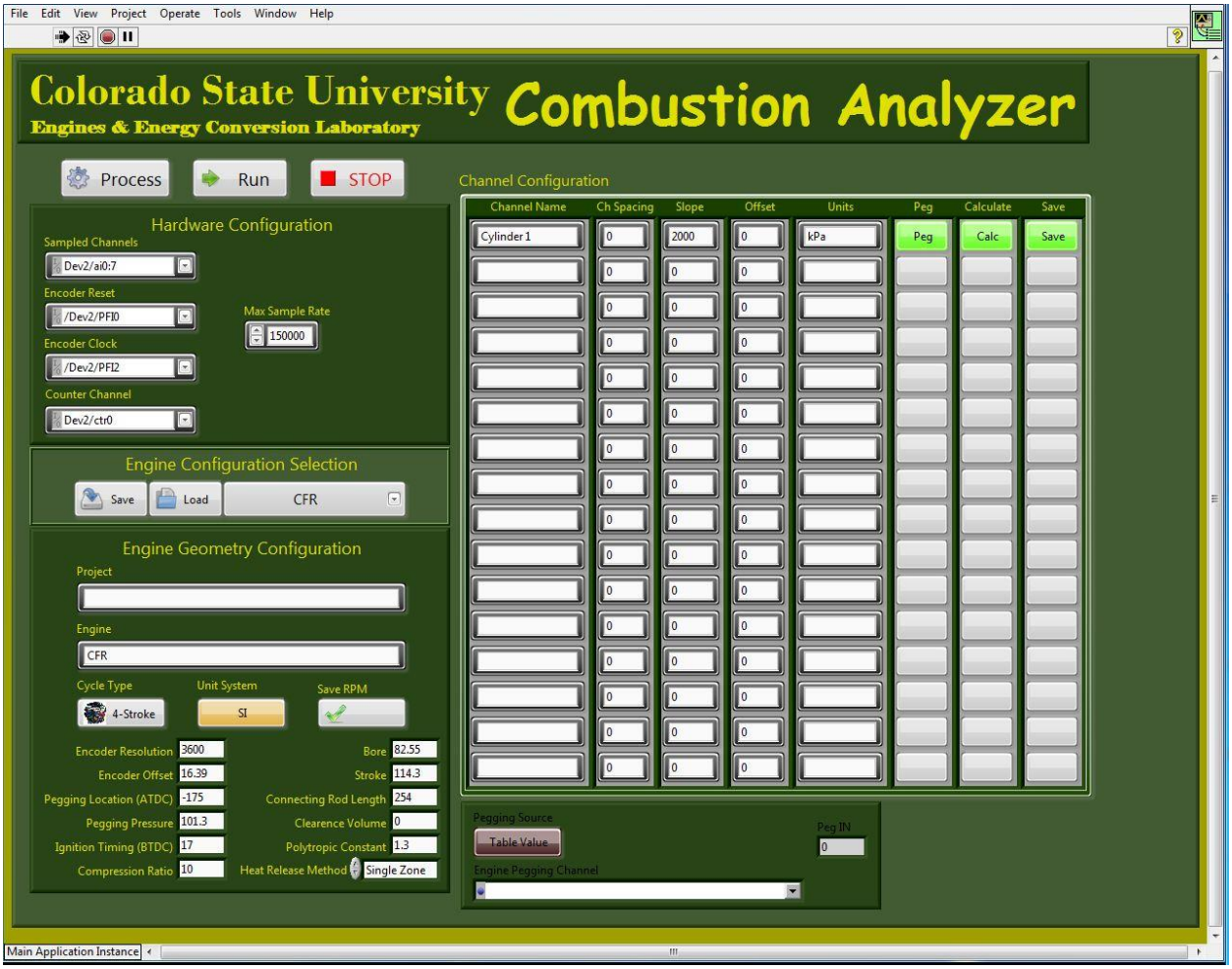

Figure B- 1 Combustion Analyzer configuration input opening screen.

Figure B-2 shows the engine monitoring page, specifically the cylinder pressure display showing real time pressure [kPa] vs. crank angle, θ [0° = TDC]. For this particular image a plot is shown with the engine motoring. Calculated values for peak pressure, location of peak pressure, imep, nmep, pmep, ignition delay, and burn duration are provided in real time as well as the Coefficient of Variance for those parameters as indicated.

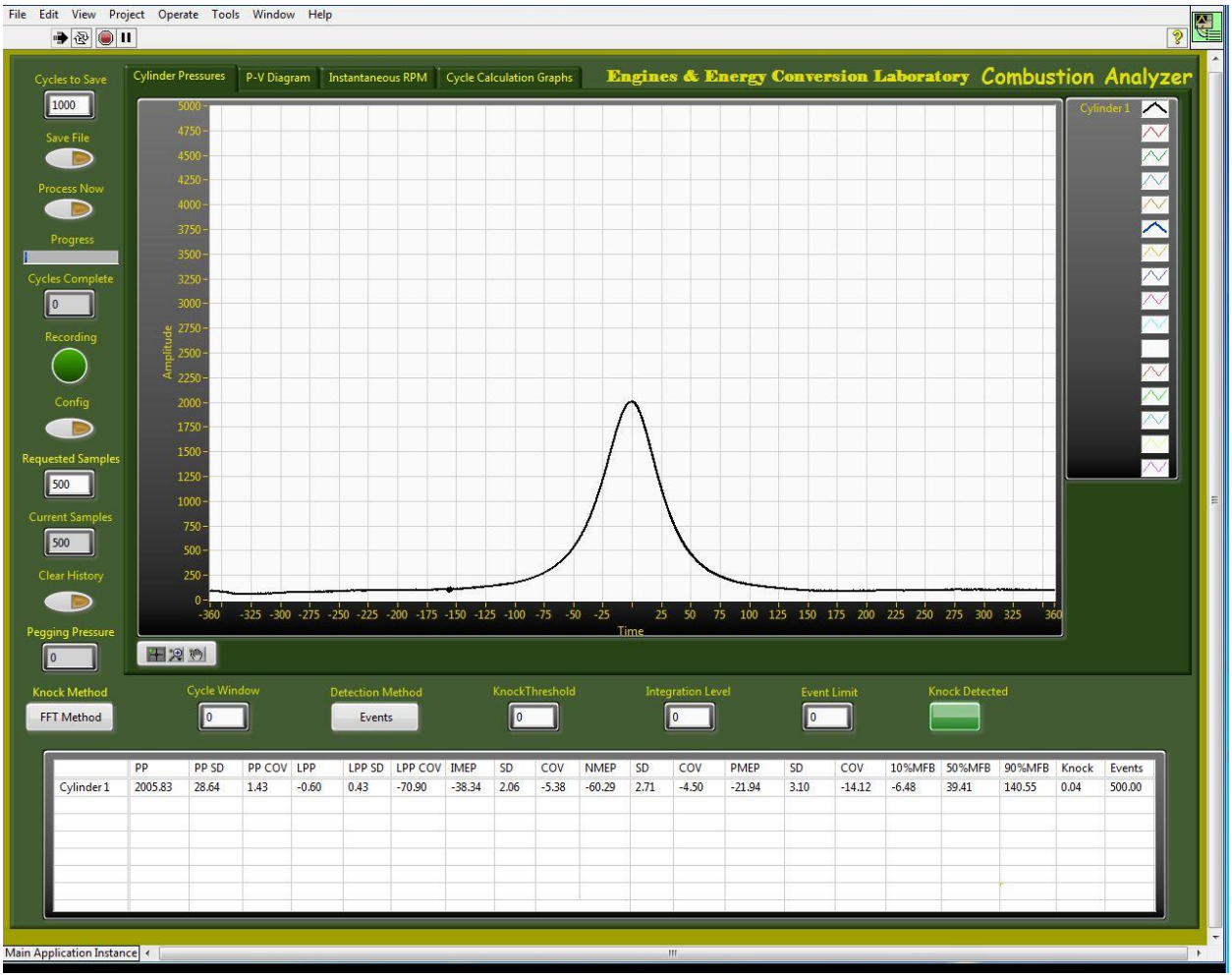

	PP	PP SD	PP COV	LPP	LPP SD	LPP COV	IMEP	SD	COV	NMEP	SD	COV	PMEP	SD	COV	10%MFB	50%MFB	90%MFB	Knock	Events
Cylinder 1	2005.83	28.64	1.43	-0.60	0.43	-70.90	-38.34	2.06	-5.38	-60.29	2.71	-4.50	-21.94	3.10	-14.12	-6.48	39.41	140.55	0.04	500.00

Figure B- 2 Engine operations monitoring page, cylinder pressure display.

Figure B-3 also shows an in-cylinder pressure vs. crank angle plot for the engine operating at a compression ratio of 10:1, ignition timing of 17°bTDC, burning natural gas. Note that nmep is shown as 895 kPa with location of peak pressure at 16°aTDC and other parameters as indicated.

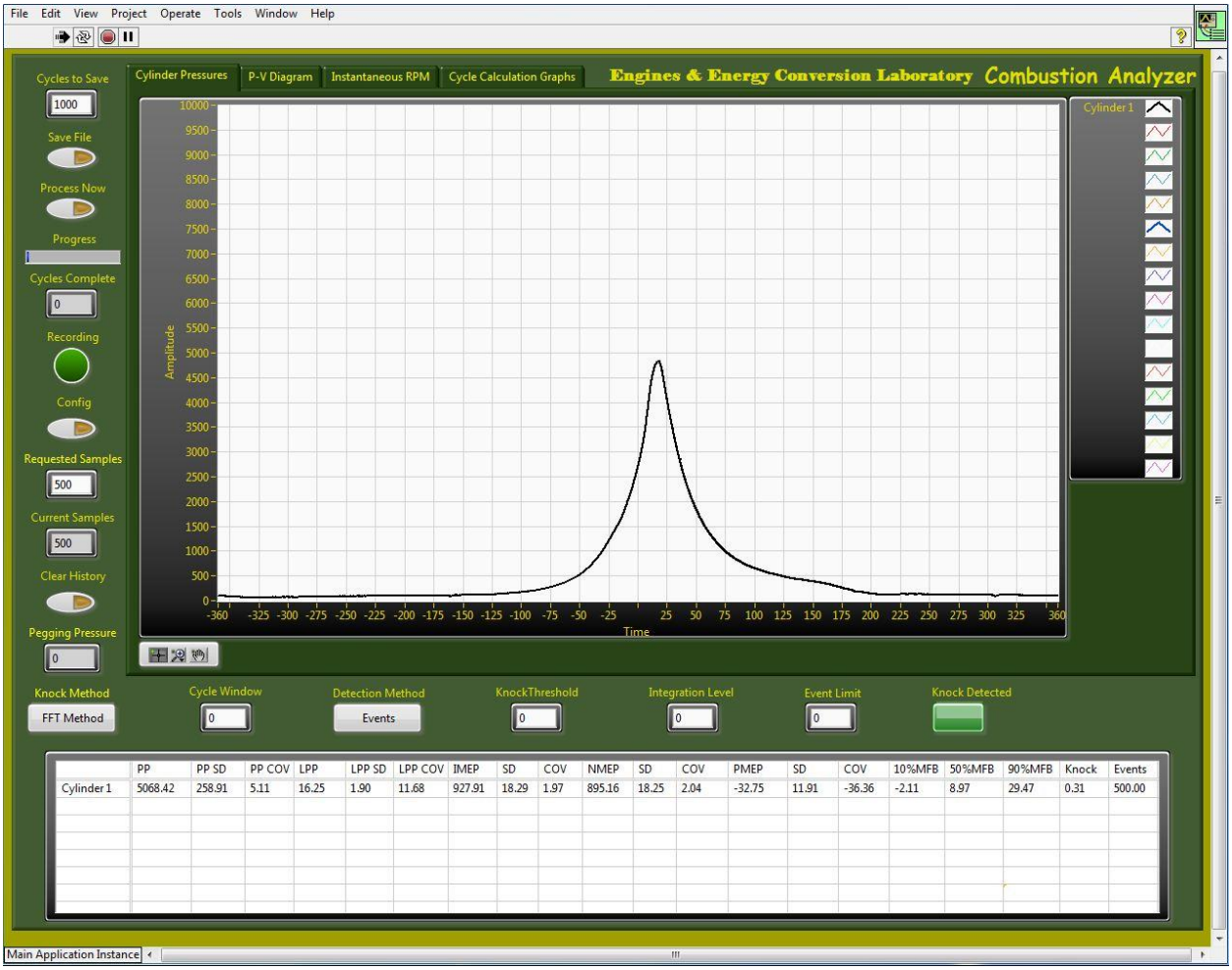

	PP	PP SD	PP COV	LPP	LPP SD	LPP COV	IMEP	SD	COV	NMEP	SD	COV	PMEP	SD	COV	10%MFB	50%MFB	90%MFB	Knock	Events
Cylinder 1	5068.42	258.91	5.11	16.25	1.90	11.68	927.91	18.29	1.97	895.16	18.25	2.04	-32.75	11.91	-36.36	-2.11	8.97	29.47	0.31	500.00

Figure B- 3 Engine operations monitoring page, cylinder pressure display.

Figure B-4 shows the pressure vs. volume curve for the operating engine. Scaling may be altered as necessary and is frequently desired to be shown in logarithmic scale for this particular plot.

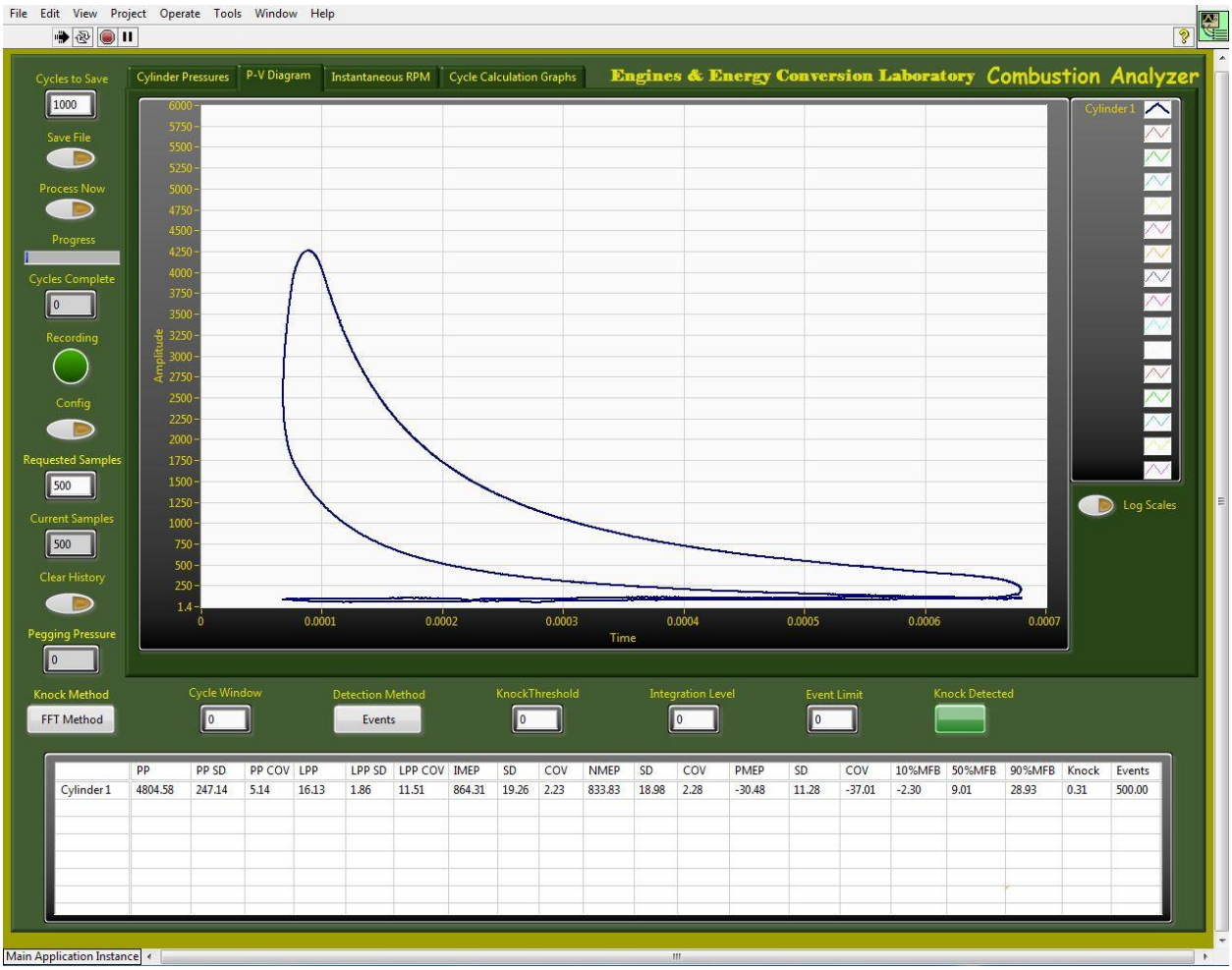

	PP	PP SD	PP COV	LPP	LPP SD	LPP COV	IMEP	SD	COV	NMEP	SD	COV	PMEP	SD	COV	10%MFB	50%MFB	90%MFB	Knock	Events
Cylinder 1	4804.58	247.14	5.14	16.13	1.86	11.51	864.31	19.26	2.23	833.83	18.98	2.28	-30.48	11.28	-37.01	-2.30	9.01	28.93	0.31	500.00

Figure B- 4 Engine operations monitoring page, P-V plot displayed (operating)

Figure B-5 shows the instantaneous RPM plot for the operating engine. For the CFR engine, a nominally constant speed device, the oscillation of actual engine speed as a function of crank can be observed in this plot.

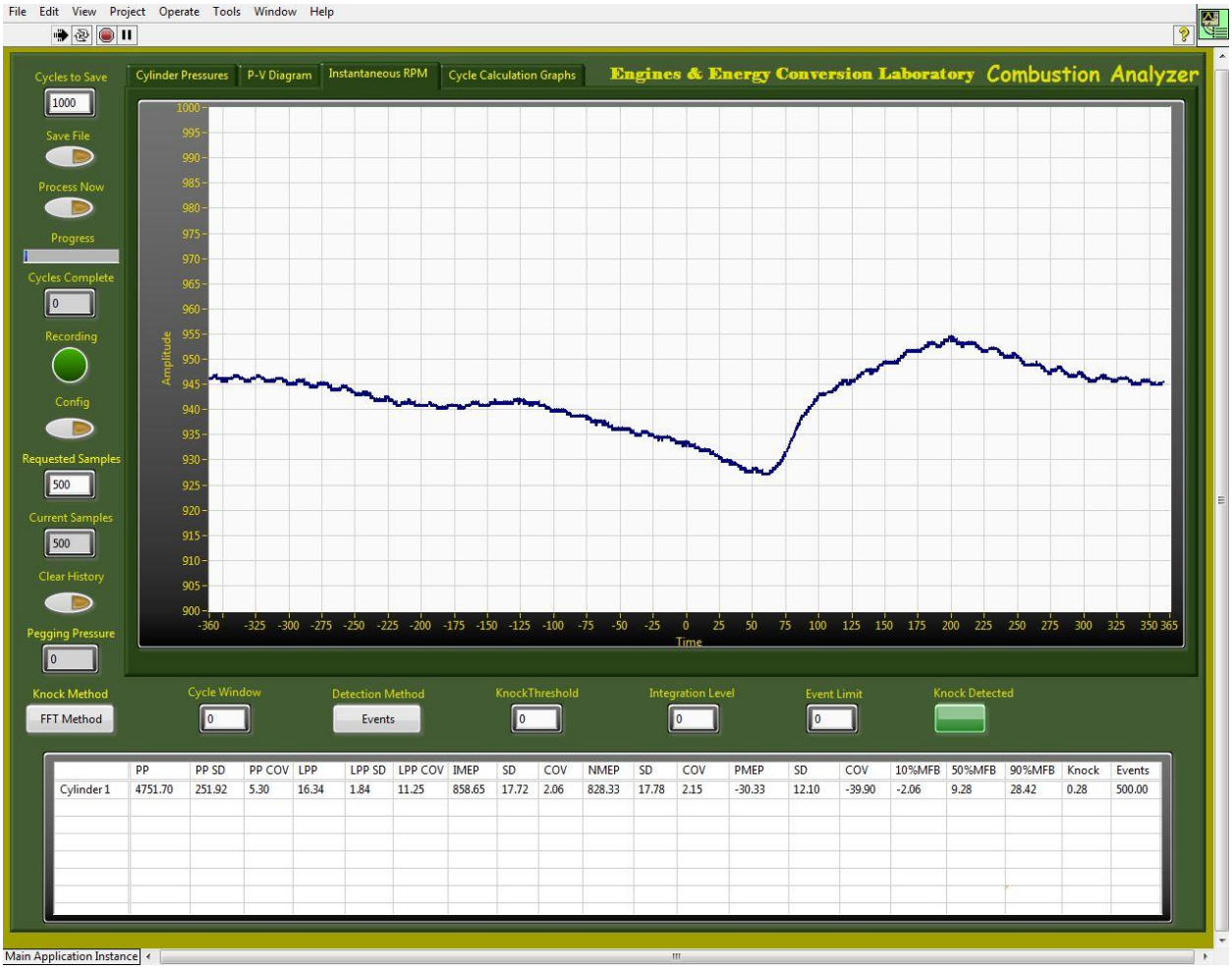

Figure B- 5 Engine operations monitoring page, instantaeous RPM plot displayed.

Figure B-6 knock detection screen for the analyzer. The plot is of the Fast Fourier Transform amplitude at 6 kHz (±200 Hz) for each engine cycle, shown in real time. This plot is illustrative of function only, no threshold values for amplitude level, integration level and event recurrance have been entered.

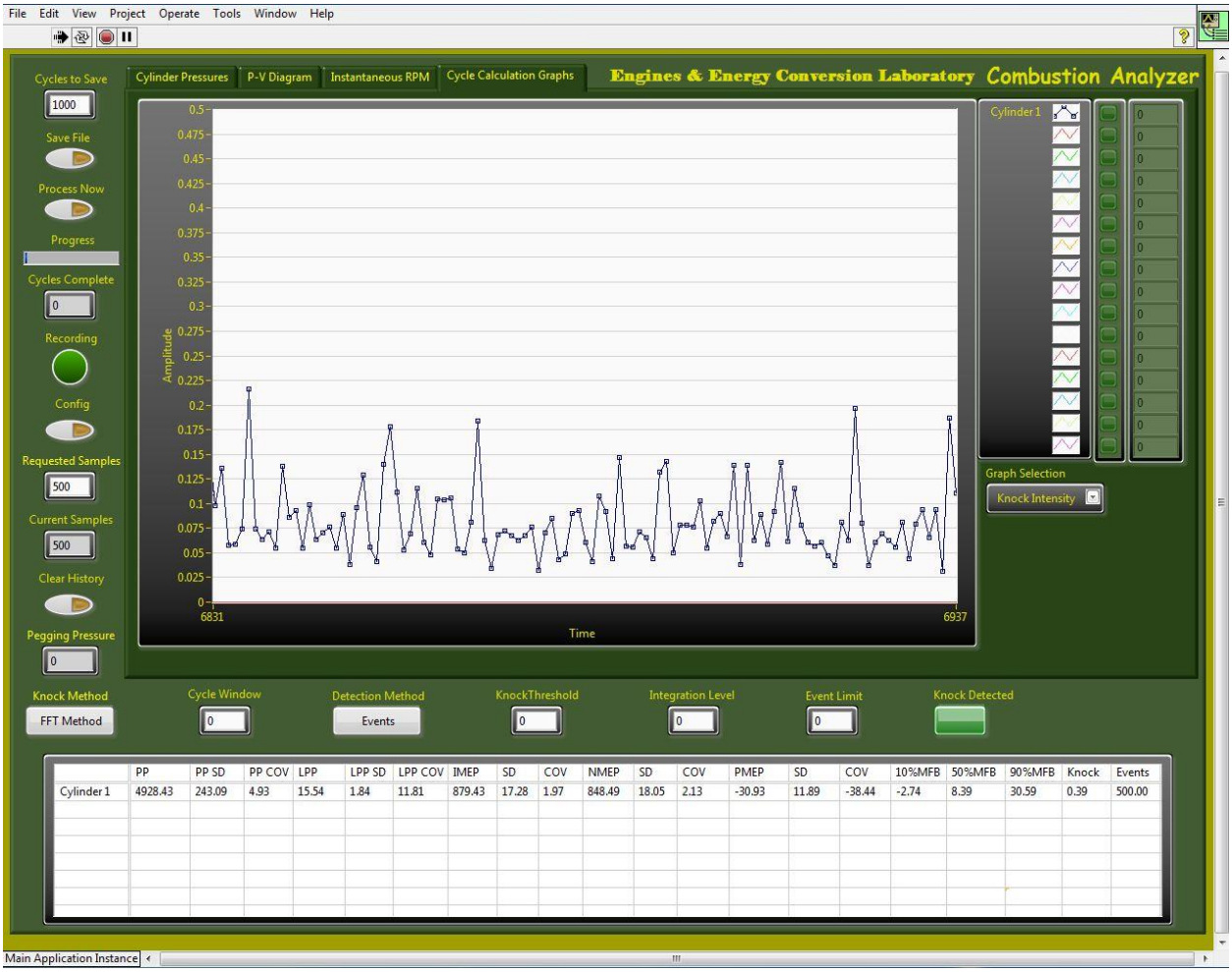

	PP	PP SD	PP COV	LPP	LPP SD	LPP COV	IMEP	SD	COV	NMEP	SD	COV	PMEP	SD	COV	10%MFB	50%MFB	90%MFB	Knock	Events
Cylinder 1	4928.43	243.09	4.93	15.54	1.84	11.81	879.43	17.28	1.97	848.49	18.05	2.13	-30.93	11.89	-38.44	-2.74	8.39	30.59	0.39	500.00

Figure B- 6 Engine operations monitoring page, FFT amplitude displayed.

Figure B-7 is a block diagram excerpt showing the combustion loop module of the combustion analyzer program.

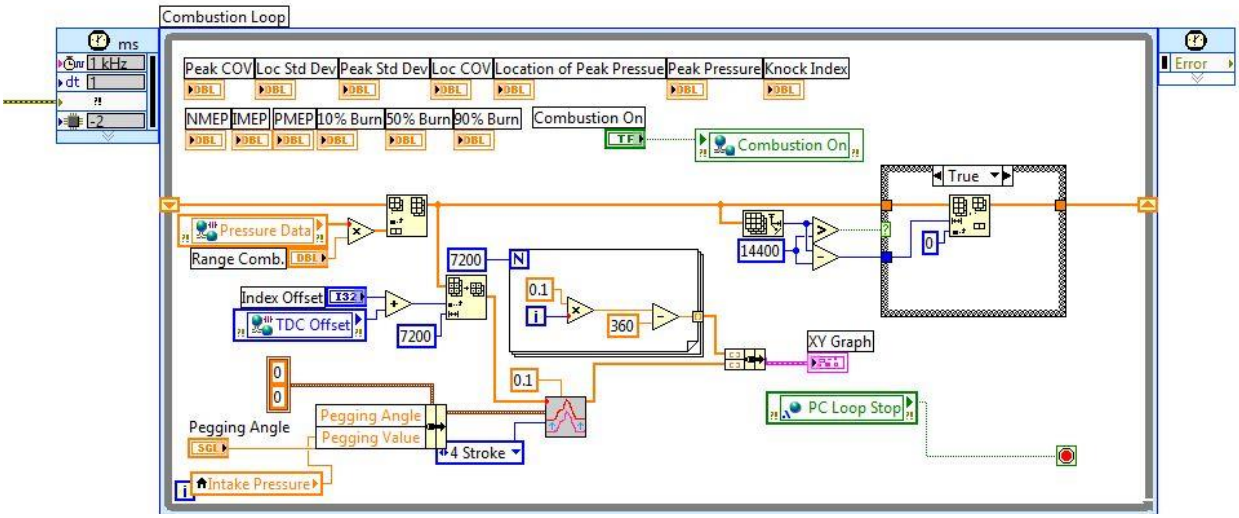

Figure B- 7 Combustion loop module of combustion analyzer block diagram.

B-1 CFR TEST CELL VI

The LabVIEW© program CFR Host VI is developed for operation of the test cell to include the fuel blending system, control of engine operations and emissions monitoring and logging. Figure B-8 shows the Operational Parameters screen of program. From this screen the operator can monitor key temperatures (inlet air, exhaust, engine coolant), exhaust and intake pressure, engine RPM and output power. Additionally, intake boost pressure is controlled by enabling remote air control and setting air setpoint (intake air boost pressure) to desire levels to elevate or reduce engine nmep. The intake air vent icon is a safety shutdown feature that allows the operator to isolate fuel and combustion air (removing power from fail shut isolation solenoid valves for fuel and air) while venting the intake manifold to atmosphere (removing power from the fail open intake ventilation solenoid valve). When activated the icon changes from green to red.

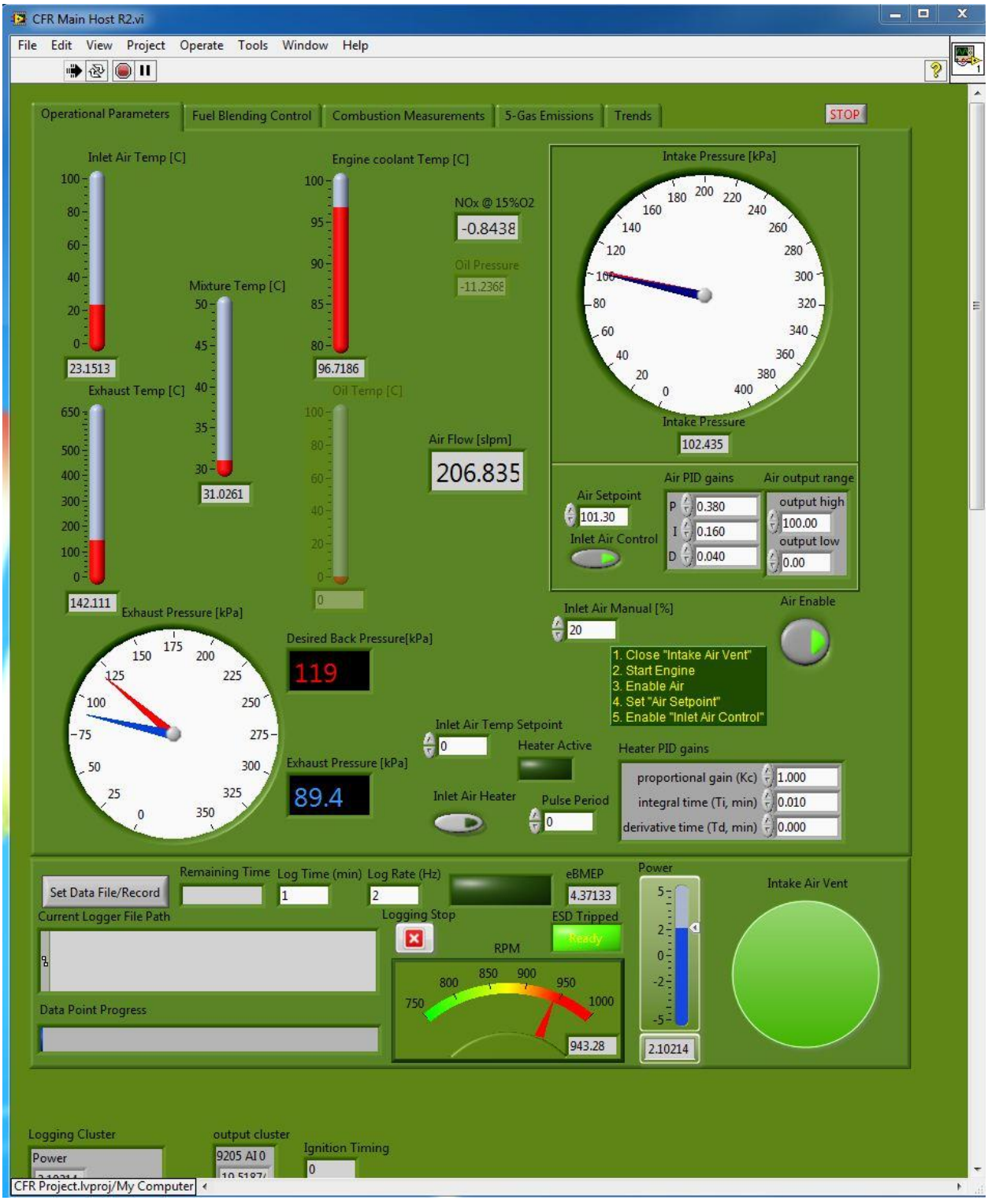

Figure B- 8 CFR Host VI Operational Parameters screen.

Figure B-9 shows the Fuel Blending Control screen for the CFR Host VI. This screen allows the operator to set operating characteristics of the fuel blending system and monitor performance of the system is real time. Fuel injector maximum duty cycle, desired air-fuel ratio, Air-Fuel Recorder range presets are entered. Stoichiometric conditions are controlled with air-fuel control selected from a choice of broad-band O_2 sensor input (Air-Fuel Recorder) control or mass flow control (combustion air mass flow meter output to summed fuel component mass flow output). Either system will compare air-fuel ratio with desired and adjust accordingly. The fuel system is enabled from this screen physically operating the fuel injectors which send proportioned fuel to the engine.

Figure B- 9 Fuel blending control display of the CFR Host VI program.

Figure B-10 shows the 5-Gas Emissions display of the CFR Host VI. The display provides real time broadcast of the data output from the 5-Gas Analyzer monitoring engine exhaust for the CFR. The data set enabled consists of value for total hydrocarbons (THC), oxygen (O_2), nitrogen oxides or NOx (NO and NO_2), carbon dioxide (CO_2), and carbon monoxide (CO). It is noted that all of the displays for the CFR Host VI allow the operator to monitor RPM, bmep, and output power as well as to observe/active intake air ventilation in the event of an emergency shutdown of the engine.

Figure B-11 shows a block diagram excerpt of the fuel blending module of the CFR Host VI and is included to give the reader an organization frame of reference for the program.

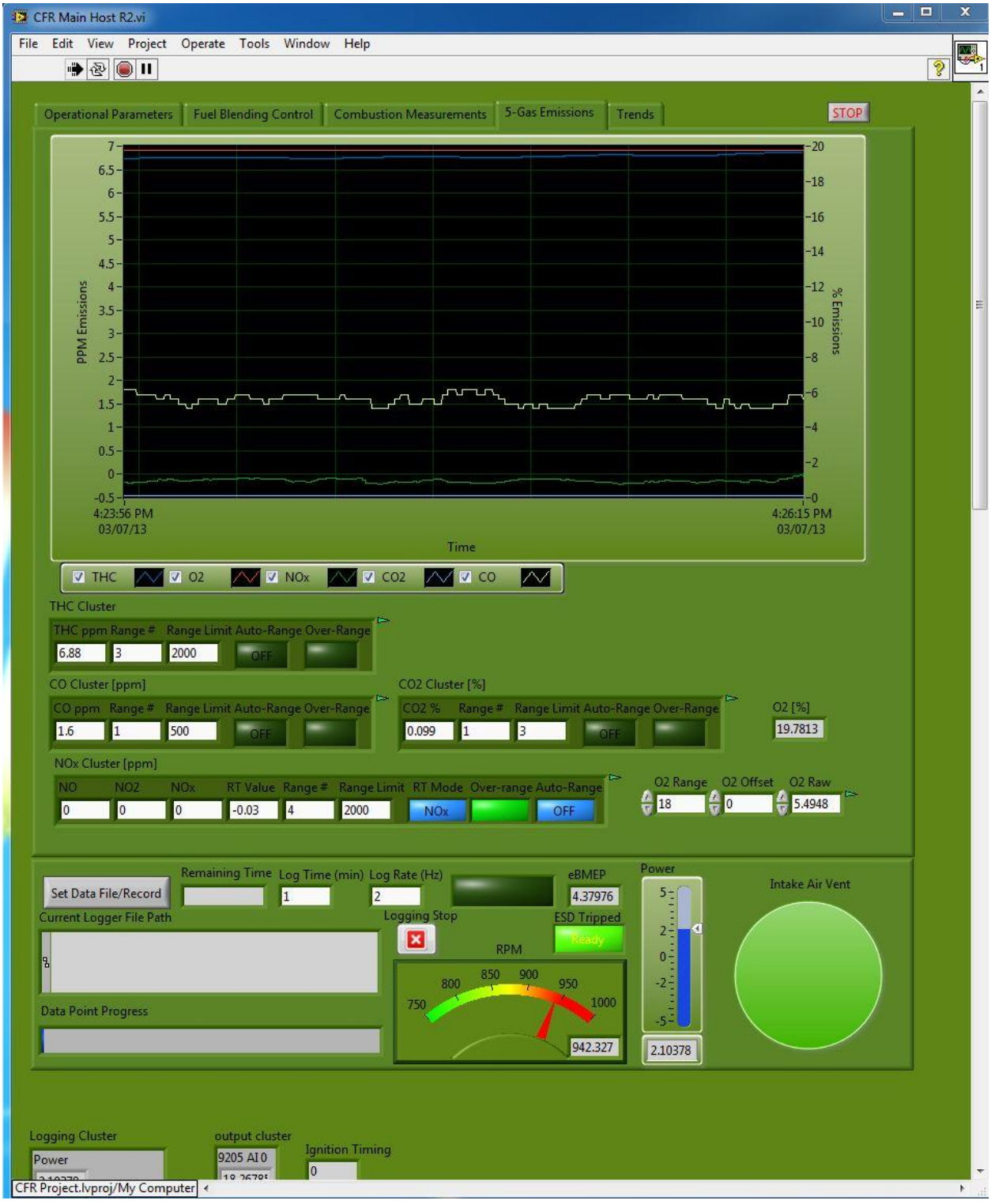

Figure B- 10 5-Gas Emissions display for the CFR Host VI.

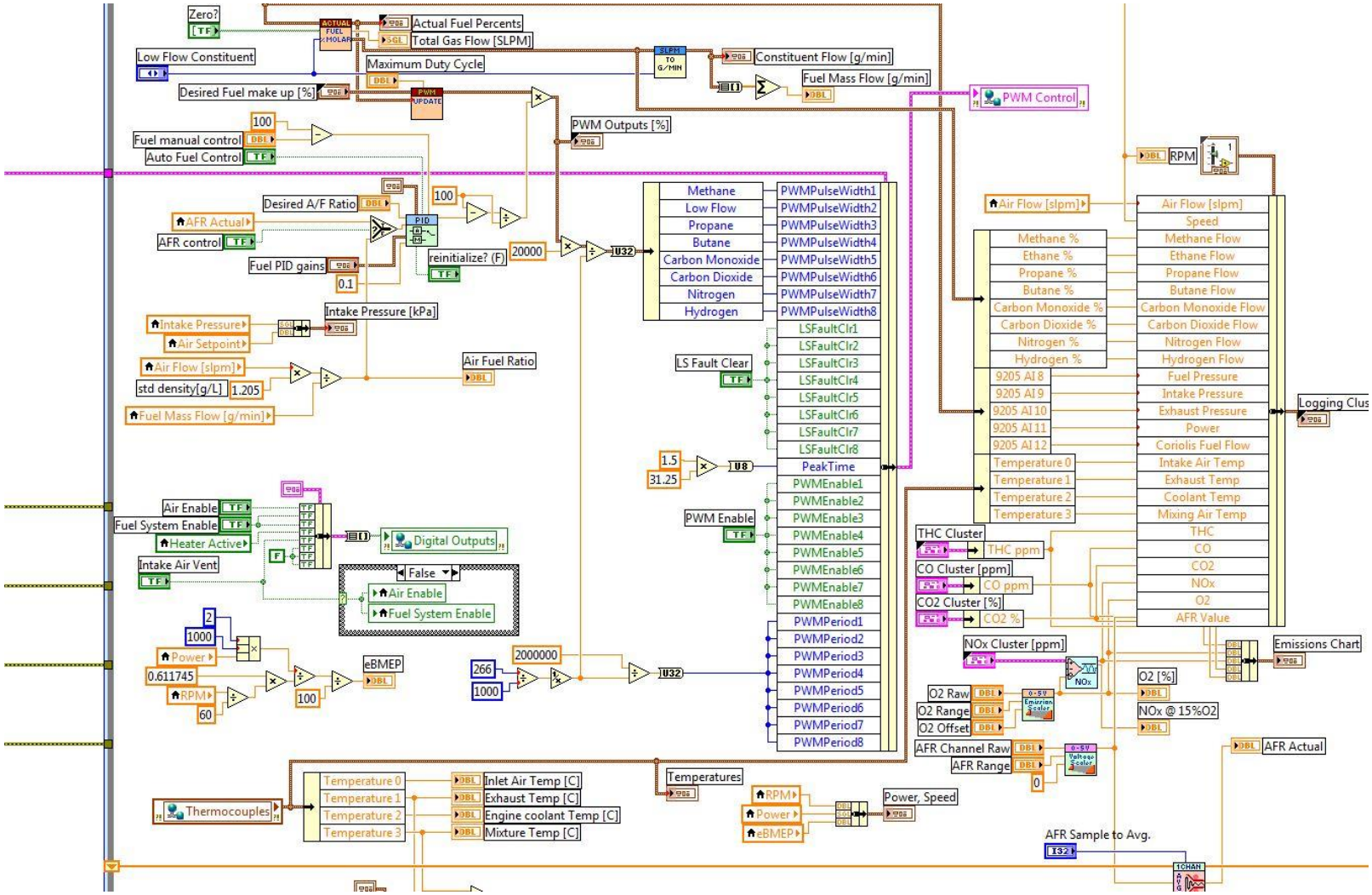

Figure B- 11 Block Diagram of CFR Host VI Fuel Blending Module

B-2 ELECTRONIC IGNITION

A third system enabling automated operation and control of the CFR engine is the electronic ignition system installed in the test cell. The Altronic CD200 system allows the operator to monitor and adjust ignition timing during engine operation without any mechanical interface to the engine. Figure B-11 shows the program terminal display while the engine is operating with ignition timing set at 17.0°bTDC.

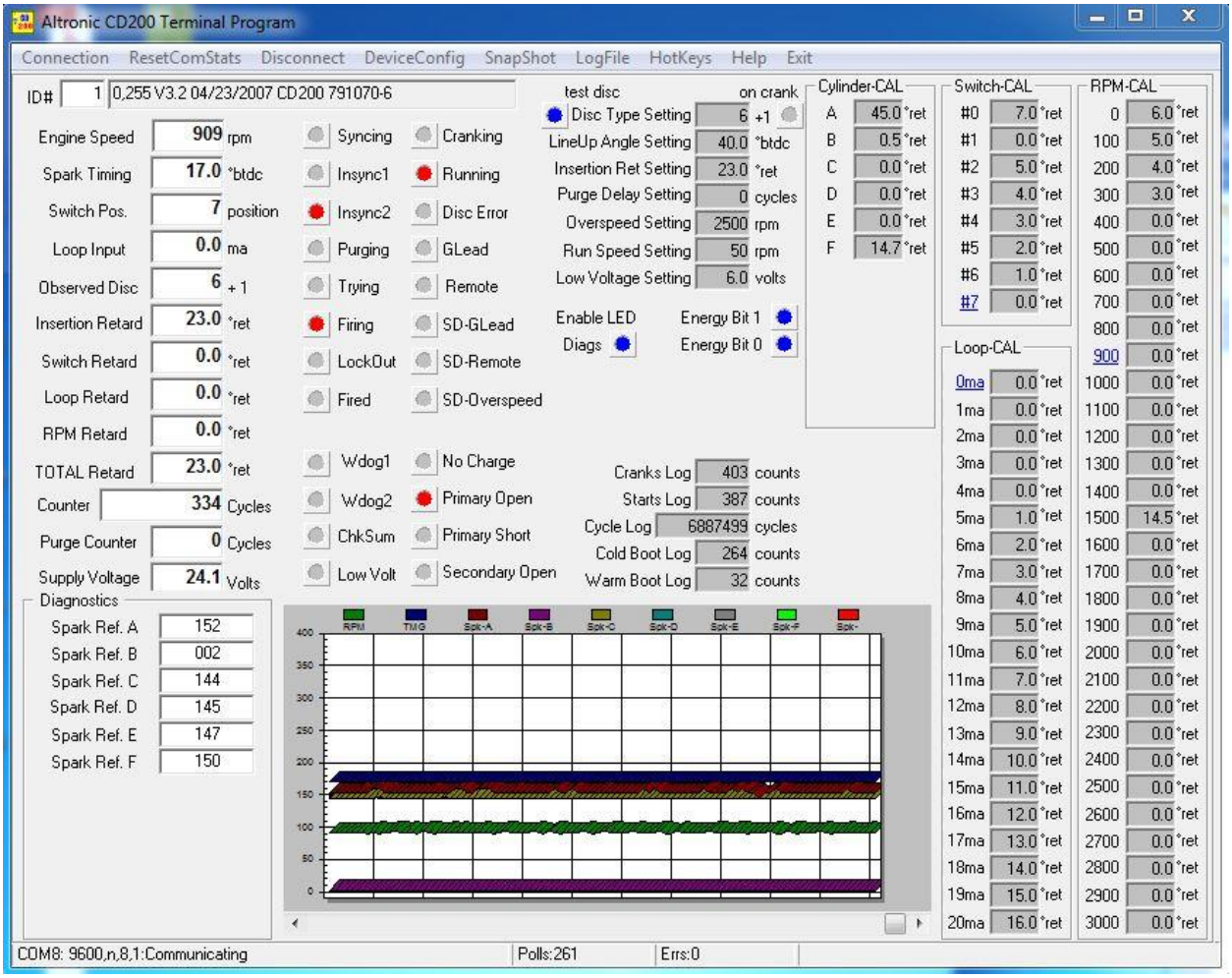

Figure B- 12 Electronic Ignition Terminal Program Display

Appendix C NEURAL NETWORK STATISTICAL ANALYSIS

Table C- 1 Results of Neural Network Predictive Model for Producer Gas Blends

											Neural Network Predicted Values			
Blend Name	N2	CO2	CO	H2	CH4	CO+H2	Diluent	A/Fs	LHV	MN	All Variables:	Less CO+H2 & Diluent:	Less A/Fs	Less LHV
AF Gap A	0.05	0.19	0.34	0.34	0.08	0.69	0.24	3.26	11472	62.2	53.6	54.6	58.9	59.6
AF Gap B	0.00	0.19	0.20	0.33	0.29	0.53	0.19	6.11	19307	93.5	83.0	79.5	91.4	93.4
AF Gap C	0.14	0.00	0.19	0.47	0.20	0.66	0.14	7.56	24548	56.3	46.7	44.5	52.2	56.5
AF Gap D	0.11	0.05	0.09	0.47	0.28	0.56	0.16	8.65	27128	56.3	58.4	56.1	56.4	56.3
AF Gap E	0.10	0.06	0.11	0.25	0.48	0.36	0.16	9.37	28348	78.0	98.1	90.6	78.2	77.4
Banham	0.00	0.20	0.21	0.36	0.23	0.57	0.20	5.39	17316	80.3	75.7	74.1	81.9	80.3
Blend #1	0.07	0.17	0.37	0.39	0.00	0.76	0.24	2.55	9664	35.9	33.8	34.4	29.6	30.2
Blend #2	0.48	0.14	0.18	0.18	0.02	0.36	0.62	1.20	4362	96.7	103.8	106.5	94.0	93.7
Blend #3	0.11	0.06	0.12	0.26	0.45	0.38	0.17	8.96	27214	71.0	93.5	86.3	79.7	73.7
Blend #4	0.15	0.15	0.20	0.50	0.00	0.70	0.30	2.78	10195	25.7	29.3	29.3	24.3	25.7
Blend #5	0.15	0.00	0.20	0.50	0.15	0.70	0.15	6.80	22536	31.9	39.4	37.9	36.1	60.5
Chroen (O2)	0.00	0.20	0.39	0.40	0.00	0.79	0.21	2.64	10004	25.9	33.2	33.9	29.0	28.3
City Energy	0.29	0.00	0.00	0.26	0.44	0.27	0.29	8.81	26273	92.0	88.3	79.5	85.2	73.4
CPC	0.57	0.01	0.21	0.19	0.02	0.40	0.58	1.45	5292	66.2	72.1	70.0	75.3	67.2
Cranfield	0.00	0.22	0.17	0.52	0.08	0.69	0.22	4.14	14121	51.1	44.7	45.7	51.8	62.6
Dil Gap A	0.12	0.07	0.13	0.28	0.40	0.41	0.18	8.28	25360	90.2	86.7	79.4	86.5	89.6
Dil Gap B	0.03	0.24	0.26	0.43	0.04	0.68	0.28	2.89	10285	46.3	48.9	46.8	42.9	42.5
Dil Gap C	0.16	0.16	0.19	0.50	0.00	0.68	0.32	2.67	9785	21.5	31.7	32.0	24.5	26.0
Dil Gap D	0.23	0.19	0.45	0.07	0.07	0.52	0.41	1.94	7024	97.6	104.1	106.9	97.3	95.3
Dil Gap F	0.41	0.14	0.22	0.17	0.05	0.40	0.56	1.62	5570	97.6	93.5	94.5	94.3	94.3
Gussing	0.03	0.23	0.24	0.40	0.10	0.64	0.26	3.58	12186	68.2	60.3	61.1	61.5	63.8
Harboore	0.41	0.12	0.23	0.19	0.05	0.42	0.53	1.80	6335	91.1	89.3	89.8	93.1	93.6
Hyder	0.05	0.07	0.13	0.27	0.47	0.41	0.12	9.74	29597	79.4	92.4	84.4	78.1	77.1
IISc	0.49	0.12	0.19	0.19	0.02	0.38	0.61	1.23	4503	96.0	95.0	96.8	92.9	93.6
Meadow Vale	0.09	0.08	0.31	0.16	0.37	0.47	0.17	6.40	20088	86.0	93.7	87.1	86.1	86.1
Plasma	0.03	0.17	0.38	0.40	0.02	0.78	0.21	2.88	10720	23.2	33.8	35.2	30.7	29.7
Repotec	0.05	0.20	0.25	0.40	0.10	0.65	0.25	3.70	12629	58.5	55.1	55.1	61.0	62.5
S4 Avg	0.05	0.19	0.35	0.35	0.05	0.71	0.24	2.95	10613	46.6	52.1	57.0	48.4	48.0
S4 Example	0.02	0.11	0.41	0.43	0.03	0.84	0.13	3.56	13129	29.9	24.3	26.8	29.6	30.0
TEMCO	0.19	0.14	0.53	0.07	0.07	0.59	0.34	2.18	7993	91.3	83.0	82.8	97.2	93.6
Victoria 1	0.11	0.05	0.10	0.49	0.25	0.58	0.17	8.32	26237	56.1	52.0	47.6	56.3	56.2
Viking	0.33	0.15	0.20	0.30	0.02	0.50	0.49	1.73	6282	70.0	70.1	71.0	69.9	70.5
VT 4/7/08	0.08	0.09	0.38	0.24	0.21	0.62	0.17	4.92	16293	58.1	63.0	58.6	59.1	58.4
VT 4/9/08	0.02	0.08	0.52	0.20	0.18	0.72	0.10	4.48	15327	60.5	48.8	43.7	59.9	60.5
WTG	0.01	0.18	0.44	0.22	0.15	0.66	0.19	3.75	12838	73.3	67.7	66.4	60.6	73.0
											"Bad" Predictions, > 30% error			

Table C- 2 Neural Network Data Set #1 Summary

Testing Summary Data Set #1: 9 Independent Variables

Summary	
Net Information	
Name	Net Trained on Data Set #1
Configuration	Linear Predictor
Location	This Workbook
Independent Category Variables	0
Independent Numeric Variables	9 (N2, CO2, CO, H2, CH4, CO+H2, Diluent, A/Fs, LHV)
Dependent Variable	Numeric Var. (MN)
Testing	
Number of Cases	35
% Bad Predictions (30% Tolerance)	8.5714%
Root Mean Square Error	8.306
Mean Absolute Error	6.842
Std. Deviation of Abs. Error	4.710
Data Set	
Name	Data Set #1
Number of Rows	35
Manual Case Tags	NO
Variable Matching	Automatic
Indep. Category Variables Used	None
Indep. Numeric Variables Used	Names from training
Dependent Variable	Numeric Var. (MN)

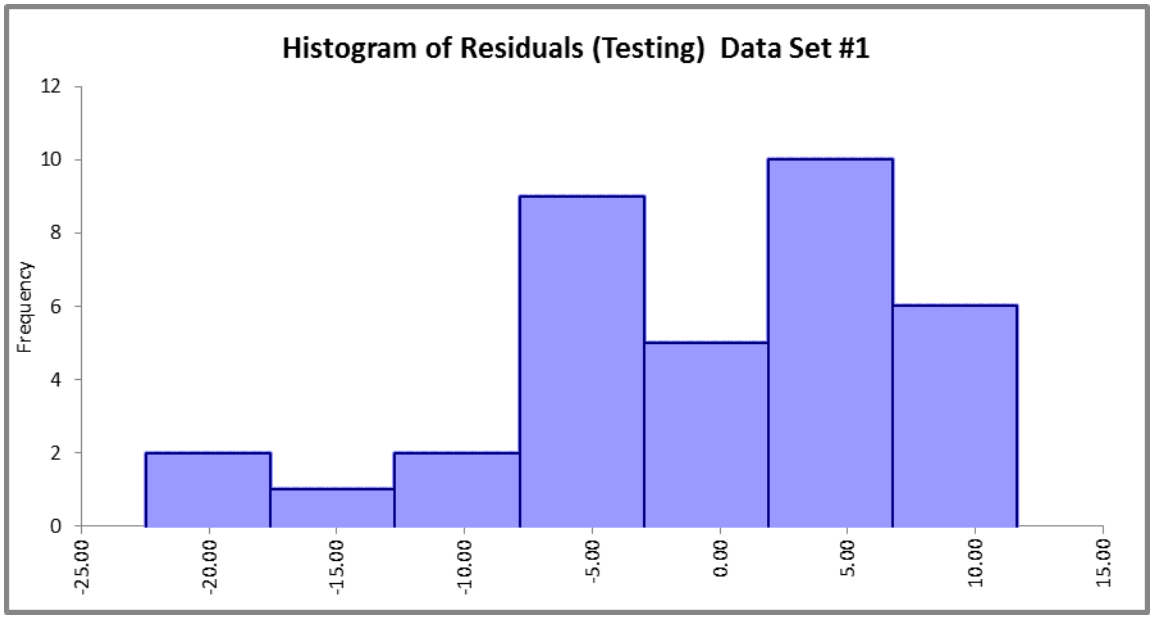

Figure C- 1 Data Set #1 Residuals

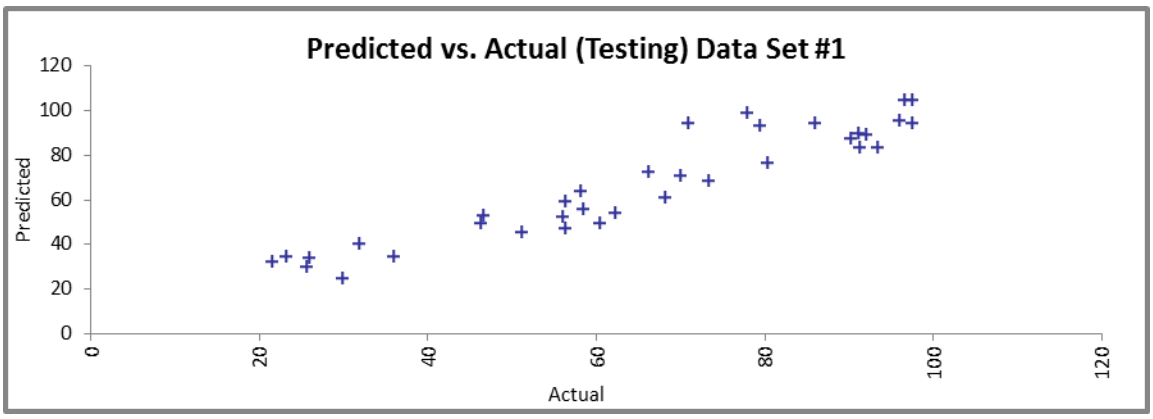

Figure C- 2 Data Set #1: Predicted vs. Actual Values

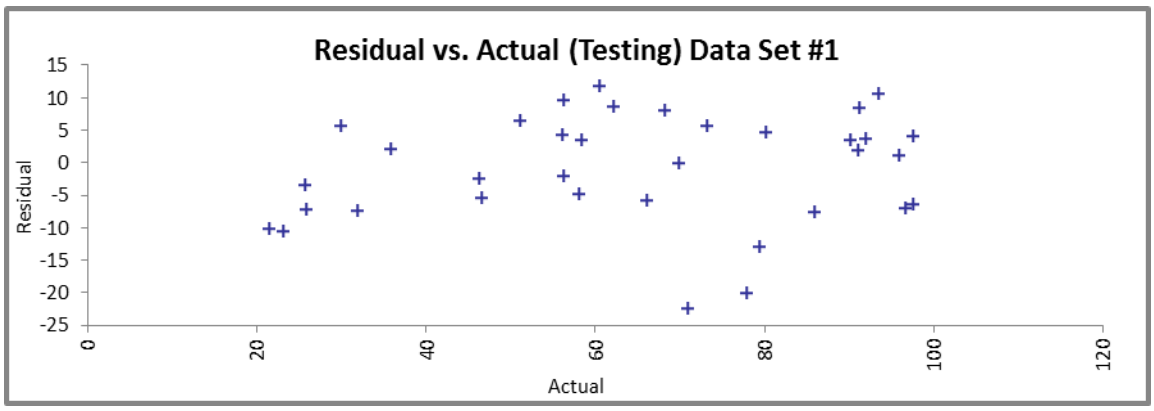

Figure C- 3 Data Set #1: Residual vs. Actual Values

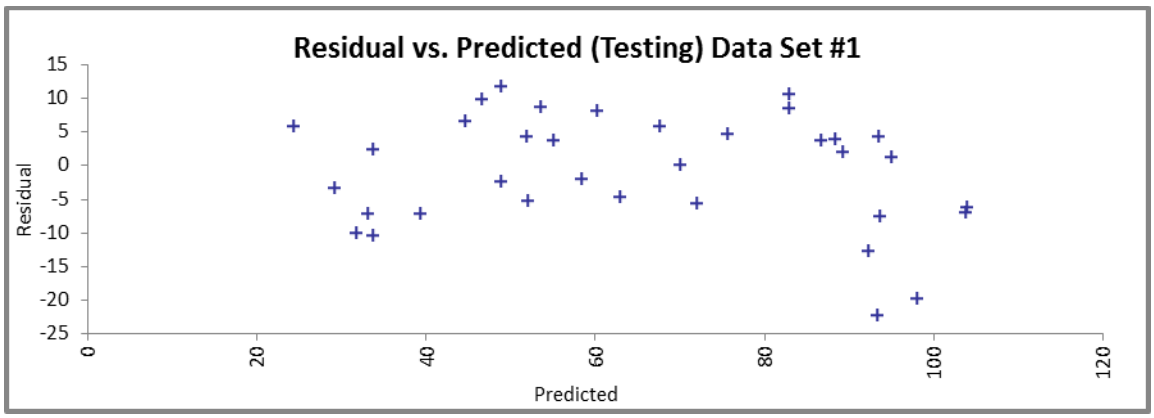

Figure C- 4 Data Set #1: Residual vs. Predicted Values

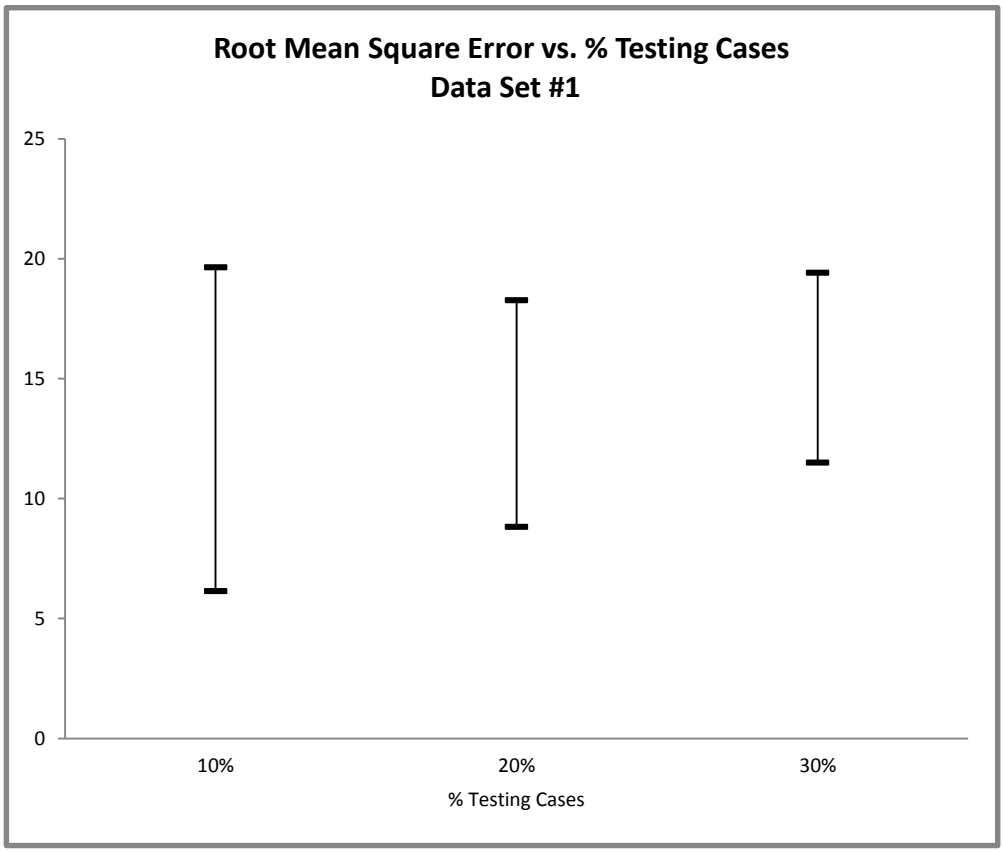

Figure C- 5 Data Set #1 Sensitivity Analysis

Table C- 3 Data Set #1 RMS Error

10%	20%	30%
6.127	8.816	11.49
9.220	12.85	12.45
13.78	13.64	13.08
16.19	13.81	19.12
19.63	18.26	19.41

Table C- 4 Neural Network Data Set #2 Summary

Testing Summary **Data Set #2: 7 Independent Variables**

Summary	
Net Information	
Name	Net Trained on Data Set #2
Configuration	Linear Predictor
Location	This Workbook
Independent Category Variables	0
Independent Numeric Variables	7 (N2, CO2, CO, H2, CH4, A/Fs, LHV)
Dependent Variable	Numeric Var. (MN)
Testing	
Number of Cases	35
% Bad Predictions (30% Tolerance)	8.5714%
Root Mean Square Error	8.259
Mean Absolute Error	6.829
Std. Deviation of Abs. Error	4.645
Data Set	
Name	Data Set #2
Number of Rows	35
Manual Case Tags	NO
Variable Matching	Automatic
Indep. Category Variables Used	None
Indep. Numeric Variables Used	Names from training
Dependent Variable	Numeric Var. (MN)

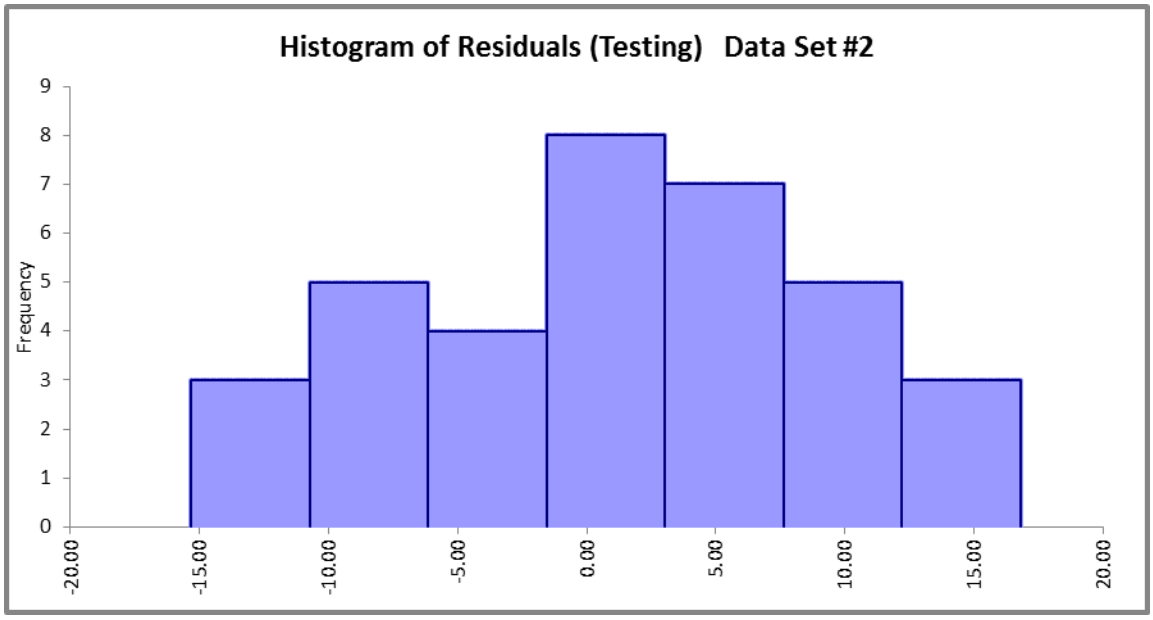

Figure C- 6 Data Set #2 Residuals

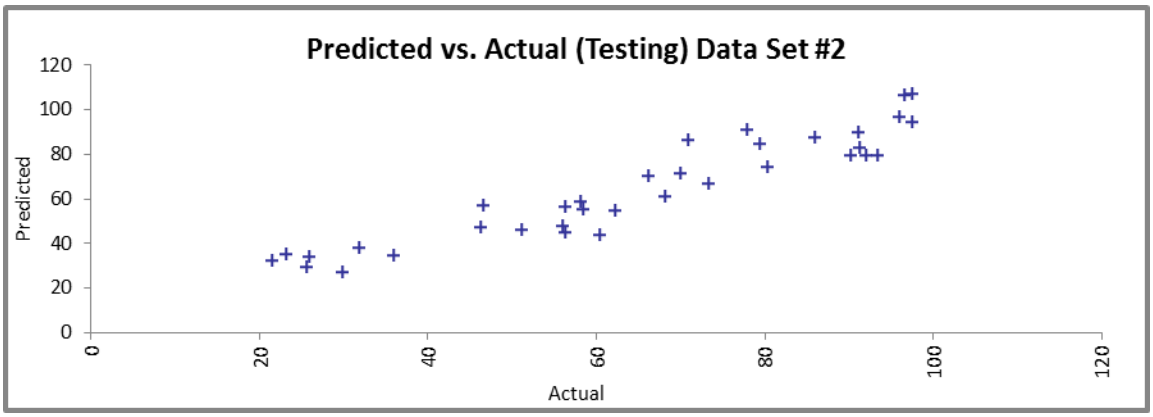

Figure C- 7 Data Set #2: Predicted vs. Actual Values

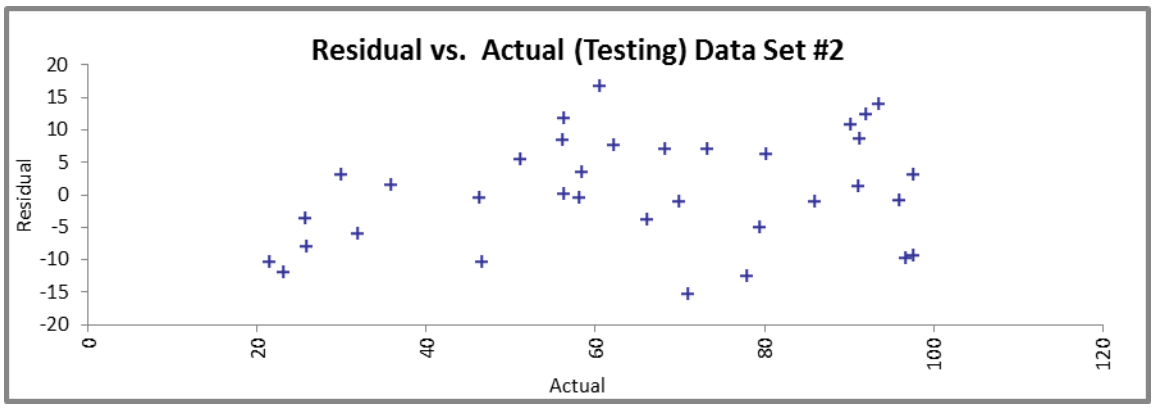

Figure C- 8 Data Set #2: Residual vs. Actual Values

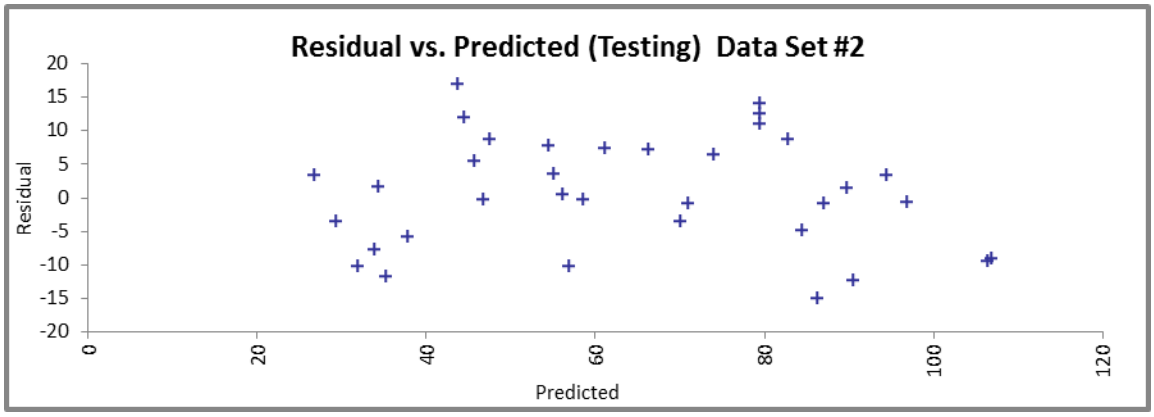

Figure C- 9 Data Set #2: Residual vs. Predicted Values

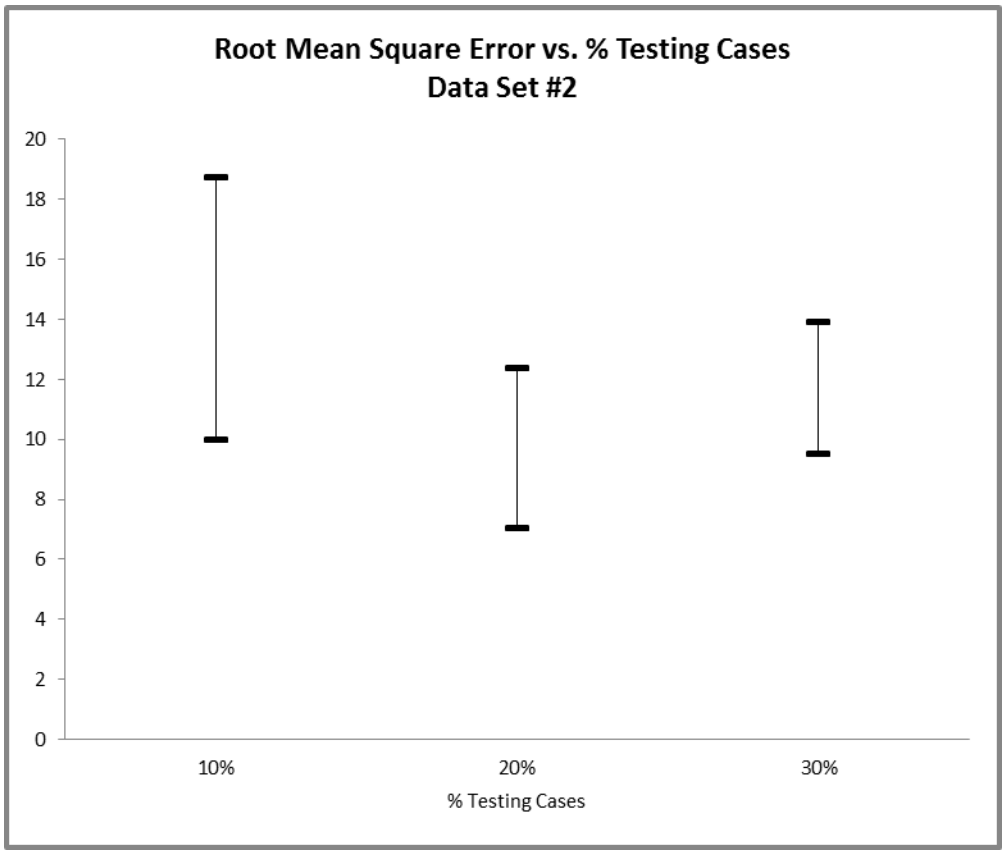

Figure C- 10 Data Set #2 Sensitivity Analysis

Table C- 5 Data Set #2 RMS Error

10%	20%	30%
9.960	6.992	9.475
10.51	9.439	10.38
11.44	9.864	11.15
16.58	10.22	11.72
18.69	12.33	13.87

Table C- 6 Neural Network Data Set #3 Summary

Testing Summary **Data Set #3: 6 Independent Variables**

Summary	
Net Information	
Name	Net Trained on Data Set #3
Configuration	GRNN Numeric Predictor
Location	This Workbook
Independent Category Variables	0
Independent Numeric Variables	6 (N2, CO2, CO, H2, CH4, LHV)
Dependent Variable	Numeric Var. (MN)
Testing	
Number of Cases	35
% Bad Predictions (30% Tolerance)	2.8571%
Root Mean Square Error	4.423
Mean Absolute Error	3.258
Std. Deviation of Abs. Error	2.991
Data Set	
Name	Data Set #3
Number of Rows	35
Manual Case Tags	NO
Variable Matching	Automatic
Indep. Category Variables Used	None
Indep. Numeric Variables Used	Names from training
Dependent Variable	Numeric Var. (MN)

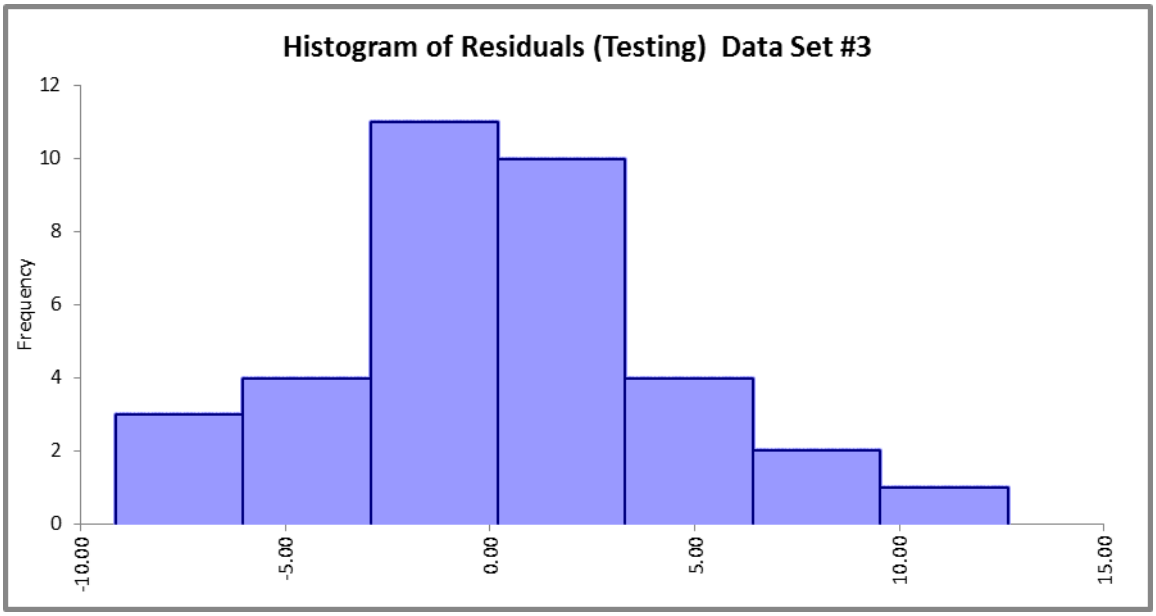

Figure C- 11 Data Set #3 Residuals

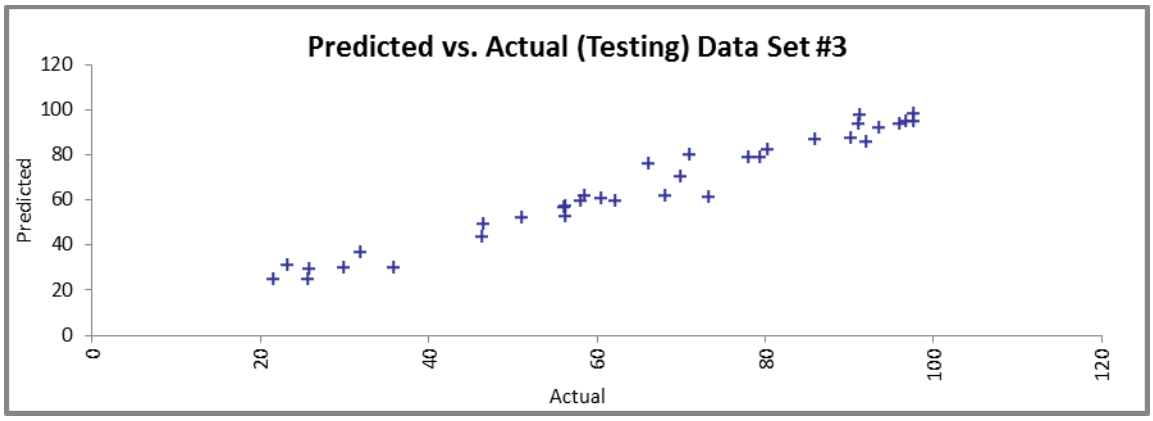

Figure C- 12 Data Set #3: Predicted vs. Actual Values

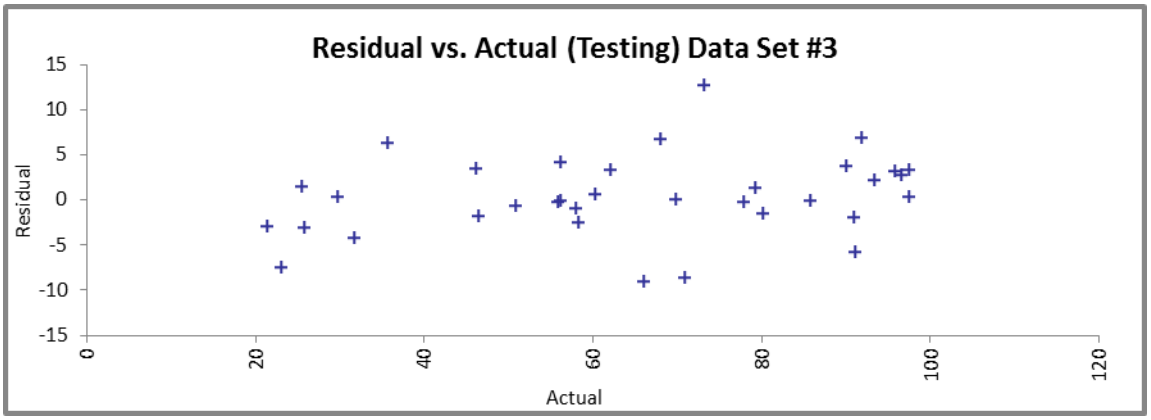

Figure C- 13 Data Set #3: Predicted vs. Actual Values

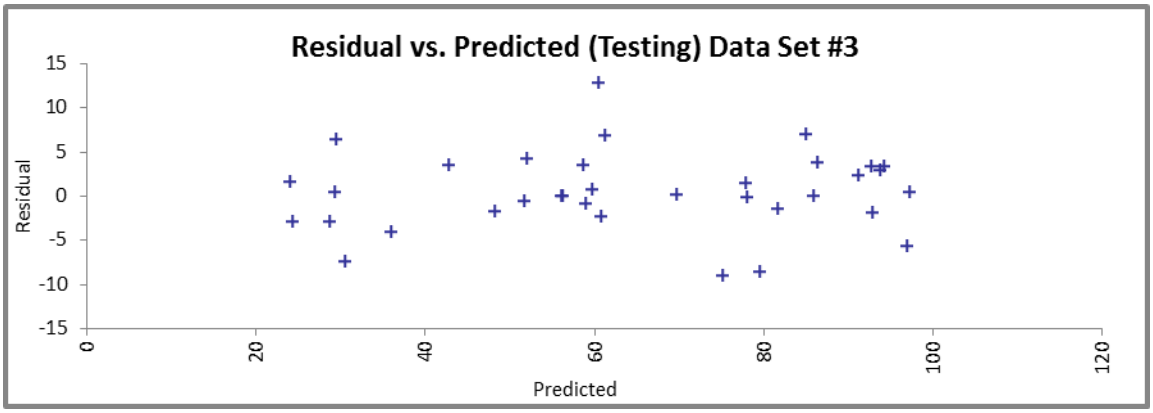

Figure C- 14 Data Set #3: Residual vs. Predicted Values

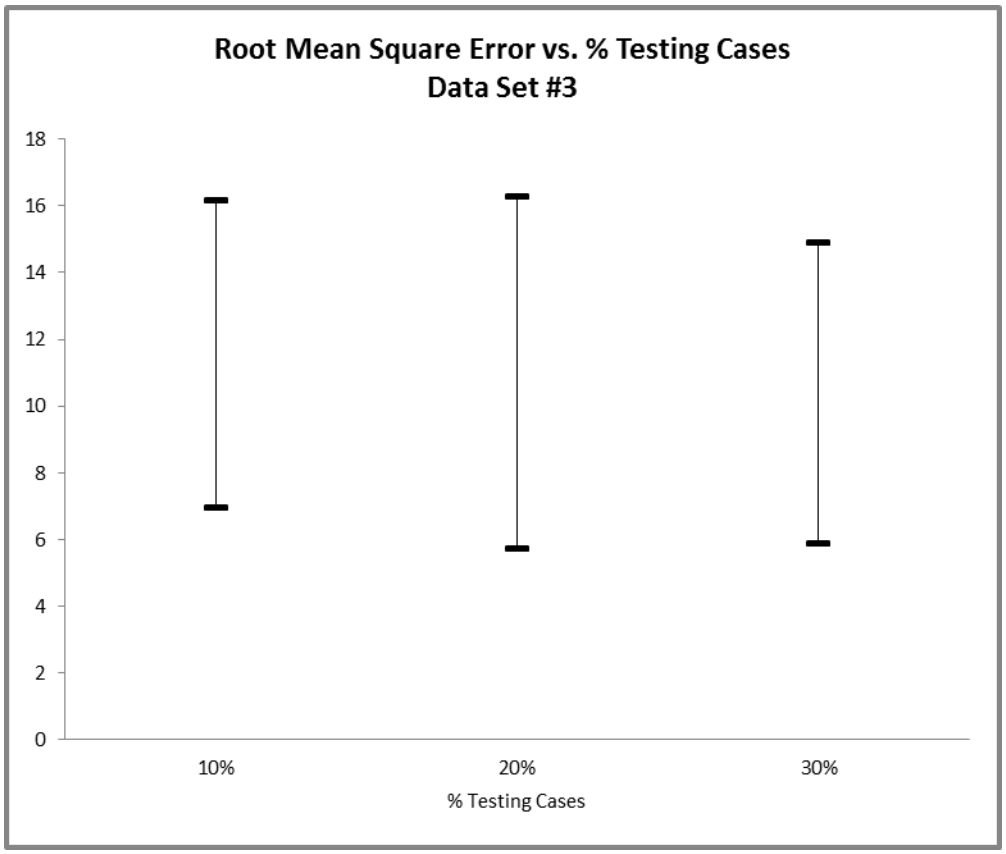

Figure C- 15 Data Set #3 Sensitivity Analysis

Table C- 7 Data Set #3 RMS Error

10%	20%	30%
6.910	5.706	5.843
7.870	6.170	8.388
10.60	9.873	14.68
13.03	13.79	14.81
16.13	16.24	14.87

Table C- 8 Neural Network Data Set #4 Summary

Testing Summary **Data Set #4: 5 Independent Variables**

Summary	
Net Information	
Name	Net Trained on Data Set #4
Configuration	GRNN Numeric Predictor
Location	This Workbook
Independent Category Variables	0
Independent Numeric Variables	5 (N2, CO2, CO, H2, CH4)
Dependent Variable	Numeric Var. (MN)
Testing	
Number of Cases	35
% Bad Predictions (30% Tolerance)	2.8571%
Root Mean Square Error	6.568
Mean Absolute Error	3.394
Std. Deviation of Abs. Error	5.624
Data Set	
Name	Data Set #4
Number of Rows	35
Manual Case Tags	NO
Variable Matching	Automatic
Indep. Category Variables Used	None
Indep. Numeric Variables Used	Names from training
Dependent Variable	Numeric Var. (MN)

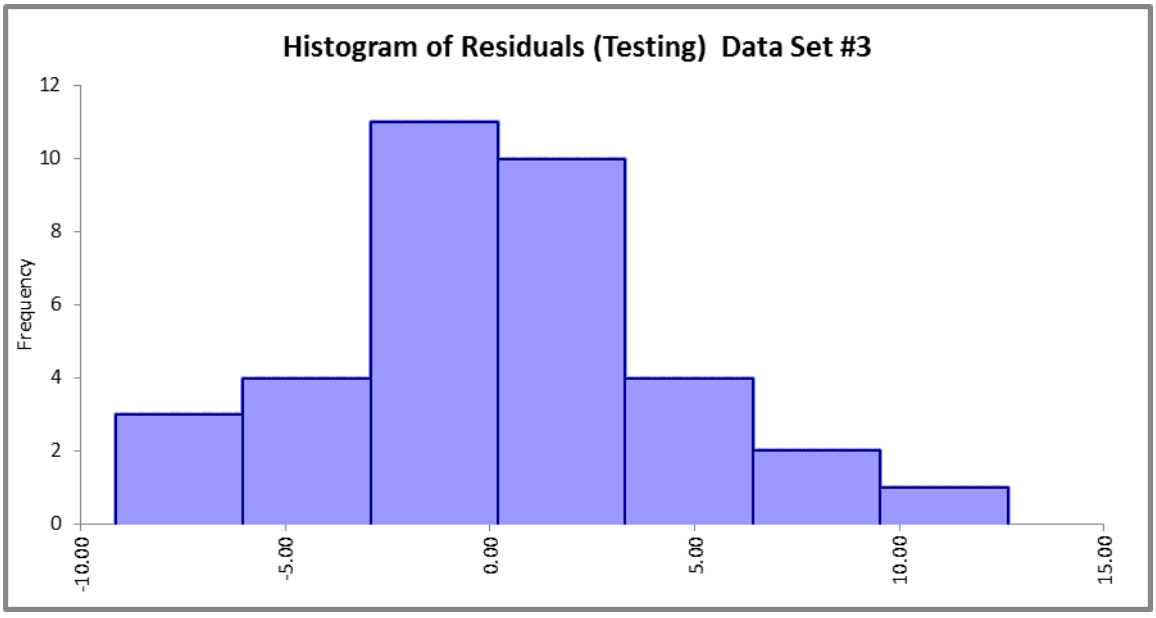

Figure C- 16 Data Set #3 Residuals

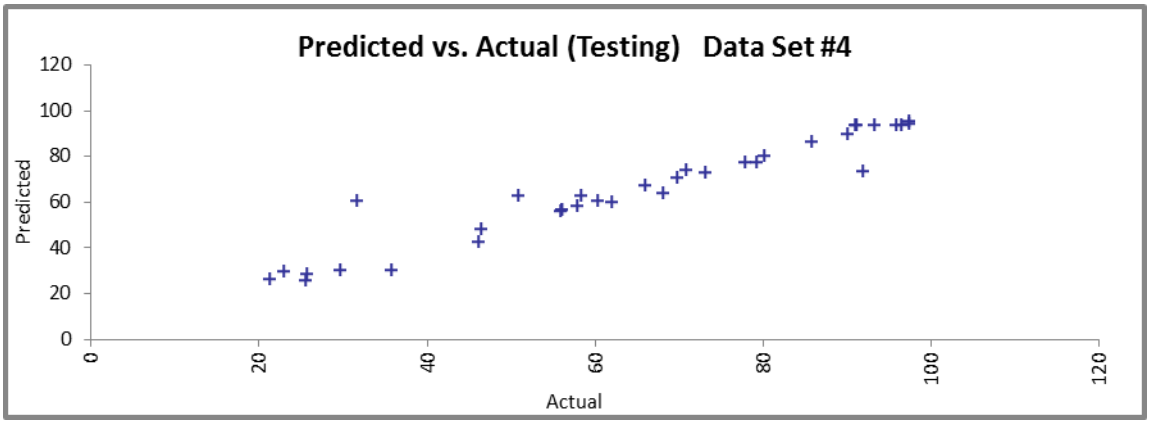

Figure C- 17 Data Set #4: Predicted vs. Actual Values

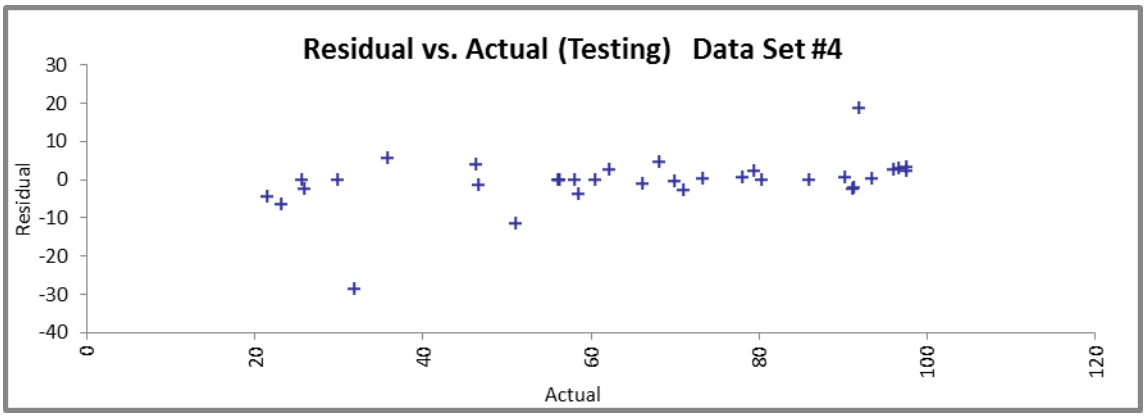

Figure C- 18 Data Set #4: Residual vs. Actual Values

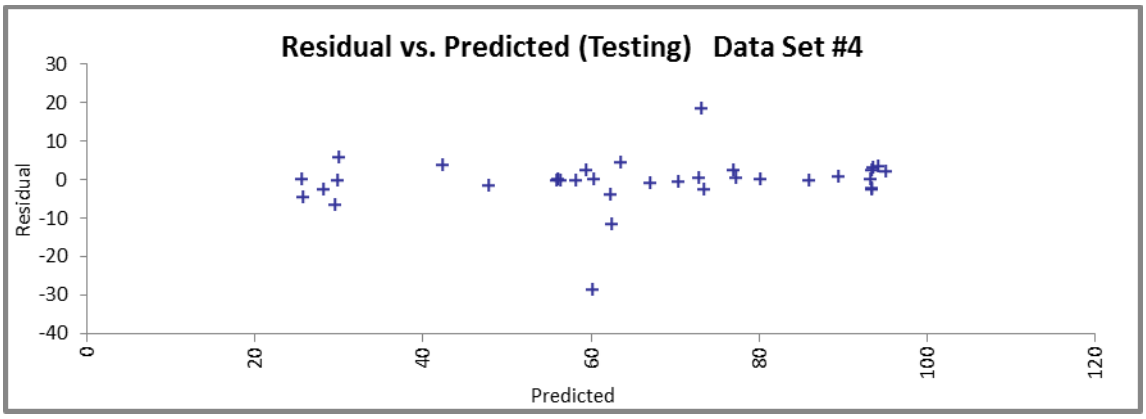

Figure C- 19 Data Set #3: Residual vs. Predicted Values

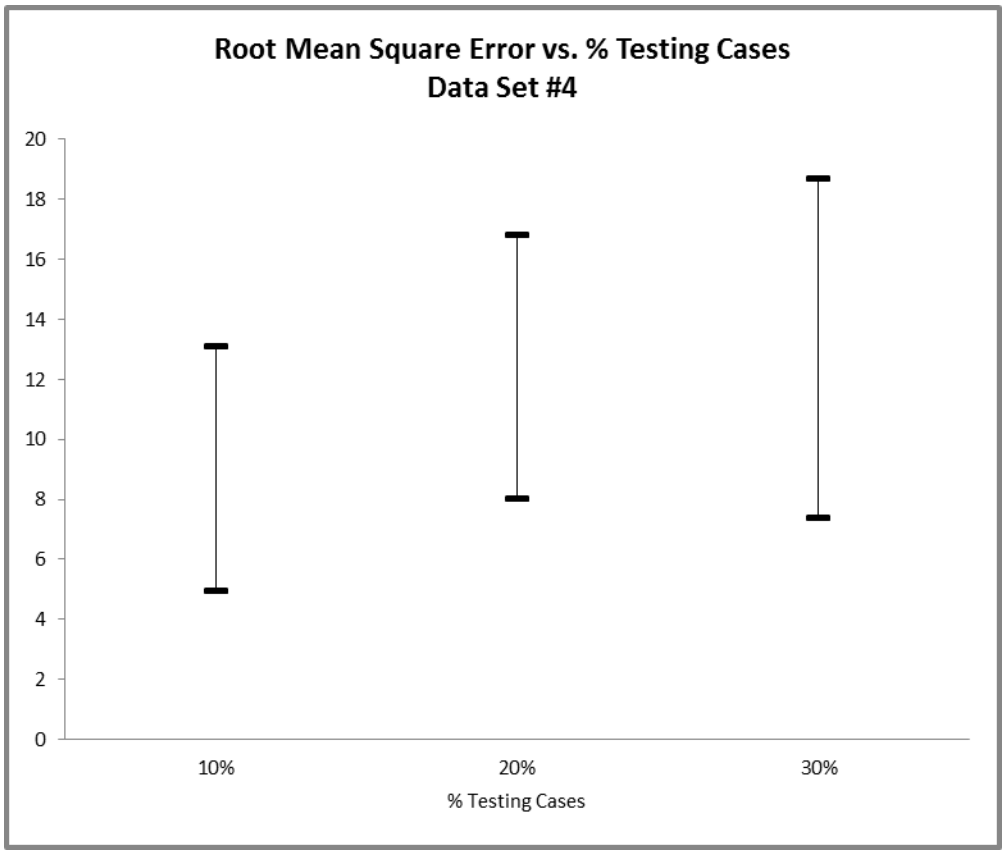

Figure C- 20 Data Set #4 Sensitivity Analysis

Table C- 9 Data Set #4 RMS Error

10%	20%	30%
4.922	7.971	7.327
10.35	12.00	11.14
10.92	13.09	13.31
11.40	13.57	15.09
13.07	16.78	18.65

Appendix D DATA TABLES

Table D- 1 Methane Number Raw Data, Blends 3, 5, and Check Case

	NA	NA	12 BAR	12 BAR	12 BAR	NA	NA	12 BAR	12 BAR	12 BAR	NA	NA	12 BAR	12 BAR	12 BAR
Syngas Blend	3	3	3	3	3	5	5	5	5	5	Check Case	Check Case	Check Case	Check Case	Check Case
Date	7/6/2012	7/16/2012	6/18/2012	6/18/2012	6/18/2012	7/13/2012	6/19/2012	7/13/2012	7/13/2012	7/13/2012	7/30/2012	7/30/2012	7/30/2012	7/30/2012	7/30/2012
	Case 1	Case 2	Case 3	Case 4	Case 5	Case 1	Case 2	Case 3	Case 4	Case 5	Case 1	Case 2	Case 3	Case 4	Case 5
Engine Data															
Timing (Degrees BTDC)	17	23	17	23	23	17	23	17	23	23	17	23	17	23	23
Knock Index	0.1	0.1	0.1	0.1	0.1	0.1	0.1	0.1	0.1	0.1	0.1	0.1	0.1	0.1	0.1
Events/Cycles	10/200	10/200	10/200	10/200	10/200	10/200	10/200	10/200	10/200	10/200	10/200	10/200	10/200	10/200	10/200
Compression Ratio	13.69	10.6	11.07	9.42	9.04	8.83	7.98	7.00	9.71	6.46	14.24	10.79	11.01	8.57	12.46
Methane Number															
Integral Value	22.12	24.61	25.63	32.57	21.14	25.43	24.50	23.42	24.91	22.44	23.72	25.35	22.13	24.49	24.05
A:F Ratio (Stoic)	8.96	8.96	8.96	8.96	8.96	6.80	6.80	6.80	6.80	6.80	17.04	17.04	17.04	17.04	17.04
Power (kW)	2.10	2.01	3.73	3.72	3.71	1.87	1.69	3.64	3.57	3.55	2.35	2.26	3.65	3.63	3.68
Speed	942.43	942.36	957.33	955.41	959.75	941.54	938.43	957.80	957.49	957.12	945.10	944.50	956.43	956.06	957.08
E-BMEP	0.00	0.00	0.00	0.00	0.00	0.00	0.00	0.00	0.00	0.00	0.00	0.00	0.00	0.00	0.00
Ignition Timing	0.00	0.00	0.00	0.00	0.00	0.00	0.00	0.00	0.00	0.00	0.00	0.00	0.00	0.00	0.00
Coolant Temp (°C)	94.91	94.84	94.20	94.16	94.02	95.05	94.44	94.27	94.53	94.16	95.00	95.05	94.94	94.72	94.96
Intake Air Temp (°C)	29.93	31.11	30.65	31.00	30.53	29.95	29.53	30.97	31.50	31.22	29.21	29.22	29.25	29.29	29.44
Mixing Air Temp (°C)	41.41	42.35	39.34	38.67	39.07	41.41	40.98	39.16	38.76	39.12	56.09	969.62	51.86	37.86	37.84
Exhaust Temp (°C)	386.67	388.70	485.83	468.02	497.09	406.85	411.40	540.48	509.31	545.22	392.98	401.97	464.81	507.76	438.13
Oil Temp	0.00	0.00	0.00	0.00	0.00	0.00	0.00	0.00	0.00	0.00	0.00	0.00	0.00	0.00	0.00
Intake Pressure (kPa)	101.35	101.25	149.05	183.05	156.98	101.16	101.25	173.24	196.89	177.12	101.44	101.35	141.09	151.30	150.23
Exhaust Pressure (kPa)	100.27	106.24	153.02	210.57	165.09	100.09	105.41	188.01	213.48	182.81	107.50	107.80	153.41	158.08	159.96
Fuel Pressure (kPa)	153.25	153.83	215.69	234.64	225.57	179.18	175.32	278.24	279.43	282.46	127.27	126.79	171.48	177.88	189.92
Oil Pressure	0.00	0.00	0.00	0.00	0.00	0.00	0.00	0.00	0.00	0.00	0.00	0.00	0.00	0.00	0.00
Coriolis Fuel Flow	0.00	0.00	0.00	0.00	0.00	0.00	0.00	0.00	0.00	0.00	0.00	0.00	0.00	0.00	0.00
Methane Flow	14.60	15.07	22.62	20.10	23.79	7.30	7.36	12.86	11.33	12.93	16.06	16.09	23.26	21.28	29.54
Low Flow	1.86	1.99	2.83	2.68	2.85	0.00	0.00	0.00	0.00	0.00	1.80	1.77	2.52	2.41	3.26
Propane Flow	0.00	0.00	0.00	0.00	0.00	0.00	0.00	0.00	0.00	0.00	0.00	0.00	0.00	0.00	0.00
Butane Flow	0.00	0.00	0.00	0.00	0.00	0.00	0.00	0.00	0.00	0.00	0.00	0.00	0.00	0.00	0.00
Carbon Monoxide Flow	4.14	3.62	5.93	5.30	6.21	9.89	9.73	17.36	15.16	18.16	0.00	0.00	0.00	0.00	0.00
Carbon Dioxide Flow	0.00	0.00	0.00	0.00	0.00	0.00	0.00	0.00	0.00	0.00	0.00	0.00	0.00	0.00	0.00
Hydrogen Flow	8.41	8.72	12.41	12.90	13.32	24.53	23.73	43.01	37.24	42.88	0.00	0.00	0.00	0.00	0.00
Nitrogen Flow	3.31	3.47	5.63	5.06	5.89	7.39	7.29	12.72	10.88	12.91	0.00	0.00	0.00	0.00	0.00
Air Flow [slpm]	168.85	168.76	260.26	335.58	272.37	154.85	152.57	272.10	335.84	277.73	184.01	184.33	264.77	286.53	277.56
Methane Flow %	8%	9%	9%	8%	9%	4%	4%	4%	4%	4%	11%	11%	12%	13%	11%
Low Flow %	1%	1%	1%	1%	1%	0%	0%	0%	0%	0%	1%	1%	1%	1%	1%
Carbon Monoxide Flow %	2%	2%	2%	2%	2%	5%	5%	6%	5%	6%	0%	0%	0%	0%	0%
Carbon Dioxide Flow %	0%	0%	0%	0%	0%	0%	0%	0%	0%	0%	0%	0%	0%	0%	0%
Hydrogen Flow %	5%	5%	5%	5%	5%	12%	12%	14%	12%	14%	0%	0%	0%	0%	0%
Nitrogen Flow %	2%	2%	2%	2%	2%	4%	4%	4%	4%	4%	0%	0%	0%	0%	0%
A:F Ratio (calc)	9.03	8.96	9.02	12.85	9.04	6.90	6.88	6.94	9.86	6.91	17.09	17.15	17.09	20.06	14.06
Equivalence Ratio (Φ)	0.99	1.00	0.99	0.70	0.99	0.99	0.99	0.98	0.69	0.98	1.00	0.99	1.00	0.85	1.21
Pressure Data															
Avg. Peak (kPa)	6306.45	6038.33	7723.84	8213.44	7803.24	5048.49	4800.39	6483.24	7347.43	6555.91	6327.16	6319.94	7252.76	7258.16	8299.66
Peak Std. Dev. (kPa)	475.49	270.66	447.50	614.57	241.15	115.25	44.48	132.53	146.37	52.29	508.58	222.92	381.34	220.46	711.19
Peak COV (%)	7.54	4.48	5.79	7.48	3.09	2.28	0.93	2.04	1.99	0.80	8.04	3.53	5.26	3.04	8.57
Max Peak (kPa)	7783.10	6676.94	8983.04	9891.03	8378.88	5428.79	4911.64	6803.82	7724.15	6698.19	7630.13	6865.97	8549.90	7862.07	10438.56
Min Peak (kPa)	5120.94	5296.43	6570.42	6916.78	6809.64	4725.50	4678.49	6081.84	6930.69	6383.25	5185.34	5572.09	6195.91	6612.30	6841.87
Avg. Peak Loc. (°ATDC)	15.01	9.97	16.75	13.84	12.19	10.14	4.69	12.45	9.49	5.45	16.12	10.47	17.00	12.23	16.21
Peak Loc. Std. Dev (°)	1.66	1.46	1.34	1.98	1.38	1.13	0.94	1.29	1.36	0.93	1.53	1.35	1.31	1.43	1.54
Peak Loc. COV (°ATDC)	11.04	14.62	8.00	14.27	11.32	11.13	20.00	10.34	14.31	17.08	9.52	12.92	7.71	11.72	9.50
AVG IMEP (kPa)	843.05	820.85	1268.79	1278.84	1271.36	777.25	736.09	1275.37	1252.37	1255.51	906.66	879.40	1256.86	1256.36	1274.82
IMEP STD DEV (kPa)	13.10	15.40	16.83	33.57	13.40	12.14	10.48	11.07	14.27	12.28	17.00	11.29	14.47	18.72	13.26
IMEP COV (%)	1.55	1.88	1.33	2.63	1.05	1.56	1.42	0.87	1.14	0.98	1.87	1.28	1.15	1.49	1.04
AVG NMEP (kPa)	813.27	787.30	1218.43	1198.82	1214.96	746.13	706.14	1209.80	1181.36	1196.03	872.34	844.49	1201.00	1200.74	1222.09
NMEP STD DEV (kPa)	14.14	15.81	16.49	34.50	11.89	12.49	9.74	11.15	13.38	12.68	17.45	10.20	15.07	17.72	13.45
NMEP COV (%)	1.74	2.01	1.35	2.88	0.98	1.67	1.38	0.92	1.13	1.06	2.00	1.21	1.25	1.48	1.10
AVG PMEP (kPa)	-29.78	-33.55	-50.36	-80.02	-56.40	-31.12	-29.96	-65.57	-71.01	-59.47	-34.32	-34.91	-55.86	-55.62	-52.73
PMEP STD DEV (kPa)	8.45	7.47	8.31	9.51	9.79	7.81	8.93	9.29	9.69	9.92	6.72	7.72	7.97	9.22	8.10
PMEP COV (%)	-28.38	-22.25	-16.50	-11.89	-17.36	-25.09	-29.81	-14.17	-13.64	-16.68	-19.59	-22.11	-14.27	-16.57	-15.36
MFB 10% (°ATDC)	-2.81	-8.39	-2.51	-6.70	-7.20	-6.77	-10.67	-4.98	-8.58	-10.06	-1.40	-7.88	-1.93	-6.94	-3.25
MFB 50% (°ATDC)	9.23	1.62	9.34	4.99	3.34	1.93	-3.28	3.82	0.12	-2.73	10.81	2.26	10.22	3.48	9.81
MFB 90% (°ATDC)	30.05	10.45	19.63	14.72	12.50	7.86	3.53	11.00	7.07	3.30	22.76	11.06	20.29	13.41	20.36

Table D- 2 Equivalence Ratio Sweeps, Raw Data (Blends 3 and 4)

		Integrals adjusted from 1000 cycles						Integrals adjusted from 1000 cycles						
	SG3	SG3	SG3	SG3	SG3	SG3	SG4	SG4	SG4	SG4	SG4	SG4	SG4
	INITIAL						INITIAL						
Target Equivalence Ratio	POINT	1	0.9	0.8	0.7	0.6	POINT	1	0.9	0.8	0.7	0.6	0.5
Date	8/1/2012	8/1/2012	8/1/2012	8/1/2012	8/1/2012	8/1/2012	8/2/2012	8/2/2012	8/2/2012	8/2/2012	8/2/2012	8/2/2012	8/2/2012
Engine Data													
Timing (Degrees BTDC)	17	17	17	17	17	17	17	17	17	17	17	17	17
Knock Index	0.1	0.1	0.1	0.1	0.1	0.1	0.1	0.1	0.1	0.1	0.1	0.1	0.1
Events/Cycles	10/200	10/200	10/200	10/200	10/200	10/200	10/200	10/200	10/200	10/200	10/200	10/200	10/200
Compression Ratio	11.03	8.83	8.83	8.83	8.83	8.83	6.55	5.24	5.24	5.24	5.24	5.24	5.24
Methane Number (Calc)													
Integral Value	22.19	10.59	10.15	10.40	9.16	7.36	24.02	16.34	19.21	17.19	17.79	20.03	14.16
Integral Delta													
A:F Ratio (Stoic)	8.96	8.96	8.96	8.96	8.96	8.96	2.78	2.78	2.78	2.78	2.78	2.78	2.78
Power (kW)	2.91	2.78	2.80	2.72	2.61	2.35	2.90	2.65	2.64	2.47	2.12	1.74	1.38
Speed	950.79	949.39	949.75	949.24	947.62	945.34	950.54	948.63	948.69	946.41	943.74	940.86	937.50
E-BMEP	0.00	0.00	0.00	0.00	0.00	0.00	0.00	0.00	0.00	0.00	0.00	0.00	0.00
Ignition Timing	0.00	0.00	0.00	0.00	0.00	0.00	0.00	0.00	0.00	0.00	0.00	0.00	0.00
Coolant Temp (°C)	94.95	94.98	94.96	94.97	95.03	95.06	94.79	94.82	94.69	94.73	94.98	94.99	95.06
Intake Air Temp (°C)	30.08	30.18	30.24	30.30	30.41	30.45	29.52	29.56	29.70	30.24	30.95	31.16	31.53
Mixing Air Temp (°C)	39.08	107.47	42.03	41.53	41.10	39.87	36.77	36.80	37.01	38.02	38.53	38.63	39.01
Exhaust Temp (°C)	457.64	471.96	477.82	479.19	460.85	436.12	457.59	494.53	521.50	527.97	478.48	449.48	405.46
Oil Temp	0.00	0.00	0.00	0.00	0.00	0.00	0.00	0.00	0.00	0.00	0.00	0.00	0.00
Intake Pressure (kPa)	125.38	125.30	125.33	125.35	125.26	125.22	169.15	169.29	169.33	169.35	169.26	169.32	169.32
Exhaust Pressure (kPa)	130.45	130.30	130.25	129.91	130.72	131.13	152.08	157.16	159.76	178.14	180.42	182.29	205.00
Fuel Pressure (kPa)	190.68	190.80	185.43	179.96	173.17	167.81	384.05	385.93	384.47	367.32	334.34	310.53	286.41
Oil Pressure	0.00	0.00	0.00	0.00	0.00	0.00	0.00	0.00	0.00	0.00	0.00	0.00	0.00
Coriolis Fuel Flow	0.00	0.00	0.00	0.00	0.00	0.00	0.00	0.00	0.00	0.00	0.00	0.00	0.00
Methane Flow	16.30	16.29	16.09	15.82	14.42	12.89	0.00	0.00	0.00	0.00	0.00	0.00	0.00
Low Flow	10.19	10.12	9.78	9.34	8.20	7.44	0.00	0.00	0.00	0.00	0.00	0.00	0.00
Propane Flow	0.00	0.00	0.00	0.00	0.00	0.00	0.00	0.00	0.00	0.00	0.00	0.00	0.00
Butane Flow	0.00	0.00	0.00	0.00	0.00	0.00	0.00	0.00	0.00	0.00	0.00	0.00	0.00
Carbon Monoxide Flow	5.11	4.91	4.61	3.60	3.67	2.81	27.10	27.56	27.80	26.42	21.52	19.09	16.08
Carbon Dioxide Flow	3.02	2.84	1.95	1.76	1.70	1.12	20.11	20.22	19.89	18.04	16.26	14.55	12.08
Hydrogen Flow	0.00	0.00	0.00	0.00	0.00	0.00	66.50	66.78	66.36	62.84	53.97	45.19	40.26
Nitrogen Flow	4.04	4.55	4.32	3.84	2.76	3.37	19.90	19.85	19.71	18.34	16.49	14.63	12.13
Air Flow [slpm]	208.58	209.49	211.99	214.05	220.81	226.96	234.15	235.79	234.30	235.35	256.58	270.44	275.36
Low Flow Species	H2	H2	H2	H2	H2	H2	None	None	None	None	None	None	None
Methane Flow %	47%	48%	50%	52%	52%	53%	0%	0%	0%	0%	0%	0%	0%
Low Flow %	29%	30%	30%	31%	29%	31%	0%	0%	0%	0%	0%	0%	0%
Carbon Monoxide Flow %	15%	14%	14%	12%	13%	12%	57%	58%	58%	59%	57%	57%	57%
Carbon Dioxide Flow %	9%	8%	6%	6%	6%	5%	43%	42%	42%	41%	43%	43%	43%
Hydrogen Flow %	0%	0%	0%	0%	0%	0%	141%	140%	139%	141%	143%	134%	143%
Nitrogen Flow %	12%	13%	13%	13%	10%	14%	42%	42%	41%	41%	44%	44%	43%
	112%	113%	113%	113%	110%	114%	283%	281%	280%	283%	286%	278%	286%
A:F Ratio (calc)	9.00	9.03	10.00	11.10	12.73	14.80	2.90	2.90	2.90	3.13	3.93	4.67	5.68
Equivalence Ratio (Φ)	1.00	0.99	0.90	0.81	0.70	0.61	0.96	0.96	0.96	0.89	0.71	0.59	0.49
Pressure Data													
Avg. Peak (kPa)	6536.88	5183.29	5259.42	5183.09	4935.80	4439.21	5569.73	4272.04	4255.75	4075.08	3528.07	2966.17	2483.31
Peak Std. Dev. (kPa)	360.59	176.79	177.84	179.63	235.92	246.08	73.35	52.92	51.53	57.84	74.40	86.43	93.43
Peak COV (%)	5.52	3.41	3.38	3.47	4.78	5.54	1.32	1.24	1.21	1.42	2.11	2.91	3.76
Max Peak (kPa)	7674.89	5732.45	5788.16	5749.19	5589.79	5292.57	5770.84	4417.38	4438.63	4220.94	3749.51	3266.48	2811.46
Min Peak (kPa)	5655.17	4482.37	4568.67	4624.70	4041.84	3745.26	5371.85	4084.73	4087.31	3837.42	3243.61	2694.25	2236.02
Avg. Peak Loc. (°ATDC)	16.06	17.87	17.30	17.42	18.21	20.07	9.41	11.76	11.86	13.52	18.77	24.11	28.07
Peak Loc. Std. Dev (°)	1.36	1.38	1.40	1.34	1.47	1.62	1.05	0.90	0.88	0.97	1.14	1.39	1.53
Peak Loc. COV (°ATDC)	8.48	7.75	8.12	7.71	8.06	8.06	11.14	7.64	7.39	7.15	6.05	5.78	5.45
AVG IMEP (kPa)	1063.21	1014.06	1020.80	1008.36	958.59	888.45	1046.16	977.24	975.59	934.38	837.70	744.96	658.92
IMEP STD DEV (kPa)	13.58	13.04	13.55	18.16	32.53	26.67	13.07	12.76	12.30	12.42	12.04	12.01	11.56
IMEP COV (%)	1.28	1.29	1.33	1.80	3.39	3.00	1.25	1.31	1.26	1.33	1.44	1.61	1.75
AVG NMEP (kPa)	1017.82	966.10	972.87	960.60	911.35	842.18	984.34	927.30	923.77	863.34	764.55	670.95	564.73
NMEP STD DEV (kPa)	14.90	14.05	13.69	18.90	32.33	27.04	13.47	13.87	13.74	12.80	13.02	12.61	13.96
NMEP COV (%)	1.46	1.45	1.41	1.97	3.55	3.21	1.37	1.50	1.49	1.48	1.70	1.88	2.47
AVG PMEP (kPa)	-45.39	-47.96	-47.94	-47.76	-47.24	-46.27	-61.82	-49.94	-51.81	-71.03	-73.14	-74.01	-94.18
PMEP STD DEV (kPa)	14.19	14.20	13.49	13.83	12.85	12.10	16.41	16.71	15.97	15.37	14.27	13.58	12.00
PMEP COV (%)	-31.25	-29.60	-28.14	-28.96	-27.20	-26.14	-26.55	-33.47	-30.82	-21.64	-19.50	-18.35	-12.74
MFB 10% (°ATDC)	-3.12	-1.87	-2.09	-2.01	-1.65	-0.53	-5.74	-1.95	-1.82	-3.22	-0.42	2.54	5.34
MFB 50% (°ATDC)	8.73	9.72	9.30	9.48	10.21	12.28	2.01	6.74	6.90	5.86	10.24	15.00	19.66
MFB 90% (°ATDC)	18.34	19.18	19.01	19.32	19.69	21.97	9.33	52.95	53.14	12.67	18.50	25.45	32.53

Table D- 3 Methane/Hydrogen Baseline Data - NA

Boost	Naturally	Aspirated								
Methane Concentration	20	40	60	80	100	20	40	60	80	100
Date	6/4/2012	6/4/2012	6/4/2012	6/4/2012	6/4/2012	6/14/2012	6/14/2012	6/14/2012	6/14/2012	6/14/2012
Engine Data										
Timing (Degrees BTDC)										
Knock Index										
Events/Cycles										
Compression Ratio	8.53	9.66	11.23	13.01	15.08	7.68	9.42	10.52	13.01	15.72
Methane Number (Calc)	19.52%	39.75%	59.72%	84.77%	100.00%	19.47%	40.34%	58.69%	81.10%	100.00%
Integral Value										
A:F Ratio (Stoic)	22.94	19.94	18.55	17.75	17.23	22.94	19.94	18.55	17.75	17.23
Power (kW)	1.87	2.10	2.27	2.30	2.30	1.86	2.10	2.16	2.20	2.14
Speed	941.74	943.40	944.74	944.75	943.48	940.56	942.06	942.39	942.57	941.96
E-BMEP	0.00	0.00	0.00	0.00	0.00	0.00	0.00	0.00	0.00	0.00
Ignition Timing	0.00	0.00	0.00	0.00	0.00	0.00	0.00	0.00	0.00	0.00
Coolant Temp (°C)	94.81	94.92	94.96	94.88	94.82	94.63	94.69	94.69	94.66	94.74
Intake Air Temp (°C)	27.39	27.23	26.67	25.78	25.24	28.29	27.95	27.60	27.32	26.96
Mixing Air Temp (°C)	40.97	40.28	40.54	40.34	40.51	40.14	39.77	39.31	38.81	37.56
Exhaust Temp (°C)	419.81	411.78	386.27	400.56	387.74	423.58	414.48	399.61	388.77	346.28
Oil Temp	0.00	0.00	0.00	0.00	0.00	0.00	0.00	0.00	0.00	0.00
Intake Pressure (kPa)	101.22	101.29	101.33	101.37	101.30	101.20	101.30	101.32	101.29	101.34
Exhaust Pressure (kPa)	99.41	100.42	99.34	99.06	98.94	98.36	98.33	98.80	98.73	98.77
Fuel Pressure (kPa)	134.68	131.67	129.74	126.60	124.97	135.04	132.59	132.24	129.06	127.01
Oil Pressure	0.00	0.00	0.00	0.00	0.00	0.00	0.00	0.00	0.00	0.00
Coriolis Fuel Flow	0.00	0.00	0.00	0.00	0.00	0.00	0.00	0.00	0.00	0.00
Methane Flow	7.98	12.45	14.88	17.58	18.18	8.10	12.88	15.53	17.80	19.21
Low Flow	0.00	0.00	10.04	3.16	0.00	0.00	0.00	10.93	4.15	0.00
Propane Flow	0.00	0.00	0.00	0.00	0.00	0.00	0.00	0.00	0.00	0.00
Butane Flow	0.00	0.00	0.00	0.00	0.00	0.00	0.00	0.00	0.00	0.00
Carbon Monoxide Flow	0.00	0.00	0.00	0.00	0.00	0.00	0.00	0.00	0.00	0.00
Carbon Dioxide Flow	0.00	0.00	0.00	0.00	0.00	0.00	0.00	0.00	0.00	0.00
Hydrogen Flow	32.90	18.87	0.00	0.00	0.00	33.51	19.05	0.00	0.00	0.00
Nitrogen Flow	0.00	0.00	0.00	0.00	0.00	0.00	0.00	0.00	0.00	0.00
Air Flow [slpm]	163.33	173.42	175.45	181.44	183.14	164.73	173.17	175.83	181.25	182.74
Low Flow Species	H2	H2	H2	H2	H2	H2	H2	H2	H2	H2
Methane Flow %	2.3%	3.6%	4.2%	5.1%	5.3%	2.4%	3.7%	4.3%	5.1%	5.5%
Low Flow %	0.0%	0.0%	2.8%	0.9%	0.0%	0.0%	0.0%	3.0%	1.2%	0.0%
Carbon Monoxide Flow %	0.0%	0.0%	0.0%	0.0%	0.0%	0.0%	0.0%	0.0%	0.0%	0.0%
Carbon Dioxide Flow %	0.0%	0.0%	0.0%	0.0%	0.0%	0.0%	0.0%	0.0%	0.0%	0.0%
Hydrogen Flow %	9.6%	5.5%	0.0%	0.0%	0.0%	9.8%	5.5%	0.0%	0.0%	0.0%
Nitrogen Flow %	0.0%	0.0%	0.0%	0.0%	0.0%	0.0%	0.0%	0.0%	0.0%	0.0%
	12%	9%	7%	6%	5%	12%	9%	7%	6%	6%
A:F Ratio (calc)	24.36	21.14	19.63	18.22	18.19	24.18	20.48	18.78	17.86	17.18
Equivalence Ratio (Φ)	0.94	0.94	0.94	0.97	0.95	0.95	0.97	0.99	0.99	1.00

Table D- 4 Methane/Hydrogen Baseline Data – 10 bar nmep

Boost	10 bar									
Methane Concentration	20	40	60	80	100	20	40	60	80	100
Date	6/4/2012	6/4/2012	6/4/2012	6/4/2012	6/4/2012	6/14/2012	6/14/2012	6/14/2012	6/14/2012	6/14/2012
Engine Data										
Timing (Degrees BTDC)										
Knock Index										
Events/Cycles										
Compression Ratio	7.82	8.84	9.83	11.12	14.44	7.04	8.68	9.92	12.12	14.86
Methane Number (Calc)	19.84%	39.39%	60.13%	79.83%	100.00%	20.52%	41.10%	60.09%	81.29%	100.00%
Integral Value										
A:F Ratio (Stoic)	22.94	19.94	18.55	17.75	17.23	22.94	19.94	18.55	17.75	17.23
Power (kW)	2.80	2.80	2.83	2.80	2.79	2.88	2.89	2.91	2.94	2.80
Speed	949.58	949.10	949.31	948.18	949.99	950.04	950.06	949.81	949.87	948.37
E-BMEP	0.00	0.00	0.00	0.00	0.00	0.00	0.00	0.00	0.00	0.00
Ignition Timing	0.00	0.00	0.00	0.00	0.00	0.00	0.00	0.00	0.00	0.00
Coolant Temp (°C)	94.52	94.62	94.77	94.93	94.79	94.35	94.52	94.59	94.64	94.59
Intake Air Temp (°C)	27.85	27.69	27.53	27.41	27.60	29.72	29.46	29.13	28.84	28.67
Mixing Air Temp (°C)	41.34	41.58	40.45	40.45	40.78	39.26	39.51	39.39	39.21	39.09
Exhaust Temp (°C)	479.42	460.79	432.51	364.47	420.34	490.51	459.81	451.37	430.00	404.46
Oil Temp	0.00	0.00	0.00	0.00	0.00	0.00	0.00	0.00	0.00	0.00
Intake Pressure (kPa)	134.93	126.12	119.02	115.12	114.83	137.01	126.91	122.99	119.93	118.04
Exhaust Pressure (kPa)	133.56	128.53	110.05	107.80	110.32	134.77	127.24	126.73	125.97	131.79
Fuel Pressure (kPa)	172.26	159.79	150.82	144.13	141.54	175.46	160.70	157.11	151.41	147.36
Oil Pressure	0.00	0.00	0.00	0.00	0.00	0.00	0.00	0.00	0.00	0.00
Coriolis Fuel Flow	0.00	0.00	0.00	0.00	0.00	0.00	0.00	0.00	0.00	0.00
Methane Flow	11.10	15.69	17.97	19.51	20.85	11.71	16.71	19.34	21.45	22.66
Low Flow	0.00	0.00	11.92	4.93	0.00	0.00	0.00	12.85	4.94	0.00
Propane Flow	0.00	0.00	0.00	0.00	0.00	0.00	0.00	0.00	0.00	0.00
Butane Flow	0.00	0.00	0.00	0.00	0.00	0.00	0.00	0.00	0.00	0.00
Carbon Monoxide Flow	0.00	0.00	0.00	0.00	0.00	0.00	0.00	0.00	0.00	0.00
Carbon Dioxide Flow	0.00	0.00	0.00	0.00	0.00	0.00	0.00	0.00	0.00	0.00
Hydrogen Flow	44.83	24.15	0.00	0.00	0.00	45.34	23.95	0.00	0.00	0.00
Nitrogen Flow	0.00	0.00	0.00	0.00	0.00	0.00	0.00	0.00	0.00	0.00
Air Flow [slpm]	224.66	218.44	210.76	209.79	210.13	232.11	223.19	217.95	218.99	216.58
Low Flow Species	H2	H2	H2	H2	H2	H2	H2	H2	H2	H2
Methane Flow %	2.5%	3.6%	4.4%	5.0%	5.4%	2.6%	3.9%	4.4%	5.1%	5.4%
Low Flow %	0.0%	0.0%	2.9%	1.3%	0.0%	0.0%	0.0%	2.9%	1.2%	0.0%
Carbon Monoxide Flow %	0.0%	0.0%	0.0%	0.0%	0.0%	0.0%	0.0%	0.0%	0.0%	0.0%
Carbon Dioxide Flow %	0.0%	0.0%	0.0%	0.0%	0.0%	0.0%	0.0%	0.0%	0.0%	0.0%
Hydrogen Flow %	9.9%	5.6%	0.0%	0.0%	0.0%	9.9%	5.5%	0.0%	0.0%	0.0%
Nitrogen Flow %	0.0%	0.0%	0.0%	0.0%	0.0%	0.0%	0.0%	0.0%	0.0%	0.0%
	12%	9%	7%	6%	5%	12%	9%	7%	6%	5%
A:F Ratio (calc)	24.26	21.07	19.55	18.82	18.20	24.10	20.44	18.78	17.92	17.26
Equivalence Ratio (Φ)	0.95	0.95	0.95	0.94	0.95	0.95	0.98	0.99	0.99	1.00

Table D- 5 Methane/Hydrogen Baseline Data – 11 bar nmep

Boost	11 bar									
Methane Concentration	20	40	60	80	100	20	40	60	80	100
Date	6/4/2012	6/4/2012	6/4/2012	6/4/2012	6/4/2012	6/14/2012	6/14/2012	6/14/2012	6/14/2012	6/14/2012
Engine Data										
Timing (Degrees BTDC)										
Knock Index										
Events/Cycles										
Compression Ratio	7.43	8.57	9.83	10.66	12.26	6.66	9.08	10.62	11.85	14.25
Methane Number (Calc)	19.92%	40.24%	59.02%	80.02%	100.00%	19.96%	41.08%	60.36%	80.75%	100.00%
Integral Value										
A:F Ratio (Stoic)	22.94	19.94	18.55	17.75	17.23	22.94	19.94	18.55	17.75	17.23
Power (kW)	3.21	3.26	3.26	3.28	3.25	3.27	3.29	3.29	3.30	3.30
Speed	954.62	955.29	954.92	954.18	953.92	953.35	953.79	953.42	954.76	953.55
E-BMEP	0.00	0.00	0.00	0.00	0.00	0.00	0.00	0.00	0.00	0.00
Ignition Timing	0.00	0.00	0.00	0.00	0.00	0.00	0.00	0.00	0.00	0.00
Coolant Temp (°C)	94.25	94.40	94.53	94.70	94.69	94.22	94.53	94.60	94.64	94.51
Intake Air Temp (°C)	29.14	28.92	28.64	28.36	28.12	30.53	30.30	30.17	30.10	29.97
Mixing Air Temp (°C)	40.80	40.32	40.41	40.24	40.57	39.46	39.84	39.86	39.79	39.61
Exhaust Temp (°C)	519.44	501.43	477.63	472.72	467.42	521.28	489.55	461.07	447.63	440.42
Oil Temp	0.00	0.00	0.00	0.00	0.00	0.00	0.00	0.00	0.00	0.00
Intake Pressure (kPa)	154.09	139.98	134.44	131.58	129.13	153.87	136.93	134.00	129.92	130.10
Exhaust Pressure (kPa)	163.10	150.59	144.74	142.77	139.61	151.97	142.26	140.88	131.24	131.82
Fuel Pressure (kPa)	194.28	175.33	169.65	163.43	158.23	194.71	173.23	170.60	163.45	161.08
Oil Pressure	0.00	0.00	0.00	0.00	0.00	0.00	0.00	0.00	0.00	0.00
Coriolis Fuel Flow	0.00	0.00	0.00	0.00	0.00	0.00	0.00	0.00	0.00	0.00
Methane Flow	12.85	17.84	20.32	22.57	23.81	13.08	18.12	21.21	23.53	25.54
Low Flow	0.00	0.00	14.11	5.64	0.00	0.00	0.00	13.93	5.61	0.00
Propane Flow	0.00	0.00	0.00	0.00	0.00	0.00	0.00	0.00	0.00	0.00
Butane Flow	0.00	0.00	0.00	0.00	0.00	0.00	0.00	0.00	0.00	0.00
Carbon Monoxide Flow	0.00	0.00	0.00	0.00	0.00	0.00	0.00	0.00	0.00	0.00
Carbon Dioxide Flow	0.00	0.00	0.00	0.00	0.00	0.00	0.00	0.00	0.00	0.00
Hydrogen Flow	51.67	26.49	0.00	0.00	0.00	52.44	25.98	0.00	0.00	0.00
Nitrogen Flow	0.00	0.00	0.00	0.00	0.00	0.00	0.00	0.00	0.00	0.00
Air Flow [slpm]	259.65	247.30	239.77	242.12	241.22	262.99	242.10	238.07	239.01	243.05
Low Flow Species	H2	H2	H2	H2	H2	H2	H2	H2	H2	H2
Methane Flow %	2.5%	3.7%	4.2%	4.8%	5.3%	2.5%	3.9%	4.4%	5.2%	5.7%
Low Flow %	0.0%	0.0%	2.9%	1.2%	0.0%	0.0%	0.0%	2.9%	1.2%	0.0%
Carbon Monoxide Flow %	0.0%	0.0%	0.0%	0.0%	0.0%	0.0%	0.0%	0.0%	0.0%	0.0%
Carbon Dioxide Flow %	0.0%	0.0%	0.0%	0.0%	0.0%	0.0%	0.0%	0.0%	0.0%	0.0%
Hydrogen Flow %	9.9%	5.5%	0.0%	0.0%	0.0%	10.2%	5.5%	0.0%	0.0%	0.0%
Nitrogen Flow %	0.0%	0.0%	0.0%	0.0%	0.0%	0.0%	0.0%	0.0%	0.0%	0.0%
	12%	9%	7%	6%	5%	13%	9%	7%	6%	6%
A:F Ratio (calc)	24.26	21.10	19.59	18.78	18.29	24.17	20.45	18.72	17.81	17.18
Equivalence Ratio (Φ)	0.95	0.94	0.95	0.95	0.94	0.95	0.97	0.99	1.00	1.00

Table D- 6 Methane/Hydrogen Baseline Data – 12 bar nmep

Boost	12 bar				
Methane Concentration	20	40	60	80	100
Date	6/4/2012	6/4/2012	6/4/2012	6/4/2012	6/4/2012
Engine Data					
Timing (Degrees BTDC)					
Knock Index					
Events/Cycles					
Compression Ratio	7.14	9.83	10.58	11.23	11.72
Methane Number (Calc)	20.68%	39.88%	59.59%	80.02%	100.00%
Integral Value					
A:F Ratio (Stoic)	22.94	19.94	18.55	17.75	17.23
Power (kW)	3.64	3.56	3.66	3.28	3.66
Speed	958.16	955.26	955.39	954.18	960.89
E-BMEP	0.00	0.00	0.00	0.00	0.00
Ignition Timing	0.00	0.00	0.00	0.00	0.00
Coolant Temp (°C)	94.15	94.13	94.43	94.70	94.52
Intake Air Temp (°C)	29.85	27.30	29.48	28.36	29.26
Mixing Air Temp (°C)	40.98	40.29	202.46	40.24	40.15
Exhaust Temp (°C)	523.00	498.26	490.52	472.72	489.24
Oil Temp	0.00	0.00	0.00	0.00	0.00
Intake Pressure (kPa)	161.93	153.23	144.47	131.58	141.02
Exhaust Pressure (kPa)	159.18	153.12	147.38	142.77	147.02
Fuel Pressure (kPa)	202.14	190.40	181.28	163.43	171.54
Oil Pressure	0.00	0.00	0.00	0.00	0.00
Coriolis Fuel Flow	0.00	0.00	0.00	0.00	0.00
Methane Flow	13.93	19.45	21.98	22.57	26.24
Low Flow	0.00	0.00	14.90	5.64	0.00
Propane Flow	0.00	0.00	0.00	0.00	0.00
Butane Flow	0.00	0.00	0.00	0.00	0.00
Carbon Monoxide Flow	0.00	0.00	0.00	0.00	0.00
Carbon Dioxide Flow	0.00	0.00	0.00	0.00	0.00
Hydrogen Flow	53.40	29.32	0.00	0.00	0.00
Nitrogen Flow	0.00	0.00	0.00	0.00	0.00
Air Flow [slpm]	277.53	270.80	258.90	242.12	265.47
Low Flow Species	H2	H2	H2	H2	H2
Methane Flow %	2.6%	3.8%	4.3%	4.8%	5.4%
Low Flow %	0.0%	0.0%	2.9%	1.2%	0.0%
Carbon Monoxide Flow %	0.0%	0.0%	0.0%	0.0%	0.0%
Carbon Dioxide Flow %	0.0%	0.0%	0.0%	0.0%	0.0%
Hydrogen Flow %	9.9%	5.7%	0.0%	0.0%	0.0%
Nitrogen Flow %	0.0%	0.0%	0.0%	0.0%	0.0%
	13%	9%	7%	6%	5%
A:F Ratio (calc)	24.30	21.14	19.60	18.78	18.27
Equivalence Ratio (Φ)	0.94	0.94	0.95	0.95	0.94

Table D- 7 Motoring Data 1 – Daily Verification of Dynamic TDC

Run #	HOT														
Blend															
Date	6/18/2012	6/19/2012	6/21/2012	6/26/2012	6/27/2012	6/28/2012	7/2/2012	7/3/2012	7/5/2012	7/6/2012	7/9/2012	7/10/2012	7/11/2012	7/12/2012	7/13/2012
Pressure Data															
Avg. Peak (kPa)	2216.17	2104.11	2169.07	2168.55	2126.02	2149.19	2187.97	4324.69	2131.36	2088.19	2193.96	2104.19	2160.00	311.43	307.18
Peak Std. Dev. (kPa)	11.93	9.99	26.87	7.42	14.34	11.03	7.12	352.58	18.19	7.94	16.69	14.44	11.92	624.13	611.50
Peak COV (%)	0.54	0.47	1.24	0.34	0.67	0.51	0.33	8.15	0.85	0.38	0.76	0.69	0.55	200.41	199.07
Max Peak (kPa)	2237.58	2126.16	2208.91	2181.87	2161.58	2165.44	2205.37	4984.40	2168.36	2106.51	2219.54	2130.02	2180.61	2181.86	2135.49
Min Peak (kPa)	2184.44	2086.87	2123.58	2146.44	2107.16	2125.51	2173.49	3638.35	2102.67	2074.95	2155.78	2083.65	2134.24	101.30	101.30
Avg. Peak Loc. (°ATDC)	-0.29	-0.35	-0.34	-0.40	-0.29	-0.32	-0.42	20.58	-0.41	-0.37	-0.49	-0.34	-0.30	-323.32	-323.32
Peak Loc. Std. Dev (°)	0.30	0.29	0.30	0.37	0.32	0.31	0.33	2.07	0.31	0.37	0.29	0.30	0.30	108.93	108.94
Peak Loc. COV (°ATDC)	-104.79	-82.50	-87.74	-92.33	-109.77	-96.29	-80.11	10.04	-75.72	-98.37	-58.64	-88.32	-98.21	-33.69	-33.69
AVG IMEP (kPa)	-31.70	-29.81	-29.33	-35.23	-32.33	-31.83	-33.97	863.48	-30.09	-30.28	-34.31	-30.54	-31.45	-3.04	-3.31
IMEP STD DEV (kPa)	2.64	2.81	3.44	1.76	2.33	1.99	3.02	23.41	4.36	3.95	2.56	3.72	3.33	9.17	9.89
IMEP COV (%)	-8.32	-9.43	-11.71	-5.00	-7.22	-6.24	-8.88	2.71	-14.50	-13.04	-7.45	-12.19	-10.59	-301.67	-298.46
AVG NMEP (kPa)	-50.07	-50.85	-50.83	-54.09	-53.96	-53.66	-53.14	831.45	-52.09	-53.47	-54.09	-54.83	-52.17	-8.37	-8.64
NMEP STD DEV (kPa)	3.68	4.37	4.20	2.95	3.60	3.07	4.37	25.02	5.88	4.54	4.87	5.55	6.39	14.59	15.35
NMEP COV (%)	-7.35	-8.60	-8.26	-5.45	-6.67	-5.73	-8.23	3.01	-11.28	-8.49	-9.00	-10.12	-12.25	-174.34	-177.68
AVG PMEP (kPa)	-18.37	-21.04	-21.50	-18.86	-21.63	-21.83	-19.18	-32.03	-22.00	-23.19	-19.77	-24.29	-20.72	-5.33	-5.32
PMEP STD DEV (kPa)	4.05	3.98	4.53	3.28	3.58	3.38	4.50	6.14	7.08	5.41	4.37	5.45	6.19	5.86	5.80
PMEP COV (%)	-22.05	-18.91	-21.09	-17.37	-16.56	-15.48	-23.44	-19.18	-32.19	-23.32	-22.11	-22.45	-29.85	-109.85	-108.98
MFB 10% (°ATDC)	7.62	-9.52	6.97	-9.59	-10.10	-9.91	-9.04	0.80	-10.11	-10.41	-9.79	-10.39	-9.18	35.28	35.42
MFB 50% (°ATDC)	46.63	36.61	39.25	37.82	30.89	34.25	41.20	13.39	31.09	25.78	35.42	27.23	36.54	83.38	83.63
MFB 90% (°ATDC)	139.89	129.02	126.80	132.06	131.78	125.08	129.54	23.71	113.16	58.08	123.00	76.49	127.27	139.02	139.39

Table D- 8 Motoring Data 2 – Daily Verification of Dynamic TDC

Run #	COLD												
Blend													
Date	6/18/2012	6/19/2012	6/21/2012	6/26/2012	6/27/2012	6/28/2012	7/2/2012	7/3/2012	7/5/2012	7/6/2012	7/9/2012	7/10/2012	7/11/2012
Pressure Data													
Avg. Peak (kPa)	2138.08	2121.74	2126.94	2089.99	2097.80	2144.29	2140.73	2079.50	2062.28	2131.47	2133.41	2101.94	2127.30
Peak Std. Dev. (kPa)	9.14	5.11	9.87	6.03	20.04	8.29	8.09	25.66	10.64	6.74	10.20	35.11	11.86
Peak COV (%)	0.43	0.24	0.46	0.29	0.96	0.39	0.38	1.23	0.52	0.32	0.48	1.67	0.56
Max Peak (kPa)	2155.46	2130.99	2146.12	2109.73	2130.07	2160.29	2153.92	2137.75	2088.18	2150.63	2149.02	2149.41	2160.97
Min Peak (kPa)	2117.14	2111.02	2101.36	2079.79	2066.95	2129.38	2121.07	2042.75	2045.02	2119.71	2106.19	2052.48	2107.83
Avg. Peak Loc. (°ATDC)	-0.43	-0.47	-0.52	-0.59	-0.56	-0.43	-0.45	-0.47	-0.54	-0.45	-0.54	-0.61	-0.62
Peak Loc. Std. Dev (°)	0.36	0.29	0.30	0.30	0.33	0.32	0.31	0.32	0.28	0.38	0.34	0.32	0.36
Peak Loc. COV (°ATDC)	-83.95	-63.07	-58.65	-50.83	-58.83	-74.47	-70.21	-67.86	-51.61	-85.10	-62.49	-52.01	-57.97
AVG IMEP (kPa)	-37.82	-38.33	-33.25	-37.43	-37.88	-38.92	-37.37	-38.29	-34.21	-36.29	-37.71	-36.33	-37.79
IMEP STD DEV (kPa)	1.33	1.84	1.06	1.18	1.51	1.20	1.90	1.19	2.81	2.23	1.98	1.98	2.14
IMEP COV (%)	-3.51	-4.81	-3.20	-3.15	-3.98	-3.08	-5.08	-3.11	-8.20	-6.15	-5.25	-5.45	-5.65
AVG NMEP (kPa)	-59.19	-60.42	-60.19	-60.73	-60.64	-61.58	-58.54	-62.12	-59.16	-58.97	-60.80	-60.74	-60.37
NMEP STD DEV (kPa)	2.18	2.73	0.75	1.94	2.37	1.62	2.45	1.63	3.41	3.23	3.12	2.64	2.88
NMEP COV (%)	-3.68	-4.51	-1.25	-3.19	-3.91	-2.64	-4.19	-2.62	-5.76	-5.47	-5.14	-4.34	-4.77
AVG PMEP (kPa)	-21.37	-22.08	-26.94	-23.30	-22.76	-22.66	-21.16	-23.83	-24.95	-22.67	-23.09	-24.41	-22.58
PMEP STD DEV (kPa)	2.10	3.32	0.89	1.60	2.18	1.31	2.44	1.46	3.80	3.48	2.91	2.86	2.78
PMEP COV (%)	-9.85	-15.05	-3.30	-6.87	-9.60	-5.77	-11.52	-6.12	-15.22	-15.34	-12.60	-11.70	-12.31
MFB 10% (°ATDC)	4.19	3.79	-9.60	3.72	1.99	-9.80	-8.95	-9.09	1.33	1.41	3.40	3.01	4.05
MFB 50% (°ATDC)	35.96	35.07	25.03	33.20	33.60	29.96	34.73	31.51	32.01	32.60	36.34	35.26	37.48
MFB 90% (°ATDC)	124.08	109.65	51.96	118.55	130.30	117.55	110.29	109.18	109.94	113.29	115.76	119.18	118.58

Table D- 9 Motoring Data 3 – Daily Verification of Dynamic TDC

Run #	COLD												
Blend													
Date	6/18/2012	6/19/2012	6/21/2012	6/26/2012	6/27/2012	6/28/2012	7/2/2012	7/3/2012	7/5/2012	7/6/2012	7/9/2012	7/10/2012	7/11/2012
Pressure Data													
Avg. Peak (kPa)	2138.08	2121.74	2126.94	2089.99	2097.80	2144.29	2140.73	2079.50	2062.28	2131.47	2133.41	2101.94	2127.30
Peak Std. Dev. (kPa)	9.14	5.11	9.87	6.03	20.04	8.29	8.09	25.66	10.64	6.74	10.20	35.11	11.86
Peak COV (%)	0.43	0.24	0.46	0.29	0.96	0.39	0.38	1.23	0.52	0.32	0.48	1.67	0.56
Max Peak (kPa)	2155.46	2130.99	2146.12	2109.73	2130.07	2160.29	2153.92	2137.75	2088.18	2150.63	2149.02	2149.41	2160.97
Min Peak (kPa)	2117.14	2111.02	2101.36	2079.79	2066.95	2129.38	2121.07	2042.75	2045.02	2119.71	2106.19	2052.48	2107.83
Avg. Peak Loc. (°ATDC)	-0.43	-0.47	-0.52	-0.59	-0.56	-0.43	-0.45	-0.47	-0.54	-0.45	-0.54	-0.61	-0.62
Peak Loc. Std. Dev (°)	0.36	0.29	0.30	0.30	0.33	0.32	0.31	0.32	0.28	0.38	0.34	0.32	0.36
Peak Loc. COV (°ATDC)	-83.95	-63.07	-58.65	-50.83	-58.83	-74.47	-70.21	-67.86	-51.61	-85.10	-62.49	-52.01	-57.97
AVG IMEP (kPa)	-37.82	-38.33	-33.25	-37.43	-37.88	-38.92	-37.37	-38.29	-34.21	-36.29	-37.71	-36.33	-37.79
IMEP STD DEV (kPa)	1.33	1.84	1.06	1.18	1.51	1.20	1.90	1.19	2.81	2.23	1.98	1.98	2.14
IMEP COV (%)	-3.51	-4.81	-3.20	-3.15	-3.98	-3.08	-5.08	-3.11	-8.20	-6.15	-5.25	-5.45	-5.65
AVG NMEP (kPa)	-59.19	-60.42	-60.19	-60.73	-60.64	-61.58	-58.54	-62.12	-59.16	-58.97	-60.80	-60.74	-60.37
NMEP STD DEV (kPa)	2.18	2.73	0.75	1.94	2.37	1.62	2.45	1.63	3.41	3.23	3.12	2.64	2.88
NMEP COV (%)	-3.68	-4.51	-1.25	-3.19	-3.91	-2.64	-4.19	-2.62	-5.76	-5.47	-5.14	-4.34	-4.77
AVG PMEP (kPa)	-21.37	-22.08	-26.94	-23.30	-22.76	-22.66	-21.16	-23.83	-24.95	-22.67	-23.09	-24.41	-22.58
PMEP STD DEV (kPa)	2.10	3.32	0.89	1.60	2.18	1.31	2.44	1.46	3.80	3.48	2.91	2.86	2.78
PMEP COV (%)	-9.85	-15.05	-3.30	-6.87	-9.60	-5.77	-11.52	-6.12	-15.22	-15.34	-12.60	-11.70	-12.31
MFB 10% (°ATDC)	4.19	3.79	-9.60	3.72	1.99	-9.80	-8.95	-9.09	1.33	1.41	3.40	3.01	4.05
MFB 50% (°ATDC)	35.96	35.07	25.03	33.20	33.60	29.96	34.73	31.51	32.01	32.60	36.34	35.26	37.48
MFB 90% (°ATDC)	124.08	109.65	51.96	118.55	130.30	117.55	110.29	109.18	109.94	113.29	115.76	119.18	118.58

Table D- 10 Motoring Data 4 – Daily Verification of Dynamic TDC

Run #	COLD														
Blend															
Date	7/12/2012	7/13/2012	7/16/2012	7/17/2012	7/18/2012	7/19/2012	7/20/2012	7/23/2012	7/24/2012	7/25/2012	7/26/2012	7/27/2012	7/30/2012	7/31/2012	8/1/2012
Pressure Data															
Avg. Peak (kPa)	299.58	308.33	305.97	307.10	2132.94	2163.21	2082.41	2066.09	2107.34	2113.51	2149.79	2151.39	2177.58	2131.79	2156.59
Peak Std. Dev. (kPa)	595.44	614.92	607.90	611.29	9.00	10.00	19.11	15.32	6.33	12.40	13.55	15.01	7.96	15.99	10.09
Peak COV (%)	198.76	199.43	198.68	199.05	0.42	0.46	0.92	0.74	0.30	0.59	0.63	0.70	0.37	0.75	0.47
Max Peak (kPa)	2102.65	2140.97	2134.91	2157.71	2151.93	2182.51	2130.34	2099.75	2118.43	2136.49	2177.68	2181.54	2190.24	2158.07	2178.97
Min Peak (kPa)	101.30	101.30	101.30	101.30	2117.15	2141.61	2049.84	2039.21	2092.02	2093.34	2127.77	2111.66	2157.71	2093.67	2138.39
Avg. Peak Loc. (°ATDC)	-324.78	-323.34	-323.34	-323.34	-0.61	-0.47	-7.75	-0.47	-0.62	-0.50	-0.38	-0.36	-0.40	-0.55	-0.42
Peak Loc. Std. Dev (°)	106.96	108.90	108.89	108.88	0.31	0.37	50.83	0.32	0.34	0.36	0.41	0.47	0.44	0.31	0.30
Peak Loc. COV (°ATDC)	-32.93	-33.68	-33.68	-33.67	-50.50	-77.76	-656.26	-67.46	-54.33	-70.46	-108.39	-129.80	-111.66	-56.39	-70.53
AVG IMEP (kPa)	-3.65	-3.99	-3.89	-3.91	-37.78	-37.38	-36.83	-34.39	-37.54	-37.94	-36.91	-37.73	-34.60	-36.61	-34.60
IMEP STD DEV (kPa)	11.02	11.86	11.56	11.64	1.84	2.51	3.35	3.22	1.70	1.98	1.60	1.89	2.56	2.54	2.19
IMEP COV (%)	-302.04	-297.36	-297.36	-297.53	-4.87	-6.72	-9.10	-9.37	-4.53	-5.22	-4.33	-5.00	-7.39	-6.94	-6.34
AVG NMEP (kPa)	-9.07	-9.37	-8.29	-9.29	-60.42	-59.77	-60.65	-59.34	-60.13	-61.16	-59.06	-57.89	-55.72	-50.82	-83.35
NMEP STD DEV (kPa)	16.86	17.44	24.08	17.18	2.73	4.29	6.20	3.68	2.15	2.86	1.86	2.29	3.51	61.01	2.95
NMEP COV (%)	-185.78	-186.10	-290.64	-184.97	-4.52	-7.18	-10.22	-6.19	-3.57	-4.67	-3.15	-3.96	-6.30	-120.04	-3.53
AVG PMEP (kPa)	-5.42	-5.39	-4.40	-5.38	-22.64	-22.39	-23.82	-24.95	-22.59	-23.23	-22.16	-20.16	-21.12	-14.21	-48.75
PMEP STD DEV (kPa)	5.94	5.73	19.79	5.66	2.40	3.80	4.42	4.79	2.12	2.78	1.45	2.86	4.11	61.60	3.05
PMEP COV (%)	-109.51	-106.34	-450.10	-105.21	-10.62	-16.98	-18.55	-19.21	-9.38	-11.98	-6.54	-14.18	-19.48	-433.54	-6.25
MFB 10% (°ATDC)	35.87	35.70	35.59	35.66	5.53	-9.09	2.18	-9.68	3.61	4.22	5.17	14.70	-8.45	5.03	-8.78
MFB 50% (°ATDC)	84.02	83.80	83.72	83.83	37.58	30.39	30.85	26.19	35.45	34.56	34.46	28.62	39.49	36.93	31.53
MFB 90% (°ATDC)	139.80	139.57	139.36	139.62	116.09	115.39	94.97	67.09	113.84	114.67	108.98	71.90	123.05	118.49	110.08

Appendix E ACOUSTIC VELOCITY CALCULATIONS

Acoustic Velocity Determination

The following assumptions are made to compute the acoustic velocity of the combustion products in the cylinder:

1. The products behave as an ideal gas.
2. Combustion is complete and exactly stoichiometric.
3. The process is adiabatic.
4. Specific heats, c_p and c_v, and therefore the ratio of specific heats, are constant.

The combustion equation for producer gas blends is assumed to be

$$a\,H_2 + b\,CO + c\,CH_4 + d\,N_2 + e\,CO_2 + f(O_2 + 3.76\,N_2) \rightarrow x\,CO_2 + y\,H_2O + z\,N_2$$

C balance: $x = b + c + e$

H_2 balance: $y = a + 2c$

O_2 balance: $x + \frac{y}{2} = \frac{b}{2} + e + f$

N_2 balance: $z = d + 3.76f$

$$f = (b + c + e) + \frac{1}{2}(a + 2c) - \frac{b}{2} - e$$

The combustion equation for matching CH4/H2 blends is assumed to be

$$a\,H_2 + b\,CH_4 + c\,(O_2 + 3.76\,N_2) \rightarrow x\,CO_2 + y\,H_2O + z\,N_2$$

C balance: $x = b$

H_2 balance: $y = a + 2b$

O_2 balance: $x + \frac{y}{2} = c$

N_2 balance: $z = 3.76c$

$$c = b + \frac{1}{2}(a + 2b) = {}^{a}/_{2} + 2b$$

The software Engineering Equation Solver (EES) is used to solve for adiabatic flame temperature. The following scripts are written for the solution, variables defined as shown are for the producer gas blend "AF Gap A" and the matching CH4/H2 blend corresponding to methane number of 62.2:

```
"Adiabatic Flame Temperature: Producer gas with reactant species CH4, CO, H2, CO2, and N2.
Product species assumed to be CO2, H20, and N2.
    Reaction:
    a H2 + b CO + c CH4 + d N2 + e CO2 + f (O2 + 3.76 N2) --> x CO2 + y H2O + z N2"

    a=.343
    b=.343
    c=.078
    d=.05
    e=.186
    f=.5
    x=.61
    y=.5
    z=1.92

HR=a*enthalpy(H2,T=300)+b*enthalpy(CO,T=300)+c*enthalpy(CH4,T=300)+d*enthalpy(N2,T=300)
+e*enthalpy(CO2,T=300)+f*enthalpy(O2,T=300)+f*3.76*enthalpy(N2,T=300)

HP=HR

HP=x*enthalpy(CO2,T=T)+y*enthalpy(H2O,T=T)+z*enthalpy(N2,T=T)

"Adiabatic Flame Temperature Calculation: CH4 and H2
```

Product species assumed to be CO2, H20, and N2.

Reaction:

a CH4 + b H2 + c (O2 + 3.76 N2) --> x CO2 + y H2O + z N2"

a=.622
b=.378
c=.1.43
x=.62
y=1.62
z=5.39

HR=a*enthalpy(CH4,T=300)+b*enthalpy(H2,T=300)+c*enthalpy(O2,T=300)+c*3.76*enthalpy(N2,T=300)

HP=HR

HP=x*enthalpy(CO2,T=T)+y*enthalpy(H2O,T=T)+z*enthalpy(N2,T=T)

The script was repeated for each of the blends to determine adiabatic flame temperature. Average molecular weight and specific heats are calculated using the gas calculations spreadsheet shown. Acoustic velocity is then calculated using the equation

$$C_{avg} = \sqrt{\gamma RT / MW} \qquad [m/s]$$

where

C_{avg} = *Acoustic Velocity [m/s]*

γ = *Ratio of average specific heats,* c_p/c_v

R = Universal gas constant, 8.31447 kJ/kmole·K

T = Adiabatic flame temperature [K]

MW = Average molecular weight [kg/kmole]

The results of the calculations are provided in Tables E-1 and E-2

Table E- 1 Worksheet to calculate γ_{avg} and MW_{avg}

Combustion Stoichiometry **Analysis Date:** **A/Fstoic = 3.2618** 0.948 Btu/kJ

Fuel

Constit.	AF Gap A	Mole Fraction	Mass Fraction	Molecular Weight	MW x Mass Fraction	Carbon Content	Hydrogen Content	Oxygen Content	Nitrogen Content
CH4	0.08	0.08	0.0589	16.0426	1.24490576	0.0776	0.3104	0	0
C2H6	0.00	0.00	0	30.0694	0	0	0	0	0
C3H8	0.00	0.00	0	44.0962	0	0	0	0	0
C4H10	0.00	0.00	0	58.123	0	0	0	0	0
C5H12	0.00	0.00	0	72.1498	0	0	0	0	0
C6H14	0.00	0.00	0	86.1766	0	0	0	0	0
CO	0.34	0.34	0.45506	28.0104	9.61877136	0.3434	0	0.3434	0
H2	0.34	0.34	0.03275	2.0158	0.69222572	0	0.6868	0	0
N2	0.05	0.05	0.0656	28.0134	1.3866633	0	0	0	0.099
O2	0.00	0.00	0	31.9988	0	0	0	0	0
CO2	0.19	0.19	0.38769	44.0098	8.19462476	0.1862	0	0.3724	0
H2O	0.00	0.00	0	18.0152	0	0	0	0	0
Sums-->		1.0001	1		21.1371909	0.6072	0.9972	0.7158	0.099

MW of Elements		LHV [kJ/kg]	Mass Fraction x LHV	Cp [kJ/kg-K]	Cv [kJ/kg-K]
C	12.011	50016	2945.765442	2.2537	1.7354
H	1.0079	47489	0	1.7662	1.4897
N	14.0067	46357	0	1.6794	1.4909
O	15.9994	45742	0	1.7164	1.5734
		45355	0	1.9764	1.88
		45105	0	1.6642	1.5489
		10100	4596.144833	1.0404	0.744
		120000	3929.901887	14.307	10.183
		0	0	1.039	0.743
		0	0	0.918	0.658
		0	0	0.846	0.657
		0	0	1.8723	1.4108
	LHV_fuel	**11471.8**	**kJ/kg**	1.47087	1.077715
	=	266.668	Btu/SCF	**Avg γ =**	1.365

MWavg = 21.1372 rho = 0.86423217 kg/m^3 = 0.02452 kg/ft^3

Following Ferguson and Kirkpatrick

All Constituents		**Combustibles Only**	
α =	0.6072	α =	55.0759
β =	0.9972	β =	130.455
γ =	0.7158	γ =	44.9241
δ =	0.099	δ =	0
a_s =	0.4986	a_s =	65.2276
A/F_s =	**3.23935**	**A/F_s =**	**5.92517**

	All Constituents			**Combustables**	
	Urban and Sharp, 1994			**Urban and Sharp, 1994**	
H/C --->	y =	1.64229	H/C --->	y =	2.368646
O/C --->	z =	1.17885	O/C --->	z =	0.815677
N/C --->	f =	0.16304	N/C --->	f =	0
	A =	0.82115		A =	1.184323
	A/Fs =	**3.2618**		**A/Fs =**	**5.966214**

Mol fract sum Comb = 0.7644

Table E- 2 Producer Gas Combustion Equation Coefficients and Calculated Acoustic Velocity

	H2	CO	CH4	N2	CO2	f (a_{th})	CO2	H2O	N2	A/Fs	$T_{adiabatic}$	Avg γ	Avg MW	$c_{prod\ gas}$
	a	b	c	d	e	f	x	y	z		[K]		[kg/kmol]	[m/s]
AF Gap A	0.343	0.343	0.078	0.050	0.186	0.50	0.61	0.50	1.92	3.24	2257	1.36	21.14	34.81
AF Gap B	0.330	0.196	0.288	0.000	0.186	0.84	0.67	0.91	3.15	6.07	2238	1.34	18.96	36.30
AF Gap C	0.470	0.188	0.202	0.141	0.000	0.73	0.39	0.87	2.89	7.51	2318	1.38	13.39	44.50
AF Gap D	0.471	0.093	0.275	0.110	0.051	0.83	0.42	1.02	3.24	8.59	2271	1.36	13.31	43.94
AF Gap E	0.246	0.114	0.479	0.104	0.057	1.14	0.65	1.20	4.38	9.31	2247	1.34	16.79	38.59
Banham	0.356	0.211	0.233	0.000	0.201	0.75	0.64	0.82	2.81	5.36	2235	1.35	19.19	36.11
Blend #1	0.390	0.370	0.000	0.070	0.170	0.38	0.54	0.39	1.50	2.53	2284	1.38	20.59	35.62
Blend #2	0.180	0.180	0.020	0.480	0.140	0.22	0.34	0.22	1.31	1.19	1817	1.38	25.33	28.65
Blend #3	0.260	0.120	0.450	0.110	0.060	1.09	0.63	1.16	4.21	8.90	2246	1.34	16.83	38.57
Blend #4	0.500	0.200	0.000	0.150	0.150	0.35	0.35	0.50	1.47	2.76	2209	1.38	17.41	38.15
Blend #5	0.500	0.200	0.150	0.150	0.000	0.65	0.35	0.80	2.59	6.75	2330	1.38	13.22	45.01
Chroen (O2)	0.402	0.393	0.000	0.001	0.204	0.40	0.60	0.40	1.50	2.62	2302	1.38	13.22	44.74
City Energy	0.264	0.003	0.440	0.289	0.003	1.01	0.45	1.15	4.10	8.75	2201	1.35	15.91	39.38
CPC	0.187	0.210	0.022	0.567	0.014	0.24	0.25	0.23	1.48	1.44	1944	1.39	23.11	31.23
Cranfield	0.524	0.171	0.081	0.003	0.222	0.51	0.47	0.68	1.92	4.11	2229	1.36	16.98	38.54
Dil Gap A	0.282	0.130	0.403	0.119	0.065	1.01	0.60	1.09	3.92	8.23	2245	1.34	16.89	38.55
Dil Gap B	0.426	0.255	0.043	0.032	0.245	0.43	0.54	0.51	1.63	2.87	2198	1.36	20.34	34.98
Dil Gap C	0.495	0.188	0.000	0.158	0.158	0.34	0.35	0.50	1.44	2.65	2187	1.38	17.68	37.65
Dil Gap D	0.069	0.451	0.069	0.225	0.186	0.40	0.71	0.21	1.72	1.92	2137	1.36	28.38	29.22
Dil Gap F	0.174	0.222	0.048	0.411	0.145	0.29	0.42	0.27	1.52	1.60	1948	1.37	25.23	29.68
Gussing	0.400	0.240	0.100	0.030	0.230	0.52	0.57	0.60	1.99	3.55	2209	1.36	20.10	35.22
Harboore	0.193	0.228	0.053	0.407	0.119	0.32	0.40	0.30	1.60	1.79	1999	1.38	24.26	30.70
Hyder	0.273	0.133	0.473	0.054	0.067	1.15	0.67	1.22	4.38	9.68	2261	1.34	16.32	39.26
IISc	0.190	0.190	0.015	0.485	0.120	0.22	0.33	0.22	1.31	1.22	1846	1.38	24.81	29.22
Meadow Vale	0.156	0.310	0.366	0.088	0.080	0.96	0.76	0.89	3.72	6.35	2268	1.35	20.86	34.88
Plasma	0.398	0.380	0.016	0.033	0.173	0.42	0.57	0.43	1.62	2.86	2306	1.37	20.24	36.08
Repotec	0.400	0.250	0.100	0.050	0.200	0.53	0.55	0.60	2.02	3.68	2226	1.36	19.62	35.83
S4 Avg	0.354	0.354	0.051	0.051	0.192	0.45	0.60	0.45	1.76	2.93	2257	1.37	21.30	34.71
S4 Example	0.427	0.411	0.028	0.021	0.114	0.47	0.55	0.48	1.80	3.54	2378	1.38	18.41	38.51
TEMCO	0.066	0.528	0.070	0.192	0.143	0.44	0.74	0.21	1.84	2.17	2227	1.37	27.74	30.24
Victoria 1	0.486	0.096	0.252	0.113	0.053	0.79	0.40	0.99	3.10	8.26	2273	1.36	13.22	44.15
Viking	0.301	0.196	0.016	0.333	0.154	0.28	0.37	0.33	1.39	1.72	2004	1.38	22.46	31.95
VT 4/7/08	0.242	0.377	0.212	0.084	0.086	0.73	0.67	0.67	2.84	4.89	2299	1.36	20.56	35.59
VT 4/9/08	0.203	0.517	0.175	0.023	0.081	0.71	0.77	0.55	2.70	4.45	2356	1.37	21.93	34.94
WTG	0.221	0.440	0.151	0.012	0.176	0.63	0.77	0.52	2.39	3.73	2286	1.36	23.29	33.29

Table E- 3 Matching CH_4/H_2 Blend Combustion Equation Coefficients and Calculated Acoustic Velocity

	MN	CH4	H2	c (a_{th})	CO2	H2O	N2	A/Fs	$T_{adiabatic}$	Avg γ	Avg MW	$c_{CH4/H2}$
		a	b	c	x	y	z		[K]		[kg/kmol]	[m/s]
AF Gap A	62.2	0.622	0.378	1.433	0.622	1.622	5.388	18.323	2284	1.331563	10.74047	48.52
AF Gap B	93.5	0.935	0.065	1.903	0.935	1.935	7.153	17.267	2257	1.303847	15.13086	40.21
AF Gap C	56.3	0.563	0.437	1.345	0.563	1.563	5.055	18.626	2291	1.337364	9.912888	50.69
AF Gap D	56.3	0.563	0.437	1.345	0.563	1.563	5.055	18.626	2291	1.337364	9.912888	50.69
AF Gap E	78.0	0.780	0.220	1.670	0.780	1.780	6.279	17.700	2269	1.316968	12.9567	43.79
Banham	80.3	0.803	0.197	1.705	0.803	1.803	6.409	17.627	2267	1.31495	13.27932	43.20
Blend #1	35.9	0.359	0.641	1.039	0.359	1.359	3.905	20.225	2324	1.359089	7.051421	61.03
Blend #2	96.7	0.967	0.033	1.951	0.967	1.967	7.334	17.193	2255	1.301273	15.57972	39.57
Blend #3	71.0	0.710	0.290	1.565	0.710	1.710	5.884	17.948	2275	1.323272	11.97483	45.72
Blend #4	25.7	0.257	0.743	0.886	0.257	1.257	3.329	21.635	2348	1.371036	5.620688	69.01
Blend #5	31.9	0.319	0.681	0.979	0.319	1.319	3.679	20.704	2333	1.363681	6.490349	63.84
Chroen (O2)	25.9	0.259	0.741	0.889	0.259	1.259	3.341	21.601	2348	1.370794	5.648741	68.83
City Energy	92.0	0.920	0.080	1.880	0.920	1.920	7.069	17.304	2258	1.305069	14.92046	40.52
CPC	66.2	0.662	0.338	1.493	0.662	1.662	5.614	18.142	2280	1.327742	11.30154	47.19
Cranfield	51.1	0.511	0.489	1.267	0.511	1.511	4.762	18.939	2298	1.342648	9.183495	52.85
Dil Gap A	90.2	0.902	0.098	1.853	0.902	1.902	6.967	17.349	2260	1.306549	14.66797	40.91
Dil Gap B	46.3	0.463	0.537	1.195	0.463	1.463	4.491	19.276	2305	1.347675	8.510208	55.09
Dil Gap C	21.5	0.215	0.785	0.823	0.215	1.215	3.093	22.449	2361	1.37619	5.031562	73.27
Dil Gap D	97.6	0.976	0.024	1.964	0.976	1.976	7.385	17.173	2255	1.300557	15.70596	39.40
Dil Gap F	97.6	0.976	0.024	1.964	0.976	1.976	7.385	17.173	2255	1.300557	15.70596	39.40
Gussing	68.2	0.682	0.318	1.523	0.682	1.682	5.726	18.058	2278	1.325865	11.58208	46.56
Harboore	91.1	0.911	0.089	1.867	0.911	1.911	7.018	17.326	2259	1.305807	14.79421	40.72
Hyder	79.4	0.794	0.206	1.691	0.794	1.794	6.358	17.655	2268	1.315736	13.15308	43.43
IISc	96.0	0.960	0.040	1.940	0.960	1.960	7.294	17.209	2256	1.301832	15.48153	39.72
Meadow Vale	86.0	0.860	0.140	1.790	0.860	1.860	6.730	17.460	2262	1.310057	14.07885	41.83
Plasma	23.2	0.232	0.768	0.848	0.232	1.232	3.188	22.098	2356	1.374087	5.270018	71.47
Repotec	58.5	0.585	0.415	1.378	0.585	1.585	5.179	18.507	2288	1.335178	10.22148	49.85
S4 Avg	46.6	0.466	0.534	1.199	0.466	1.466	4.508	19.253	2305	1.347356	8.552289	54.95
S4 Example	29.9	0.299	0.701	0.949	0.299	1.299	3.566	20.976	2338	1.366022	6.209813	65.39
TEMCO	91.3	0.913	0.087	1.870	0.913	1.913	7.029	17.321	2259	1.305643	14.82227	40.68
Victoria 1	56.1	0.561	0.439	1.342	0.561	1.561	5.044	18.637	2291	1.337565	9.884835	50.77
Viking	70.0	0.700	0.300	1.550	0.700	1.700	5.828	17.986	2276	1.324194	11.83456	46.02
VT 4/7/08	58.1	0.581	0.419	1.372	0.581	1.581	5.157	18.528	2289	1.335573	10.16537	50.00
VT 4/9/08	60.5	0.605	0.395	1.408	0.605	1.605	5.292	18.405	2286	1.333214	10.50201	49.12
WTG	73.3	0.733	0.267	1.600	0.733	1.733	6.014	17.862	2273	1.321173	12.29744	45.06